E-20-H75
vols. 5 + 13
1/3

Spatial Assessment of Ozone and Particulate Matter in the Gulf Coast Region, Response to Controls and Advanced Field Monitoring as Part of the GC-ARCH SuperSite Study.

Draft Final Report to
University of Texas, Austin

From

K. Baumann, F. Ift, J. Z. Zhao, M. Bergin W. Younger, R. Weber, H. Park, T. Odman, Y. Hu and A. Russell
Georgia Institute of Technology
Atlanta, GA 30332-0512
trussell@ce.gatech.edu

As part of the Gulf Coast Aerosol Research Characterization Program (GC-ARCH), researchers at the Georgia Institute of Technology conducted a variety of studies and experiments to better characterize ozone and particulate matter evolution in the Gulf Coast region, including the Houston, TX, area as well as other Gulf Coast states. As documented in the attached reports, the studies included conducting field experiments during the TexAQS study, analysis of the particulate matter (PM) from coastal and near coastal monitors along the Gulf Coast, assessing a statistical approach for estimating control requirements for meeting the PM NAAQS and numerical simulation of part of the TexAQS period as well as the same period using future emissions. Notable findings and accomplishments from the research include:

- The PILS instrument was used to help calibrate the Aerodyne AMS to help it provide quantitative measurements of ionic species.
- Ground level and elevated (top of Williams Tower)…
- More from field study
- Spatial analysis of PM and ozone along the coast showed significant correlation (by species, when available). The correlation decreases inland, suggesting that much of the time, the coastal region is impacted by significantly different conditions than inland, and that transport to/from the coast inland has a less dominant effect. Numerical air quality modeling suggests that this is, indeed, the case, and that transport along the coast can be insignificant.
- Statistical analysis of daily speciated PM data over three years suggests that there is relatively little uncertainty in the necessary level of controls in PM precursors IF one assumes a linear and proportional response to controls. That is to say that the data are well represented by a log-normal distribution and that the year-to-year variability is small. However, more comprehensive mathematical modeling suggests that reductions in sulfate will meet with increases in nitrate.
- Numerical modeling of a 10-day period during TexAQS found good results for ozone, sulfate, organic carbon and elemental carbon. Surprisingly, the simulations found nitrate levels lower than observed, opposite of the findings in most other regions. While a new release of CMAQ is expected to address the over-estimates in other regions, those same improvements will exacerbate the underestimates found here. It appears as though the reason for the underestimate is due to simulated ammonia/ammonium (total ammonia) levels being low, suggesting a low bias in the emissions.

- Simulation of future year emissions found relatively little change in air quality in the Gulf Coast region, though significant reductions in ozone and some PM species inland. The reductions inland are driven by Tier II regulations (which also apply to the Gulf Coast areas) and both Acid Rain and NOx SIP-Call reductions (which have less impact in the Gulf coastal areas).

Data developed as part of the project includes continuous (1 min) measurements of various meteorological parameters, trace gases (NO, NO_x, NO_y, CO, SO_2, and O_3), and discrete, 6 to 24 h integrated filter-based measurements of $PM_{2.5}$ mass and composition, including aerosol gases (NH_3, HONO, HNO_3, HCl, SO_2, and light organic acids), were made at the LaPorte municipal airport (LP), near the Houston ship channel, during TexAQS2000. These discrete measurements were made by means of a three-channel Particle Composition Monitor (PCM) used in previous experiments carried out in the Southeastern U.S. within the framework of the Southern Oxidant Study (SOS), and described in greater detail by *Baumann et al.* [2003]. Similar PCM measurements supplemented by semi-continuous (30 min) O_3 and TEOM mass measurements were made on the 62nd floor of the Williams Tower (WT), 254 m agl, and ~12 km west of downtown Houston. The exact locations and periods of measurements are summarized in Table 1. The methods and quality of the measurements is briefly described and assessed first. In the second step, the results are compared and investigated for systematic differences induced by the difference in sampling height above ground. Lastly, special diurnal features and events are presented and discussed.

Table 1: Measurement site name, location and period during the TexAQS2000.

Site name	**Abbr.**	**Coordinates**			**Msmt Period**
		latitude N	**longitude W**	**elevation masl**	
LaPorte Airport	LP	29.671	95.069	8	08/15 - 09/14 2000
Williams Tower	WT	29.750	95.475	284	08/15 - 09/13 2000

The School's Air Quality Mobile Laboratory (AQML) was deployed at the LaPorte Municipal Airport (29.671 °N, 95.069 °W, 8 masl), collecting high temporal resolution atmospheric chemical and physical data from August 15 to September 14, 2000. The parameters sampled included O_3, CO, SO_2, NO, NOx, NOy, PM mass, PM composition, atmospheric pressure, surface and near surface temperature, relative humidity, visible and UV-B radiation, wind

direction, and wind speed. The AQML utilized a standard 10 m meteorological triangular Al tower mounted to the rear side of it. The meteorological parameters measured, their units, the sensor height in m above ground level (magl), the sensors' specifications and accuracies are listed in Table 2.

Table 2: Meteorological parameters measured with the AQML.

Parameter	**unit**	**height magl**	**sensor specifications**	**accuracy**
barometric p	mbar	2.0	Vaisala PTB100A 800-1060mbar	±0.3 mbar
rel. humidity	%	10.4	Vaisala HMP45A 0-100%	±1%RH (<90%)
air temp.	°C	11.0	aspir. RMYoung RTD –40-+60°C	±0.05°C
air temp.	°C	2.8	aspir. RMYoung RTD –40-+60°C	±0.05°C
soil temp.	°C	-0.1	Omega RTD1000 –40-+60°C	±0.05°C
visible rad.	W m^{-2}	11.3	LICOR LI-200SA pyr. 400-1100nm	±5 %
UV-B rad.	W m^{-2}	11.3	YES UVB-1 pyranom. 280-320 nm	±5 % (0-60zenith)
wind directn.	deg N	11.6	RM Young 05305AQ 0-360 deg	±3 deg
wind speed	m s^{-1}	11.6	RM Young 05305AQ 0-40 m s^{-1}	±0.2 m s^{-1}

Further detail can be found in the attached report by Baumann (2003). In addition, data was gathered and processed for air quality modeling of the region, as well as spatial analysis of the PM and ozone in the region. Four sources were utilized: GC-ARCH collaborators, EPA-AQS data base (EPA, 2003), the Southeastern Aerosol Research and Characterization (SEARCH) Study, and the Assessment of Spatial Aerosol Composition in Atlanta (ASACA) study (Butler et al., 2003).

Quality assurance procedures were followed closely in the conduct of this project. The Quality Assurance Project Plan (QAPP) is attached.

At present, the work has led, in part or in full, to four publications in preparation and three conference presentations that have been given. The conference presentations given to date are:

Baumann K, F Ift, JZ Zhao, MH Bergin, and AG Russell, Measurement of trace gases and $PM_{2.5}$ mass and composition near the ground and at 254 m agl during TexAQS 2000, *Proceedings of the 4th Conference on Atmospheric Chemistry: Urban, Regional, and Global-Scale Impacts of Air Pollutants, Orlando, FL, Amer. Meteor. Soc.*, 242-247, 2002

Park S, A Sahabi, H Lee, K Kim, A Marmur, J Tong, AG. Russell, The assessment of spatial aerosol composition, *AEES annual symposium, Atlanta GA,* April 7, 2003:

Park SK, AG Russell and E Edgerton, The statistical analysis of PM 2.5 in Atlanta: An application to the control strategy, *AAAR PM*, Pittsburgh PA, March 31-April 3, 2003

A copy of the proceedings document is attached. Also attached are: 1. A comprehensive description of the field experimental study, 2. A report describing the spatial analysis of the PM and ozone, 3. Results of air quality modeling of a period during the GC-ARCH study, and 4. A report describing the analysis of control requirements using probability distributions applied to sulfate and organic carbon.

As noted, many of the analysis projects are still underway, and will proceed with alternative funding (e.g., the modeling). Data sets can be supplied to interested individuals and other members of the GC-ARCH team.

References

Baumann, K., Chameides, W.L., Ift, F., and Zhao, J.Z. 2001. Discrete measurements of reactive gases and particle mass and composition during the 1999 Atlanta Supersite Experiment. *J. Geophys. Res. 108*, 8416, doi: 10.1029 /2001 JD001210, 2003.

Baumann K, F Ift, JZ Zhao, MH Bergin, and AG Russell, Measurement of trace gases and $PM_{2.5}$ mass and composition near the ground and at 254 m agl during TexAQS 2000, *Proceedings of the 4th Conference on Atmospheric Chemistry: Urban, Regional, and Global-Scale Impacts of Air Pollutants, Orlando, FL, Amer. Meteor. Soc.*, 242-247, 2002.

Butler, A., Andrew, K. and Russell, A.G. (2003) Spatial Characterization of Aerosols in Atlanta during the Supersite" *J. Geophys. Res.* (in press).

Edgerton, ES (2003) Presentation at Supersite P.I. Meeting, January, 23, 2003, Atlanta, GA

Measurements of trace gases and $PM_{2.5}$ mass and composition near the ground and at 254 m agl during TexAQS2000.

Final Report

Karsten Baumann

EAS-GIT

1. INTRODUCTION

Continuous (1 min) measurements of various meteorological parameters, trace gases (NO, NO_x, NO_y, CO, SO_2, and O_3), and discrete, 6 to 24 h integrated filter-based measurements of $PM_{2.5}$ mass and composition, including aerosol gases (NH_3, HONO, HNO_3, HCl, SO_2, and light organic acids), were made at the LaPorte municipal airport (LP), near the Houston ship channel, during TexAQS2000. These discrete measurements were made by means of a three-channel Particle Composition Monitor (PCM) used in previous experiments carried out in the Southeastern U.S. within the framework of the Southern Oxidant Study (SOS), and described in greater detail by *Baumann et al.* [2003]. Similar PCM measurements supplemented by semi-continuous (30 min) O_3 and TEOM mass measurements were made on the 62nd floor of the Williams Tower (WT), 254 m agl, and ~12 km west of downtown Houston. The exact locations and periods of measurements are summarized in Table 1. The methods and quality of the measurements is briefly described and assessed first. In the second step, the results are compared and investigated for systematic differences induced by the difference in sampling height above ground. Lastly, special diurnal features and events are presented and discussed.

Table 1: Measurement site name, location and period during the TexAQS2000.

Site name	Abbr.	Coordinates			Msmt Period
		latitude N	longitude W	elevation masl	
LaPorte Airport	LP	29.671	95.069	8	08/15 - 09/14 2000
Williams Tower	WT	29.750	95.475	284	08/15 - 09/13 2000

2. INSTRUMENTATION

2.1 Air Quality Mobile Laboratory (AQML)

The School's Air Quality Mobile Laboratory (AQML) was deployed at the LaPorte Municipal Airport (29.671 °N, 95.069 °W, 8 masl), collecting high temporal resolution atmospheric chemical and physical data from August 15 to September 14, 2000. The parameters sampled included O_3, CO, SO_2, NO, NOx, NOy, PM mass, PM composition, atmospheric pressure, surface and near surface temperature, relative humidity, visible and UV-B radiation, wind direction, and wind speed. The AQML utilized a standard 10 m meteorological triangular Al tower mounted to the rear side of it, as depicted in Figure 1. The meteorological parameters measured, their units, the sensor height in m above ground level (magl), the sensors' specifications and accuracies are listed in Table 2.

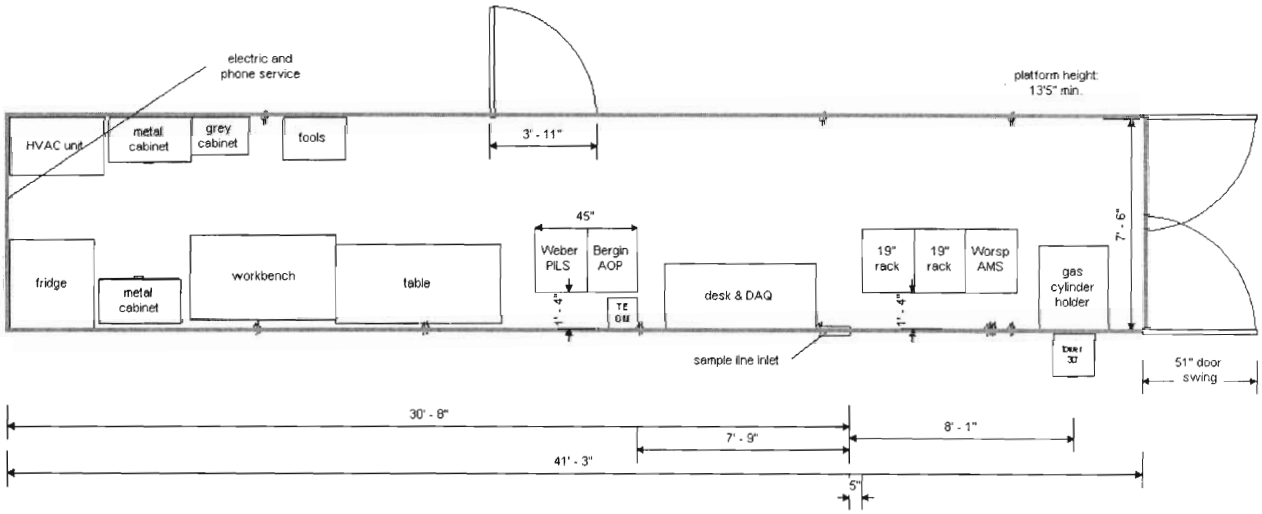

Figure 1: Top view dimensions and overview arrangements of the AQML.

Table 2: Meteorological parameters measured with the AQML.

Parameter	unit	height magl	sensor specifications	accuracy
barometric p	mbar	2.0	Vaisala PTB100A 800-1060mbar	±0.3 mbar
rel. humidity	%	10.4	Vaisala HMP45A 0-100%	±1%RH (<90%)
air temp.	°C	11.0	aspir. RMYoung RTD –40-+60°C	±0.05°C
air temp.	°C	2.8	aspir. RMYoung RTD –40-+60°C	±0.05°C
soil temp.	°C	-0.1	Omega RTD1000 –40-+60°C	±0.05°C
visible rad.	W m^{-2}	11.3	LICOR LI-200SA pyr. 400-1100nm	±5 %
UV-B rad.	W m^{-2}	11.3	YES UVB-1 pyranom. 280-320 nm	±5 % (0-60zenith)
wind directn.	deg N	11.6	RM Young 05305AQ 0-360 deg	±3 deg
wind speed	m s^{-1}	11.6	RM Young 05305AQ 0-40 m s^{-1}	±0.2 m s^{-1}

2.2 Particle Composition Monitor (PCM)

The measurement principle of our PCM is based on successive separation of particles larger than 2.5 microns aerodynamic diameter, followed by the separation of gaseous species from the particles prior to $PM_{2.5}$ collection on Teflon membrane and quartz fiber filters backed by specifically impregnated filters as backup adsorbers. The sampler operates three channels each controlled at a nominal flow rate of 16.7 lpm. $PM_{2.5}$ separation is achieved by standard, Teflon coated cyclone heads, after the sample air is pulled through 30 cm long, 14 mm ID, Teflon coated inlet tubes. Denuders and filter packs are mounted on top of the cyclone heads, the sampling occurs from bottom to top, see Figure 2.

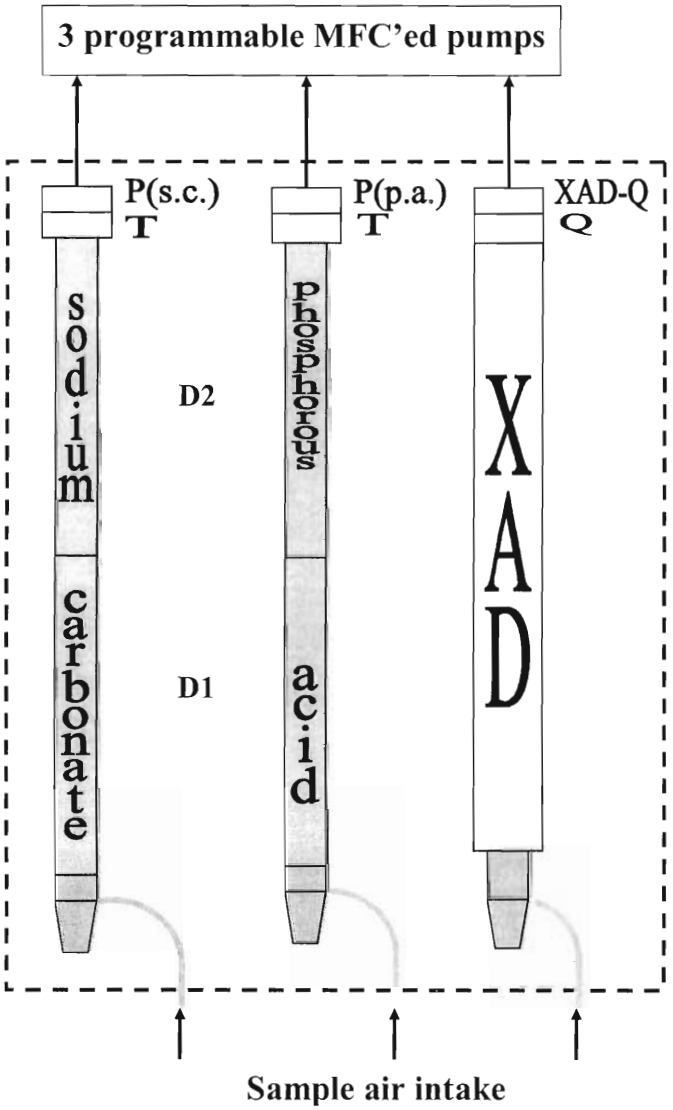

Figure 2: Three-channel Particle Composition Monitor (PCM) used during TexAQS2000. The phophosous acid channel is also labeled channel 1, the sodium carbonate channel 2, and the channel utilizing XAD is 3.

$D_{1,2}$	3-channel etched glass sc/pa-impregnated denuders in tandem set-up.
P...	Whatman 41 cellulose [paper] filter.
pa...	phosphorous acid coating solution: 10%/90% DDW/MeOH by volume, with 1g of PA per 100ml of solution, yielding a 122 mM solution.
Q...	Pallflex #2500 QAT-UP Quartz fiber filter, pre-baked for 2 h at 600°C.
sc...	sodium carbonate coating solution: 15.7g of Na_2CO_3 dissolved with 5 mg glycerol in 400ml DDW, 600 ml methanol added, yielding a 148 mM solution.
T...	Zeflour™ P5PJ047, unringed Teflon membrane, 2μm pore size.
XAD	XAD-4, porous macroreticular, non-polar, polystyrene-divinyl-benzene resin, applied to 8-channel etched glass denuders, same type as used in IOGAPS, see *Gundel et al.* [1995].

Each PCM sample is analyzed at the AREC (formerly SCISSAP) analytical laboratory at Georgia Tech. A thorough QA/QC protocol [see Quality Integrated Work Plan submitted to the U.S. EPA in August 1998 in fulfillment of requirement for Quality Assurance Plans for environmental data operations, and Standard Operating Procedures listed therein] ensures highest quality of the suite of species that are analyzed and reported; which are i) gaseous HCl, HONO, HNO_3, SO_2, HCOOH, CH_3COOH, $(COOH)_2$, NH_3; ii) particle-phase ($PM_{2.5}$) mass concentration, and its individual components Na^+, K^+, NH_4^+, Ca^{++}, Cl^-, F^-, NO_3^-, $SO_4^=$, $HCOO^-$, CH_3COO^-, $C_2O_4H^-$, elemental and organic carbon (EC, OC) with an estimate for semi-volatile OC, as well as the water-soluble fraction of the particle-phase OC for a few select samples. Details of the underlying assumptions for the calculations arriving at the final ambient concentrations for each species are summarized in Appendix A.

3. METHODS

3.1 $PM_{2.5}$ Mass Concentration

All Teflon filter samples were stored refrigerated at 4-8 °C immediately after collection until return to the home laboratory after the field experiment, where their initial gravimetric mass was determined. They were subsequently dehydrated in a desiccator located in a temperature- (21°C) and humidity- (40%) controlled clean room in order to remove humidity artifacts. The samples remained in the desiccator for at least 4 days, in most cases longer. The mass loss between the intial and final (desiccated) weight is plotted for both channels in Figure 3. The final masses

were determined gravimetrically from the desiccated channel 1 and 2 Teflon filters using a Mettler Toledo MT5 Electronic Balance with an experimentally determined detection limit of 1.2 ± .02 μg and an instrumental precision of 0.37 % for 1μg (from repeated weighings of a 1 mg standard weight). The MT5 is highly linear in the 1 to 500 mg range and exhibits an accuracy better than 0.001 %.

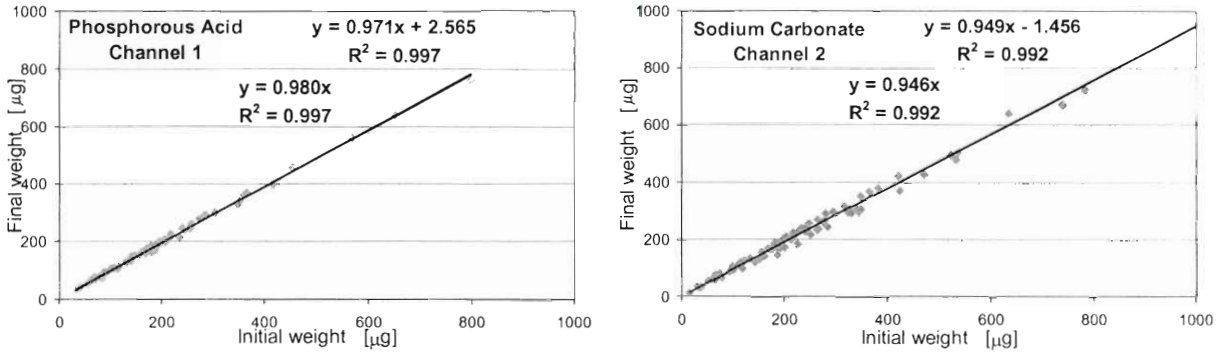

Figure 3: Average Teflon sample filter mass loss due to desiccation: The $PM_{2.5}$ collected downstream of the phophorous acid coated denuder pair loses 2 ±0.6 % (left), and downstream of the sodium carbonate coated denuder pair 5 ±0.9 % (right), incl. the ± standard error on the slopes. The standard error on the intercepts are ±1.4 and ±2.7, respectively.

The mass loss induced by desiccation is relatively minor, ranging between 2 and 5 % as indicated by the regression slopes in Figure 3. Higher losses were reported in earlier studies, and are thought mainly due to the more immediate determination of the intial weight after sample collection. Note, that the samples for this study were stored for severel weeks, before they were weighed for the first time. Also note, that desiccation occurred under ambient pressure, and tests proving that none of the lost mass is attributed to any water-solube species quantified and detected by the ion chromatopragh are described in *Baumann et al.* [2003].

Figure 4 compares the gravimetric mass concentrations determined from the two channels Teflon filter samples collected at both LP and WT during the study. Channel 2 Teflon masses were systematically higher by 13 ±5 % (corresponding 2.7 ±2.9 μg m^{-3}) at LaPorte, and by 21 ±7 % (2.6 ±2.8 μg m^{-3}) at Williams Tower, which is suspected to be due to artifacts caused by the glycerol-containing sodium carbonate coating solution used in the channel 2 denuders [*Finn et al.*, 2001]. Therefore, only channel 1 (phophorous acid denuded) Teflon filter mass concentrations were considered for any further evaluation. The semi-volatile fractions of NH_4^+,

NO_3^-, and the organic acids (from paper backup filters, considering corresponding blank levels and denuder efficiencies) are added to the gravimetric mass determined from the channel 1 Teflon filters.

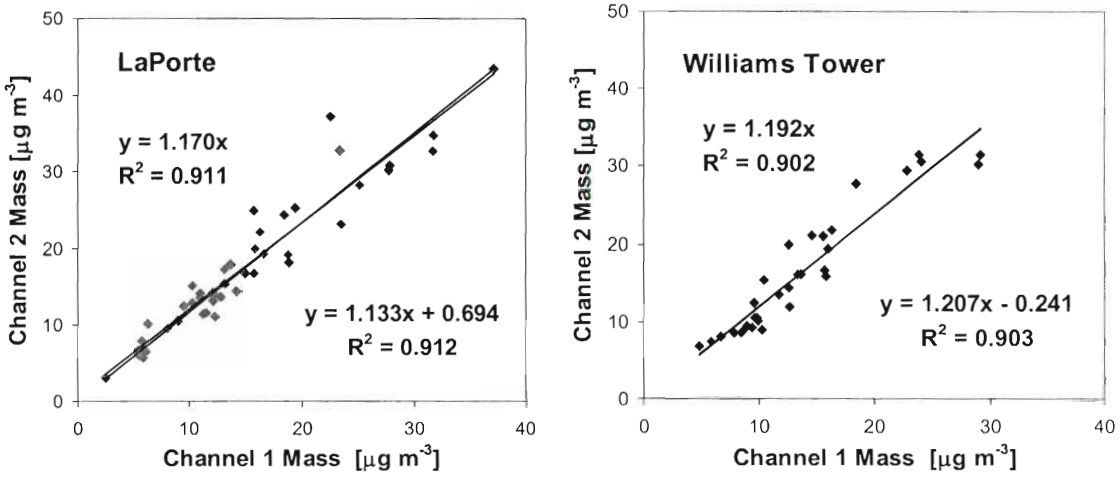

Figure 4: Sodium carbonate denuded (channel 2) Teflon filter $PM_{2.5}$ mass concentration compared with simultaneously collected phophorous acid denuded (channel 2) mass concentration, showing a systematic bias towards positive artifact in channel 2, possibly due to the use of glycerol in the Na_2CO_3 denuder coating solution [see *Finn et al.*, 2001].

At both sites, LP and WT, fine particle mass was measured utilizing a Tapered Element Oscillating Microbalance (TEOM 1400A, Rupprecht & Patashnick) in a semi-continuous fashion, allowing 30 minute time-resolution of the ambient $PM_{2.5}$ mass concentration measurement. Both TEOMs were operated with a commercially available naphion drier upstream of the oscillating sensor. The differences were that i) the cap, case and air temperature at LP were controlled at 50 °C, and 40 °C at WT; ii) an additional active humidity control was employed at the LP site via a heated copper inlet line controlled at 50 °C; and iii) the naphion drier sheeth air was supplied by the return flow from the TEOM sensor return at the WT set-up, whereas the LP set-up used indoor (trailer) air for this. As indicated in Figure 5, the TEOM mass concentrations at LP were systematically low relative to the gravimetric filter mass by 7 ±6 %, most likely attributed to the active, and more rigorous humidity control employed with the LP-TEOM. At the WT site, on the other hand, the TEOM averages seemed to be 7 ±4 % higher than the desiccated filter masses.

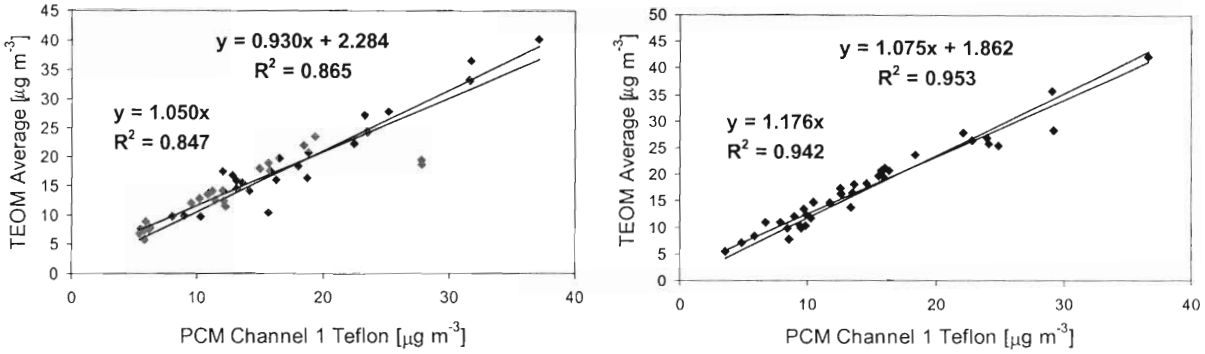

Figure 5: TEOM fine mass concentrations averaged over and compared with the gravimetric Teflon filter values from the discrete PCM sample intervals for LP (left) and WT (right).

3.2 PCM Species

3.2.1 Reactive Gases

Separation of the gases is achieved by means of appropriately coated denuders. During TexAQS2000 a phosphorous acid coating solution was used in channel 1, which selectively removed NH_3, while a sodium carbonate solution was used in channel 2 capturing the acidic gases HNO_3, HONO, SO_2, HCl, acetic, formic, and oxalic acids. Denuders were 3-annuli edged glass tubes that have a theoretical removal efficiency, based on molecular diffusion assuming 100% adsorption of 99.9% for NH_3, and 99.7% for HNO_3 at 0.1s residence time [Possanzini et al., 1983]. The effective denuder efficiencies are actually governed by the adsorption ability and sticking coefficient of the individual species, and were experimentally determined by extraction and analysis of two identical denuders set-up in series; see Table 3. Atmospheric concentrations of all the above gas-phase compounds were determined for each sample collected during the first half of the study, considering the listed denuder efficiencies, with exception of HONO and HNO_3, for which the amounts of nitrite and nitrate found on the second denuder were considered artifact due to heterogeneous reactions involving NO_2, O_3, and water vapor according to *Ferm and Sjodin* [1985]; see *Baumann et al.* [2003] for details. Therefore, HONO and HNO_3 were reported as differences from the amounts found in the extractions of the second from the first denuder. Please refer to Appendix A for more details of the calculations arriving at ambient concentrations, i.e. mixing ratios (ppbv) for the reactive gases and underlying assumptions, esp. for the light organic acids (LOA), acetic, formic and oxalic acids.

3.2.2 Water-Soluble Ionic Species

Correspondingly coated paper filters were placed downstream of the Teflon filters in order to capture volatilization losses (as a result of the altered gas-phase/solid phase equilibrium after removal of gaseous species through the denuders) of the Teflon filters. The chemical analysis followed ion chromatography (IC) using a Dionex DX-500 with EG-40 eluent generator. Details of the calculations arriving at ambient concentrations, i.e. mass per volume ambient air ($\mu g\ m^{-3}$) for the PM species, and underlying assumptions are given in Appendix A.

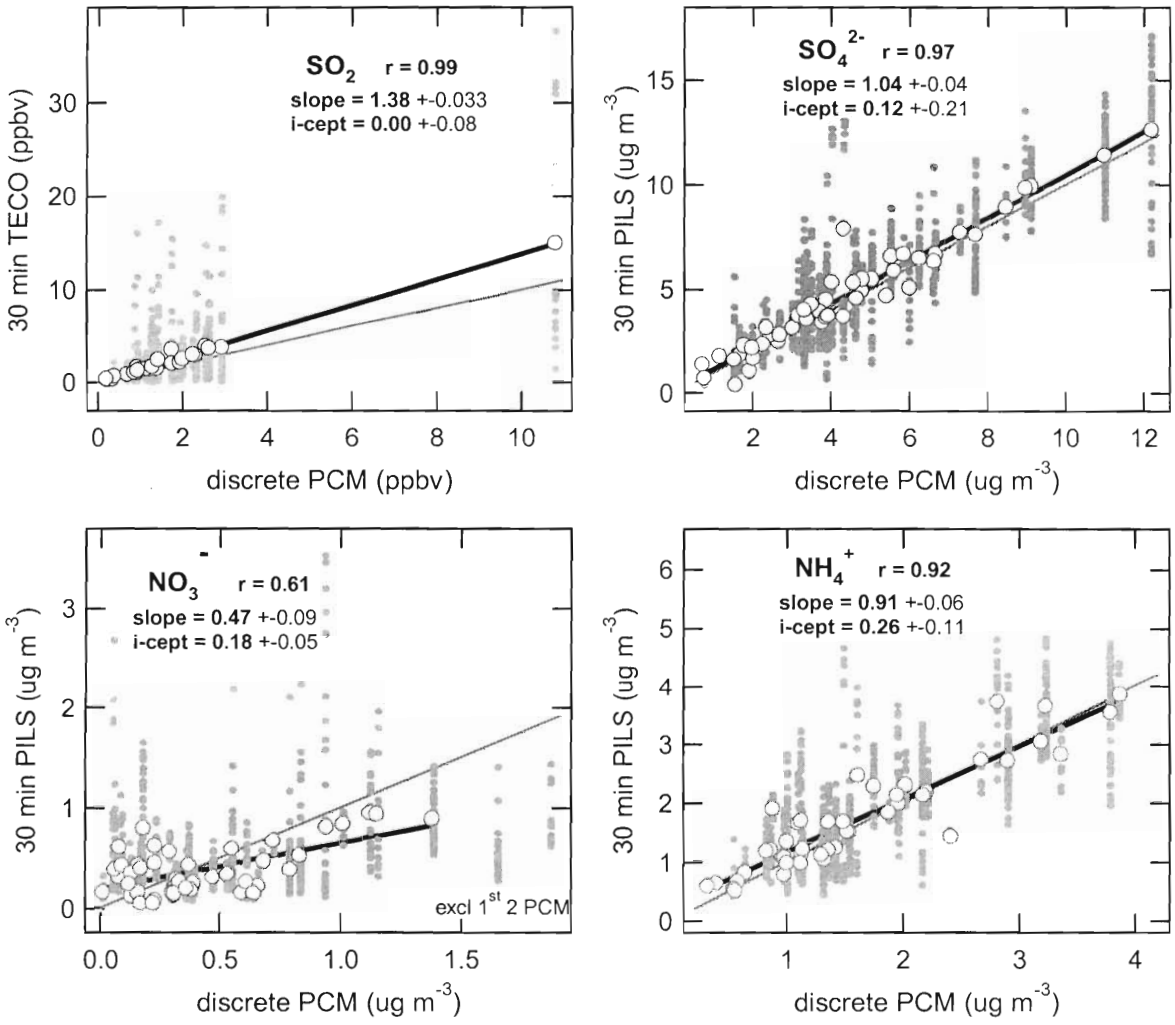

Figure 6: Comparison of main PCM derived compounds with higher resolution Particle-Into-Liquid Sampler (PILS) measurements at the LP site.

The accuracy of the measurement of the major water-soluble fine PM species using the PCM was assessed by comparison with higher time-resolved measurements of the Particle-Into-Liquid Sampler (PILS) conducted simultaneously during the study at the LP site. The correlations depicted in Figure 6 show generally good agreement between sulfate and ammonium, with the PCM values being 4 ±4 % low, and 9 ±6 % high relative to PILS, however, nitrate values were more uncertain, mainly due to their generally much lower ambient ambundance, reaching below the PCM's detection limit.

3.2.3 Elemental and Organic Carbon (EC/OC)

The third channel served the measurement of particulate organic and elemental carbon (OC/EC) by the thermal optical transmittance (TOT) [*Birch and Cary*, 1996]. This channel minimizes positive artifacts to occur on the quartz filter by passing the aerosol sample through a 28.5 cm long 8-annuli XAD coated denuder at 0.8 s residence time. If denuders are used that quantitatively remove these gases that are otherwise susceptible to uptake, the positive artifact is in principle eliminated. However, the imposed change in equilibrium between particle and gas phase species can now cause an increased volatility of semi-volatile species associated with the collected particles thus generating a negative artifact and necessitating a backup adsorber [*Eatough et al.*, 1985]. An XAD coated quartz filter was used as backup adsorber in PCM channel 3 on an experimental basis. Results of tests adressing positive and negative artifacts associated with quartz filter sampling and subsequent EC/OC analysis, are discussed in Zhao et al. [2001]. Since OC represents only pure carbon from the TOT analysis, other organic elements (OOE) bound to carbon in the organic species had to be considered. Assuming an average organics molecular weight to carbon weight ratio of 0.4 [*White and Roberts*, 1977; *Countess et al.*, 1980; *Japar et al.*, 1984], OOE is typically calculated to be 0.4*OC. However, applying a simple mass balance approach, the organic mass to organic carbon ratio (OM/OC) was estimated, indicating that an OOE factor larger than 0.4 was needed to achieve mass closure in most cases, as discussed later.

Table 3: Data Quality Indicators (DQI) for gas-phase and particle-phase species measured using the Particle Composition Monitor (PCM).
D (pa)... phosphorous acid-coated denuder; D (sc)... sodium carbonate-coated denuder; P... Whatman 41 cellulose [paper] filter; Q... Pallflex #2500 QAT-UP Quartz fiber filter, pre-baked at 600°C for 2h; T... Zeflour™ P5PJ047, unringed Teflon membrane, 2μm pore size; XAD... XAD-4, porous macroreticular, non-polar, polystyrene-divinyl-benzene resin ($725 m^2 g^{-1}$).

* from linear regression with cont. SO_2 UV absorption measurements.
** from NIST standards.
*** from linaer regression with TEOM measurements for LP and WT, respectively.
\# from linear regression with PILS measurements at LP [*Baumann, 2002*].

Gas Phase

	Site	NH_3	HNO_3	HONO	SO_2	HCl	HCOOH	CH_3COOH	$(COOH)_2$
Retrieved from		D (pa)	D (sc)	D (sc)			D (sc)	D (sc)	D (sc)
D-eff [%]	LP	91±18	90±22	91±8	87±19	97±6	83±10	81±18	78±17
	WT	92±22	85±23	88±9	91±18	96±17	83±11	89±19	73±21
DL [ppbv]	LP	0.49	0.33	0.03	0.07	0.18	0.08	0.21	0.01
	WT	1.40	0.36	0.04	0.20	0.15	0.11	0.28	0.02
Bias [%]	n/a	10	11		6	14	6	12	20
Accuracy [%]	LP	-27 *							

Particle Phase

	Site	NH_4^+	NO_3^-	SO_4^{-2}	EC	OC	SVOC	M_{tot}
Retrieved from		T+P	T+P	T	Q	Q	XAD-Q	T
DL [$\mu g\ m^{-3}$]	LP	0.23	0.09	0.06	0.42	0.80	0.51	1.1
	WT	0.22	0.10	0.05	0.59	0.93	0.51	1.1
BIAS [%]	LP	12	33	13	7	5	25	12
	WT	13	19	3	7	5	25	12
Accuracy [%]	LP/WT	+9#	+53#	-4#	-9 **	+10 **		-7/+7***

	Site	Na^+	K^+	Ca^{2+}	Cl^-	F^-	$HCOO^-$	CH_3COO^-	$C_2O_4H^-$
Retrieved from		T	T	T	T	T	T+P	Q	Q
DL [$\mu g\ m^{-3}$]	LP	0.15	0.10	0.18	0.07	0.02	0.88	1.71	0.18
	WT	0.10	0.07	0.14	0.07	0.02	0.84	0.84	0.16
BIAS [%]	LP	20	35	17			17	11	25
	WT	22	37	26			17	11	27

3.3 Continuously Measured Meteorological Parameters and Gaseous Tracers

All meteorological and trace gas quantities were continuously aquired at a rate of 1 Hz, reduced to and qa/qc'ed for 1 min averages, and reported as 30 min averages.

3.3.1 Ozone

O_3 was measured using a pressure and temperature compensated commercial UV absorption instrument (model TEI 49-C, TEI, Inc., Franklin, MA), being absolutely calibrated by the known absorption coefficient of O_3 at 254 nm. The linearity and precision of the analyzer at LP was checked on average once every 22 hours. Precision check mixing ratios of 0, 90, 180, 270, and 360 ppbv were provided by a primary standard calibrator with active feedback control (model TEI 49C-PS). The calibrator was supplied with O_3-free (zero) air from a cartridge of activated carbon that effectively removed O_3 from the ambient air. Each precision check resulted in a 5 point linear regression. Assuming normal distribution of the regressions' intercepts, the O_3 analyzer's detection limit was 1.0 ppbv for the 1 min average; whereas the slopes of the linear regressions yielded ±4 % precision. The accuracy is estimated to be the same. The same type analyzer was deployed at WT and was subjected to the primary standard calibration procedure before and after the study yielding a similar level of quality.

3.3.2 Carbon Monoxide

CO was measured by gas filter correlation, nondispersive infrared absorption (model TEI 48C-TL with a hand-selected PbSe detector matched with an optimal preamplifier, and an absorption cell with gold-plated mirrors). The signal output was pressure compensated while the absorption cell temperature was controlled at 44 ±0.1 °C during the entire study. A zero trap of 0.5 % Pd on alumina catalyst bed (type E221 P/D, Degussa Corp.) kept at 180 °C quantitatively oxidized CO to CO_2 at an efficiency greater 99 %, and allowed the switching of zero modes every 11 min for 2 min. NIST traceable calibration gas of 405 ±4 ppmv CO in N_2 (Scott-Marrin Inc., Riverside, CA) was introduced into the sample stream by mass flow controlled standard addition and dynamic dilution at the instrument inlet for 2 min approximately every 11 h. The detection limit for a 1 min average based on the 1 Hz data was 107 ppbv, and 20 ppbv for a 1/2 h average. The instrument's precision, determined from the standard addition span checks, was ±9 % at ~570 ppbv. The accuracy was estimated as the RMS error of uncertainties in the calibration tank concentration (2 %), the mass flow controllers (4 % each MFC), the background variation (4 %), and potential inaccuracies from interpolation of the measured ambient CO during span checks (15 %). Thus, the total uncertainty in the CO measurement is estimated at ±17 % for the entire measuring range. The instrument's linearity within its 5000 ppbv range was determined from all calibrations performed during the study (zero excluded), and revealed an r^2 of 0.98.

3.3.3 Sulfur Dioxide

SO_2 was measured by use of a commercial, pulsed UV fluorescence instrument (model TEI 43C-TL) with pressure and temperature compensated signal output. It's response time was ~45 s and therefore, required longer zeroing and calibration periods compared to the CO instrument: zero for 4 min once every 55 min; calibration - via mass flow controlled standard addition of 30.6 ±0.3 ppmv SO_2 in N_2 NIST traceable calibration gas (Scott-Marrin Inc.) and dynamic dilution at the instrument inlet - was performed for 4 min once every 11 hours. Zero [SO_2-free] air was produced by passing ambient air through a HEPA glass fiber in-line filter (Balston) impregnated with a 0.15 molar Na_2CO_3 solution. At a flow rate of 0.9 slm, the filter removed >99 % of the SO_2 in the sample. Calibrations were performed and evaluated analogous to the CO measurements resulting in a detection limit of 0.2 ppbv for 1/2 h averages, and a precision of ±4 % at 60-130 ppbv. Since the instrument's measurement principle is known to be sensitive to organic hydrocarbons (HC), the efficiency of the internal HC removal through a semi-permeable wall was enhanced by introducing an activated carbon trap into the flow of the low-[HC]-side of the wall, and thereby further increasing the [HC] gradient across the wall. NO is known to be another interferent, and its level of interference was examined by standard addition of NO calibration gas earlier before the study, resulting in a 2-3 % increase of signal. The reported data were not corrected for this relatively small interference. The accuracy was estimated as the RMS error of uncertainties in the calibration tank concentration (2 %), the mass flow controllers (4 % each MFC), the background variation (12 %), the NO interference (2 %), and potential inaccuracies from interpolation of the measured ambient SO_2 during span checks (10 %). Thus, the total uncertainty in the SO_2 measurement is estimated at ±17 % for the entire measuring range. The instrument's linearity within its 200 ppbv range was determined from all calibrations during the study, and revealed an r^2 of 0.99.

3.3.4 Reactive Nitrogen Oxides

Proto-type Air Quality Design (AQD, Golden, Colorado) NO/NO_y and NO/NO_x analyzers were deployed for the measurement of NO, NO_x, and total reactive nitrogen oxides (NO_y) that include NO, NO_2, NO_3, N_2O_5, HONO, HNO_3, aerosol nitrate, PAN and other organic nitrates. The NO_y measurements were based on the principal method of metal-surface induced reduction

of the more highly oxidized species to NO, and its subsequent chemiluminescence detection (CLD) with excess ozone. The metal surface here was a 35 cm long, 0.48 cm ID MoO tube (Rembar Co., Dobbs Ferry, NY), temperature controlled at 350 ±2 °C, and housed inside an inlet box mounted to the met tower ~9 m above ground. The NOx measurements made 4.5 m agl, utilized a Xe/Hg photolysis system with an average NO_2 conversion fraction of 12 ±3 % at 1 s s±ample residence time. The data quality of these and the above trace gas measurements are summarized on the basis of 30 min averages in Table 4. The accuracy of the nitrogen oxides measurements is further assessed below by comparison with measurements made by the NOAA-Aeronomy Laboratory on a 15 m walk-up tower adjacent to our MAQL.

Table 4: Detection limits (DL), precision (P), and accuracy (A) based on 30 min averages of the O_3, CO, SO_2, NO, NO_x, and NO_y measurements performed at the LaPorte (LP) site.

	DL	**P**	**A**
	ppbv	**%**	**%**
O_3	0.2	± 4	± 4
CO	20	± 9	±17
SO_2	0.2	± 4	±17
NO	0.0005	±10	±15
NO_x	0.02	±15	±25
NO_y	0.01	±15	±20

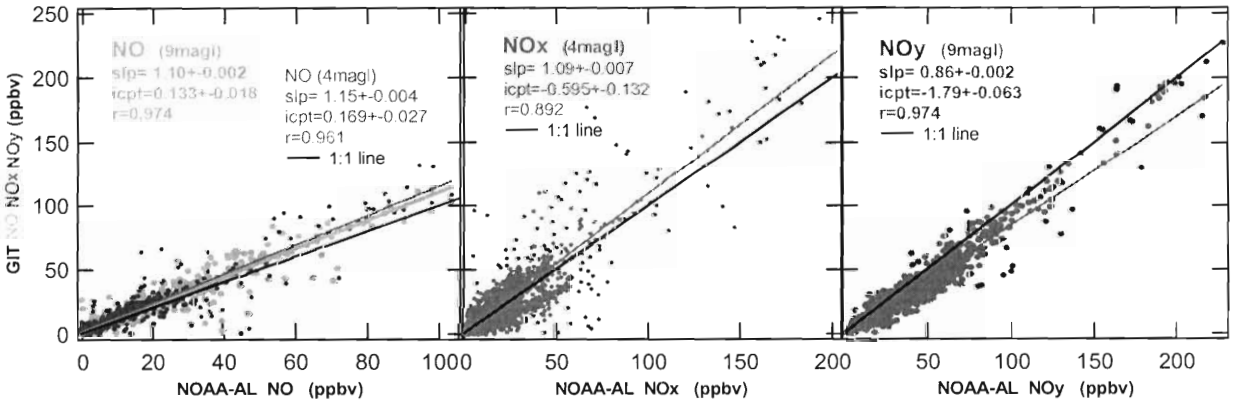

Figure 7: Comparison of our NO (left), NOx (center), and NOy (right) measurements made at different heights agl on the MAQL tower, with the corresponding measurements made by the NOAA AL group (courtesy of Dr. Eric Williams) on a 15 m walk-up tower near-by.

The NO, NOx, and NOy comparison in Figure 7 shows generally good agreement, esp. considering the difference in sample height above ground. It is interesting to note that the NO measured closer to the ground (4m) shows average 5% larger concentration levels than the one higher above (9m), indicating influences from source near the ground, such as very local traffic (vehicle movements of other investigators) but more likely exhalations from the soil of the airport compound. Details of the determination of the data quality indicators for the odd nitrogen oxides measurements are described in Appendix B.

4 RESULTS

4.1 General Overview

LaPorte was influenced predominantly and in particular during the first half of the study period by a strong land-sea breeze circulation with veering wind directions, causing periodic short-term impacts of plumes from nearby sources with significantly reduced (titrated) nighttime ozone levels. The combination of this air flow pattern and the relative vicinity of various emission sources led to vertically confined ozone plumes, which caused the highest ozone readings of the study at LaPorte on August 30 and 31, with maximum hourly averages of 219 and 196 ppbv, respectively, while the elevated site at Williams Tower, only saw ~50% lower ozone maxima, which can be seen in Figures 8a) and b). With exception of this episode, the $PM_{2.5}$ mass and sulfate concentrations generally follow the trends in daily ozone maxima, which points to very rapid ozone production in these plumes as suggested by other investigators. The occasional deviation from this agreement between $[PM_{2.5}]$ and $[O_3]_{max}$ also indicates that ozone is formed much faster than $PM_{2.5}$ under these specific conditions, which stands in contrast to the conditions typically leading to O_3 and $PM_{2.5}$ pollution in the southeastern U.S., where regional stagnation leads to simultaneous buildup of these pollutants as in a 'rising tide'.

While the first half of the study period was characterized by a persistent land-sea-breeze pattern and maximum ozone levels on August 30 and 31, the second half showed a break in this pattern about midway, which was preceeded by maximum fine PM mass concentration on September 6. The last week of the study saw the highest wind speeds and daytime humidity levels, lowest temperatures and generally lowest pollution levels.

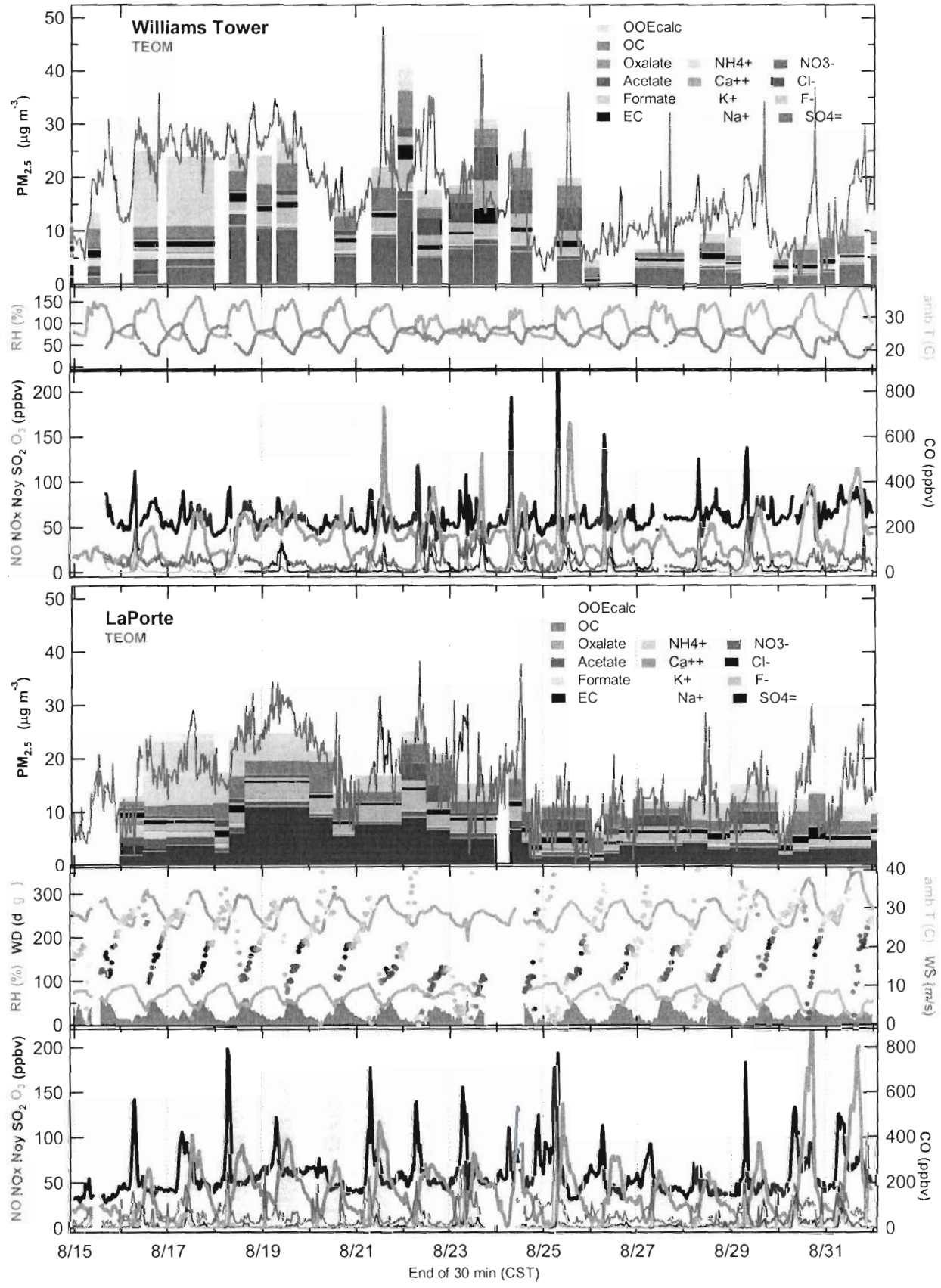
Williams Tower
TEOM
OOEcalc
OC
Oxalate
Acetate
Formate
EC
NH4+
Ca++
K+
Na+
NO3-
Cl-
F-
SO4=
PM2.5 (µg m-3)
RH (%)
amb T (C)
NO NOx Noy SO2 O3 (ppbv)
CO (ppbv)
LaPorte
TEOM
WD (deg)
WS (m/s)
8/15
8/17
8/19
8/21
8/23
8/25
8/27
8/29
8/31
End of 30 min (CST)

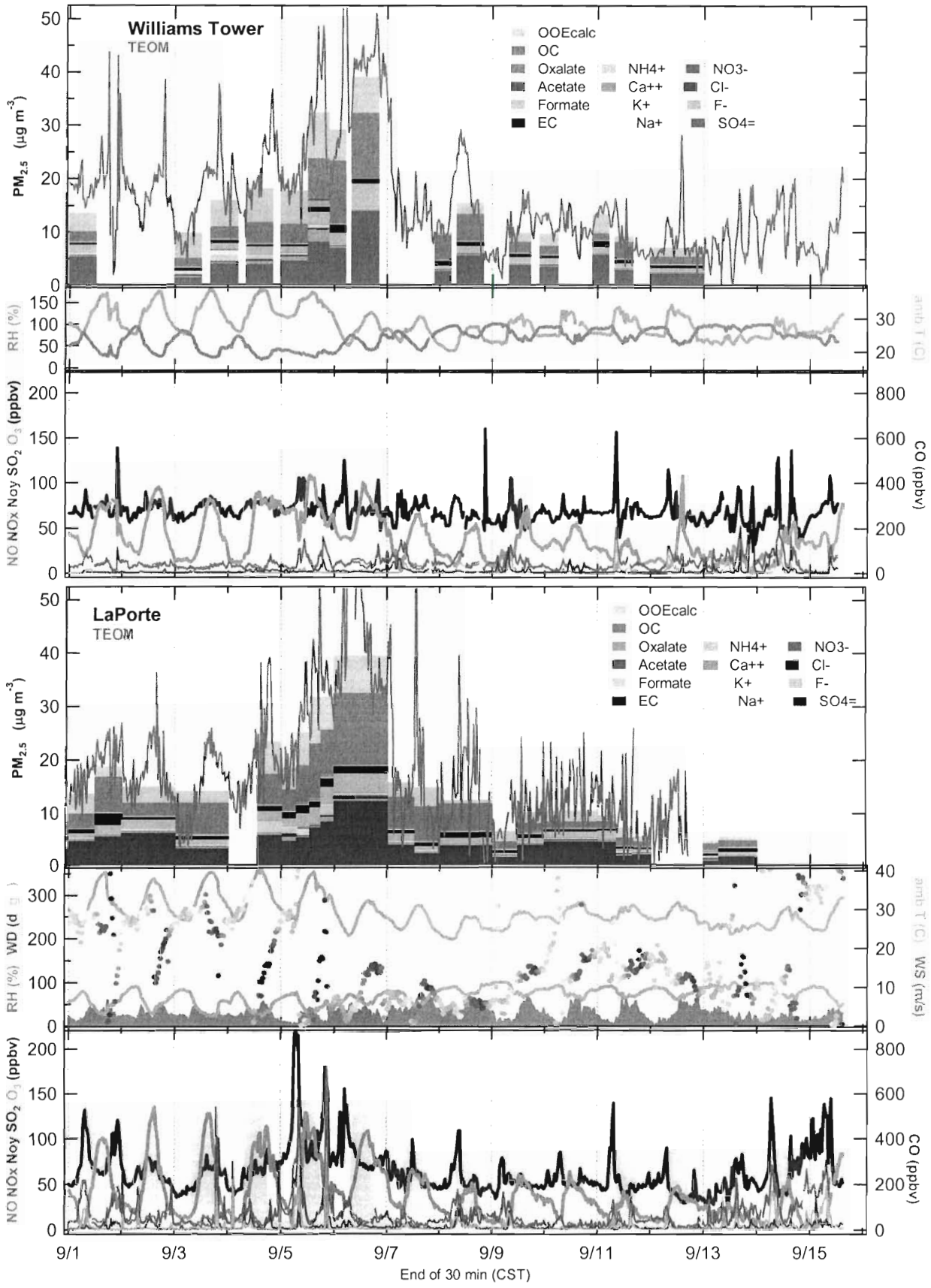
Williams Tower
TEOM
OOEcalc
OC
Oxalate
Acetate
Formate
EC
NH4+
Ca++
K+
Na+
NO3-
Cl-
F-
SO4=
PM2.5 (µg m-3)
RH (%)
amb T (C)
NO NOx Noy SO2 O3 (ppbv)
CO (ppbv)
LaPorte
TEOM
WD (d
WS (m/s)
9/1
9/3
9/5
9/7
9/9
9/11
9/13
9/15
End of 30 min (CST)

Figure 8: $PM_{2.5}$ mass and composition (top), meteorological quantities (center), and trace gas indicator species (bottom) as measured at both the WT and the LP site, during the first two weeks of the study period (a), and the second half (b); the LP wind direction data are color-coded for time of day, i.e. red for early afternoon, light blue and green for late night and early morning. Note, that the trace gases shown for WT were measured by the Batelle National Lab and are courtesy of Drs. Chet Spicer and Carl Berkowitz.

Comparison of the 30 min ozone and fine PM (TEOM) data between LP and WT reveals a systematically higher O3 concentration during middays at LP relative to WT, while nighttime concentrations are significantly higher at WT, pointing to a decoupling of the lower atmosphere and the penetration of more regional background ozone down to the high rise WT site, but not as far down to the ground reaching the LP site. Figure 9 shows the average diurnal gradient from the difference in the 30 min ozone data measured simultaneously at LP and WT. Negative gradients represent higher values closer to the ground, i.e. at LP relative to WT. The PM2.5 seems more homogeneously mixed, although the mean gradient shows the similar trend. Lastly, the ambient temperature difference between LP and WT is minor compared to the near surface gradient measured between 2.8 and 11 m agl at LP, which indicates very strong near-surface nocturnal inversions, and well-mixed convective surface layer during daytime .

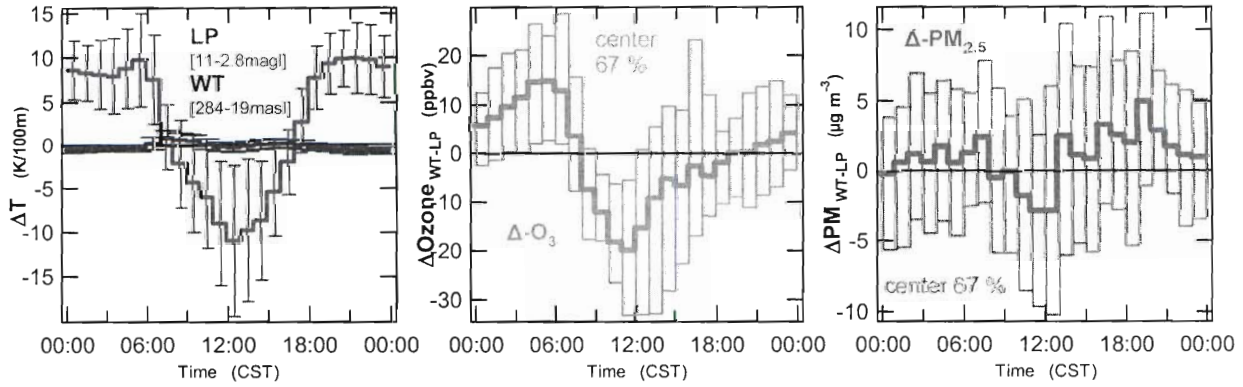

Figure 9: Vertical gradients of temperature (left), ozone (middle), and fine PM (right) from 30 min differences between WT (284 masl) and LP (19 masl) data; the red temperature trace is a true vertical gradient, since it has been measured on the LP tower between 2.8 and 11 magl.

A charge balance based on the sulfate-nitrate-ammonium system indicates slightly acidic conditions with 16 ±17 ne m^{-3} at LaPorte and 25 ±47 ne m^{-3} at Williams Tower, as illustrated in Figure 10. In the context of aerosol acidity, *it is important to note that* [NH_3], the only neutralizing species measured during the first half of the study, averaged 3.2 ±1.5 ppbv at LaPorte, and 2.9 +1.9 ppbv at Williams Tower.

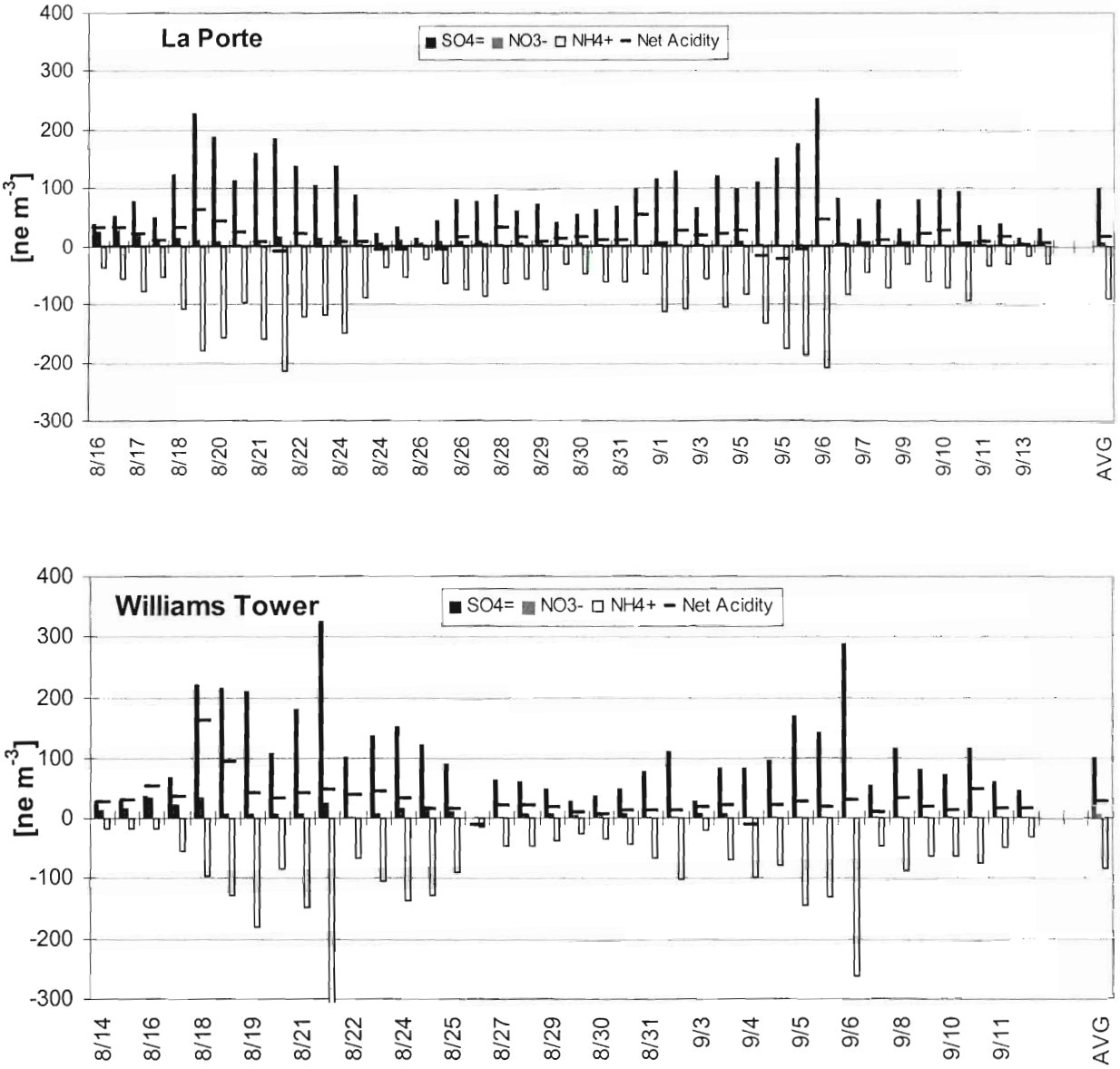

Figure 10: Charge balance within the $SO_4^{=}/NO_3^{-}/NH_4^{+}$ system for PCM samples collected at LP (top) and WT (bottom).

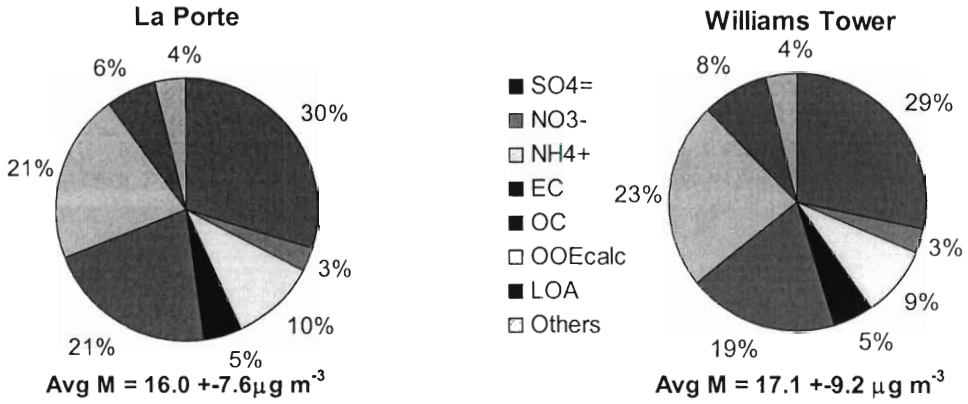

Figure 11: Average mass composition for LP (left) and WT (right); LOA are the combined lightorganic acids acetic, formic and oxalic in their PM phase; Others include Na^+, K^+, Ca^{++}, Cl^-, and F^-. OOEcalc denotes the other organic elements as calculated from mass closure.

Adding the other organic elements (OOEcalc from Fig. 11) to the light organics (LOA) and organic carbon (OC), the sum of all organics in the particle-phase comprises 48 % and 50 % of the total PM2.5 mass measured at LP and WT, respectively. While the average fine PM mass concentration at WT is insignificantly higher (see Fig. 11), the OC/EC ratio is equal at 4.4 at both sites, with slightly higher variability (±3.2 vs 2.4) at the WT site. The OM/OC ratio derived with OOE from mass closure is higher also at WT with 2.6 ±1.5, versus 2.4 ±1.3 at the LP site.

REFERENCES

Baumann, K., Chameides, W.L., Ift, F., and Zhao, J.Z. 2001. Discrete measurements of reactive gases and particle mass and composition during the 1999 Atlanta Supersite Experiment. *J. Geophys. Res. 108*, 8416, doi: 10.1029 /2001 JD001210, 2003.

Baumann K, F Ift, JZ Zhao, MH Bergin, and AG Russell, Measurement of trace gases and $PM_{2.5}$ mass and composition near the ground and at 254 m agl during TexAQS 2000, *Proceedings of the 4th Conference on Atmospheric Chemistry: Urban, Regional, and Global-Scale Impacts of Air Pollutants, Orlando, FL, Amer. Meteor. Soc.*, 242-247, 2002.

Birch, M.E., and R.A. Cary, Elemental carbon-based method for monitoring occupational exposures to particulate diesel exhaust, *Aerosol Science and Technology 25*, 221-241, 1996.

Countess, R.J., G.T. Wolff, and S.H. Cadle, The Denver Winter Aerosol: A Comprehensive Chemical Characterization, *J. Air Pollut. Control Assoc. 30*, 1194-1200, 1980.

Eatough, D.J., V.F. White, L.D. Hanson, N.L. Eatough, and E.C. Ellis, Hydration of nitric acid and its collection in the atmosphere by diffusion denuders, *Anal. Chem. 57*, 743-748, 1985.

Finn, D., B. Rumburg, C. Claiborn, L. Bamesberger, W.F. Siems, J. Koenig, T. Larson, and G. Norris, Sampling Artifacts from the Use of Denuder Tubes with Glycerol Based Coatings in the Measurement of Atmospheric Particulate Matter, *Environ. Sci. Technol. 35*, 40-44, 2001.

Gundel, L.A., V.C. Lee, K.R.R. Mahanama, R.K. Stevens, and J.M. Daisey, Direct determination of the phase distributions of semi-volatile polycyclic aromatic hydrocarbons using annular denuders, *Atmos. Environ. 29*, 1719-1733, 1995.

Japar, S.M., A.C. Szkarlat, R.A. Gorse Jr., E.K. Heyerdahl, R.L. Johnson, J.A. Rau, and J.J. Huntzicker, Comparison of Solvent Extraction and Thermal-Optical Carbon Analysis Methods: Application to Diesel Vehicle Exhaust Aerosol, *Environ. Sci. Technol. 18*, 231-234, 1984.

Possanzini, M. et al., New design of a high-performance denuder for the sampling of atmospheric pollutants, *Atmos. Environ. 17*, 2605-2610, 1983.

White, W.H. and P.T. Roberts, On the Nature and Origins of Visibility-Reducing Aerosols in the Los Angeles Air Basin, *Atmos. Environ. 11*, 803-812, 1977.

Zhao, J.Z., K. Baumann, F. Ift, and W.L. Chameides, Investigating the adsorption artifact during aerosol sampling of semi-volatile organic carbon, *J. Geophys. Res., submitted,* 2001.

Acknowledgements

The authors greatfully acknowledge Prof. J. Lester from the Univ of Houston, Clearlake, for laboratory support. This study was carried out as part of the Southern Oxidants Study (SOS), sponsored by EPA and TNRCC.

APPENDIX A

Measurements of reactive gas species and PM compounds using the Particle Composition Monitor (PCM)

GIT's Particle Composition Monitor (PCM) is equipped with 3 separate mass flow controlled channels for the sampling of airborne $PM_{2.5}$ on discrete time scales between 24 and 6 hours, depending on pollution level. Prior to collection of $PM_{2.5}$ on filter media, important inorganic and organic gas species such as NH_3, SO_2 and HNO_3 , as well as semi-volatile polycyclic aromatic compounds (PAH), pesticides, and halogenated species are effectively removed from the sample stream by means of specially coated diffusion tubes (denuders). The following species are quantitated and reported:

Gaseous: NH_3, HNO_3, HONO, SO_2, HCl, HF, acetic, formic, and oxalic acids.

$PM_{2.5}$: NH_4^+, Na^+, K^+, Ca^{2+}, NO_3^-, acetate, formate, oxalate, SO_4^{2-}, Cl^-, F^-, elemental, organic, and "semi-volatile" organic carbon (EC, OC, svOC).

PCM channel set up

ch 1: flow direction → Dpa-Dpa-T-Ppa → to pump

ch 2: flow direction → Dsc-Dsc-T-Psc → to pump

ch 3: flow direction → Dxad-Q-Qxad → to pump

D... triple-annuli etched quartz glass denuders, 15/24 cm long (0.06/0.1 s res time at 16.7 lpm) Eight annuli D used for xad channel, 28.5 cm long (0.8 s res time at 16.7 lpm)

P... Whatman 41 cellulose [paper] filter

pa... phosphorous acid coating solution: 10%/90% DDW/MeOH by volume, with 1g of PA per 100ml of solution, yielding a 122 mM solution.

Q... Pallflex #2500 QAT-UP Quartz fiber filter, pre-baked at 600°C for 2h.

sc... sodium carbonate coating solution: 15.7g of Na_2CO_3 dissolved with 5 mg glycerol in 400ml DDW, 600 ml methanol added, yielding a 148 mM solution.

T... Zeflour™ P5PJ047, unringed Teflon membrane, 2μm pore size.

xad... XAD-4, porous macroreticular, non-polar, polystyrene-divinyl-benzene resin ($725 m^2 g^{-1}$).

The use of glycerol in the sc coating solution has demonstrated to introduce a mass artifact on the T downstream; we therefore report only channel 1 T-masses. The final gravimetric mass reported includes the semi-volatile contributions from the backup absorbers. Only ammonium, nitrate, and the light organic acids are considered 'semi-volatile'. We assume an effective artifact from heterogeneous NO_2+O_3 reactions on sc denuder walls, therefore subtract nitrite and nitrate found on second from first for HONO and HNO_3, respectively. Nevertheless, a denuder efficiency is calculated and reported for all species, but is taken into account only for the light organic acids; for all other species, it is assumed to be one. We carried one field blank (B) of each medium for each set of ~3 PCM loadings, which serves two purposes, a) the determination of detection limits, and b) the correction of the reported data for systematic artifacts.

Calculation of Gas and $PM_{2.5}$ Concentrations

Field Blanks were carried for each sample medium type (DB/TB/PB) about once a day; averages of all the blanks were applied to each individual sampling period.

GASES

All gases (except for HONO and HNO_3)

$$c_{n,gas} = \frac{\left\{c_{n,ion}(D1) + c_{n,ion}(D2) - 2 * c_{n,ion}(DB)\right\} * M_n}{\Phi_{n,tot}}$$

where

$c_{n,ion}(D1/D2/DB)$: concentration of species n from Denuder 1, 2, Blank, resp.

M_n: mass correction factor = $\frac{M_{gas}}{M_{ion}}$

with $M_{gas/ion}$: molar mass of gaseous/conjugated ionic species, resp.

Note: Denuder efficiencies are only considered for the light organic acids (acetic, formic, and oxalic acids). For all other species, they are assumed to be 1.

HONO and HNO_3

$$c_{HONO/HNO_3} = \{c_{Nitrite/Nitrate}(D1) - c_{Nitrite/Nitrate}(D2)\} * M_{(HONO/Nitrite)/(HNO_3/Nitrate}$$

assuming equal denuder efficiency for NO_2 and 100% denuder efficiency for HONO; subtraction of NO_2^- artifact due to reaction $2\ NO_2 + H_2O \rightarrow HNO_3 + HONO$ (*Ferm and Sjodin*, 1985)

$PM_{2.5}$

Na^+, K^+, Ca^{2+}, Cl^-, F^-, SO_4^{2-} (considered non-volatile)

$$c_{n,ion} = c_{n,ion}(T) - c_{n,ion}(TB)$$

where

$c_{n,ion}(T/TB)$: concentration of species *n* from Teflon filter/blank, resp.

NH_4^+, NO_3^-, Acetate, Formate, Oxalate (considered semi-volatile)

appropriately coated paper backup filter applied

$$c_n = c_{n,ion}(T) + c_{n,ion}(P) - c_{n,ion}(TB) - c_{n,ion}(PB) - \left\{\left(1 - \Phi_{n,tot}\right) * \frac{c_{n,gas}}{M_n}\right\}$$

where

$c_{n,ion}(P/PB)$: concentration of species *n* from paper filter/blank, resp.

Again, efficiencies are only considered for the light organic acids.

Total Mass, M_{tot}

All Teflon sample filters were dehydrated in a desiccator located in a temperature- (21°C) and humidity- (35%) controlled clean room in order to remove humidity artifacts. The samples remained in the desiccator for at least 4 days, in most cases longer.

The final mass was determined gravimetrically from the desiccated channel 1 Teflon filters. Channel 2 Teflon masses are systematically higher, which is suspected to be due to artifacts caused by the glycerol-containing sodium carbonate coating solution used in the channel 2 denuders (*Finn et al.*, 2001).

The semivolatile fractions of NH_4^+, NO_3^-, and the organic acids (from paper filters/blanks and denuder efficiencies) are added to the gravimetric mass determined from the Teflon filter and blank.

Elemental/Organic Carbon/Other Organic Elements (EC/OC/OOE)

Calculated from the quartz filters/blanks in the same fashion as Na^+, Ca^{2+}, etc.

OC concentrations from XAD-Q are not taken into account here.

Since OC represents only pure carbon from TOT analysis, other organic elements (OOE) bound to carbon in the organic species have to be considered. Assuming an average organics molecular weight to carbon weight ratio of 0.4 (*White and Roberts*, 1977; *Countess et al.*, 1980; *Japar et al.*, 1984), OOE is calculated to be 0.4*OC.

APPENDIX B

Determination of data quality indicators for the reactive odd nitrogen measurements

The sample air was drawn continuously through a 15 cm long 0.64 cm OD SS tube, which extended ~5 cm to the outside bottom of the box and was coupled to two SS crosses, where the flow was diverted to a MoO converter tube for the NO_y and a bypass PFA tube of same length for the NO measurement, at 1 slm respectively. All SS components were Teflon coated and temperature controlled at 40 ^{o}C. A stream selector assembly with mass flow controllers (MFC) housed inside the inlet box, which reduced the sample residence time inside the PFA tubing between the inlet box on the tower and the CLD unit inside the mobile lab at the ground to < 0.2 s. NO and NO_y measure modes were switched every 2 minutes. Automated calibrations were performed via a programmed set of NO, NO_2, n-propyl nitrate (NPN), and HNO_3 standard additions to the sample inlet on average 2 times per day in ambient air, and about once per day in zero air. The calibrations allowed the determination of specific parameters that are relevant for the assessment of the overall instrument performance, such as sensitivity, artifacts, detection limits, and conversion efficiencies of the MoO tube.

In summary, the NO detection limit for a 1 min integration time was 3 ±0.5 pptv in ambient air and 2 ±0.1 pptv in zero air at a signal-to-noise ratio of 2, respectively. The instrument's overall sensitivity to ambient NO (S_NO) averaged to 3.57 ±0.6 Hz pptv^{-1} in ambient air and 4.39 ±0.15 Hz pptv^{-1} in zero air. A difference in signal was present when sampling zero air in NO measure mode versus NO zero mode, displaying a NO artifact (A_NO), which was 28 ±4 pptv. A_NO was interpolated between calibrations and subtracted from the ambient NO measurements. Since the zero volume efficiency was less than 100 %, i.e. on average 97 ±3 %, the instrument's zero varied with ambient NO and NO_y levels, respectively. Thus, during low level periods sporadically occurring at night, the NO_zero signal counts typically averaged 1300 Hz ±2 %. The accuracy of the NO measurements had uncertainty due to variations in instrument zeroes, sensitivities, MFC calibrations, and the level of calibration standard used. The MFC calibrations before and after the study were within 2 %. The biggest contributor to the overall uncertainty was the variable level of ambient NO before and after the standard addition and the interpolation necessary for the S_NO determination, which is estimated here at ±13 %.

Therefore, the overall uncertainty of the NO measurement is estimated at ±15 % as RMS error of all the above potential inaccuracies.

Each calibration cycle allowed the determination of the instrument's sensitivity to NO_2, NPN, and HNO_3. The NO_2 sensitivity (S_NO_2) in ambient air averaged 3.72 ±0.44 Hz $pptv^{-1}$ revealing a NO_2 conversion efficiency Q_NO_2 of 94 ±8 %. With each calibration cycle the conversion efficiencies for NPN and HNO_3, species that are typically harder to convert than NO_2, were also determined via standard addition. NPN cal gas was delivered mass flow controlled to the converter inlet from a NIST traceable compressed air tank of 3.88 ±0.19 ppmv NPN in O_2-free N_2 (Scott-Marrin Inc.). HNO_3 was supplied from a permeation tube (Kin-Tek) inside an oven controlled at 40 ±0.1 °C via a critical orifice controlled zero air flow of ~10 sccm. The permeation rate was verified before and after the study via dissolution of HNO_3 using a small scale impinger and subsequent IC analysis of NO_3^-. The conversion efficiencies for both NPN and HNO_3 in ambient air were 87 ±18 % and 80 ±53 %, respectively, suggesting that NO_2 is typically converted the easiest and HNO_3 the hardest. The variability and relative differences in conversion efficiencies of these three NO_y species add uncertainty to the NO_y measurement as considered below. The NO_y zeroes averaged 1450 Hz ±10 %, and an artifact A_NOy was present when sampling zero air. This artifact varied with time and level of converter decay, and was therefore considered in a time-dependent manner; it averaged 0.39 ±0.17 ppbv. Based on measured variations in NO_y over 2 – 3 h periods, the precision of our NO_y measurements ranged between ±10 and ±15 %. In addition to the potential uncertainties that contributed to the NO inaccuracies described above, our estimate for the overall accuracy of the NO_y measurements include the uncertainties in the GPT derived NO_2 calibration gas, and the unequal MoO converter efficiencies for NO_2, NPN, and HNO_3 resulting in an RMS error of ±20 %.

10.2 MEASUREMENT OF TRACE GASES AND $PM_{2.5}$ MASS AND COMPOSITION NEAR THE GROUND AND AT 254 M AGL DURING TEXAQS 2000

Karsten Baumann *, Frank Ift, Jing Zhi Zhao, Mike Bergin, Armistead Russell
Georgia Institute of Technology, Atlanta, Georgia

1. INTRODUCTION

Continuous (1 min) measurements of various meteorological parameters, trace gases (NO, NO_x, NO_y, CO, SO_2, and O_3), and discrete, 6 to 24 h integrated filter-based measurements of $PM_{2.5}$ mass and composition, including aerosol gases (NH_3, HONO, HNO_3, HCl, SO_2, and light organic acids), were made at the LaPorte municipal airport (LP), near the Houston ship channel, during TexAQS2000. These discrete measuremnts were made by means of a three-channel Particle Composition Monitor (PCM) used in previous experiments carried out in the Southeastern U.S. within the framework of the Southern Oxidant Study (SOS), and described in greater detail by Baumann et al. (2001). Similar PCM measurements supplemented by semi-continuous (30 min) O_3 and TEOM mass measurements were made on the 62nd floor of the Williams Tower (WT), 254 m agl, and ~12 km west of downtown Houston. The quality of the measurements is briefly assessed here, and the results are compared and investigated for systematic differences induced by the difference in sampling height above ground.

2. METHODS

The measurement principle of our PCM is based on successive separation of particles larger than 2.5 microns aerodynamic diameter, followed by the separation of gaseous species from the particles prior to $PM_{2.5}$ collection on Teflon membrane and quartz fiber filters backed by specifically impregnated filters as

---

* *Corresponding author address:* Karsten Baumann, Georgia Tech, School of Earth and Atmospheric Sciences, Atlanta, GA 30332-0340;
e-mail: kb@eas.gatech.edu

backup adsorbers. The sampler operates three channels each controlled at a nominal flow rate of 16.7 lpm. $PM_{2.5}$ separation is achieved by standard, Teflon coated cyclone heads, after the sample air is pulled through 30 cm long, 14 mm ID, Teflon coated inlet tubes. Separation of the gases is achieved by means of appropriately coated denuders. During TexAQS2000 a phosphorous acid coating solution was used in channel 1, which selectively removed NH_3, while a sodium carbonate solution was used in channel 2 capturing the acidic gases HNO_3, HONO, SO_2, HCl, acetic, formic, and oxalic acids. Denuders were 3-annuli edged glass tubes that have a theoretical removal efficiency, based on molecular diffusion assuming 100% adsorption of 99.9% for NH_3, and 99.7% for HNO_3 at 0.1s residence time (Possanzini et al., 1983). The effective denuder efficiencies are actually governed by the adsorption ability and sticking coefficient of the individual species, and were experimentally determined by extraction and analysis of two identical denuders set-up in series; see Table 1. Atmospheric concentrations of all the above gas-phase compounds were determined for each sample collected during the first half of the study, considering the listed denuder efficiencies, with exception of HONO and HNO_3, for which the amounts of nitrite and nitrate found on the second denuder were considered artifact due to heterogeneous reactions involving NO_2, O_3, and water vapor according to Ferm and Sjodin (1985); see Baumann et al. (2001) for details. Therefore, HONO and HNO_3 were reported as differences from the amounts found in the extractions of the second from the first

denuder. Correspondingly coated paper filters were placed downstream of the Teflon filters in order to capture volatilization losses

Table 1a: PCM data quality indicators for gaseous species, as retrieved from phosphorous acid and sodium carbonate coated denuders (D(pa) and D(sc), resp): denuder efficiencies (D-eff), detection limits (DL) from blank analysis, bias (precision estimate based on side-by-side runs). SO_2 accuracy has been determined from linear regression with continuous SO_2 UV fluorescence measurements.

	Site	NH_3	HNO_3	HONO	SO_2	HCl	HCOOH	CH_3COOH	$(COOH)_2$
Medium		D(pa)	D(sc)	D(sc)	D(sc)	D(sc)	D(sc)	D(sc)	D(sc)
D-eff [%]	LP	91±18	90±22	91±8	87±19	97±6	83±10	81±18	78±17
	WT	92±22	85±23	88±9	91±18	96±17	83±11	89±19	73±21
DL [ppbv]	LP	0.49	0.33	0.03	0.07	0.18	0.08	0.21	0.01
	WT	1.40	0.36	0.04	0.20	0.15	0.11	0.28	0.02
Bias [%]	n/a	10	11		6	14	6	12	20
Accuracy [%]	LP				-27				

Table 1b: Same as Table 1a for particulate species. EC/OC accuracy has been determined from NIST standards, total mass (M_{tot}) accuracy from linear regression with TEOM measurements.

	Site	NH_4^+	NO_3^-	SO_4^{-2}	EC	OC	SVOC	M_{tot}
Medium		T+P	T+P	T	Q	Q	XAD-Q	T
DL [ug m^{-3}]	LP	0.23	0.09	0.06	0.42	0.80	0.51	1.1
	WT	0.22	0.10	0.05	0.59	0.93	0.51	1.1
BIAS [%]	LP	12	33	13	7	5	25	12
	WT	13	19	3	7	5	25	12
Accuracy [%]	n/a				-9	+10		+5/+11

	Site	Na^+	K^+	Ca^{2+}	Cl^-	F^-	$HCOO^-$	CH_3COO^-	$C_2O_4H^-$
Medium		T	T	T	T	T	T+P	Q	Q
DL [ug m^{-3}]	LP	0.15	0.10	0.18	0.07	0.02	0.88	1.71	0.18
	WT	0.10	0.07	0.14	0.07	0.02	0.84	0.84	0.16
BIAS [%]	LP	20	35	17			17	11	25
	WT	22	37	26			17	11	27

(as a result of the altered gas-phase/solid phase equilibrium after removal of gaseous species through the denuders) of the Teflon filters. The chemical analysis followed ion chromatography (IC) using a Dionex DX-500 with EG-40 eluent generator.

The third channel served the measurement of particulate organic and elemental carbon (OC/EC) by the thermal optical transmittance (TOT) (Birch and Cary, 1996). This channel minimizes positive artifacts to occur on the quartz filter by passing the aerosol sample through a 28.5 cm long 8-annuli XAD coated denuder at 0.8 s residence time. If denuders are used that quantitatively remove these gases that are otherwise susceptible to uptake, the positive artifact is in principle eliminated. However, the imposed change in equilibrium between particle and gas phase species can now cause an increased volatility of semi-volatile species associated with the collected particles thus generating a negative artifact and necessitating a backup adsorber (Eatough et al., 1985). An XAD coated quartz filter was used as backup adsorber in PCM channel 3 on an experimental basis. Results of tests adressing positive and negative artifacts associated with quartz filter sampling and subsequent EC/OC analysis, are discussed in Zhao et al. (2001). Since OC represents only pure carbon from the TOT analysis, other organic elements (OOE) bound to carbon in the organic species had to be considered. Assuming an average organics molecular weight to carbon weight ratio of 0.4 (White and Roberts, 1977; Countess et al., 1980; Japar et al., 1984], OOE is calculated to be 0.4*OC.

O_3 was measured using a pressure and temperature compensated commercial UV absorption instrument (model TEI 49-C, TEI, Inc., Franklin, MA), being absolutely calibrated by the known absorption coefficient of O_3 at 254 nm. The linearity and precision of the analyzer at LP was checked on average once every 22 hours by comparison with a primary standard. The O_3 analyzer's detection limit was 1.0 ppbv; and the precision determined from the linear regressions was ±4%. The accuracy is estimated to be the same. The same type analyzer was deployed at WT and was subjected to the primary standard calibration procedure before and after the study yielding similar quality.

CO was measured by gas filter correlation, nondispersive infrared absorption (model TEI 48C-TL with a hand-selected PbSe detector matched with an optimal preamplifier, and an absorption cell with gold-plated mirrors). The absorption cell temperature was controlled at 44 ±0.1 °C during the entire study. A catalytic zero trap kept at 180 °C quantitatively oxidized CO to CO_2 at an efficiency greater 99 %, and allowed the switching of zero modes every 11 min for 2 min. NIST traceable calibration gas of 405 ±4 ppmv CO in N_2 (Scott-Marrin Inc., Riverside, CA) was introduced into the sample stream by mass flow controlled standard addition and dynamic dilution at the instrument inlet for 2 min approximately every 11 h. The detection limit for a 1 min average based on the 1 Hz data was ~107 ppbv, and ~23 ppbv for a 1 h average. The instrument's precision, determined from the standard addition span checks, was ±9 % at ~570 ppbv. The accuracy was estimated at ±17 % for the entire measuring range based on the RMS error of uncertainties in the individual system components. The instrument's linearity within its 5000 ppbv range was determined from all calibrations performed during the study (zero excluded), and revealed an r^2 of 0.98.

SO_2 was measured by use of a commercial, pulsed UV fluorescence instrument (model TEI 43C-TL) with pressure and temperature compensated signal output. Its response time was ~45 s and therefore, required longer zeroing and calibration periods compared to the CO instrument: zero for 4 min once every 55 min; calibration - via mass flow controlled standard addition of 30.6 ±0.3 ppmv SO_2 in N_2 NIST traceable calibration gas (Scott-Marrin Inc.) and dynamic dilution at the instrument inlet - was performed for 4 min once every 11 hours. Zero [SO_2-free] air was produced by passing ambient air through a HEPA glass fiber in-line filter (Balston) impregnated with a 0.15 molar Na_2CO_3 solution. At a flow rate of 0.9 slm, the filter removed >99 % of the SO_2 in the sample. Calibrations were performed and evaluated analogous to the CO measurements resulting in a detection limit of 4.3 ppbv for 1 min, and 0.08 ppbv for 1 h averages, and a precision of ±4 % at 60-130 ppbv. Since the instrument's measurement principle is known to be sensitive to organic hydrocarbons (HC), the efficiency of the internal HC removal through a semi-permeable wall was enhanced by introducing an activated carbon trap into the flow of the low-[HC]-side of the wall, and thereby further increasing the [HC] gradient across the wall. NO is known to be another interferent, and its level of interference was examined by standard addition of NO calibration gas earlier before the study, resulting in a 2-3 % increase of signal. The reported data were not corrected for this relatively small interference. The accuracy was estimated as the RMS error of uncertainties in the individual system components, yielding ±17 % for the entire measuring range. The instrument's linearity within its 200 ppbv range was determined from all calibrations during the study, and revealed an r^2 of 0.99.

Proto-type Air Quality Design (AQD, Golden, Colorado) NO/NO_y and NO/NO_x analyzers were deployed for the measurement of NO, NO_x, and total reactive nitrogen oxides (NO_y) that include NO, NO_2, NO_3, N_2O_5, HONO, HNO_3, aerosol nitrate, PAN and other organic nitrates. The NO_y measurements were based on the principal method of metal-surface induced reduction of the more highly oxidized species to NO, and its subsequent chemiluminescence detection (CLD) with excess ozone. The metal surface here was a 35 cm

long, 0.48 cm ID MoO tube (Rembar Co., Dobbs Ferry, NY), temperature controlled at 350 ±2 °C, and housed inside an inlet box mounted to the met tower ~9 m above ground. The NOx measurements made 4.5 m agl, utilized a Xe/Hg photolysis system with an average NO_2 conversion fraction of 12 ±3 % at 1 s sample residence time. The data quality of these measurements are summarized on the basis of 1 min averages in Table 2.

Table 2: Detection limits (DL), precision (P), and accuracy (A) of the NO, NO_x, and NO_y measurements.

	DL (ppbv)	P (%)	A (%)
NO	0.003	10	15
NO_x	0.5	15	25
NO_y	0.4	15	20

3. RESULTS

At both the LaPorte and the Williams Tower site, semi-continuous $PM_{2.5}$ mass measurements were made using a Tapered Element Oscillating Microbalance
(TEOM) in addition to and much higher resolved than the discrete filter measurements. The TEOM mass concentrations were systematically low relative to the gravimetric filter mass by 5 amd 11 %, respectively, which is attributed to the active humidity control employed with both TEOM. All Teflon sample filters were dehydrated in a desiccator located in a temperature- (21°C) and humidity- (40%) controlled clean room in order to remove humidity artifacts. The samples remained in the desiccator for at least 4 days, in most cases longer. The final mass was determined gravimetrically from the desiccated channel 1 Teflon filters. Channel 2 Teflon masses were systematically higher by 15 ±13 % (corresponding 3.2 ±4 μg m^{-3}) at LaPorte, *and by 17 ±16 %* (*4.4 ±6* μg m^{-3}) at Williams Tower, which is suspected to be due to artifacts caused by the glycerol-containing sodium carbonate coating solution used in the channel 2 denuders (Finn et al., 2001). The semi-volatile fractions of NH_4^+, NO_3^-, and the organic acids (from paper backup filters, considering corresponding blank levels and denuder efficiencies) are added to the gravimetric mass determined from the Teflon filters.

LaPorte was influenced predominantly by a strong land-sea breeze circulation with veering wind directions, causing periodic short-term impacts of plumes from nearby sources with significantly reduced (titrated) nighttime ozone levels. The combination of this air flow pattern and the relative vicinity of various emission sources led to vertically confined ozone plumes, which caused the highest ozone readings of the study at LaPorte on August 30 and 31, with maximum hourly averages of 219 and 196 ppbv, respectively, while the elevated site at Williams Tower, only saw ~50% lower ozone maxima, which can be seen in Figure 1. With exception of this episode, the $PM_{2.5}$ mass and sulfate concentrations generally followed the trends in daily ozone maxima, which points to very rapid ozone production in these plumes as suggested by other investigators. The occasional deviation from this agreement between $[PM_{2.5}]$ and $[O_3]_{max}$ also indicates that ozone is formed much faster than $PM_{2.5}$ under these specific conditions, which stands in contrast to the conditions typically leading to O_3 and $PM_{2.5}$ pollution in the southeastern U.S., where regional stagnation leads to simultaneous buildup of these pollutants as in a 'rising tide'.

A charge balance based on the sulfate-nitrate-ammonium system indicates slightly acidic conditionswith 16 ±17 ne m^{-3} at LaPorte and 25 ±47 ne m^{-3} at Williams Tower, as illustrated in Figure 2. In the context of aerosol acidity, it is important to note that [NH_3], the only neutralizing species measured during the first half of the study, averaged 3.2 ±1.5 ppbv at LaPorte, and 2.9 +1.9 ppbv at Williams Tower. Figure 2 compares the $PM_{2.5}$ mass and charge balances from LaPorte and Williams Tower with previous measurements made in the Southeastern U.S. within the framework of SOS, at sub-urban and rural sites in TN, and at metropolitan Atlanta, GA, during the Atlanta Supersite Experiment in August 1999.

4. REFERENCES

Baumann K., F. Ift, J.Z. Zhao, and W.L. Chameides, under review: Discrete measurements of reactive gases and fine particle mass and composition during the 1999 Atlanta Supersite Experiment. *J. Geophys. Res.*

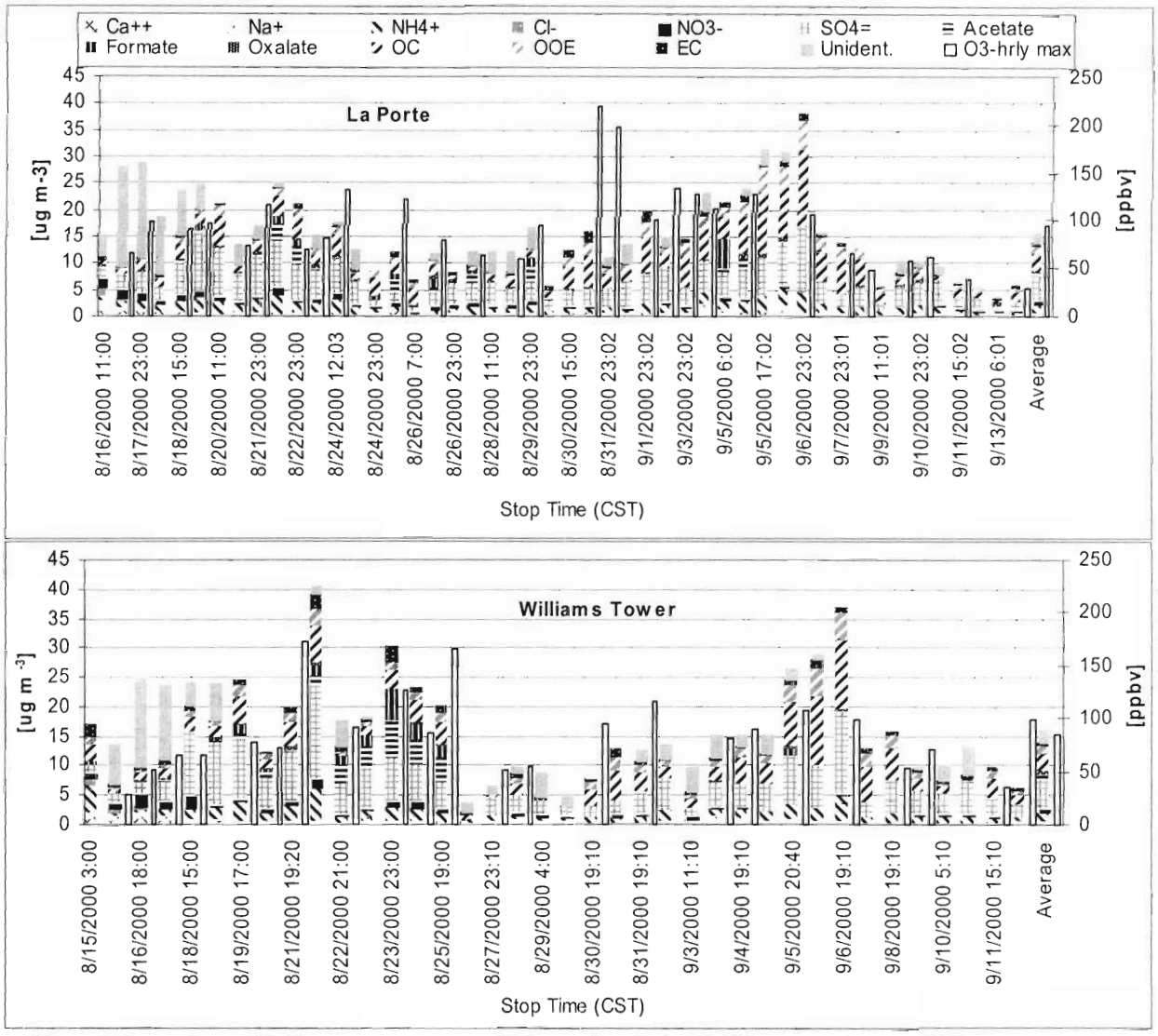

Figure 1 top and bottom: $PM_{2.5}$ mass balance and max. hourly O_3 concentrations for sample periods ranging from 6 to 24 hours in La Porte (top) and at Williams Tower (bottom).

Birch, M.E., and R.A. Cary, 1996: Elemental carbon-based method for monitoring occupational exposures to particulate diesel exhaust. *Aerosol Science and Technology*, **25**, 221-241.

Countess, R.J., G.T. Wolff, and S.H. Cadle, 1980: The Denver Winter Aerosol: A Comprehensive Chemical Characterization. *J. Air Pollut. Control Assoc.*, **30**, 1194-1200.

Eatough, D.J., V.F. White, L.D. Hanson, N.L. Eatough, and E.C. Ellis, 1985: Hydration of nitric acid and its collection in the atmosphere by diffusion denuders. *Anal. Chem.*, **57**, 743-748.

Finn, D., B. Rumburg, C. Claiborn, L. Bamesberger, W.F. Siems, J. Koenig, T. Larson, and G. Norris, 2001: Sampling Artifacts from the Use of Denuder Tubes with Glycerol Based Coatings in the Measurement of Atmospheric Particulate Matter. *Environ. Sci. Technol.*, **35**, 40-44.

Japar, S.M., A.C. Szkarlat, R.A. Gorse Jr., E.K. Heyerdahl, R.L. Johnson, J.A. Rau, and J.J. Huntzicker, 1984: Comparison of Solvent Extraction and Thermal-Optical Carbon Analysis Methods: Application to Diesel Vehicle Exhaust Aerosol. *Environ. Sci. Technol.*, **18**, 231-234.

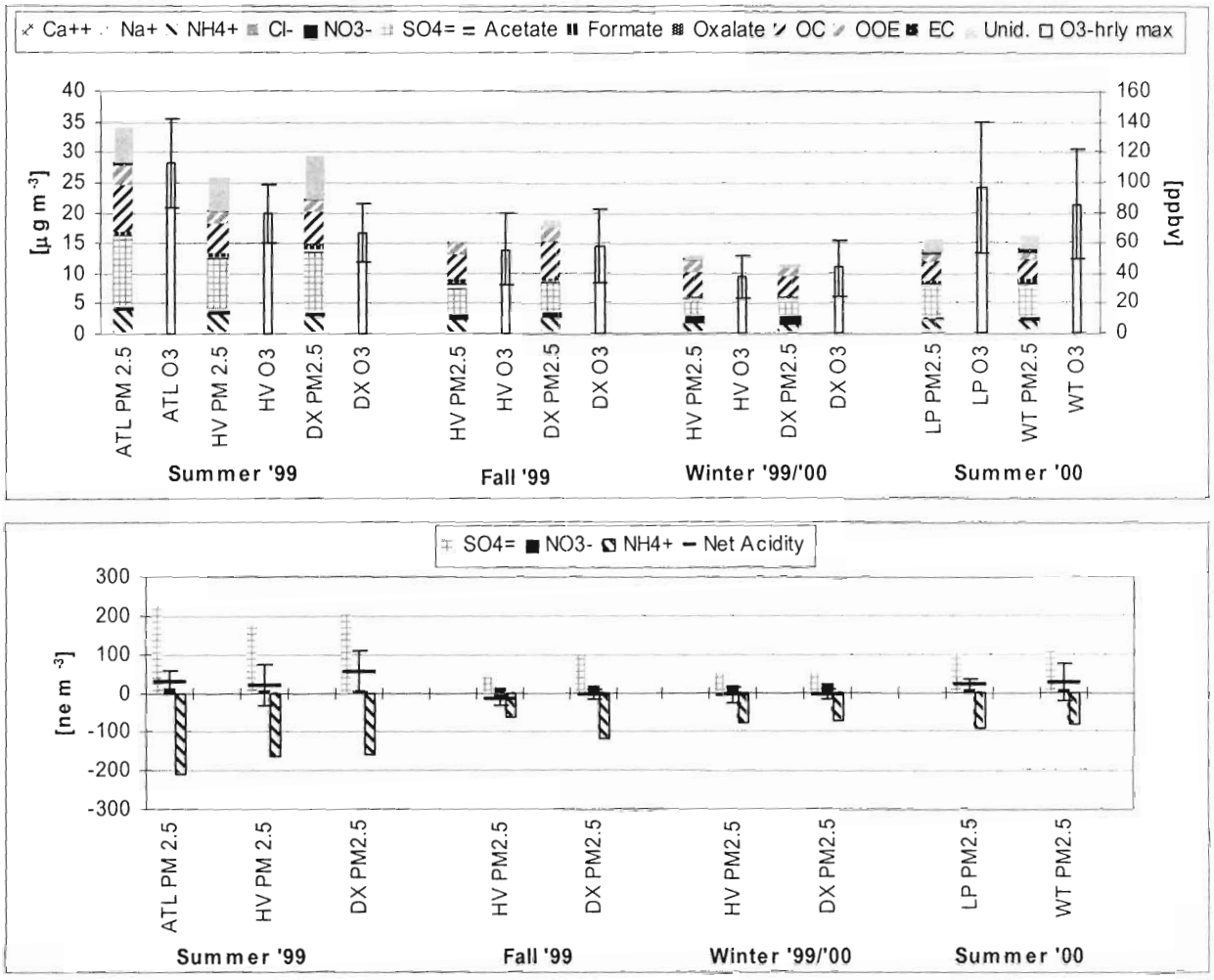

Figure 2 top and bottom: Seasonal averages of $PM_{2.5}$ and O_3 concentrations (top) and charge balance (bottom) for Atlanta, GA (ATL), Dickson, TN (DX), Hendersonville, TN (HV), La Porte (LP), and Williams Tower (WT).

Possanzini, M. et al., 1983: New design of a high-performance denuder for the sampling of atmospheric pollutants. *Atmos. Environ.*, **17**, 2605-2610.

White, W.H. and P.T. Roberts, 1977: On the Nature and Origins of Visibility-Reducing Aerosols in the Los Angeles Air Basin. *Atmos. Environ.*, **11**, 803-812.

5. ACKNOWLEDGEMENTS

The authors gratefully acknowledge Prof. J. Lester from the University of Houston, Clearlake, for laboratory support. This study was carried out as part of the Southern Oxidants Study (SOS), sponsored by EPA and TNRCC.

E-20-H75
Docs. 5 + 13
2/3

Characteristics of Ozone and PM 2.5 in the Southeastern United States

(August 12 ~ September 15, 2000)

Sun-kyoung(Helena) Park and Armistead G. Russell

Goeriga Institute of Technology, Atlanta GA

TABLES OF CONTENTS

LIST OF FIGURES

LIST OF TABLES

1. INTRODUCTION

A Clean Air Act requires EPA to set National Ambient Air Quality Standards for pollutants considered harmful to public health and the environment. Those pollutants are Carbon Monoxide (CO), Nitrogen Dioxide (NO2), Ozone (O3), Lead (Pb), Particulate Matter with size less than 10 mm (PM 10), Particulate Matter with size less than 2.5 mm (PM 2.5) and Sulfur Dioxide (SO2). Among the above pollutants, especially, ozone and PM 2.5 had been increasingly studied due to the epidemiological importance of those species. Ozone inhaled by human can inflame and damage cells that line lungs. PM 2.5 can also damage respiratory tissues because these particles are so tiny that they can be drawn into lungs. The adverse health effects of those pollutants initiated the regional studies of the ozone and the PM 2.5 levels. Studies showed that Houston and Atlanta areas were non-attainment areas for the ozone and the PM 2.5, where the pollutant levels are higher than the National Ambient Air Quality Standard (NAAQS). Thus, we analyzed ozone and the PM 2.5 levels in those two cities in detail.

We analyzed ozone and PM 2.5 total mass and species over the Southeastern United States focusing on Atlanta and Houston from August 12, 2000 to September 15, 2000. Figure 1 shows locations of measurement sites. Stations marked with blue circles in Figure 1 are built for the Assessment of Spatial Aerosol Composition in Atlanta (ASACA) project in the Department of the Environmental Engineering at Georgia Tech, those in green are stations for the Interagency Monitoring of Protected Visual Environments (IMPROVE) program, those in purple are stations of Dr. Karsten Baumann

in the Department of the Earth and Atmospheric Sciences at Georgia Tech, and red circled stations are for the South Eastern Aerosol Research and Characterization (SEARCH) study.

Each station was maintained by different projects; hence each station measured pollutants in different interval. The La Porte (LP) and Williams Tower (WT) stations measured 30-minute average ozone, PM 2.5 total mass and PM 2.5 species concentrations. The North Birmingham (BHM), Centreville (CTR), Gulfport (GFP), Jefferson Street (JST), Oak Grove (OAK), Pensacola (OLE), Pensacola (PNS), and Yorkville (YRK) stations monitored 1-hour average ozone, 24-hour average PM 2.5 total mass, and PM 2.5 species concentrations. The Fort McPherson (FTM), South Dekalb (SDK), and Tucker (TUC) stations measured 24-hour average PM 2.5 total mass and species concentrations. The Breton (BRET1), Chassahowitzka National Wildlife (CHAS1), Cohutta (COHU1), Everglades National Park (EVER1), Okefenokee National Wildlife Refuge (OKEF1), St. Marks (SAMA1), and Sipsy Wilderness (SIPS1) stations also measured 24-hour average PM 2.5 total mass and species concentrations, but those stations did not measure ammonium, one of the major PM 2.5 species.

2. CHARACTERISTICS OF OZONE

An important part of this project was to examine the characteristics of ozone, which we analyzed by comparing the ozone concentrations measured in each station. Ozone is regulated by the National Ambient Air Quality Standard (NAAQS). The standard regulated 1-hour and 8-hour average ozone concentrations as 120 ppbv and 80 ppbv, respectively. According to a Table 2, the measured ozone concentrations in every station exceeded 8-hour standard at least twice during the measured period, and seven out of ten stations exceeded 1-hour standard at least 3 times throughout the period.

Measured ozone concentrations in each station were compared in a Figure 2. Average ozone concentrations from August 12 to September 15, 2000 were between 33 ppbv (JST station) ~ 51 ppbv (YRK station). The average concentrations were relatively high in CTR, OAK, OLE and YRK stations, and relatively low in LP, WT, BHM and JST stations. In general, stations of high ozone concentrations were located in rural areas, whereas those of low ozone concentrations were in urban area. This result can be explained as follows: An ozone concentration increases or decreases as a Volatile Organic Compound (VOC) and a Nitrogen Oxide (NO_x) concentrations change. When a ratio of the VOC to the NO_x concentrations is smaller than a threshold value (5.5:1), as the NO_x concentration increases, the ozone concentration decreases. Thus, low ozone concentrations in JST and BHM stations suggest a high NO_x emission in those areas during the period.

Ozone concentrations were highly correlated between each station. Correlation coefficients of 1-hour average ozone concentrations are in a Table 3.1. High correlation coefficients of 1-hour average concentrations are mainly due to consistent diurnal variations represented in a Figure 3. In general, ozone concentrations were high between noon to 3:00pm, and they were low early in the morning (between 5:00am to 8:00am). A Table 3.2 represents correlation coefficients of 24-hour average ozone concentrations. 24-hour ozone concentrations were also highly correlated each other. Figures 4 and 5 illustrate 30-minute average ozone concentrations in LP and WT stations. Figures 6, 7, 8, 9, 10, 11, 12, and 13 illustrate 1-hour average ozone concentrations in BHM, CTR, GFP, JST, OAK, OLE, and PNS stations, respectively.

3. CHARACTERISTICS OF PM2.5 TOTAL MASS AND SPECIES

One of the most important pollutants is PM 2.5 because of its health impact. PM 2.5 is regulated by the National Ambient Air Quality Standard (NAAQS). The standard regulated daily and annual average concentrations as 65 $\mu g/m^3$ and 15 $\mu g/m^3$, respectively. According to Figure 14, average concentrations from August 12 through September 15, 2000 were relatively high in urban area such as BHM, JST and TU stations. A maximum 24-hour average PM 2.5 concentration was highest in BHM station as 50.4 $\mu g/m^3$. Therefore, during the above period, 24-hour average PM 2.5 concentrations in all stations met the standard. Figure 15 exhibits the regional comparison of PM 2.5 mass and species concentration averages.

We also calculated a correlation coefficient of PM 2.5 between each station. PM 2.5 concentrations were highly correlated between geographically closely located stations. Correlations between LP and WT stations was as high as 0.91 (Table 4). Correlation coefficients of PM 2.5 between BHM, CTR, GFP and JST stations, and OAK, OLE and PNS stations were also high. Correlation coefficient of PM 2.5 between CHAS1 and EVER1 stations were high even though these stations are not close each other. However both stations are located in Florida coast. BRET1, COHU1 and SAMA1 stations did not have enough PM 2.5 data available during the analysis period. Therefore, we did not calculate statistics of PM 2.5 concentrations for these stations. Figures 16 and 17 illustrate 30-minute PM 2.5 concentration averages in LP and WT stations. Figures 18~34 depict 24-hour PM 2.5 concentration averages in the other stations.

PM 2.5 contains five major species: sulfate, ammonium, nitrate, organic carbon and elemental carbon. We will analyze each of those species.

Average sulfate concentrations in a Figure 35 were between 1.8 $\mu g/m^3$ (EVER1 station) to 7.5 $\mu g/m^3$ (PNS station). Sulfate concentrations were relatively high in urban area such as BHM, CTR, JST, PNS and FT stations. A maximum 24-hour average sulfate concentration was observed in Fort McPherson station (16.1 $\mu g/m^3$) on August 16, 2000. Mass percentage of sulfate is plotted in a Figure 36. Sulfate occupied 23 % (TUC station) to 44 % (PNS station) of total PM 2.5 mass. Sulfate concentrations were also higly correlated between closely located stations such as LP and WT stations, CTR, GFP, JST, OAK, OLE and PNS stations, and FTM, JST, SDK, TUC and YRK stations. In a Table 5 also represents correlation coefficients between SIPS1 station and BHM, CTR, GFP, OAK, OLE, PNS and YRK stations were specified as one. However, these high correlation coefficients do not necessarily mean that sulfate concentrations in SIPSI1 station are highly correlated with those of other stations rather these results are because only two or three data points were available for calculating these correlation coefficients. Figures 37 ~ 38 illustrate 30-minute average sulfate concentrations in LP and WT stations. Figures 39 ~ 56 are 24-hour average sulfate concentrations in the other stations.

Ammonium concentrations were analyzed. Average ammonium concentrations in a Figure 57 were lowest in SDK station as 1.5 $\mu g/m^3$ and highest in BHM station as 3.4 $\mu g/m^3$. Figure 58 depicts mass percentage of ammonium in PM 2.5 total mass. Like the case of sulfate, the highest mass percentage of nitrate was observed in PNS station (13.7

%) and the lowest mass percentage was observed TUC station (7.3 %). A Table 6 showed that ammonium concentrations were highly correlated between LP and WT stations, BHM, CTR, GFP, OAK, OLE and PNS stations, and FTM, JST, SDK, TUC and YRK stations. Figures 59 ~ 60 show 30-minute average ammonium concentrations in LP and WT stations, and Figures 61 ~ 71 represent 24-hour average ammonium concentrations in the other stations.

Average nitrate concentrations were between 0.2 $\mu g/m^3$ (CTR station) 0.6 $\mu g/m^3$ (YRK station) (Figure 72). The nitrate concentration occupied less than 5 % of the total mass of the PM 2.5 (Figure 73). Average nitrate concentrations were relatively high in LP, WT, BHM, JST, YRK and FT stations. Correlation coefficients of nitrate concentrations were relatively high between CTR, GFP, OAK, OLE and PNS stations, FTM, JST, SDK and TUC stations, CHAS1, and EVER1 stations (Table 7). Figures 74 ~ 75 depict 30-minute average nitrate concentrations in LP and WT stations. Figures 76 ~ 93 are 24-hour average nitrate concentrations in the other stations.

Average organic carbon concentrations were from 1.3 $\mu g/m^3$ (EVER1 station) to 7.1 $\mu g/m^3$ (BHM station) during the above period (Figure 94). A Figure 95 represents that organic carbon occupied 15 % (TUC station) ~ 32 % (GFP station) of the total mass of the PM 2.5. Organic carbon concentrations were not highly correlated each other compared with sulfate, and ammonium. However correlation coefficients between LP and WT stations, and BHM, CTR, FTM, GFP, JST, OAK and PNS stations were relatively high. Figures 96 ~ 97 illustrated 30-minute organic carbon concentrations in LP and WT

stations. 24-hour average organic carbon concentrations in the other stations were depicted in Figures 98 ~ 115.

Average elemental carbon concentration ranged between 0.2 $\mu g/m^3$ (EVER1 station) and 2.8 $\mu g/m^3$ (BHM station) (Figure 116). Mass percentage averages of elemental carbon in PM 2.5 varied from 2.6 % (OAK station) to 11 % (BHM station) (Figure 117). Elemental carbon concentrations were highly correlated in BHM, CTR, JST, OAK, OLE and PNS stations. However, the correlation coefficient of nitrate between LP and WT stations, other species of which stations were highly correlated, was only 0.13. Figures 118 ~ 119 illustrate 30-minute average elemental carbon concentrations in LP and WT stations. Figures 120 ~ 136 represent 24-hour average elemental carbon concentrations in the other stations.

4. CONCLUSION

We analyzed characteristics of ozone and PM 2.5 concentrations in Texas, Louisiana, Mississippi, Alabama, Georgia, and Florida. Average ozone concentrations from August 12 to September 15, 2000, were lowest in Jefferson street, Georgia (33 ppbv) and highest in Yorkville, Georgia (51 ppbv). In general, ozone concentrations were relatively low in urban areas and high in rural areas. Ozone concentrations showed consistent diurnal variations in measured stations. The consistent diurnal pattern resulted in high correlation coefficients of 1-hour average ozone concentrations. 24-hour average ozone concentrations were also highly correlated.

We compared measured 1-hour and 8-hour average ozone concentrations with the National Ambient Air Quality Standard (NAAQS). Ozone concentrations in every station exceeded 8-hour standard more than once during the analysis period, and seven out of ten stations exceeded 1-hour standard at least three times.

We examined the regional trend of PM 2.5 concentrations. PM 2.5 concentrations were highest in Jefferson Street station and lowest I Everglades National Park station. In general, average PM 2.5 concentrations were high in urban areas and low in rural areas. However no station exceeded the daily PM 2.5 standard during the analysis period.

We also examined five major species concentrations of PM 2.5: sulfate, nitrate, ammonium, organic carbon and elemental carbon. On average, sulfate represented 23 %

to 44 % of total PM 2.5 mass depending on the measured locations. Ammonium and organic carbon explained around 10 % and 25 % of total PM 2.5 mass, respectively. Sum of ammonium and elemental carbon concentrations occupied less than 15 % of the total PM 2.5 mass. PM 2.5 mass concentrations were highly correlated between closely located stations, such as LP and WT stations, BHM, CTR, GFP and JST stations, OAK, OLE and PNS stations. PM 2.5 species concentrations were also highly correlated between geographically close stations.

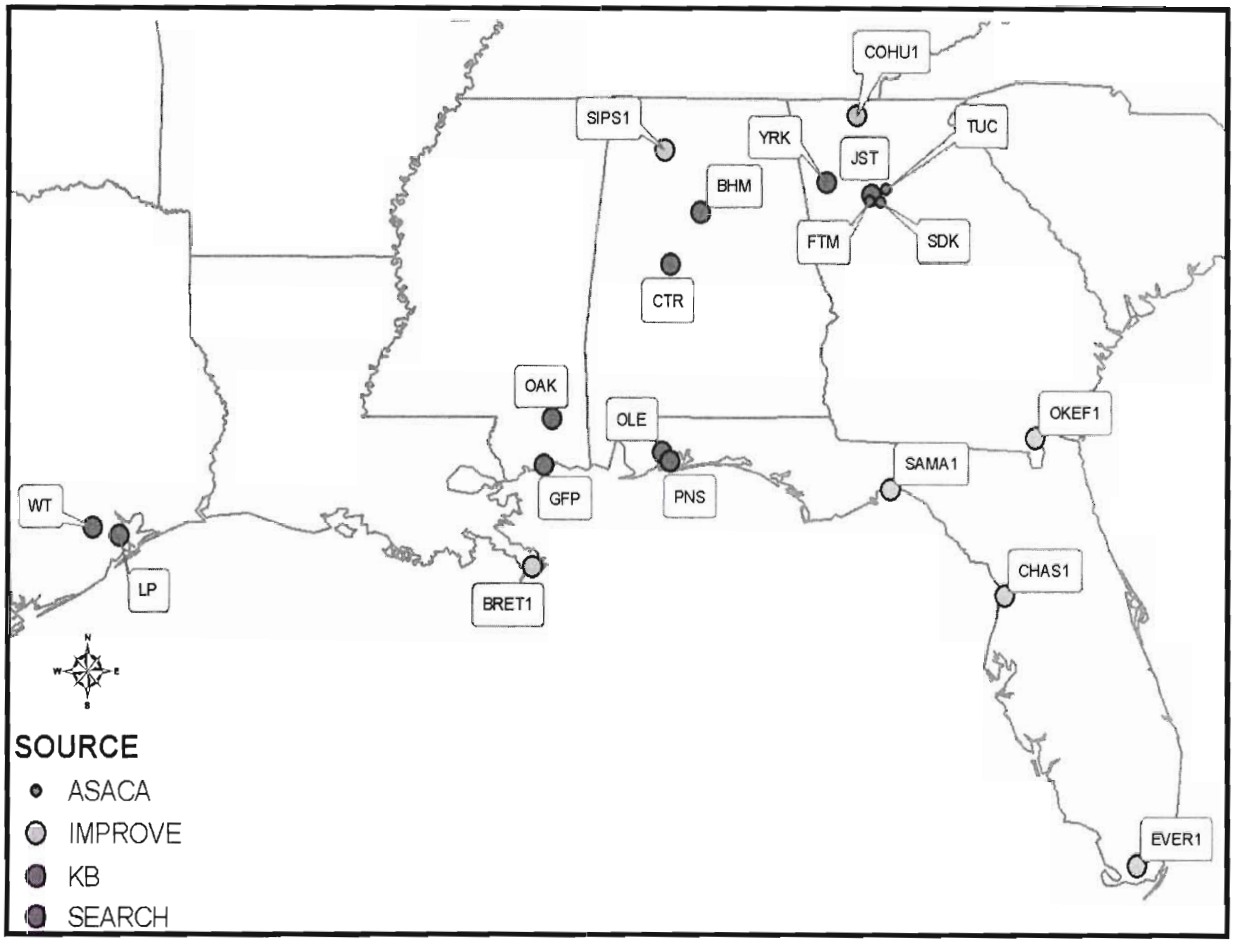

Figure 1. Locations of PM 2.5 Monitoring Sites

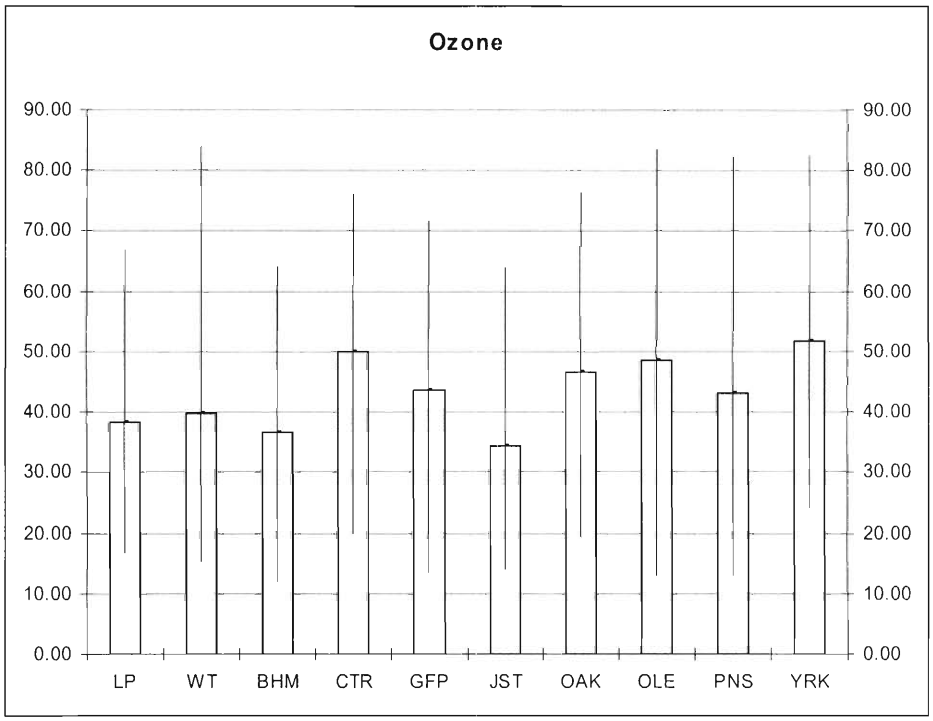

Figure 2. Maximums, minimums and averages of ozone concentrations 24-hour averages (ppbv) from August 12 to September 15, 2000

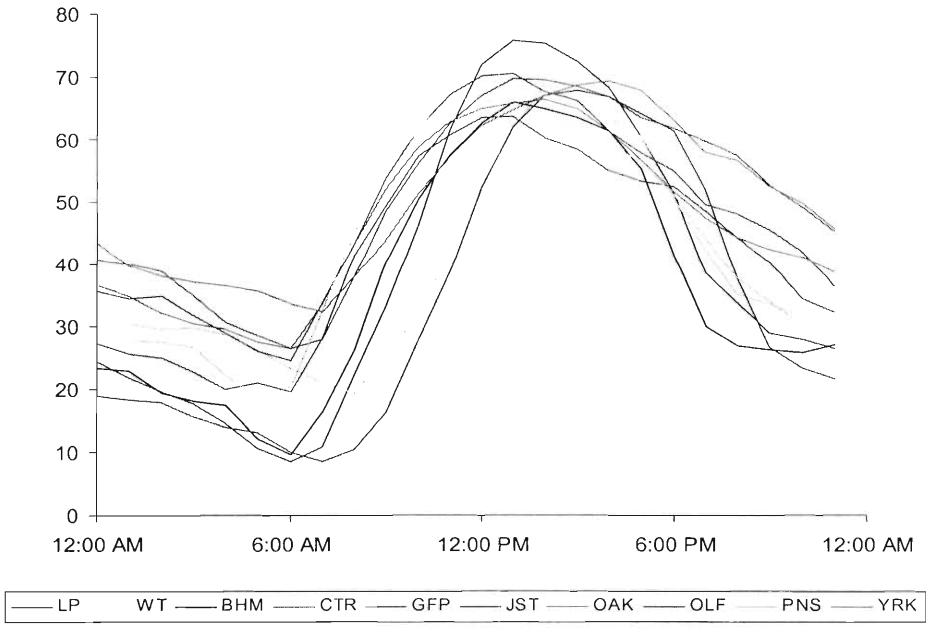

Figure 3. Diurnal ozone concentration (ppbv) averages from August 12 ~ September 15, 2000.

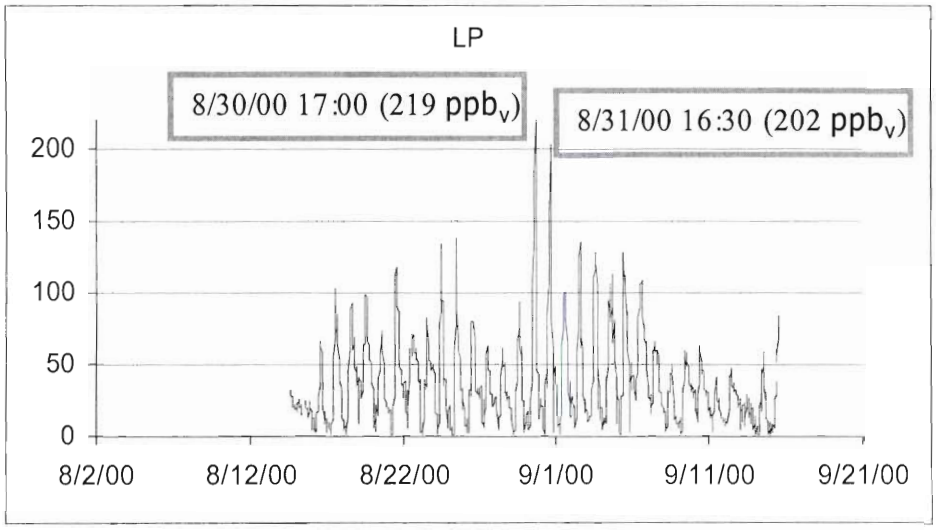

Figure 4. Ozone concentration 30-minute averages (ppbv) in La Porte.

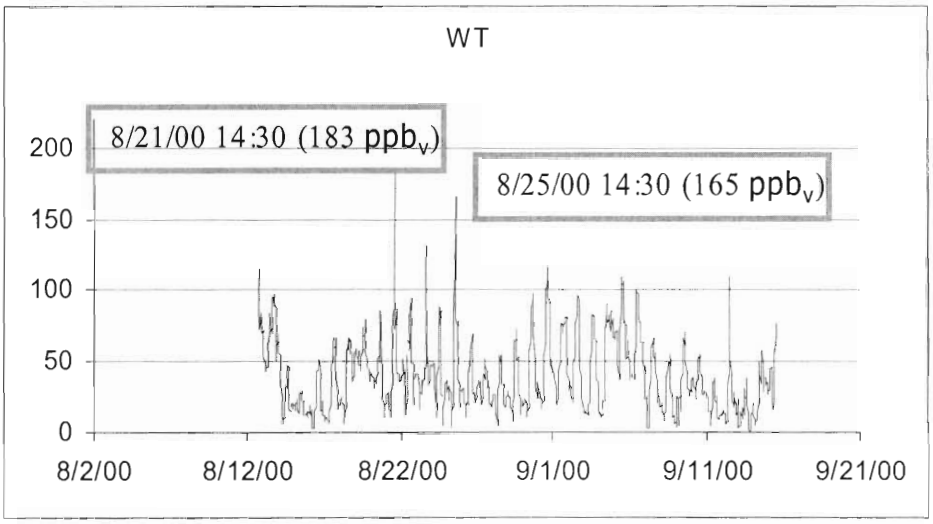

Figure 5. Ozone concentration 30-minute averages (ppbv) in Williams Tower.

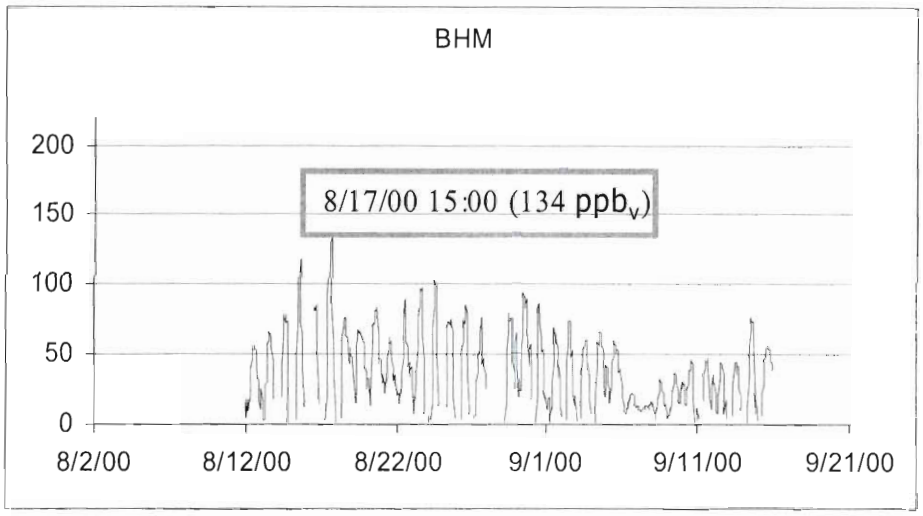

Figure 6. Ozone concentration 1-hour averages (ppbv) in North Birmingham.

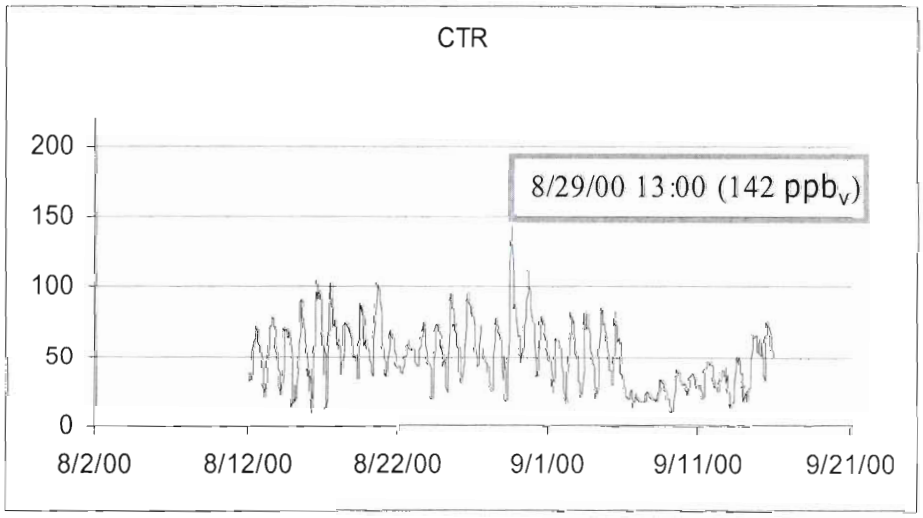

Figure 7. Ozone concentration 1-hour averages (ppbv) in Centreville.

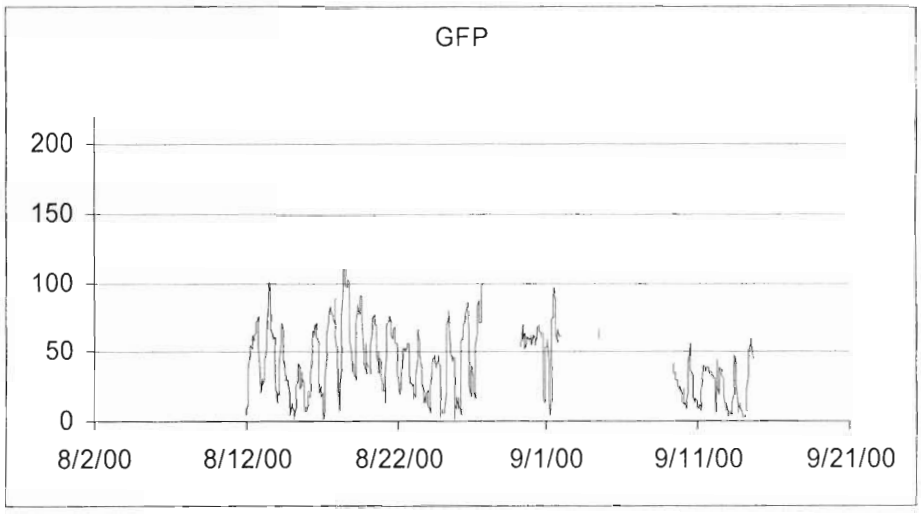

Figure 8. Ozone concentration 1-hour averages (ppbv) in Gulfport.

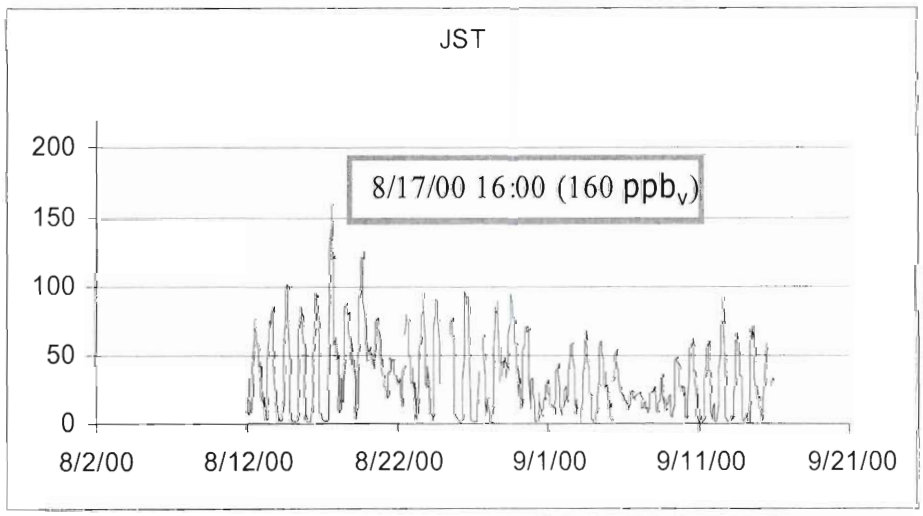

Figure 9. Ozone concentration 1-hour averages (ppbv) in Jefferson Street.

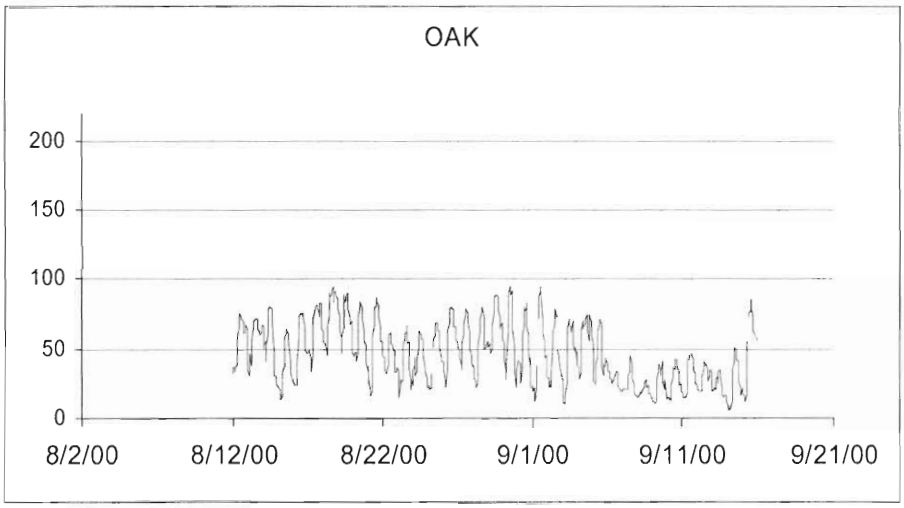

Figure 10. Ozone concentration 1-hour averages (ppbv) in Oak Grove.

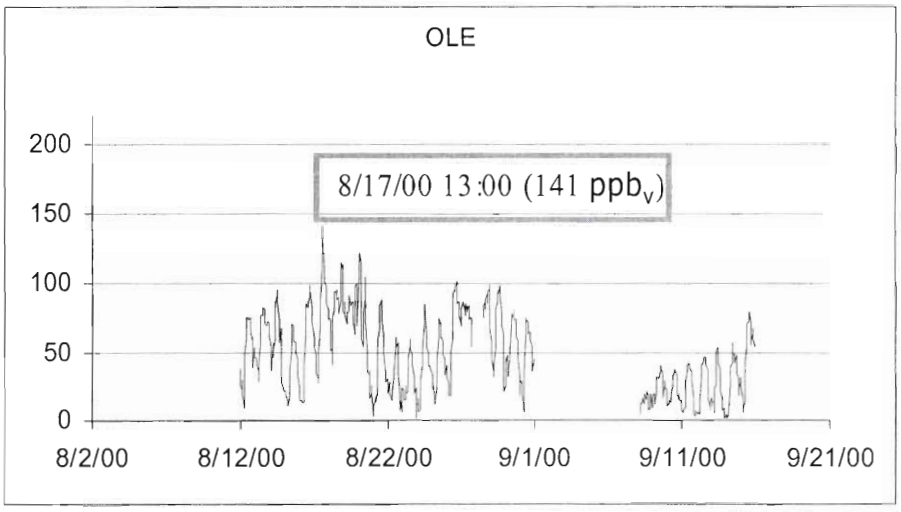

Figure 11. Ozone concentration 1-hour averages (ppbv) in Pensacola (OLE).

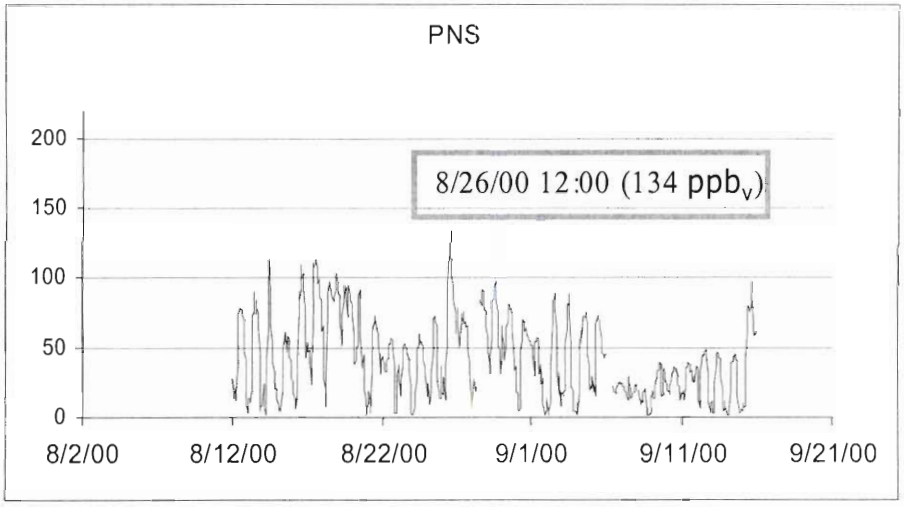

Figure 12. Ozone concentration 1-hour averages (ppbv) in Pensacola (PNS).

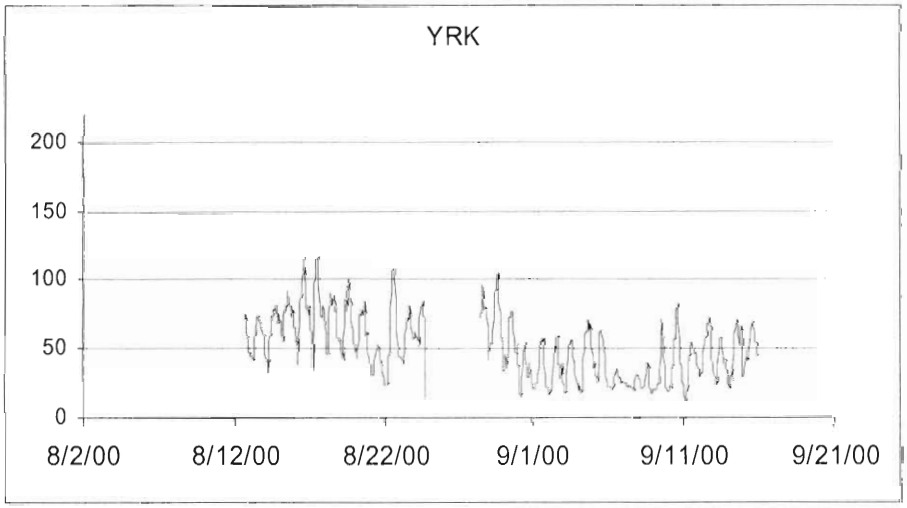

Figure 13. Ozone concentration 1-hour averages (ppbv) in Yorkville.

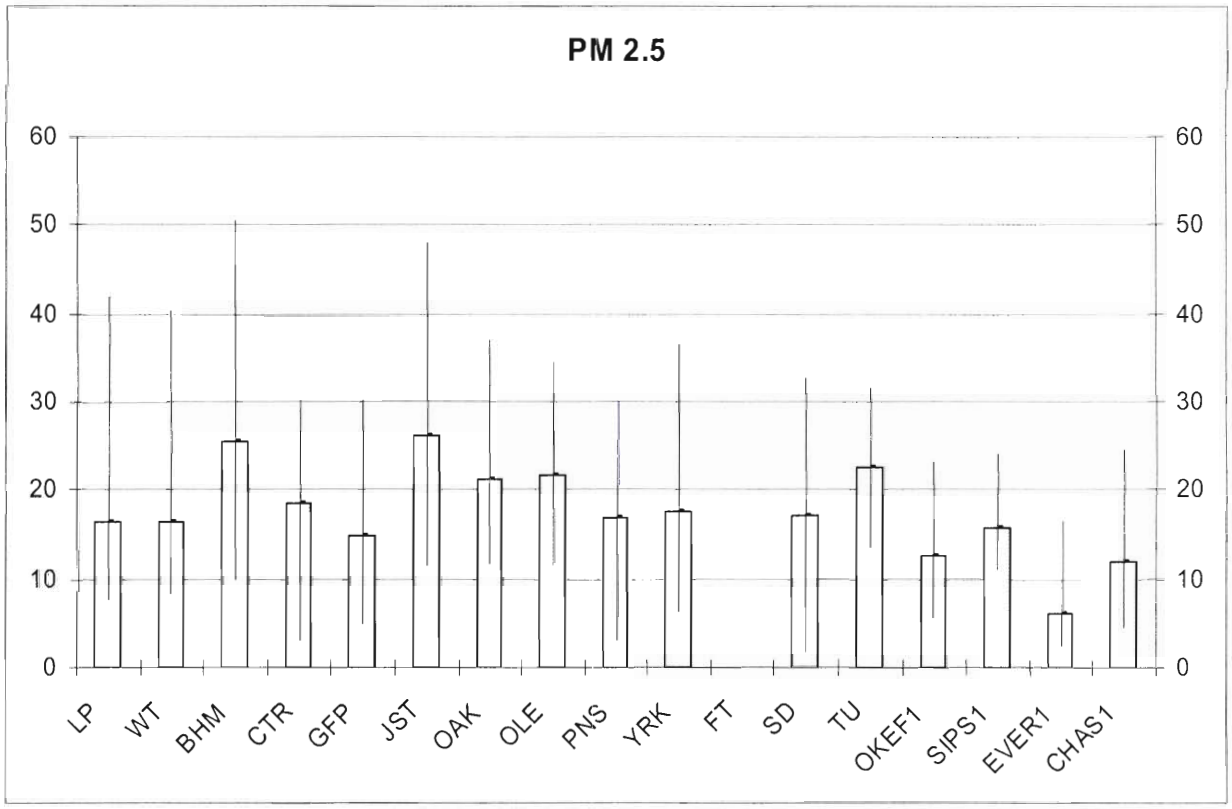

Figure 14. Maximums, minimums and averages of PM 2.5 concentrations 24-hour averages ($\mu g/m^3$) from August 12 to September 15, 2000

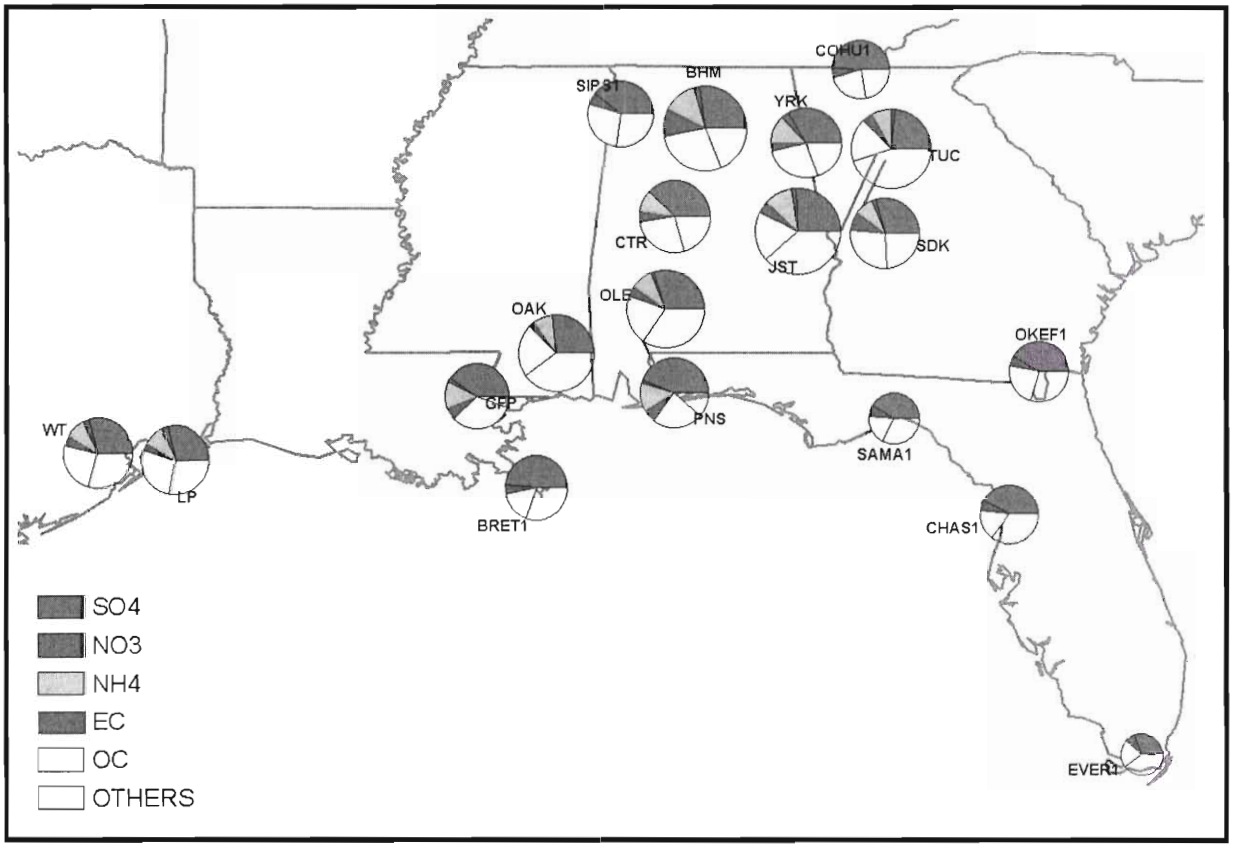

Figure 15. The regional comparison of PM 2.5 mass and species concentration averages.

The same period as in Figure 14

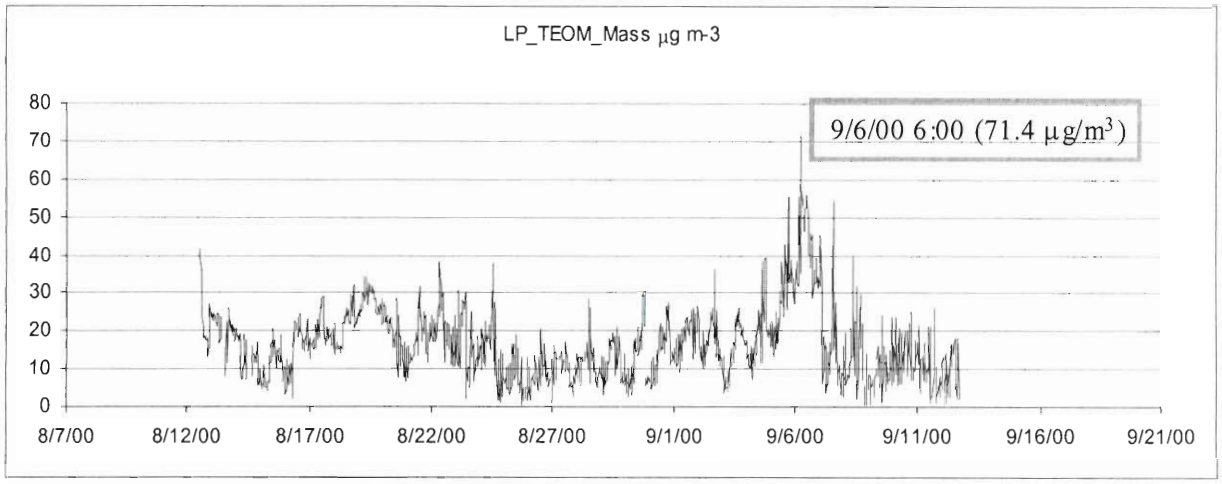

Figure 16. PM 2.5 concentration 30-minute averages ($\mu g/m^3$) in La Porte

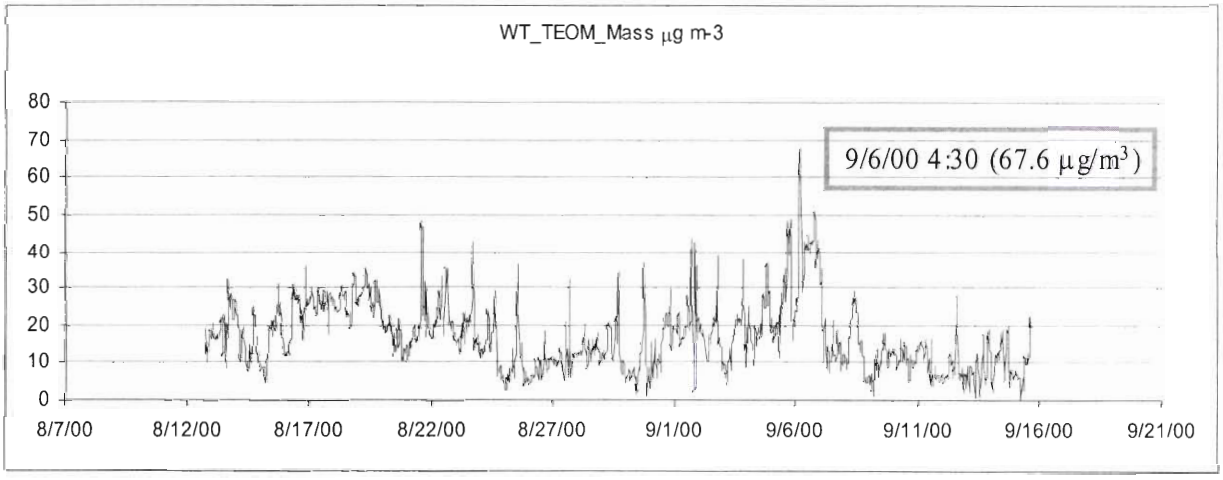

Figure 17. PM 2.5 concentration 30-minute averages ($\mu g/m^3$) in Williams Tower

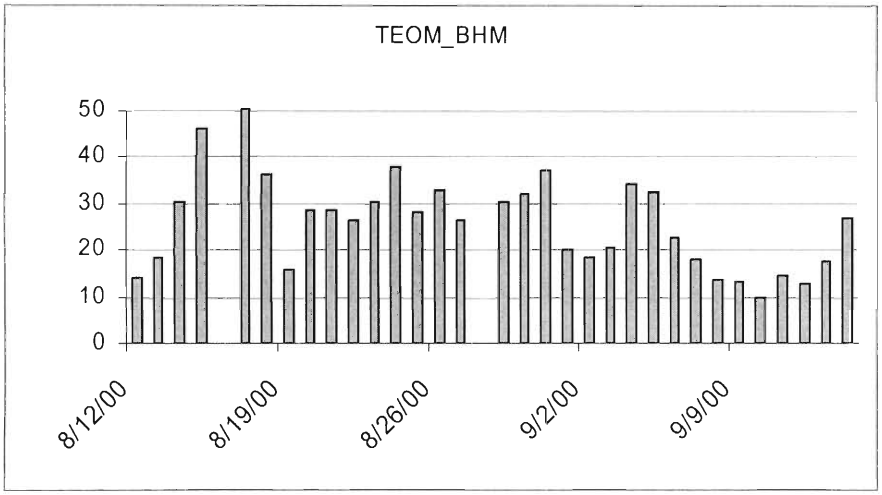

Figure 18. PM 2.5 concentration 24-hour averages ($\mu g/m^3$) in North Birmingham.

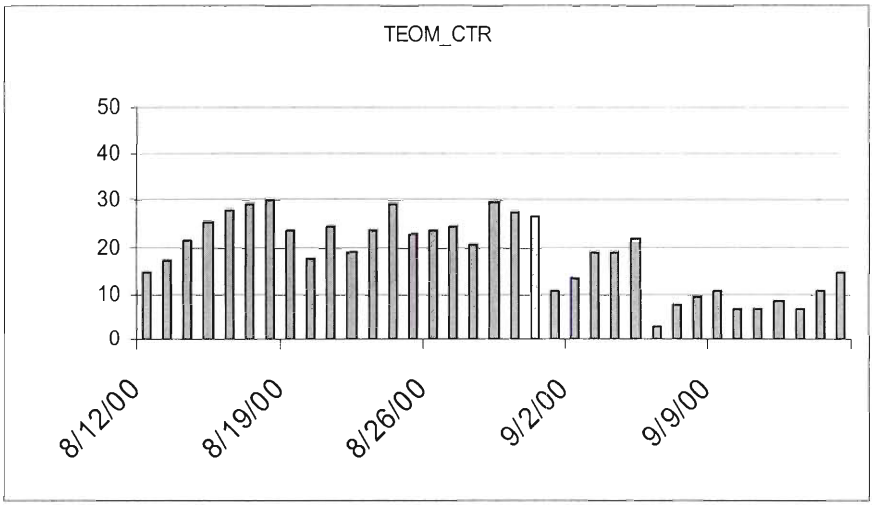

Figure 19. PM 2.5 concentration 24-hour averages ($\mu g/m^3$) in North Birmingham.

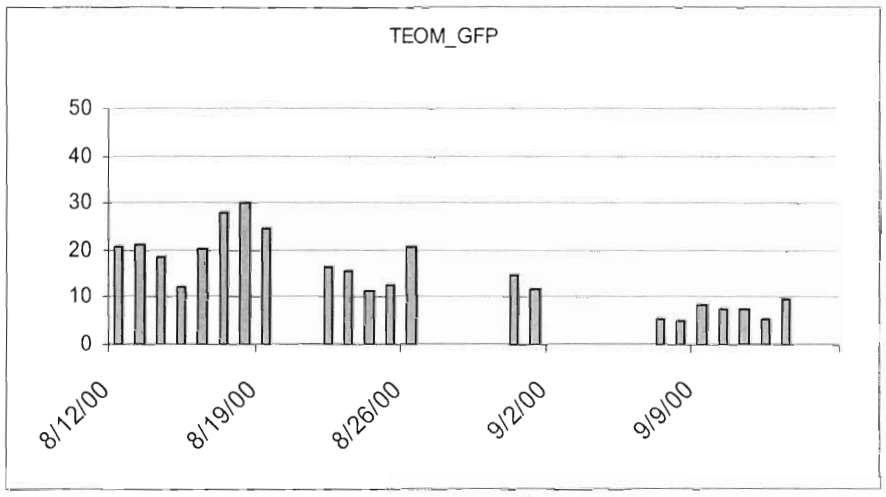

Figure 20. PM 2.5 concentration 24-hour averages ($\mu g/m^3$) in Gulfport.

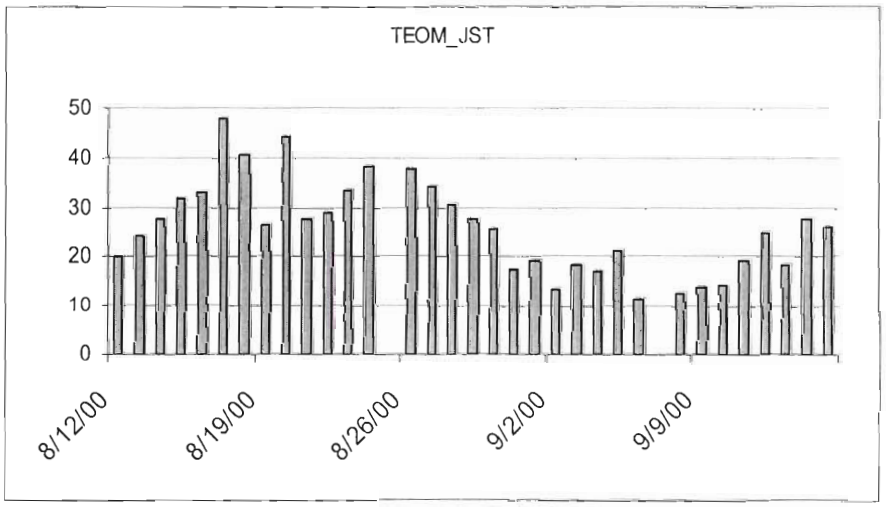

Figure 21. PM 2.5 concentration 24-hour averages ($\mu g/m^3$) in Jefferson Street.

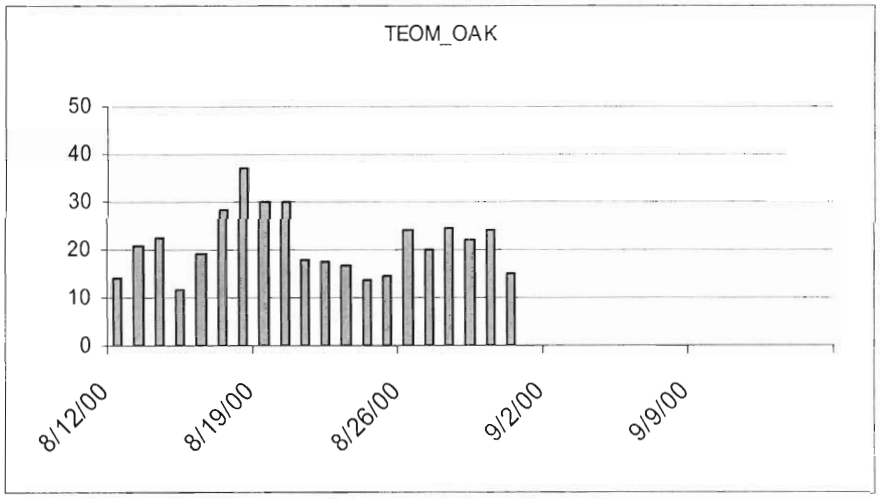

Figure 22. PM 2.5 concentration 24-hour averages ($\mu g/m^3$) in Oak Grove.

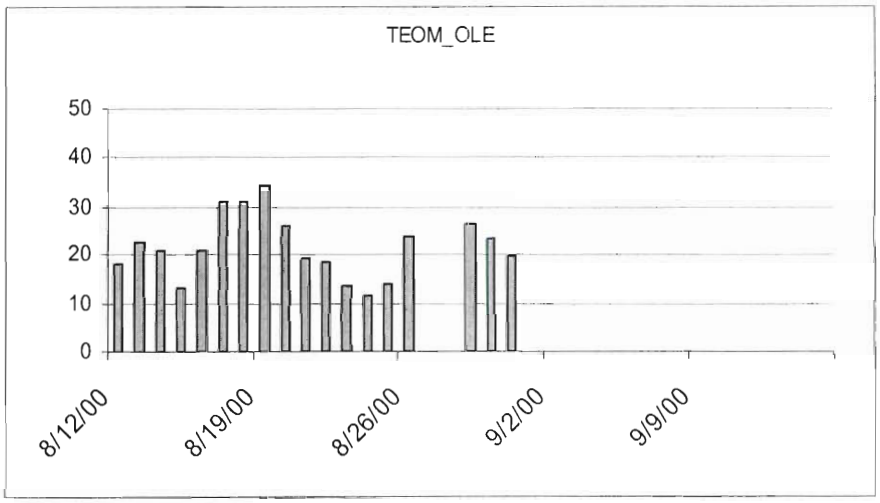

Figure 23. PM 2.5 concentration 24-hour averages ($\mu g/m^3$) in Pensacola (OLE).

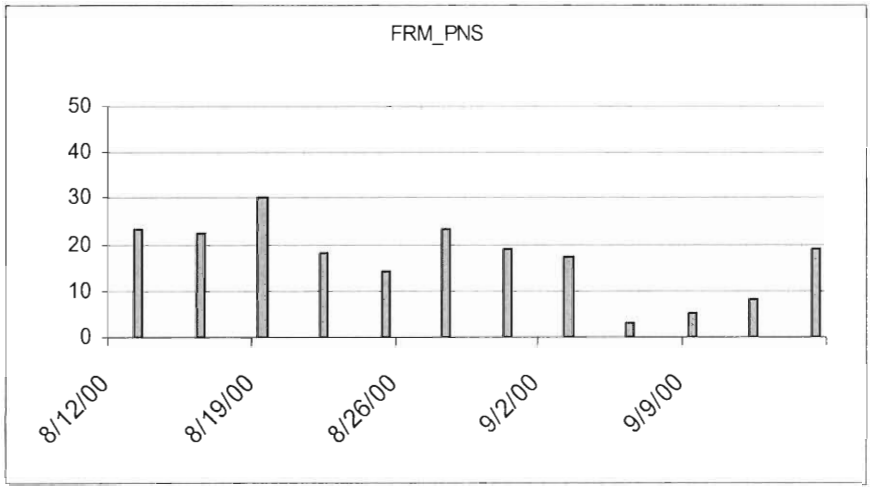

Figure 24. PM 2.5 concentration 24-hour averages ($\mu g/m^3$) in Pensacola (PNS).

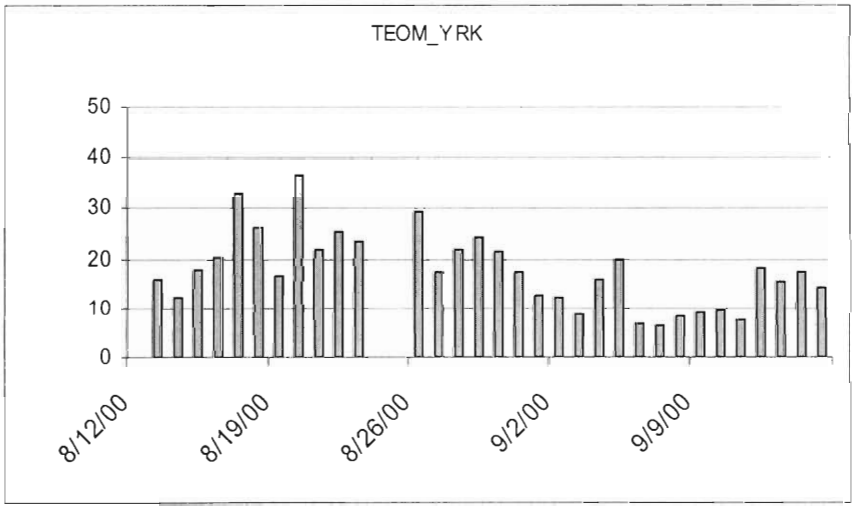

Figure 25. PM 2.5 concentration 24-hour averages ($\mu g/m^3$) in Yorkville.

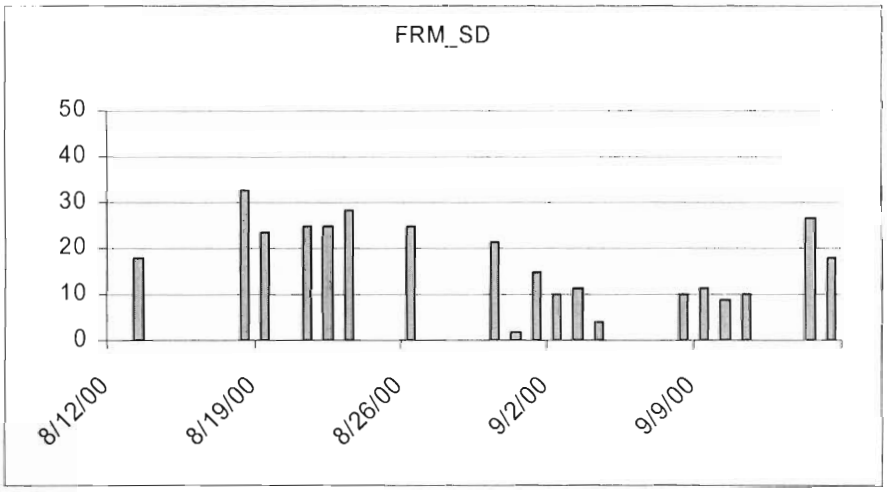

Figure 26. PM 2.5 concentration 24-hour averages ($\mu g/m^3$) in South Dekalb.

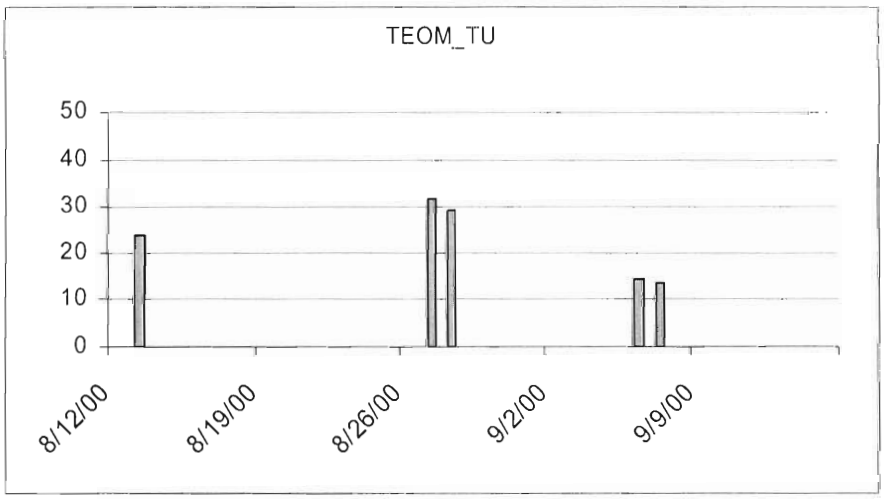

Figure 27. PM 2.5 concentration 24-hour averages ($\mu g/m^3$) in Tucker.

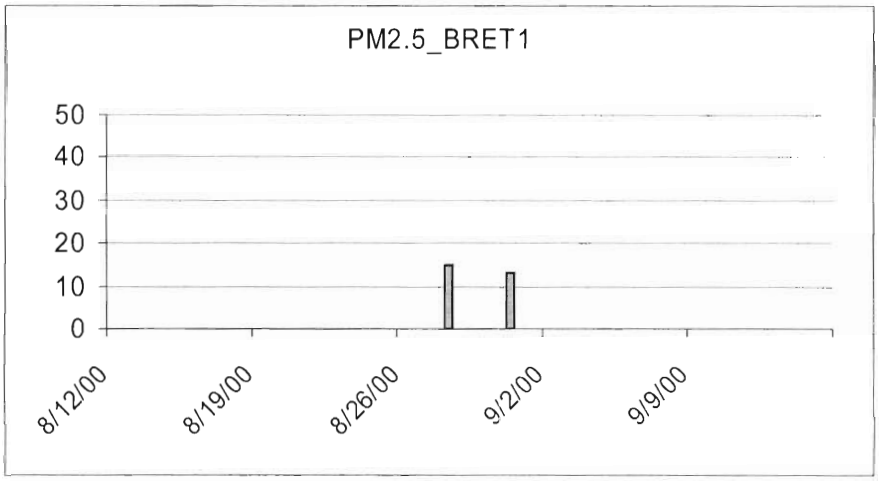

Figure 28. PM 2.5 concentration 24-hour averages ($\mu g/m^3$) in Brento.

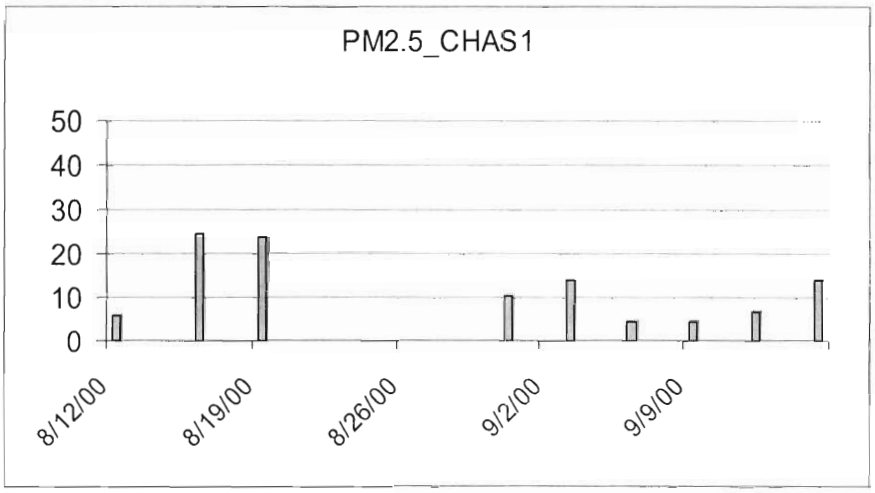

Figure 29. PM 2.5 concentration 24-hour averages ($\mu g/m^3$) in Chassahowitzka National Wildlife.

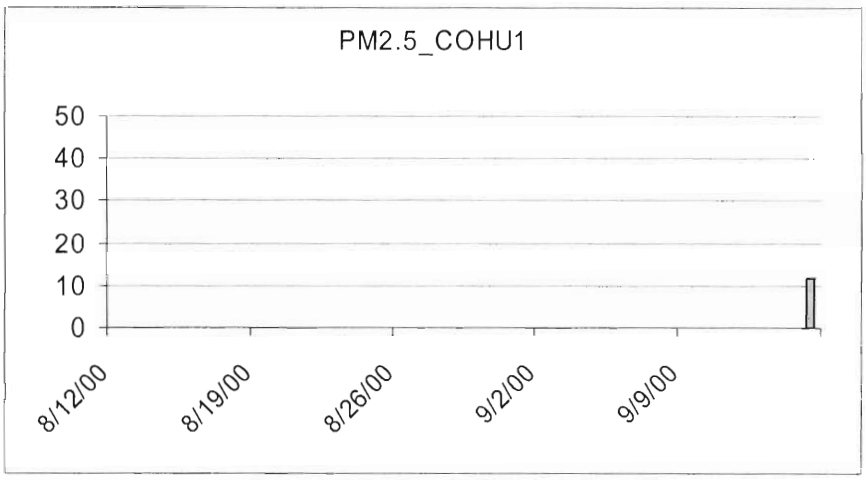

Figure 30. PM 2.5 concentration 24-hour averages ($\mu g/m^3$) in Cohutta.

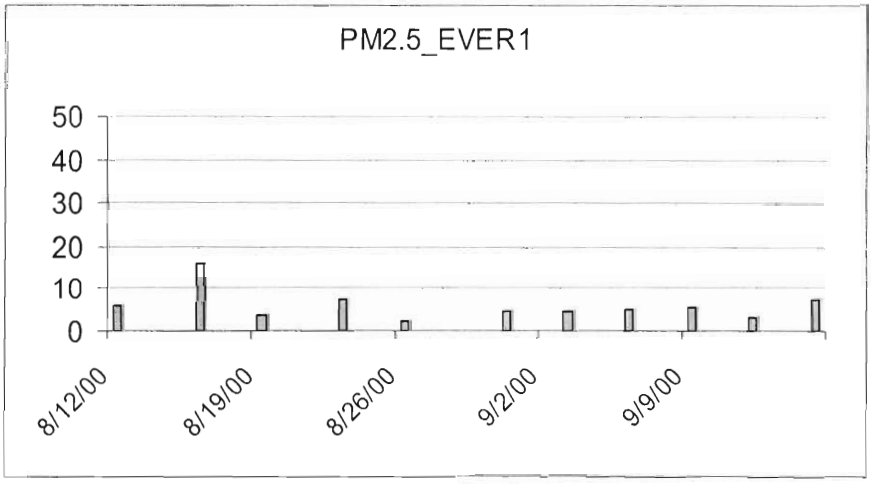

Figure 31. PM 2.5 concentration 24-hour averages ($\mu g/m^3$) in Everglades National Park.

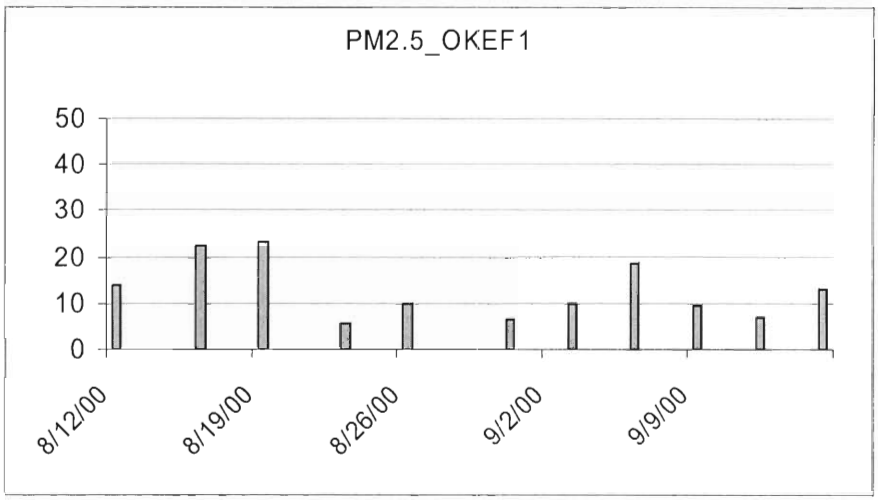

Figure 32. PM 2.5 concentration 24-hour averages ($\mu g/m^3$) in Okefenokee National Wildlife Refuge.

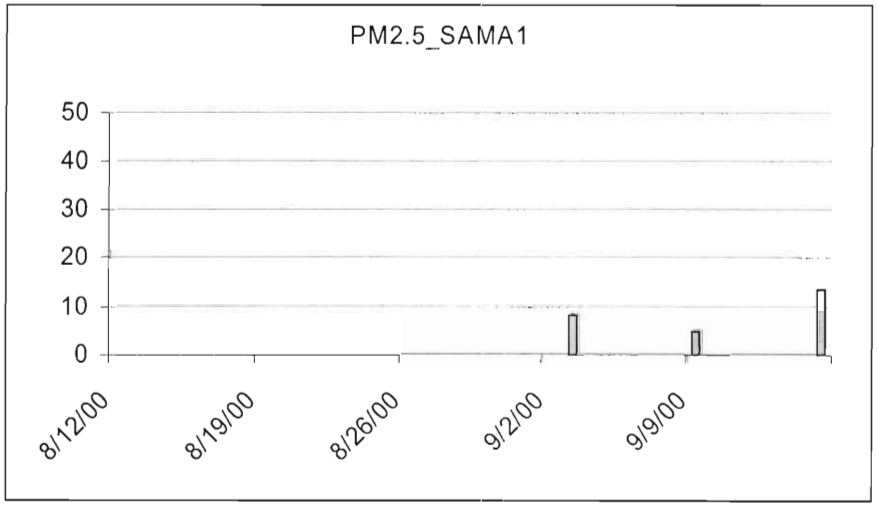

Figure 33. PM 2.5 concentration 24-hour averages ($\mu g/m^3$) in St. Marks.

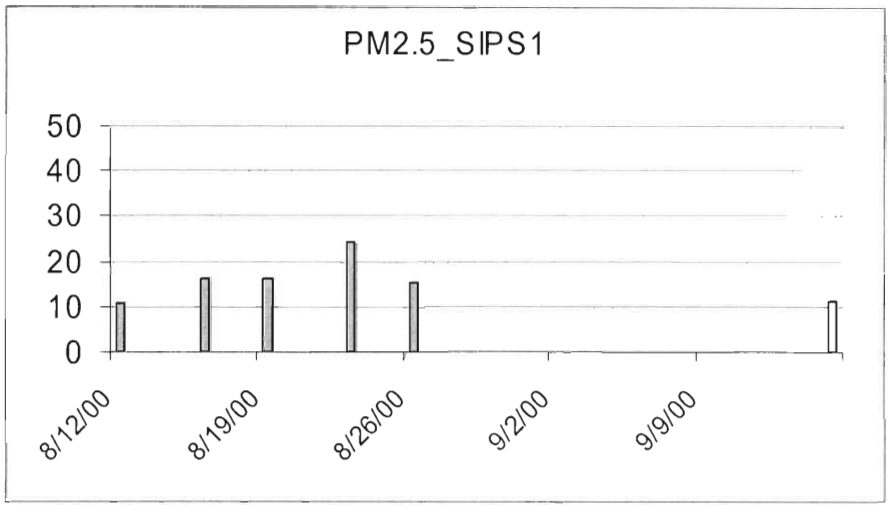

Figure 34. PM 2.5 concentration 24-hour averages ($\mu g/m^3$) in Sipsy Wilderness.

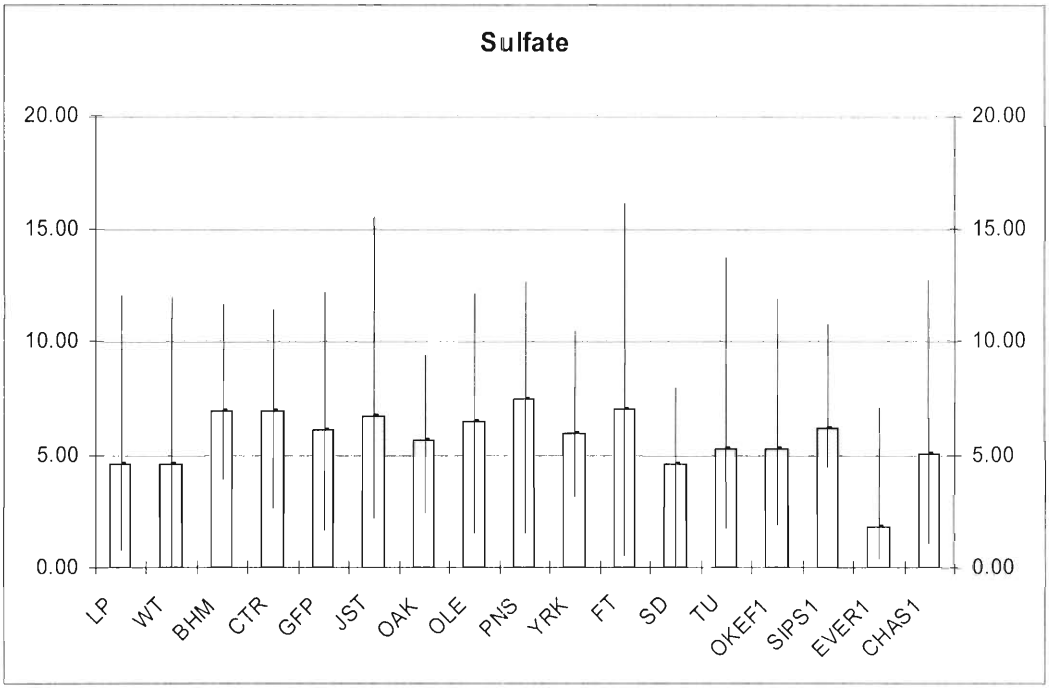

Figure 35. Maximums, minimums and averages of sulfate concentrations 24-hour averages ($\mu g/m^3$) from August 12 to September 15, 2000

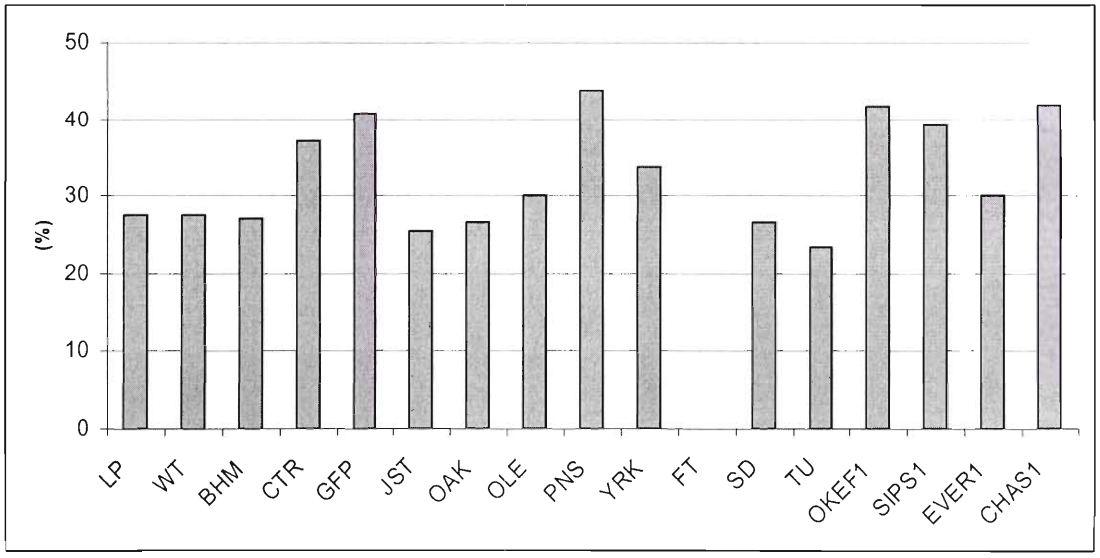

Figure 36. Mass percentage averages of sulfate in PM 2.5.

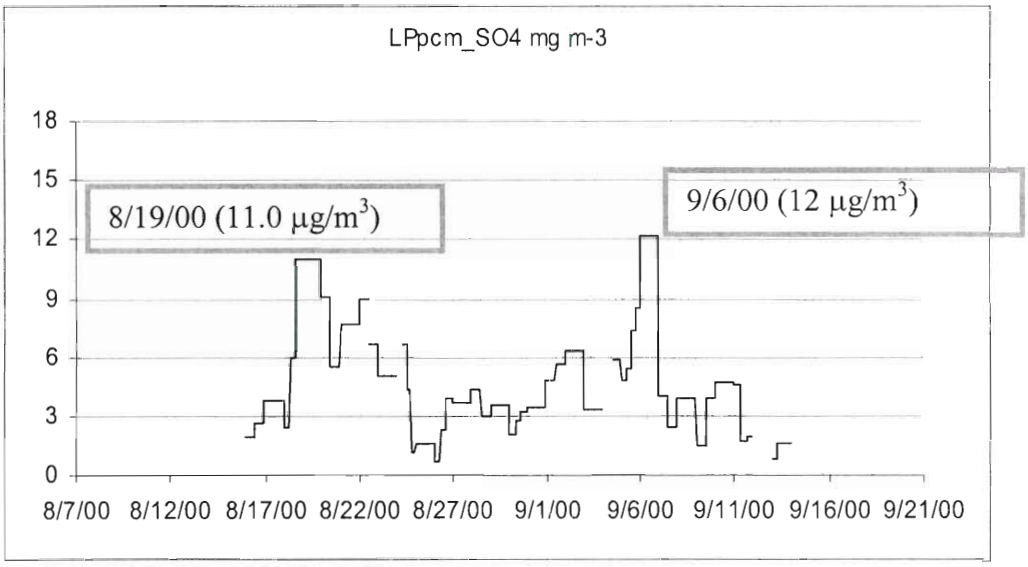

Figure 37. Sulfate concentration 30-minute averages ($\mu g/m^3$) in La Porte.

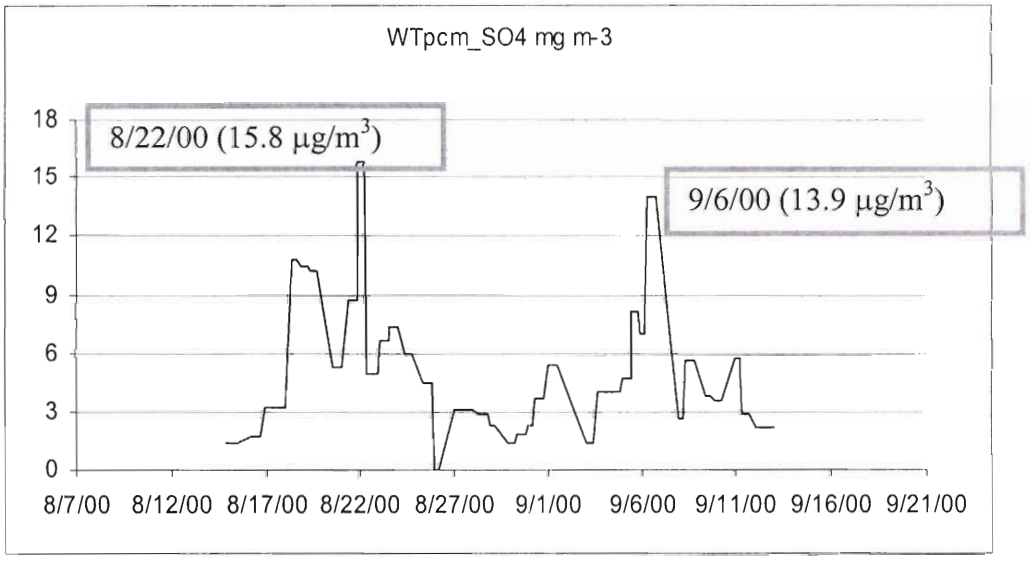

Figure 38. Sulfate concentration 30-minute averages ($\mu g/m^3$) in Williams Tower.

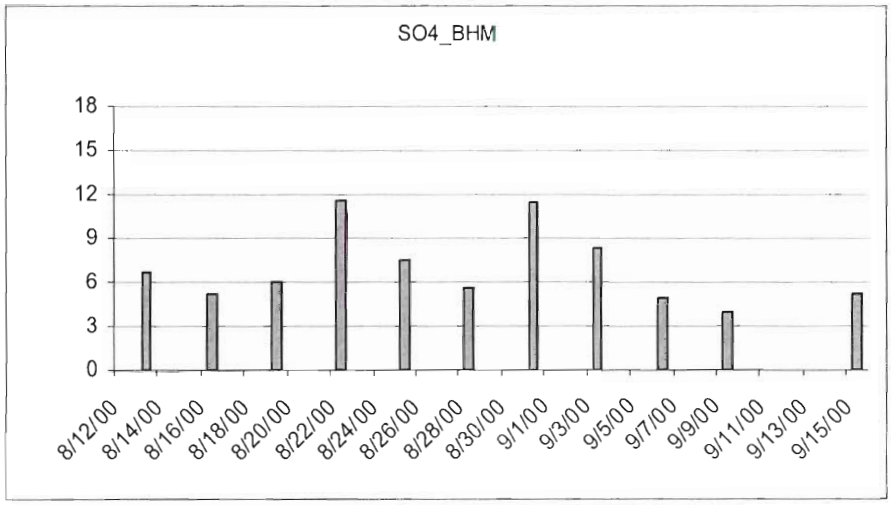

Figure 39. Sulfate concentration 24-hout averages ($\mu g/m^3$) in North Birmingham.

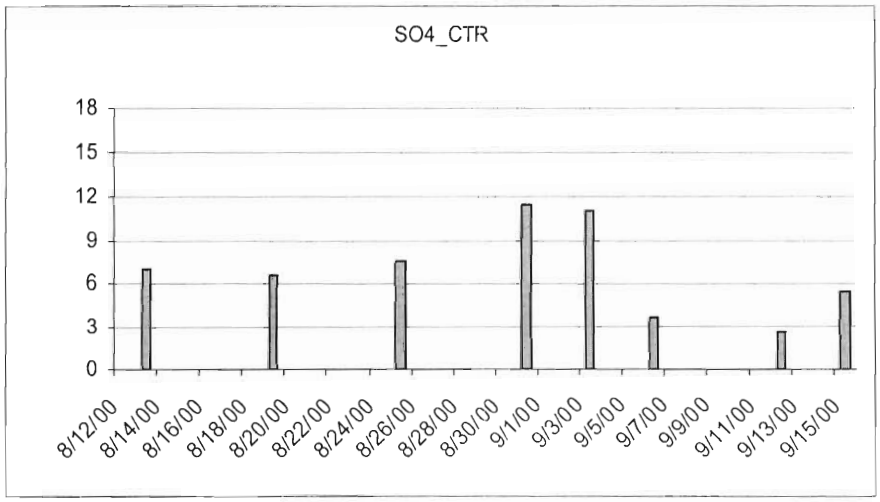

Figure 40. Sulfate concentration 24-hour averages ($\mu g/m^3$) in Centreville.

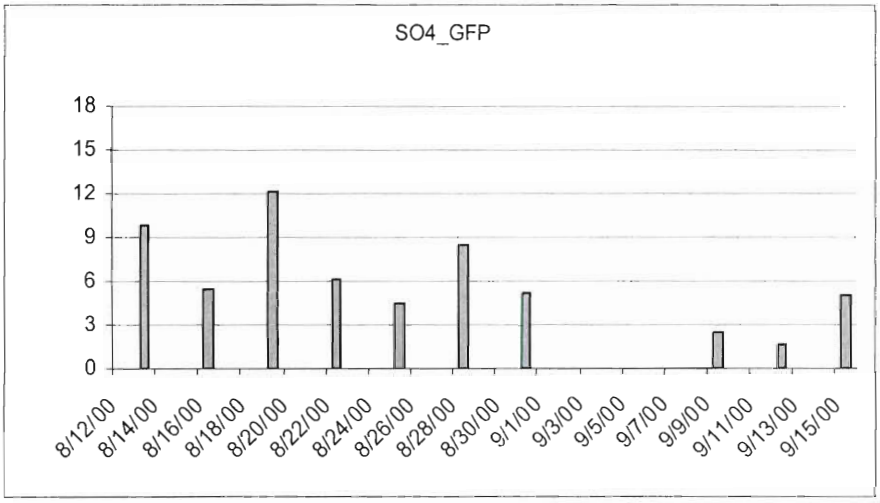

Figure 41. Sulfate concentration 24-hour averages ($\mu g/m^3$) in Gulfport.

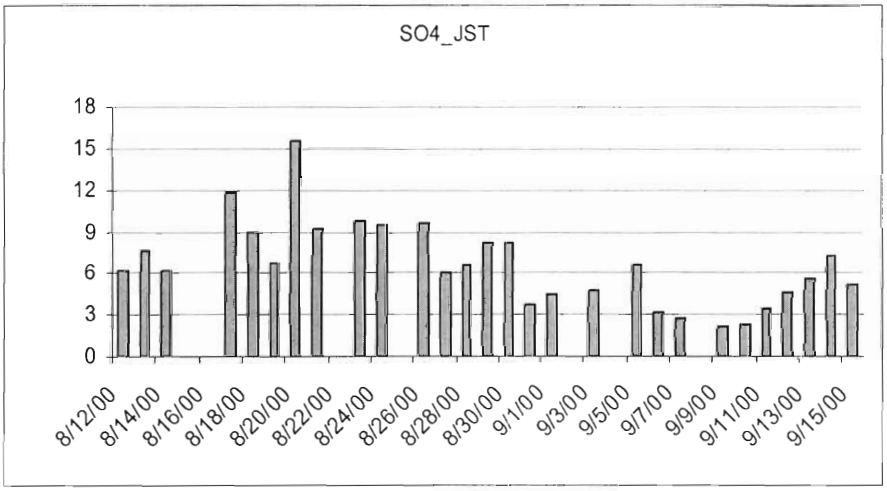

Figure 42. Sulfate concentration 24-hour averages ($\mu g/m^3$) in Jefferson Street.

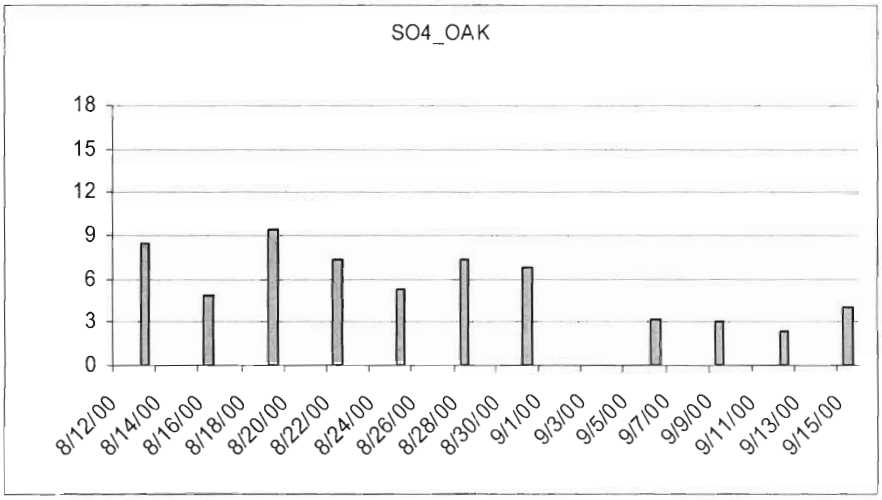

Figure 43. Sulfate concentration 24-hour averages ($\mu g/m^3$) in South Dekalb.

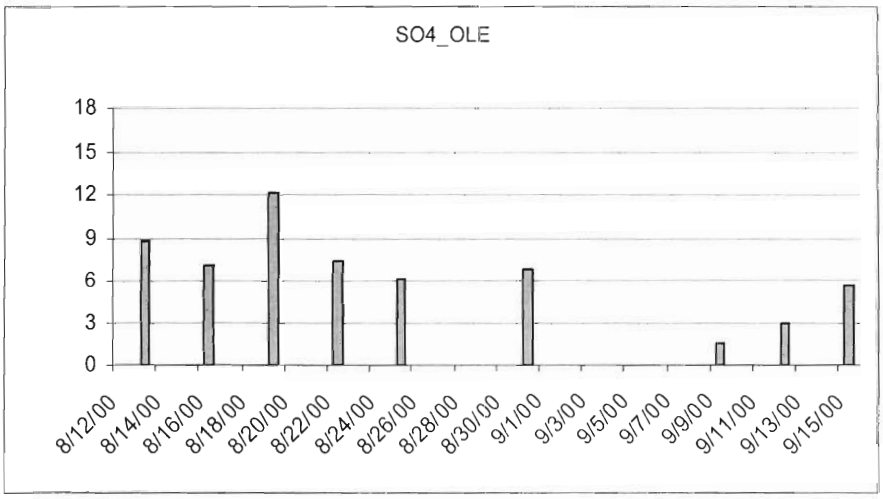

Figure 44. Sulfate concentration 24-hour averages ($\mu g/m^3$) in Pensacola (OLE).

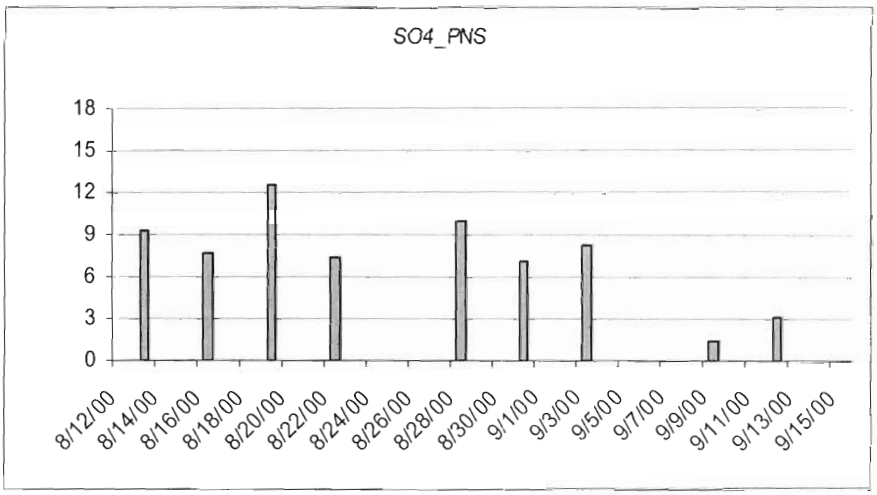

Figure 45. Sulfate concentration 24-hour averages ($\mu g/m^3$) in Pensacola (PNS).

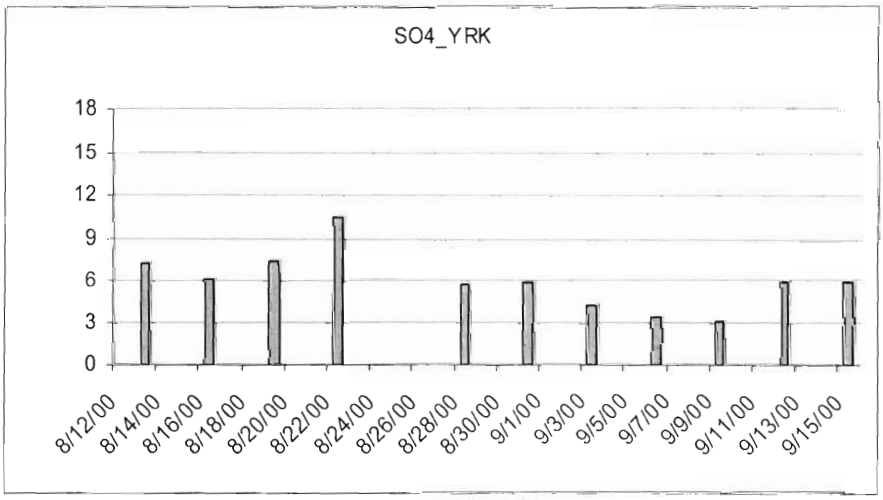

Figure 46. Sulfate concentration 24-hour averages ($\mu g/m^3$) in Pensacola (YRK).

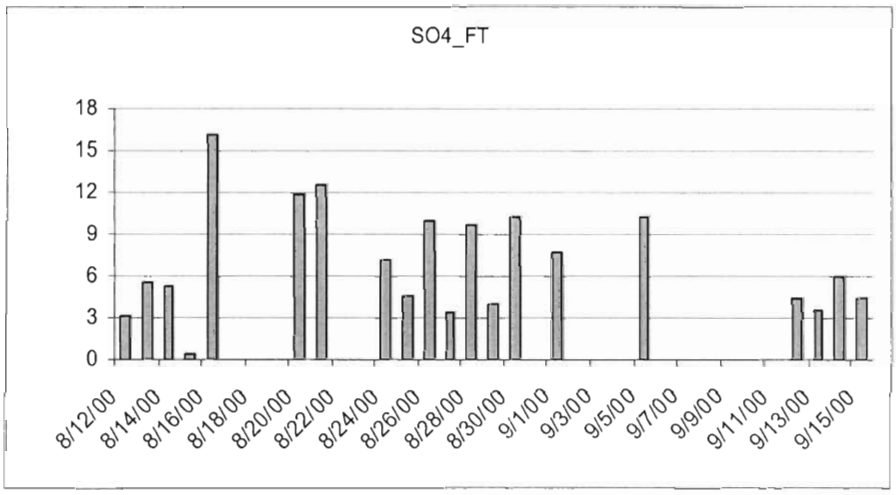

Figure 47. Sulfate concentration 24-hour averages ($\mu g/m^3$) in Fort McPherson.

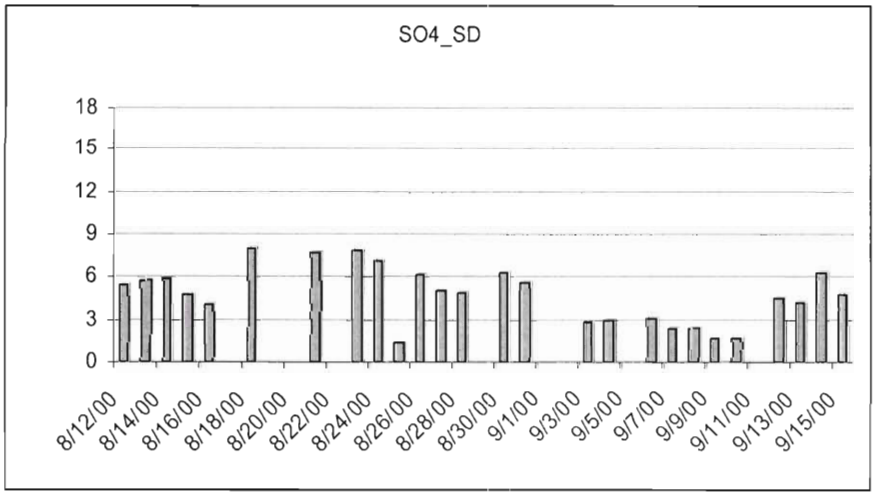

Figure 48. Sulfate concentration 24-hour averages ($\mu g/m^3$) in South Dekalb.

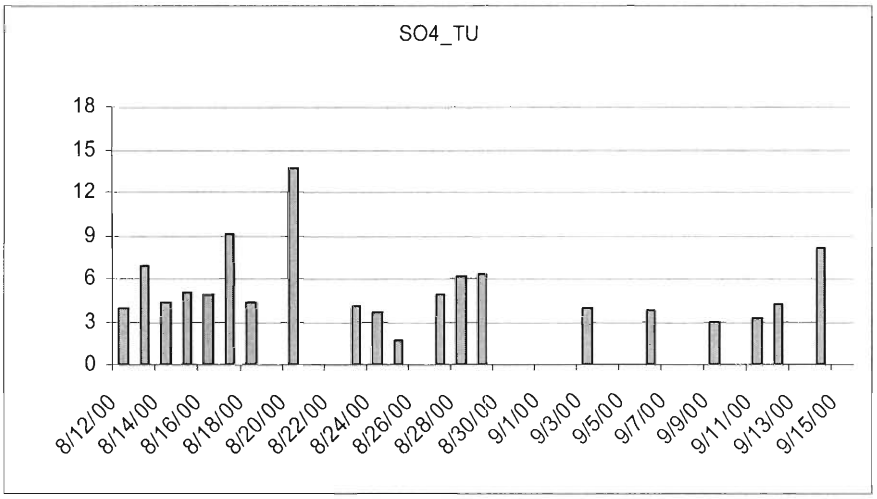

Figure 49. Sulfate concentration 24-hour averages ($\mu g/m^3$) in Tucker.

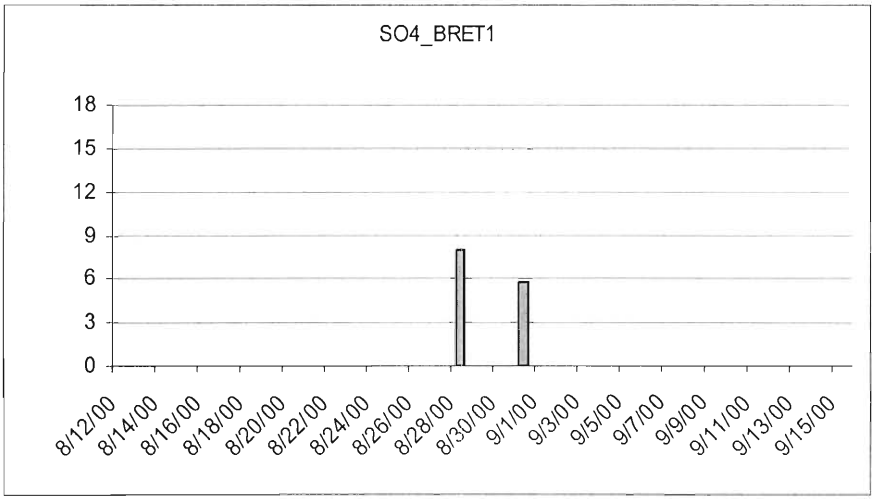

Figure 50. Sulfate concentration 24-hour averages ($\mu g/m^3$) in Breton.

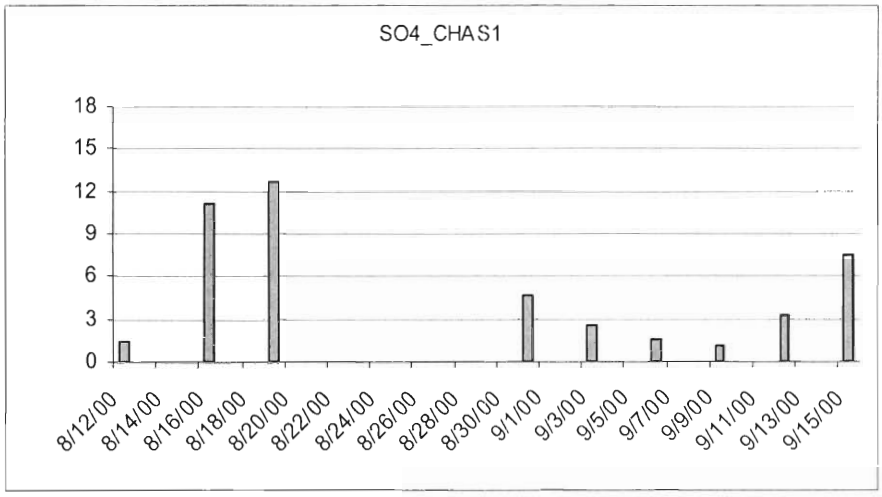

Figure 51. Sulfate concentration 24-hour averages ($\mu g/m^3$) in Chassahowitzka National Wildlife.

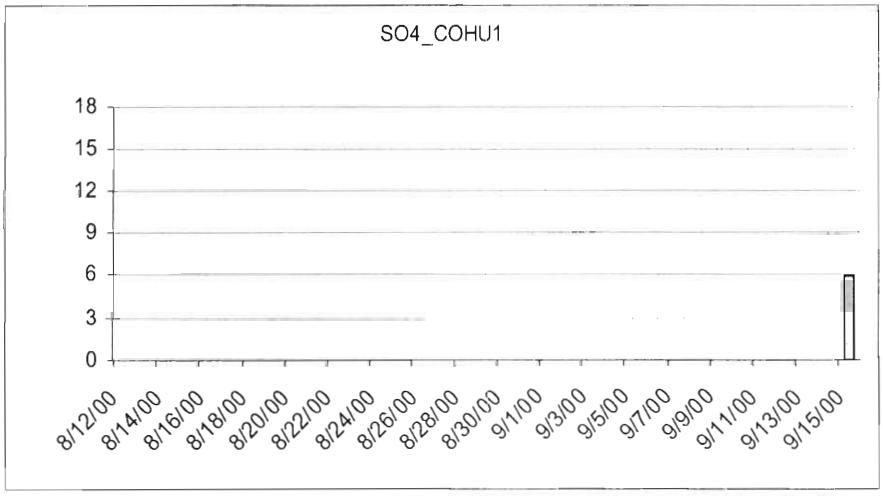

Figure 52. Sulfate concentration 24-hour averages ($\mu g/m^3$) in Cohutta.

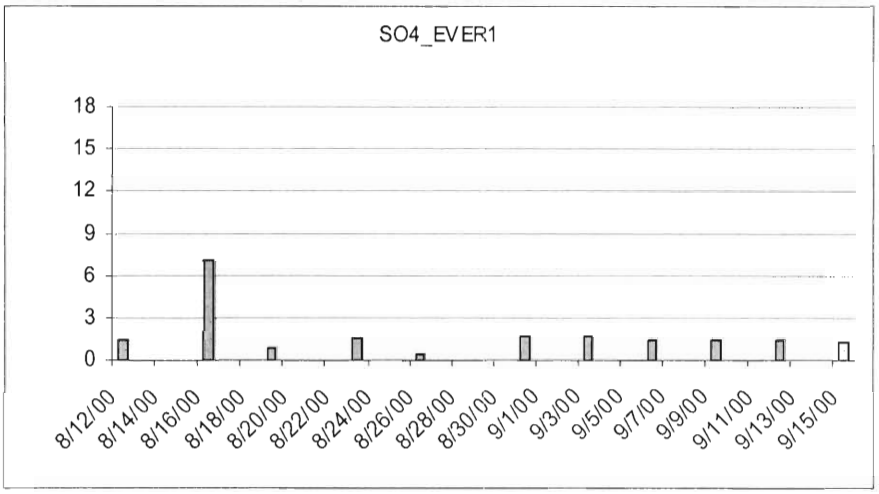

Figure 53. Sulfate concentration 24-hour averages ($\mu g/m^3$) in Everglades National Park.

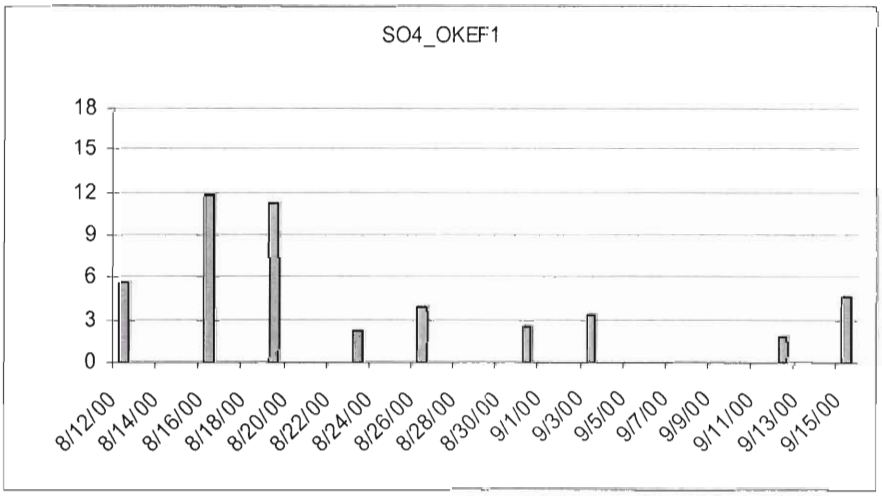

Figure 54. Sulfate concentration 24-hour averages ($\mu g/m^3$) in Okefenokee National Wildlife Refuge.

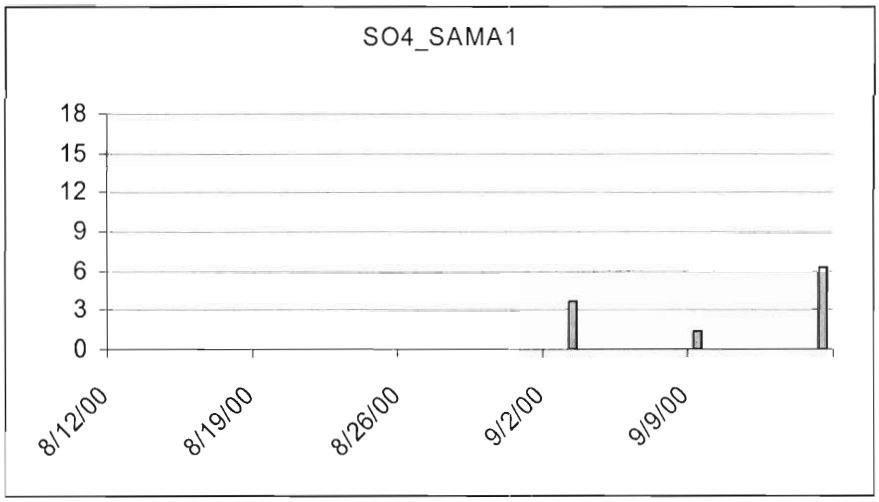

Figure 55. Sulfate concentration 24-hour averages ($\mu g/m^3$) in St. Marks.

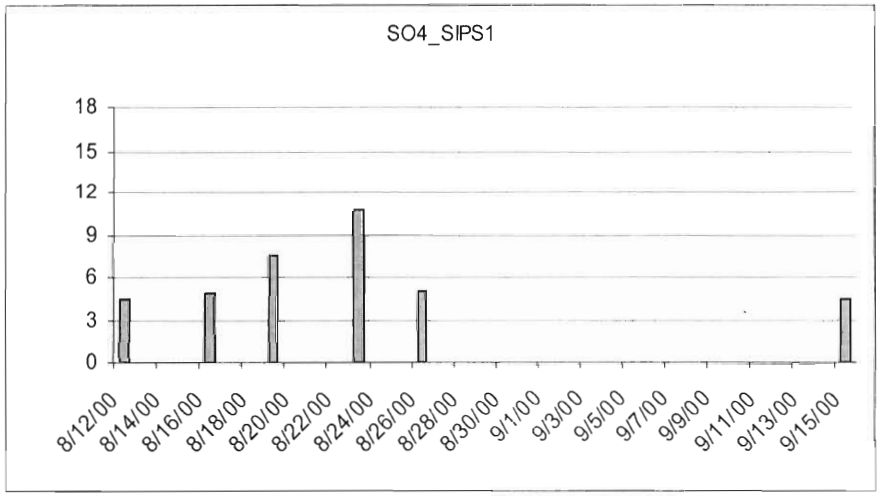

Figure 56. Sulfate concentration 24-hour averages ($\mu g/m^3$) in Sipsy Wilderness.

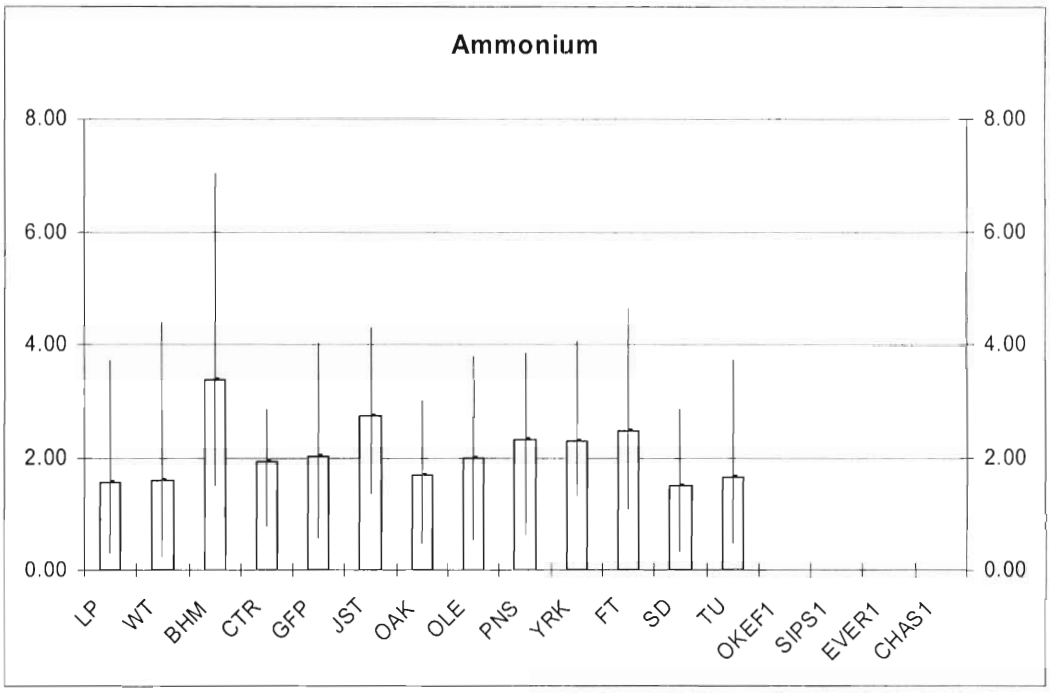

Figure 57. Maximums, minimums and averages of ammonium concentration 24-hour averages ($\mu g/m^3$) from August 12 to September 15, 2000

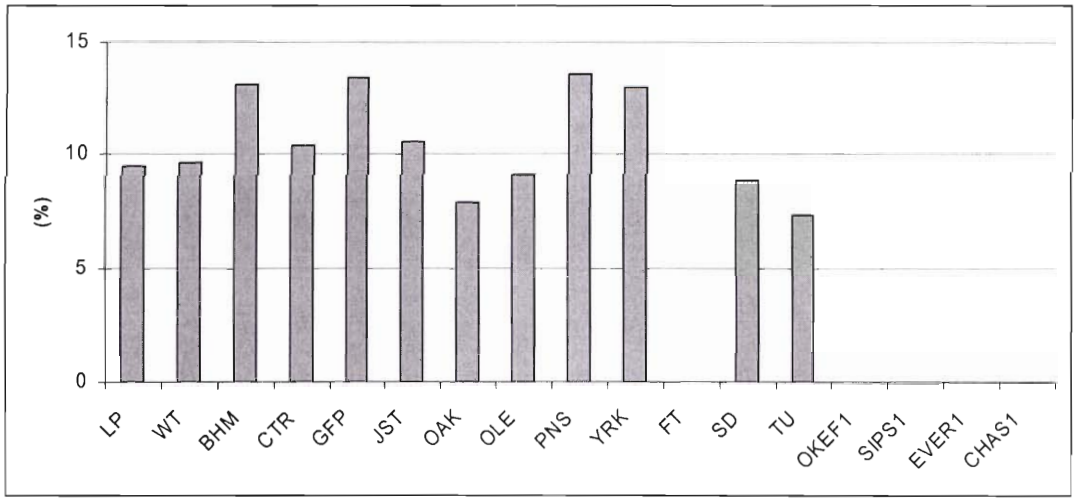

Figure 58. Mass percentage averages of ammonium in PM 2.5.

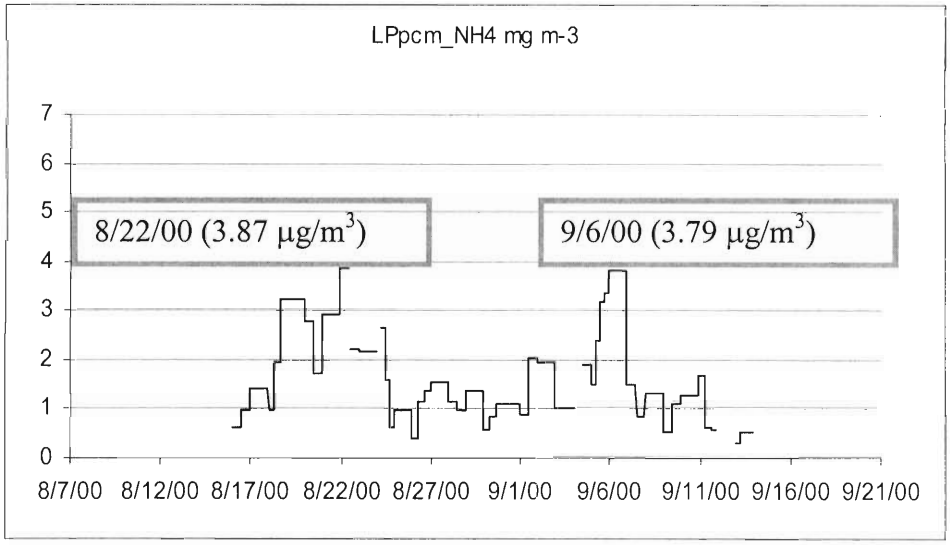

Figure 59. Ammonium concentration 30-minute averages ($\mu g/m^3$) in Sipsy Wilderness

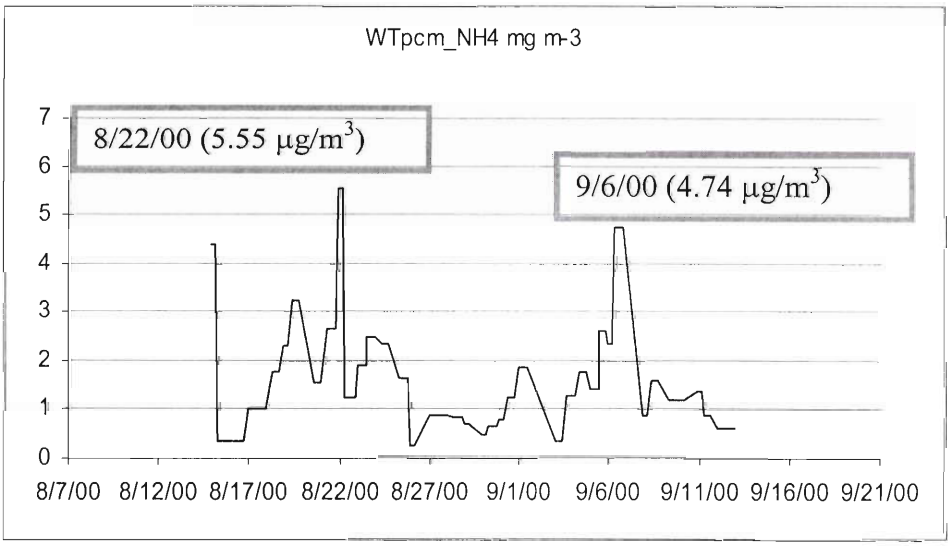

Figure 60. Ammonium concentration 30-minute averages ($\mu g/m^3$) in Sipsy Wilderness

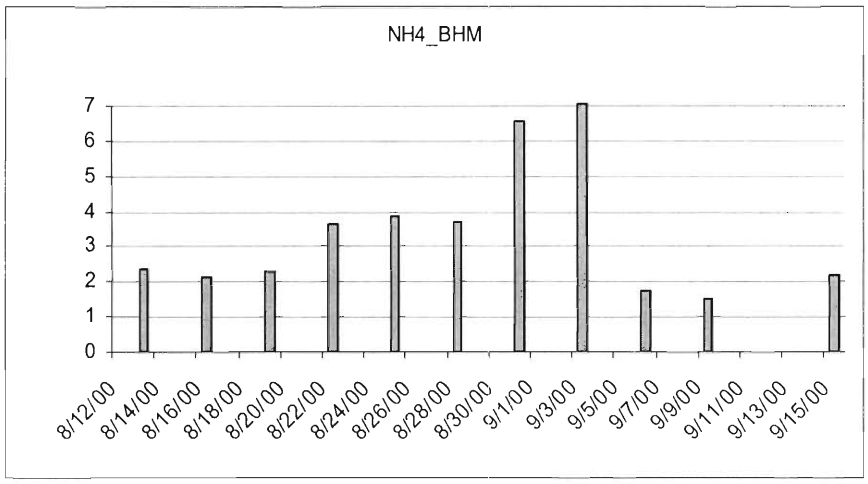

Figure 61. Ammonium concentration 24-hour averages ($\mu g/m^3$) in North Birmingham

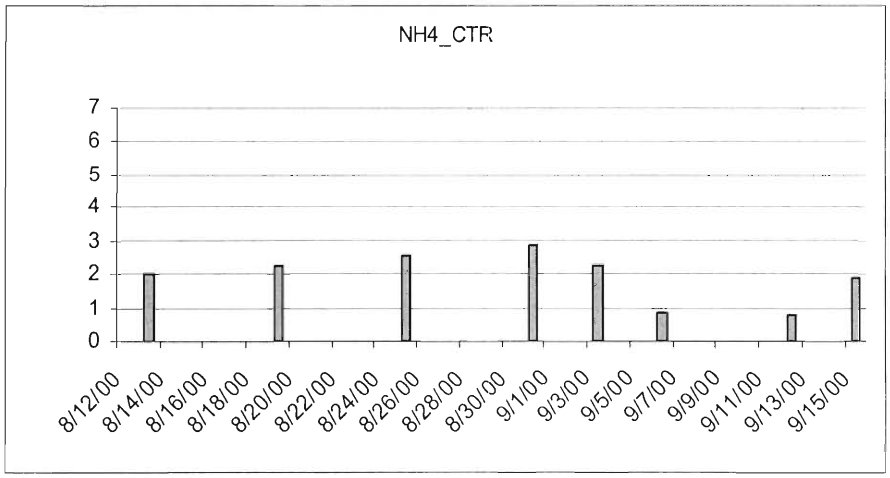

Figure 62. Ammonium concentration 24-hour averages ($\mu g/m^3$) in Centreville

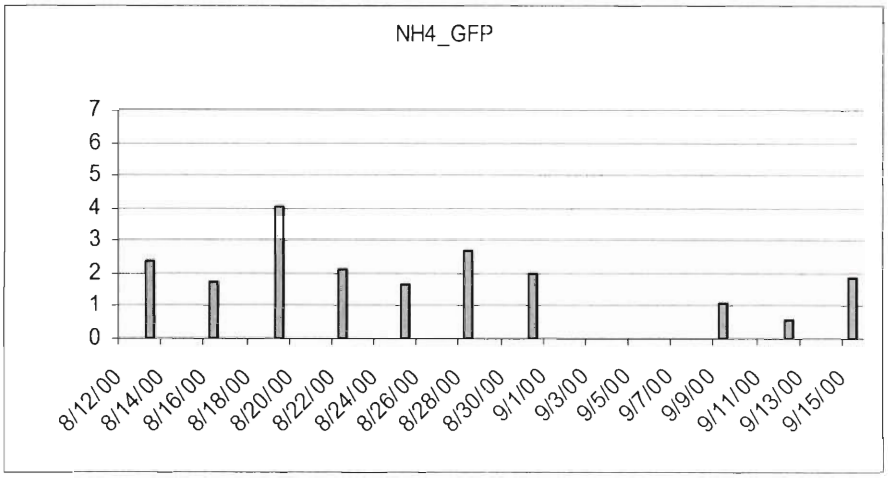

Figure 63. Ammonium concentration 24-hour averages ($\mu g/m^3$) in Gulfport

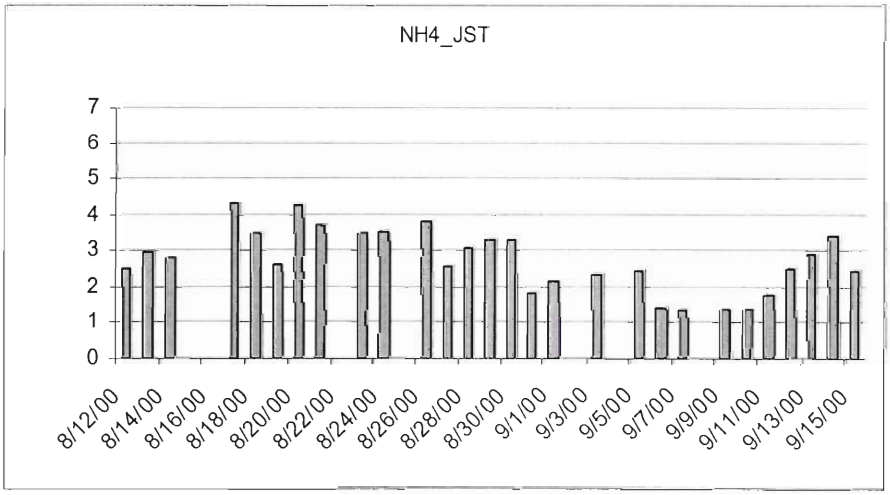

Figure 64. Ammonium concentration 24-hour averages ($\mu g/m^3$) in Jefferson Street

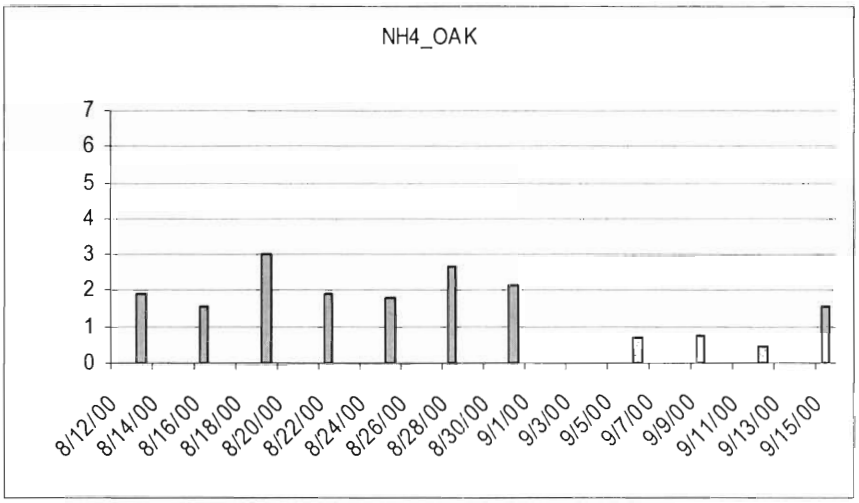

Figure 65. Ammonium concentration 24-hour averages ($\mu g/m^3$) in Oak Grove

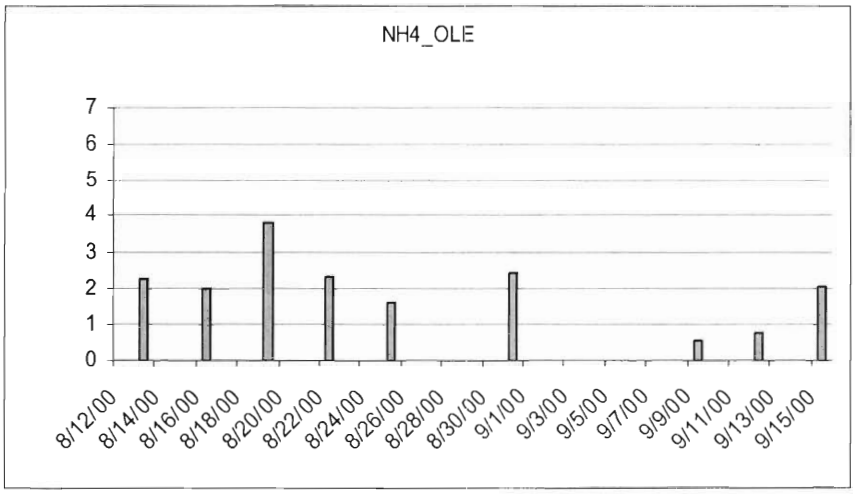

Figure 66. Ammonium concentration 24-hour averages ($\mu g/m^3$) in Pensacola (OLE)

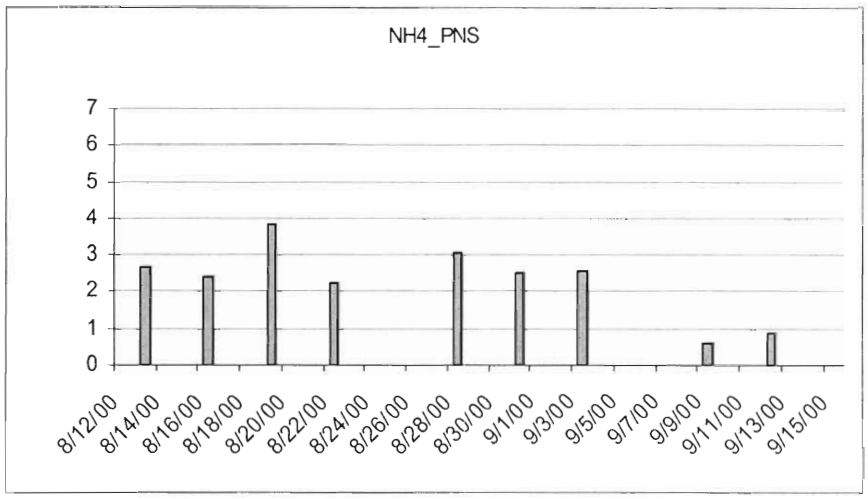

Figure 67. Ammonium concentration 24-hour averages ($\mu g/m^3$) in Pensacola (PNS)

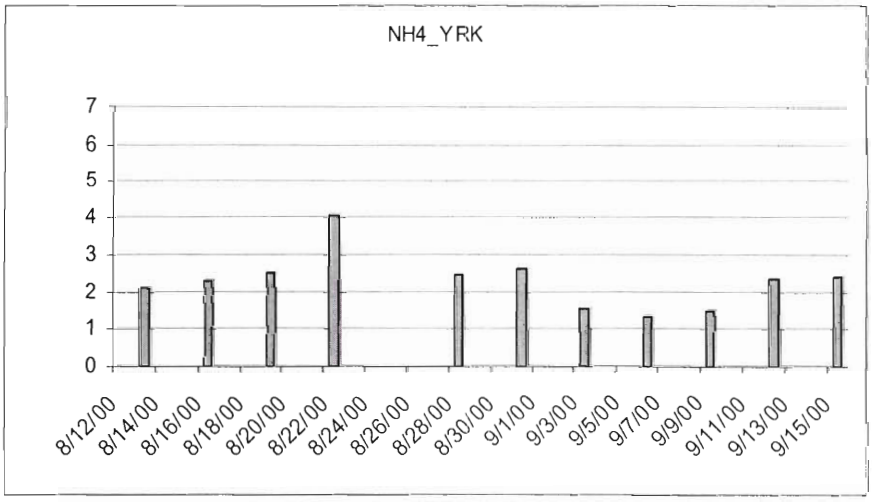

Figure 68. Ammonium concentration 24-hour averages ($\mu g/m^3$) in Yorkville

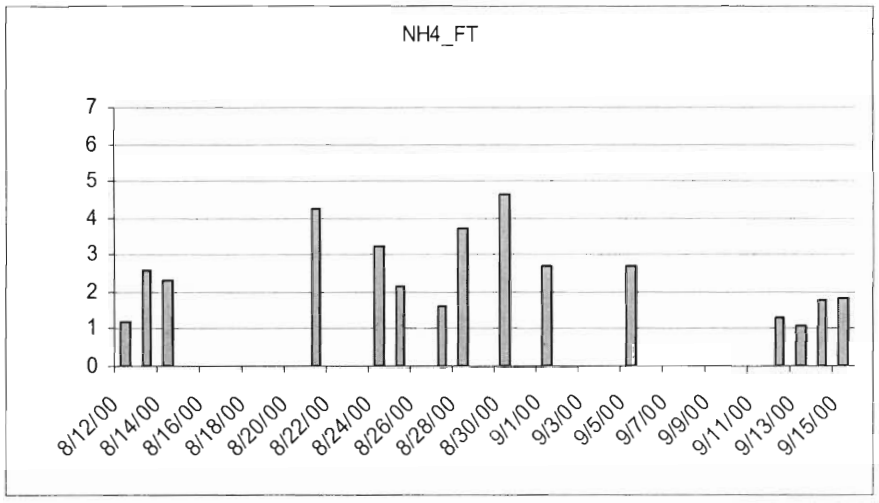

Figure 69. Ammonium concentration 24-hour averages ($\mu g/m^3$) in Fort McPherson

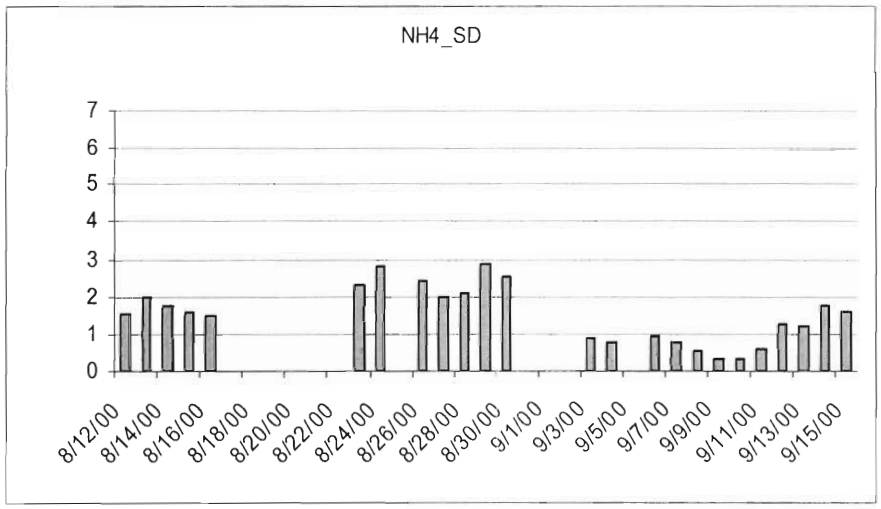

Figure 70. Ammonium concentration 24-hour averages ($\mu g/m^3$) in South Dekalb

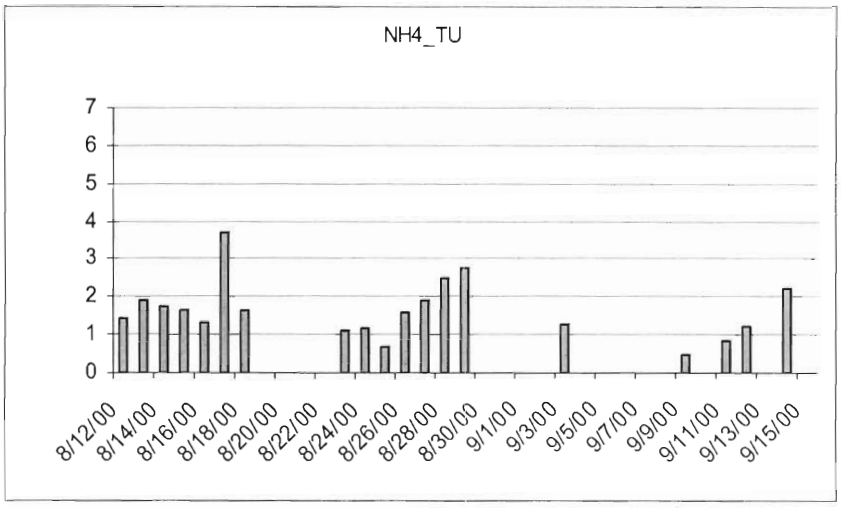

Figure 71. Ammonium concentration 24-hour averages ($\mu g/m^3$) in Tucker

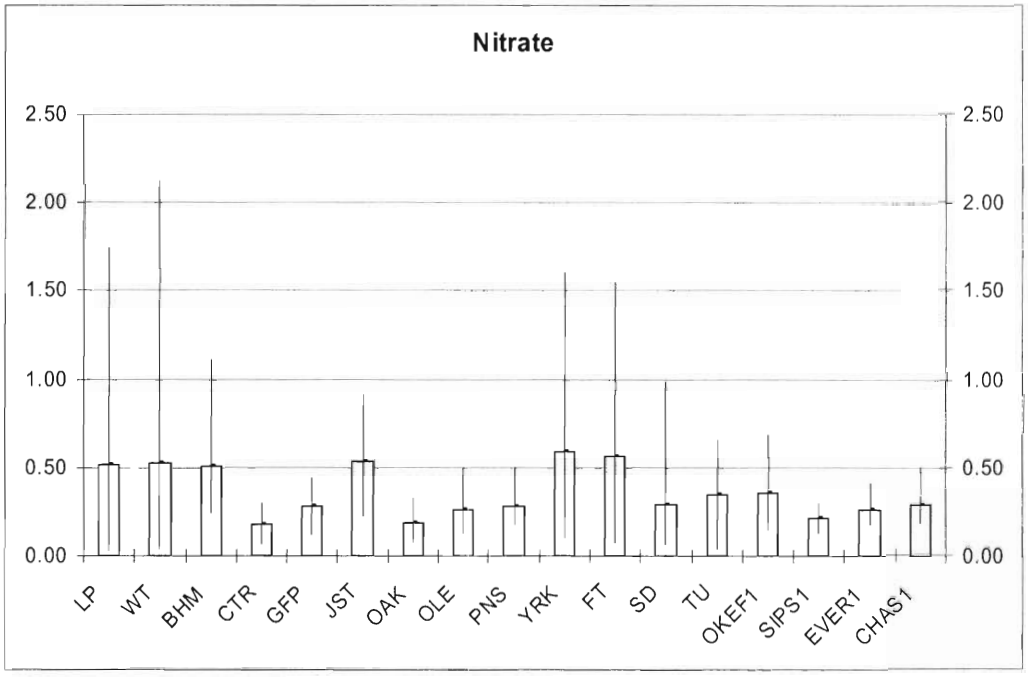

Figure 72. Maximums, minimums and averages of nitrate concentrations 24-hour averages ($\mu g/m^3$) from August 12 to September 15, 2000

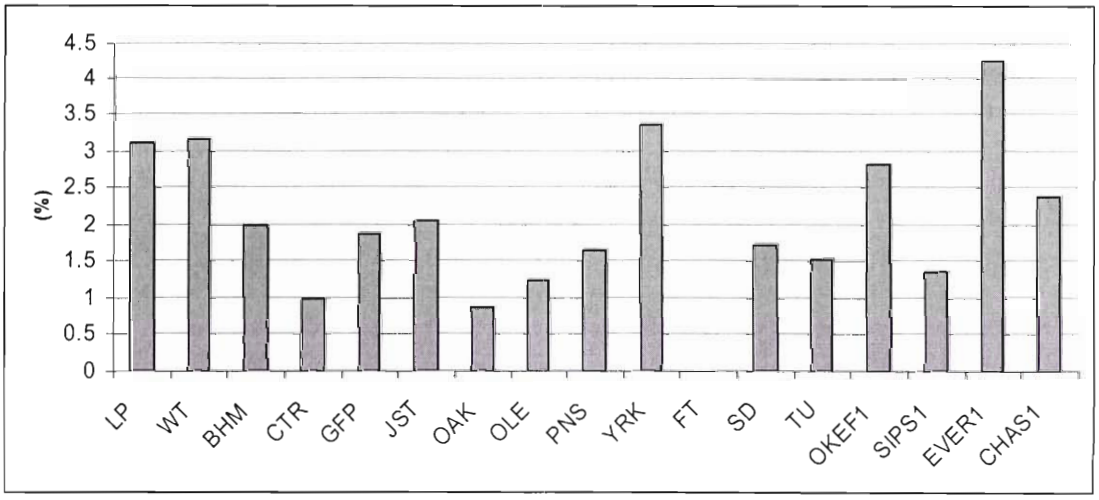

Figure 73. Mass percentage averages of nitrate in PM 2.5.

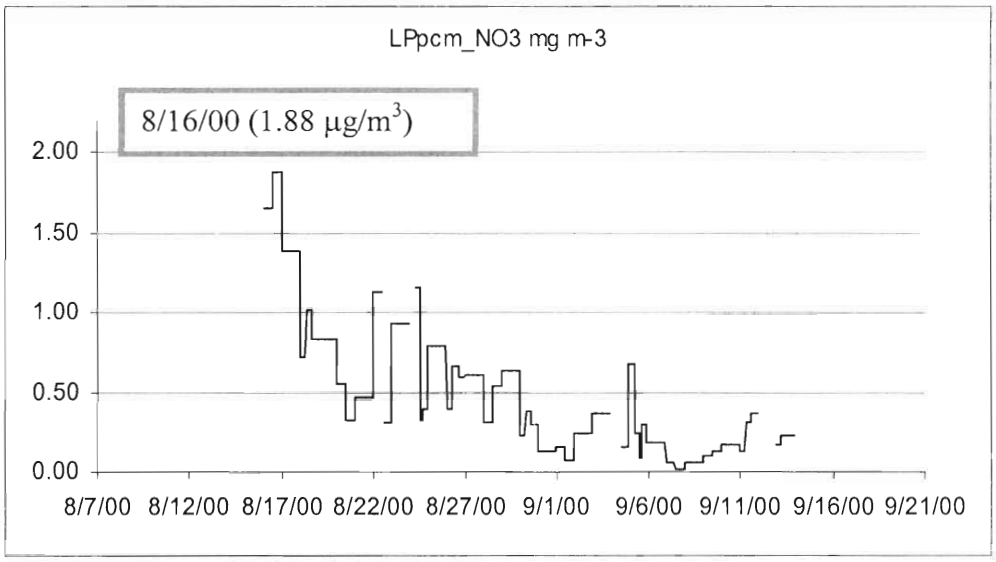

Figure 74. Nitrate concentration 30-minute averages ($\mu g/m^3$) in La Porte

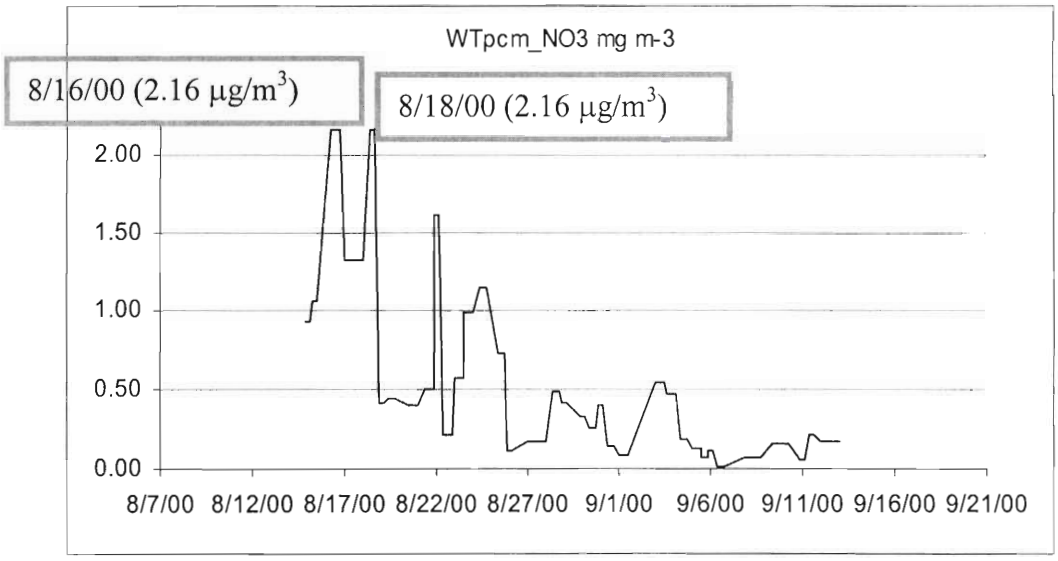

Figure 75. Nitrate concentration 30-minute averages ($\mu g/m^3$) in Williams Tower

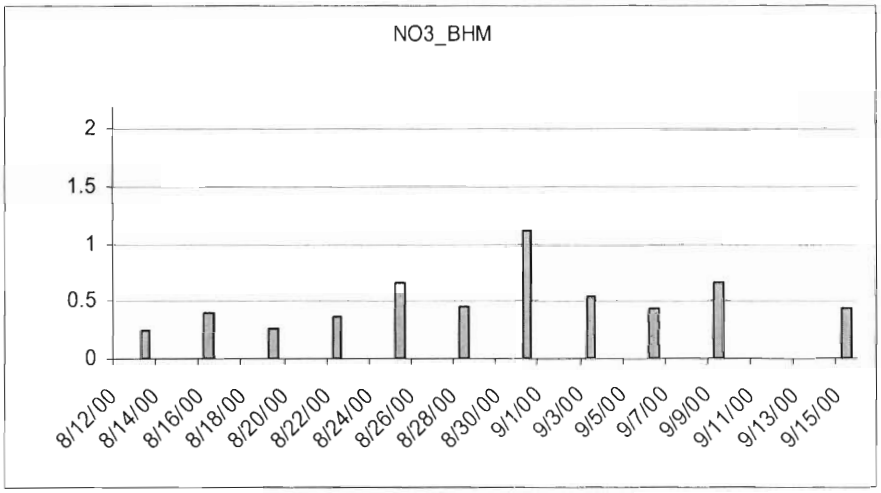

Figure 76. Nitrate concentration 24-hour averages ($\mu g/m^3$) in North Birmingham

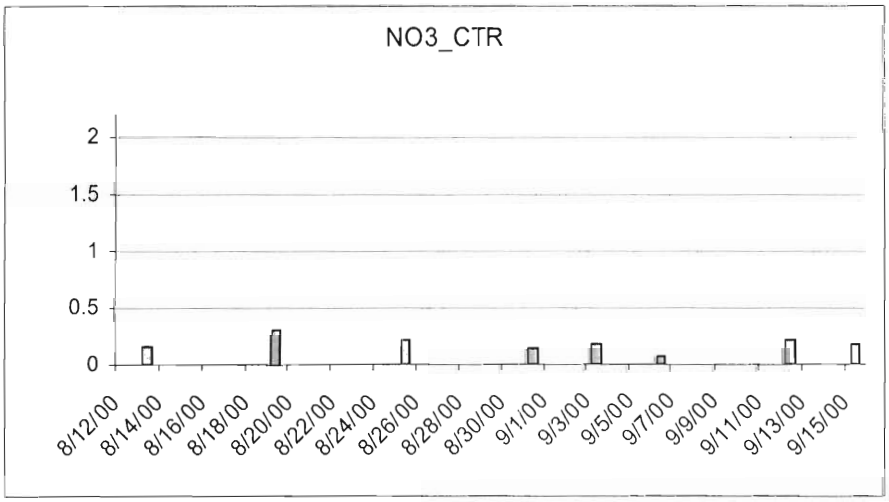

Figure 77. Nitrate concentration 24-hour averages ($\mu g/m^3$) in Centreville

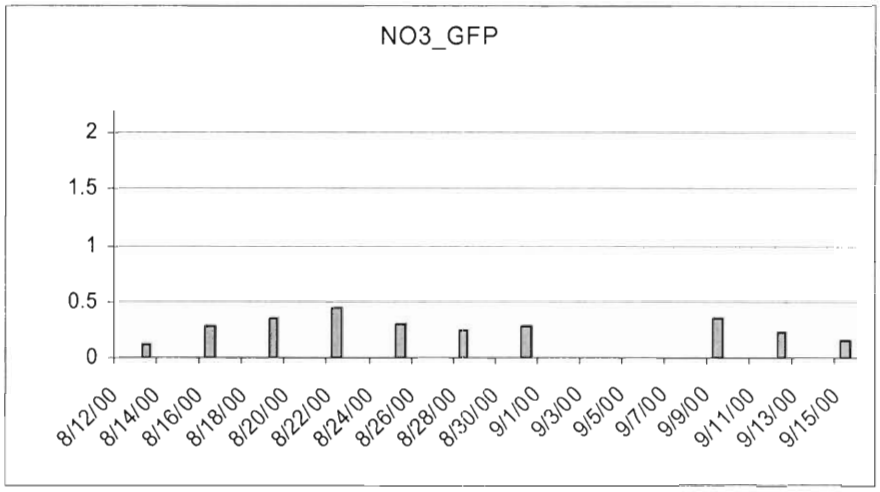

Figure 78. Nitrate concentration 24-hour averages ($\mu g/m^3$) in Gulfport

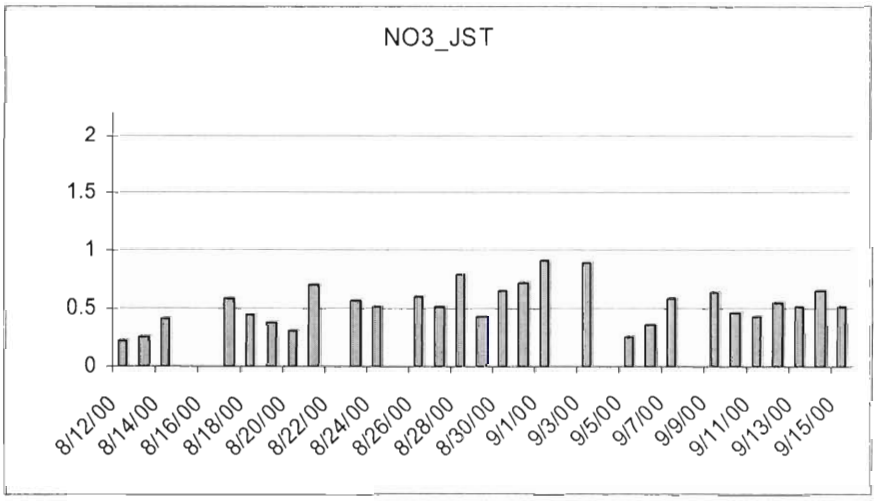

Figure 79. Nitrate concentration 24-hour averages ($\mu g/m^3$) in Jefferson Street

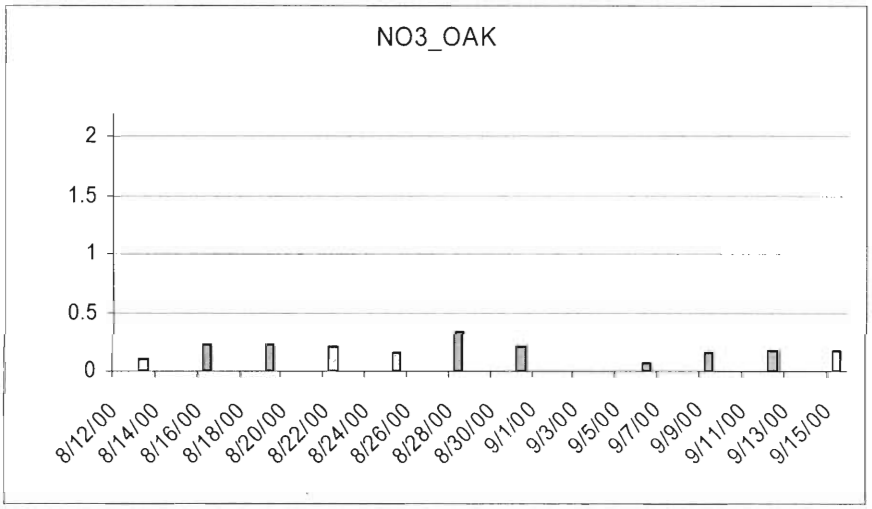

Figure 80. Nitrate concentration 24-hour averages ($\mu g/m^3$) in Oak Grove

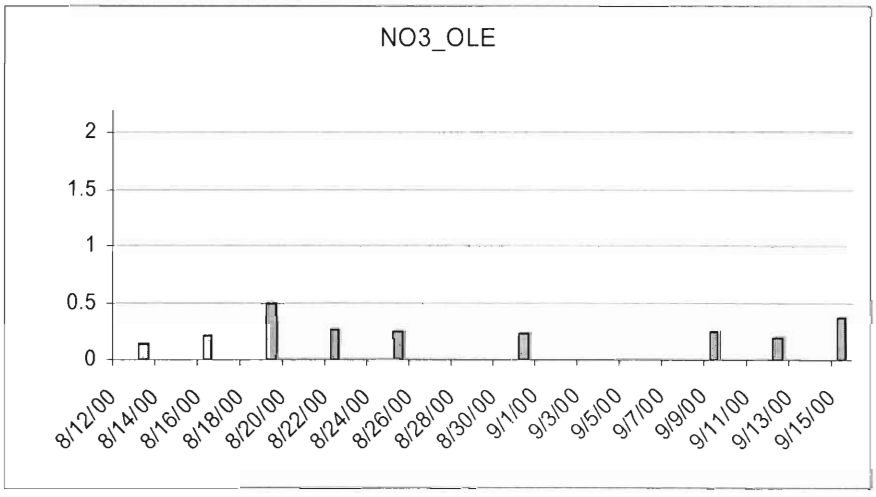

Figure 81. Nitrate concentration 24-hour averages ($\mu g/m^3$) in Pensacola (OLE)

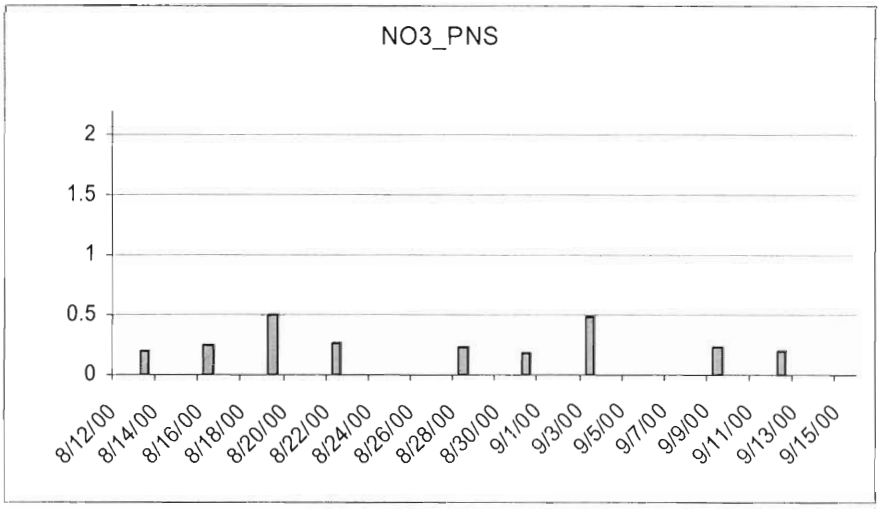

Figure 82. Nitrate concentration 24-hour averages ($\mu g/m^3$) in Pensacola (PNS)

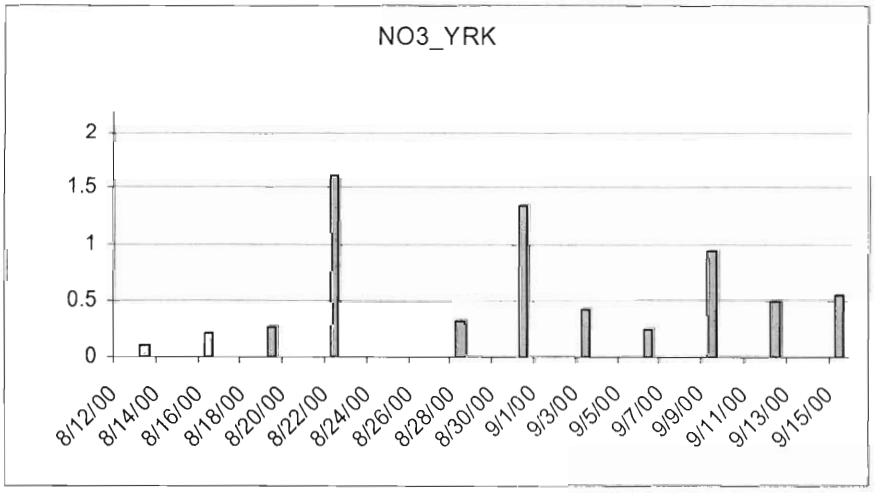

Figure 83. Nitrate concentration 24-hour averages ($\mu g/m^3$) in Yorkville

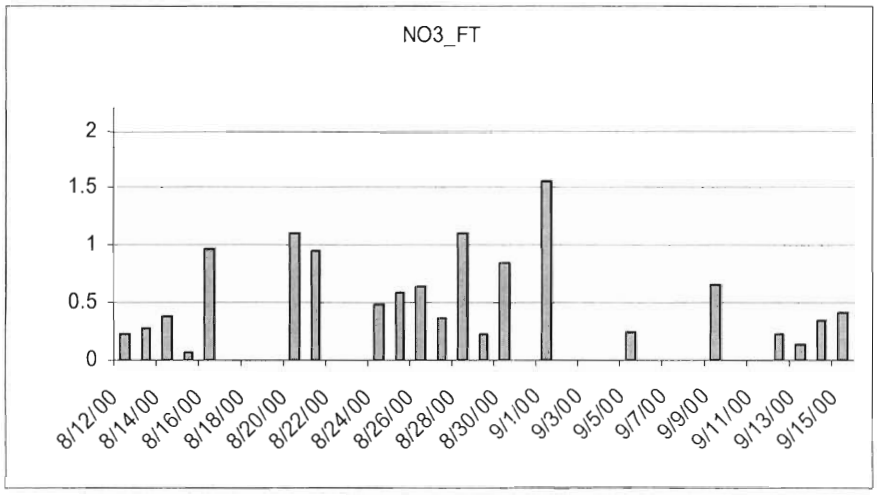

Figure 84. Nitrate concentration 24-hour averages ($\mu g/m^3$) in Fort McPherson

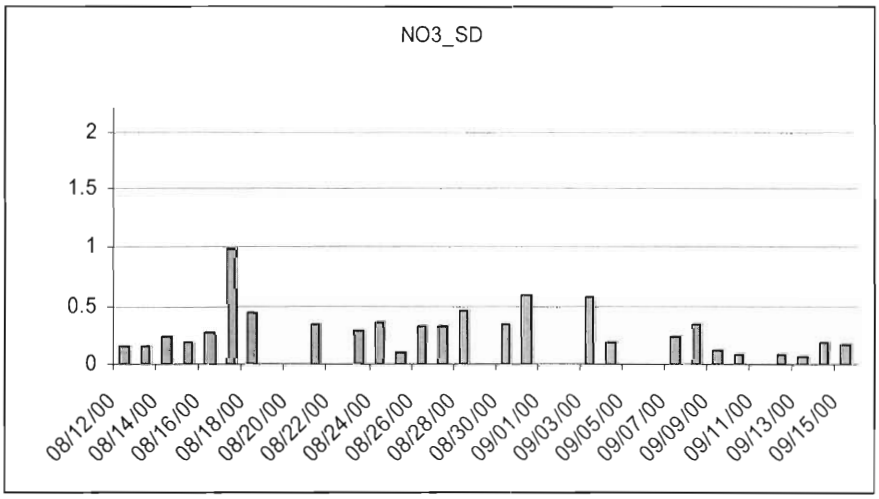

Figure 85. Nitrate concentration 24-hour averages ($\mu g/m^3$) in South Dekalb

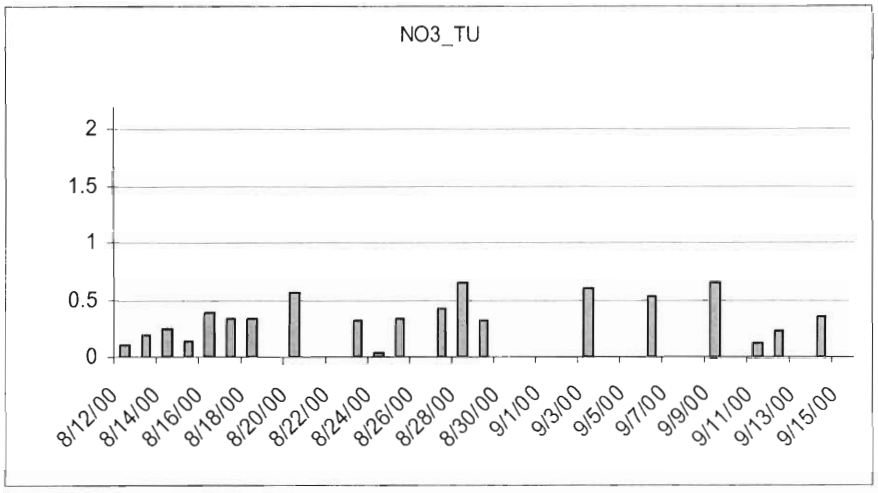

Figure 86. Nitrate concentration 24-hour averages ($\mu g/m^3$) in Tucker

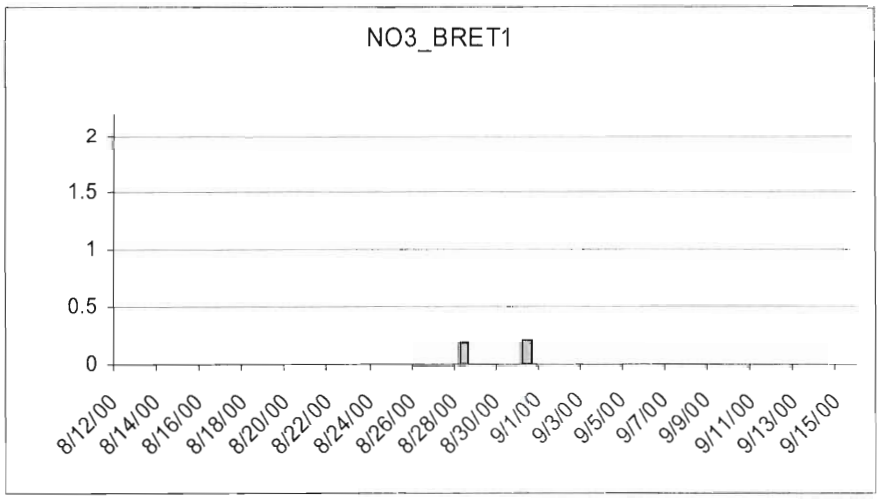

Figure 87. Nitrate concentration 24-hour averages ($\mu g/m^3$) in Breton

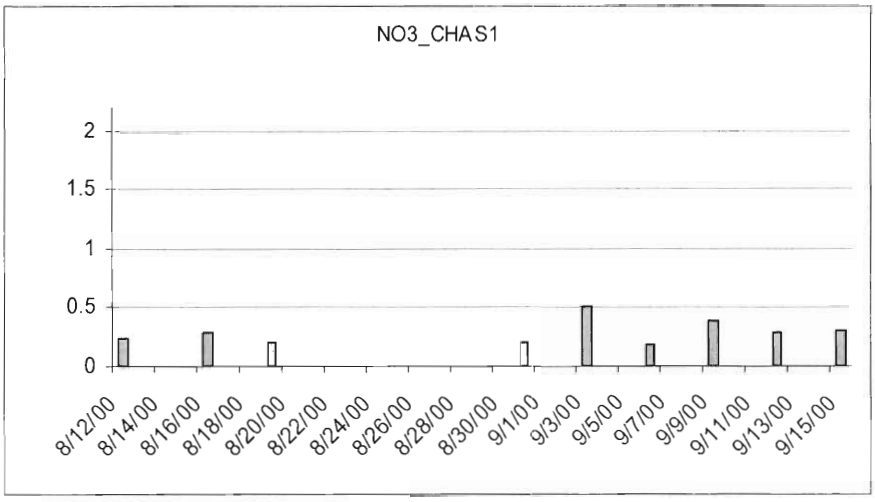

Figure 88. Nitrate concentration 24-hour averages ($\mu g/m^3$) in Chassahowitzka National Wildlife

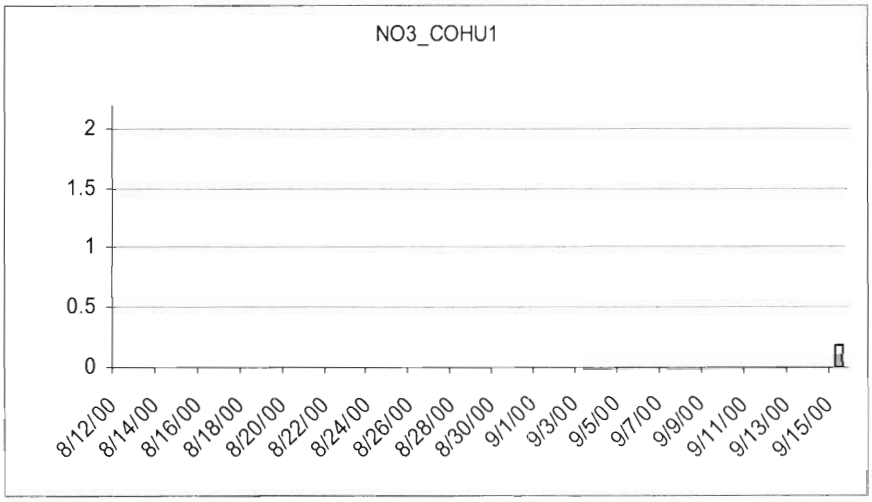

Figure 89. Nitrate concentration 24-hour averages ($\mu g/m^3$) in Cohutta

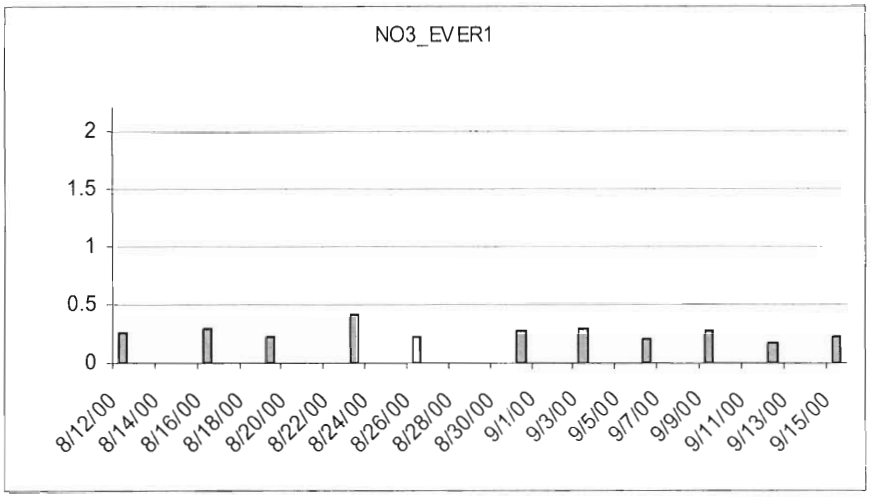

Figure 90. Nitrate concentration 24-hour averages ($\mu g/m^3$) in Everglades National Park

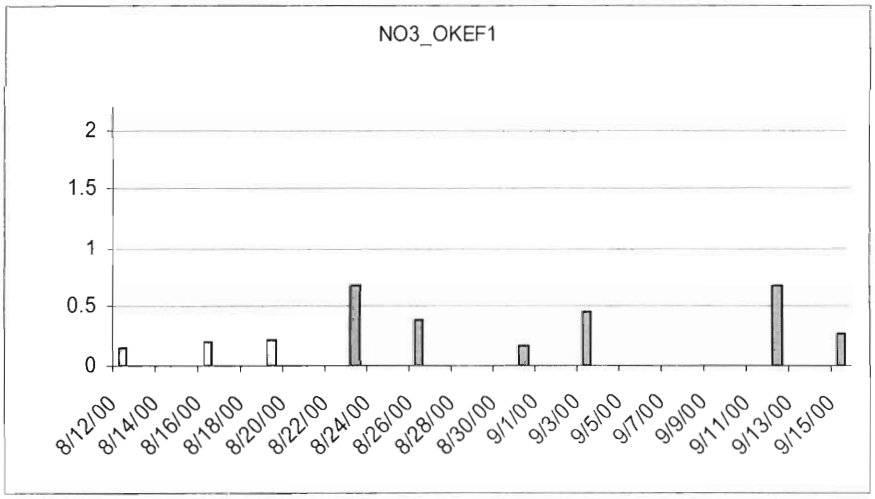

Figure 91. Nitrate concentration 24-hour averages ($\mu g/m^3$) in Okefenokee National Wildlife Refuge

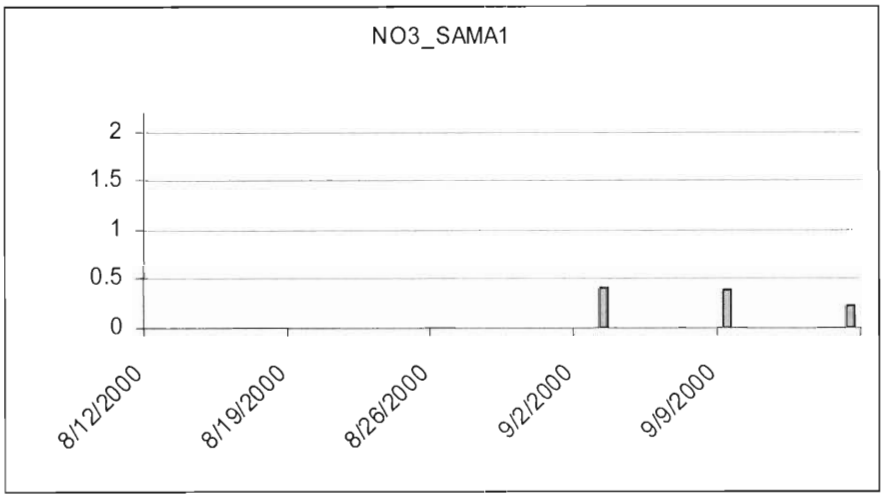

Figure 92. Nitrate concentration 24-hour averages ($\mu g/m^3$) in St Marks

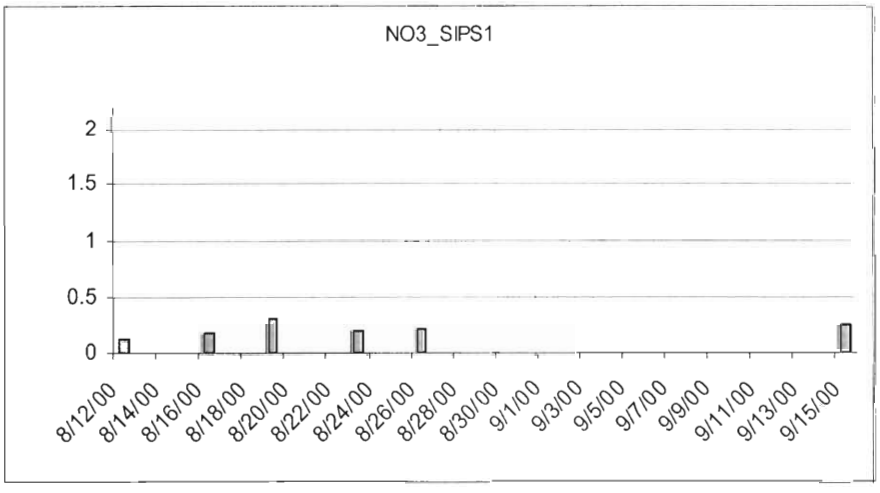

Figure 93. Nitrate concentration 24-hour averages ($\mu g/m^3$) in Sipsy Wilderness

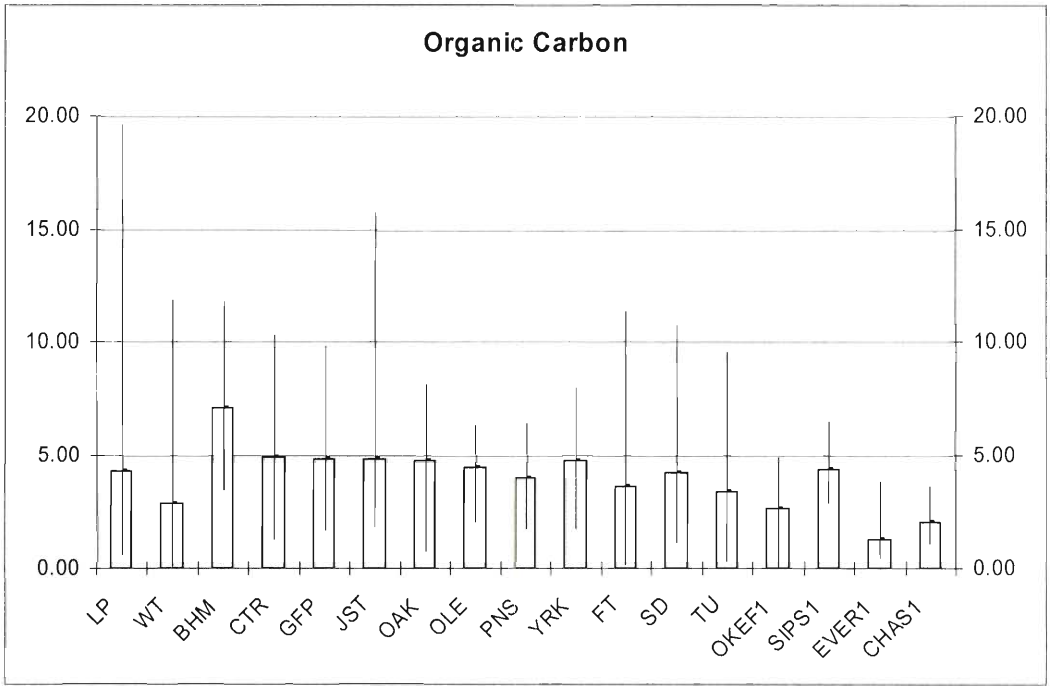

Figure 94. Maximums, minimums and averages of organic carbon concentrations 24-hour averages ($\mu g/m^3$) from August 12 to September 15, 2000

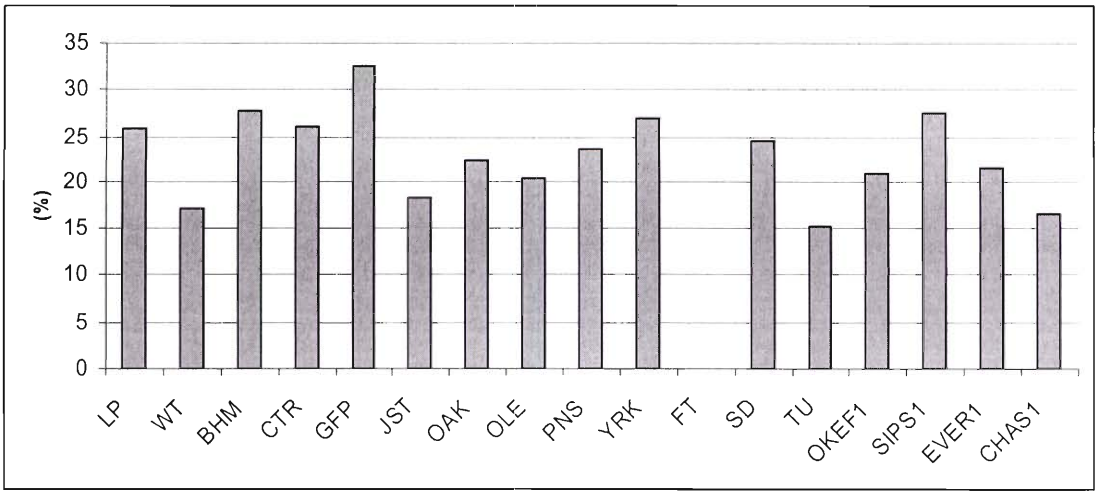

Figure 95. Mass percentage averages of organic carbon in PM 2.5.

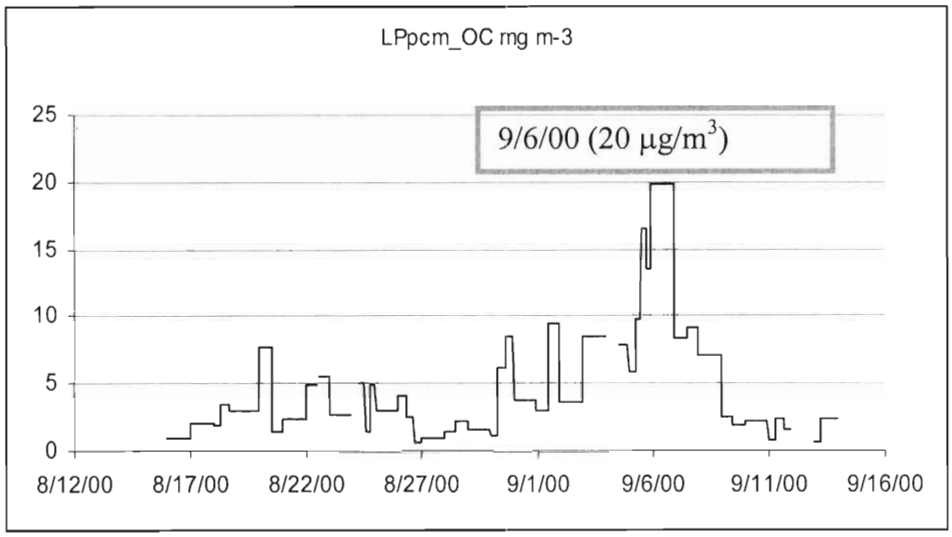

Figure 96. Organic carbon concentration 30-minute averages ($\mu g/m^3$) in La Porte

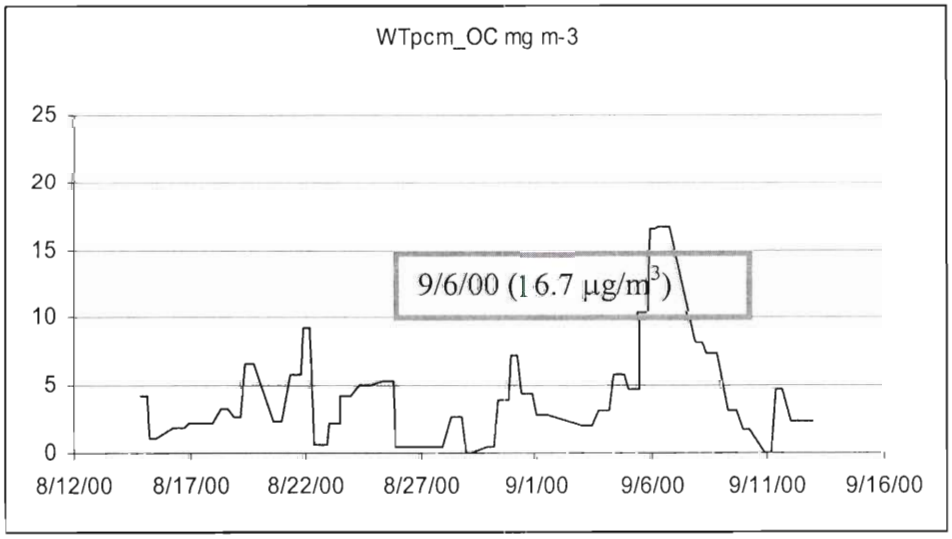

Figure 97. Organic carbon concentration 30-minute averages ($\mu g/m^3$) in Williams Tower

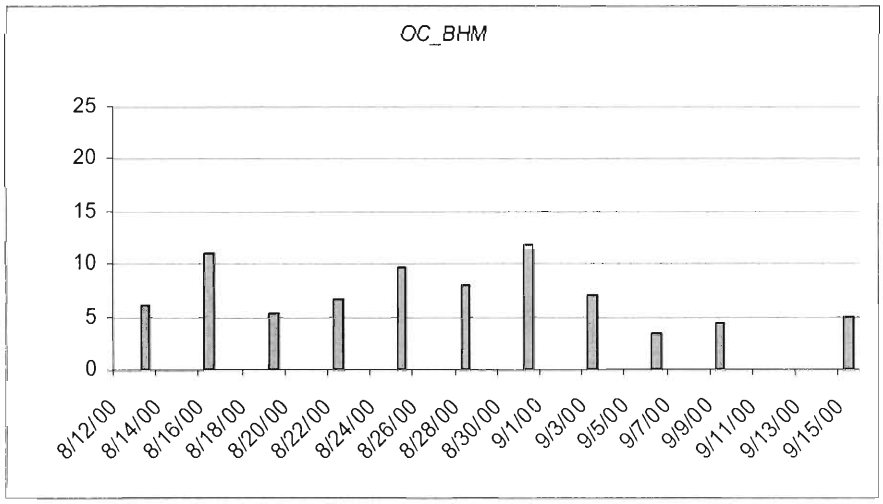

Figure 98. Organic carbon concentration 24-hour averages ($\mu g/m^3$) in North Birmingham

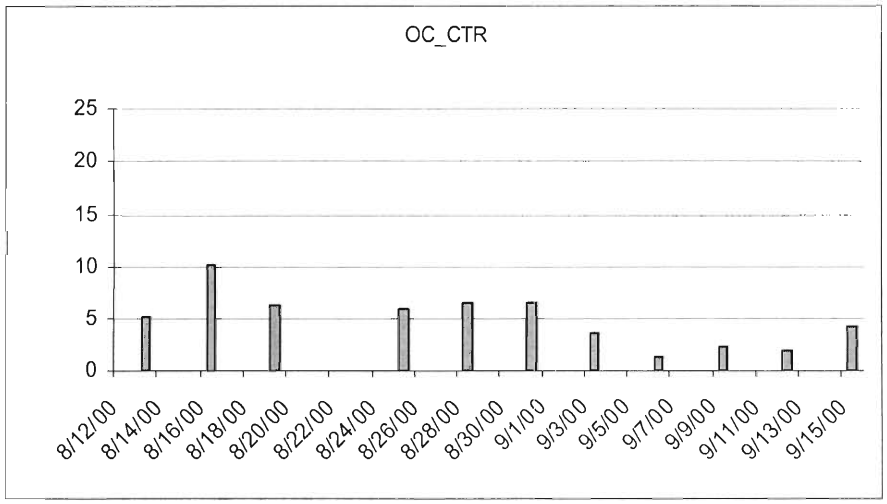

Figure 99. Organic carbon concentration 24-hour averages ($\mu g/m^3$) in Centreville

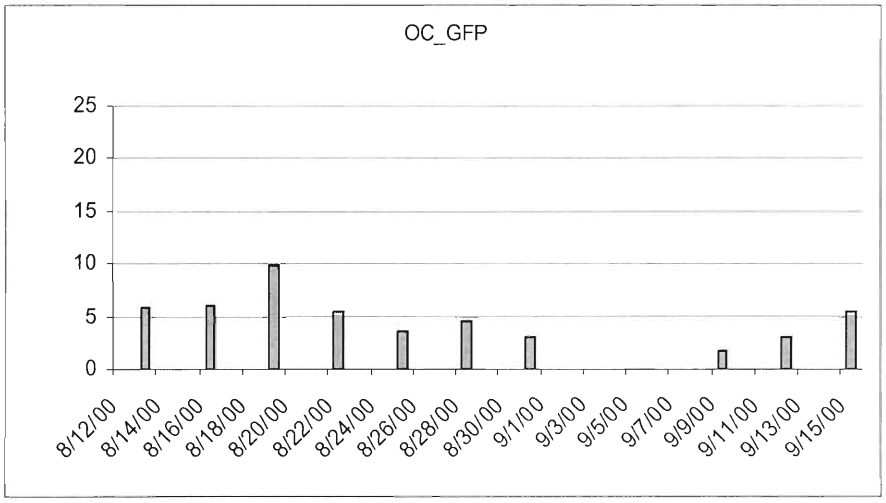

Figure 100. Organic carbon concentration 24-hour averages ($\mu g/m^3$) in Gulfport

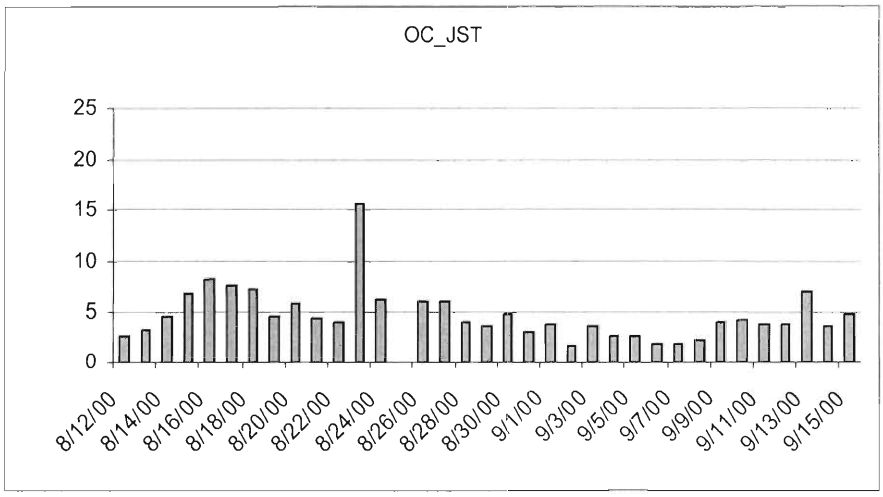

Figure 101. Organic carbon concentration 24-hour averages ($\mu g/m^3$) in Jefferson Street

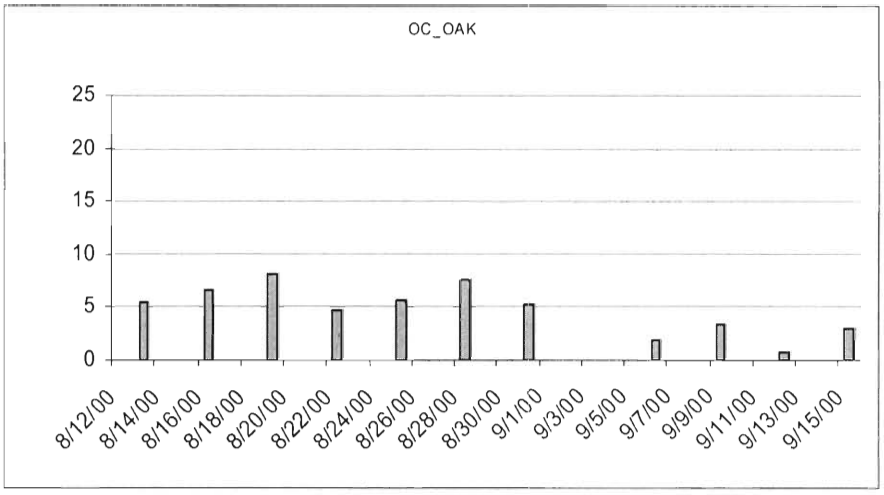

Figure 102. Organic carbon concentration 24-hour averages ($\mu g/m^3$) in Oak Grove

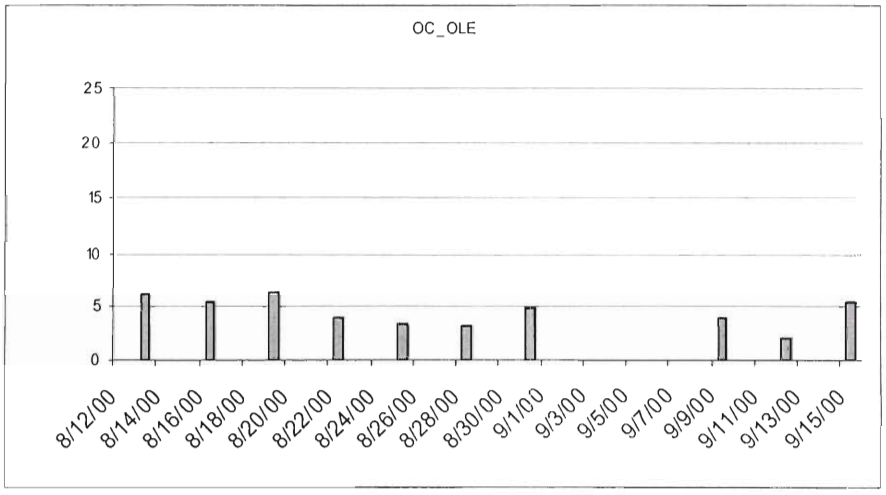

Figure 103. Organic carbon concentration 24-hour averages ($\mu g/m^3$) in Pensacola (OLE)

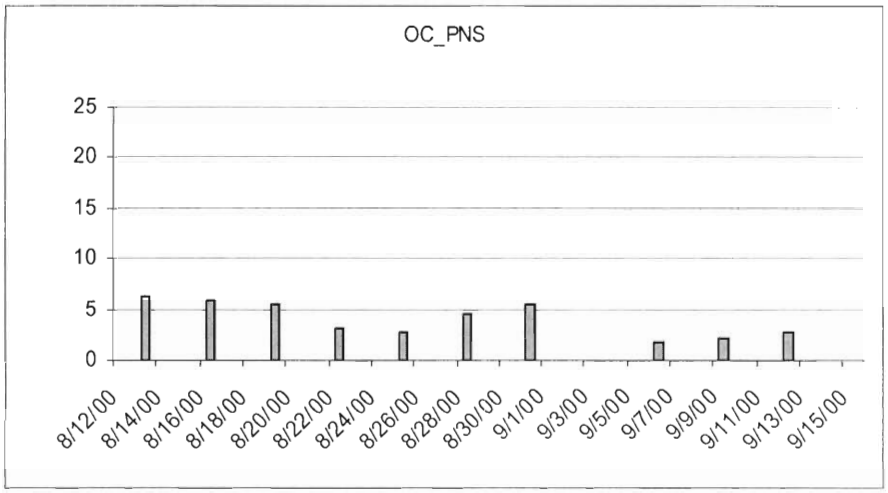

Figure 104. Organic carbon concentration 24-hour averages ($\mu g/m^3$) in Pensacola (PNS)

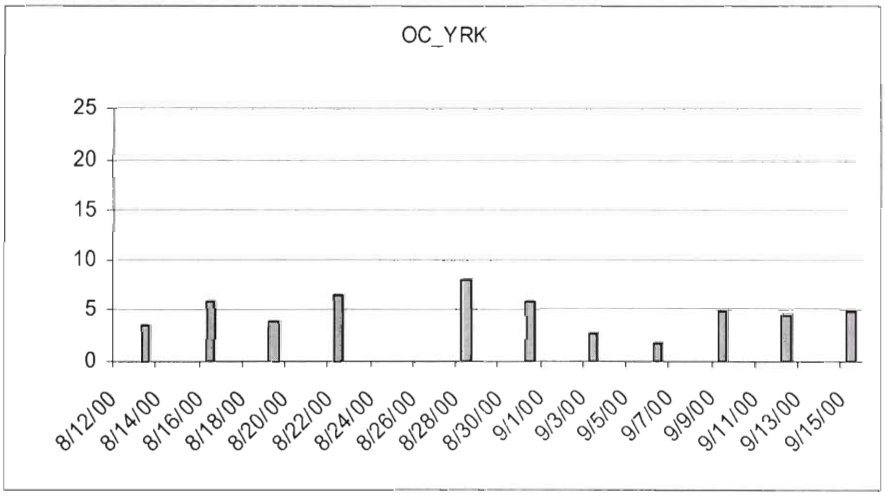

Figure 105. Organic carbon concentration 24-hour averages ($\mu g/m^3$) in Yorkville

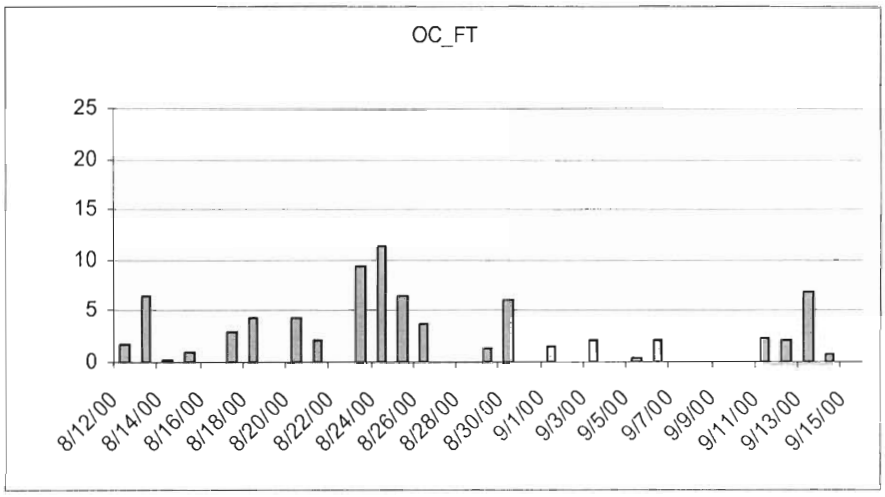

Figure 106. Organic carbon concentration 24-hour averages ($\mu g/m^3$) in Fort McPherson

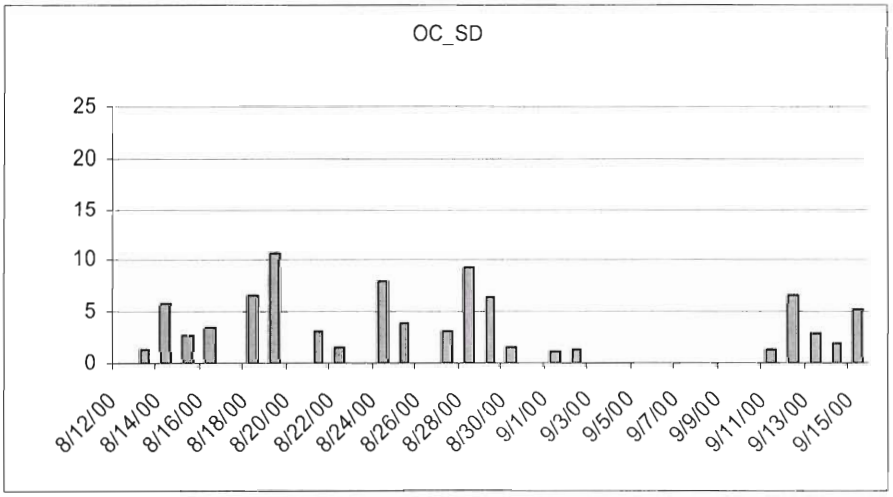

Figure 107. Organic carbon concentration 24-hour averages ($\mu g/m^3$) in South Dekalb

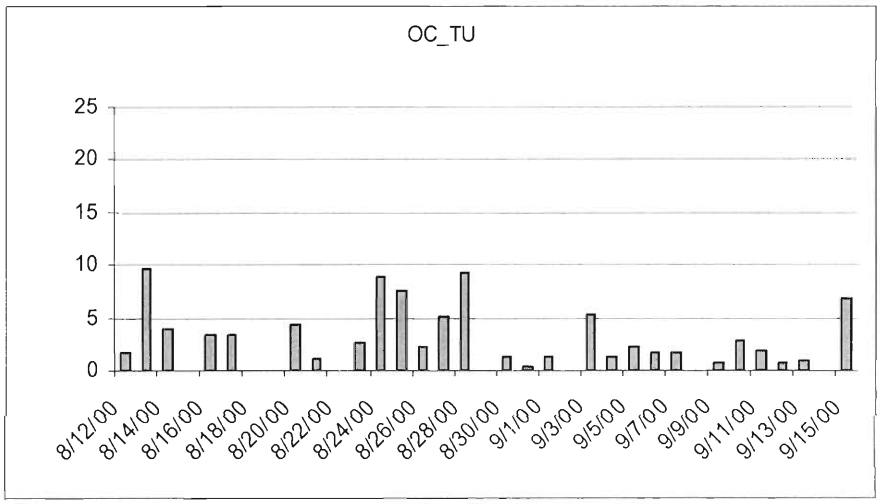

Figure 108. Organic carbon concentration 24-hour averages ($\mu g/m^3$) in Tucker

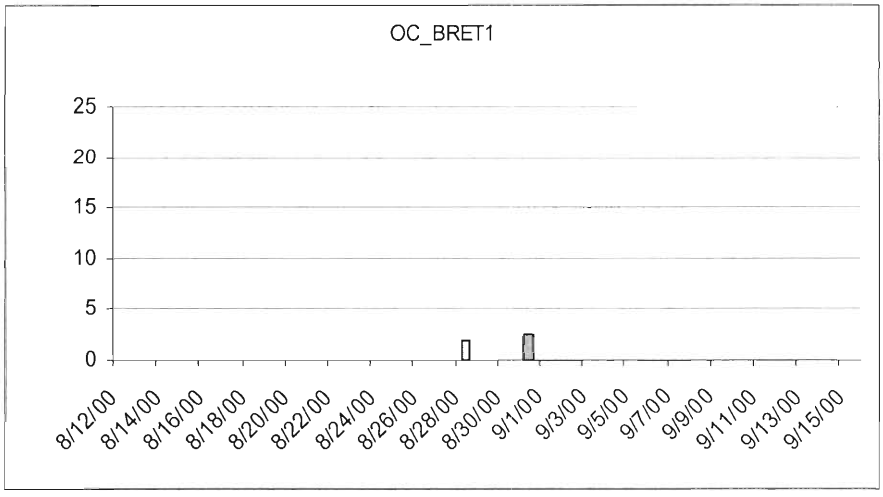

Figure 109. Organic carbon concentration 24-hour averages ($\mu g/m^3$) in Breton

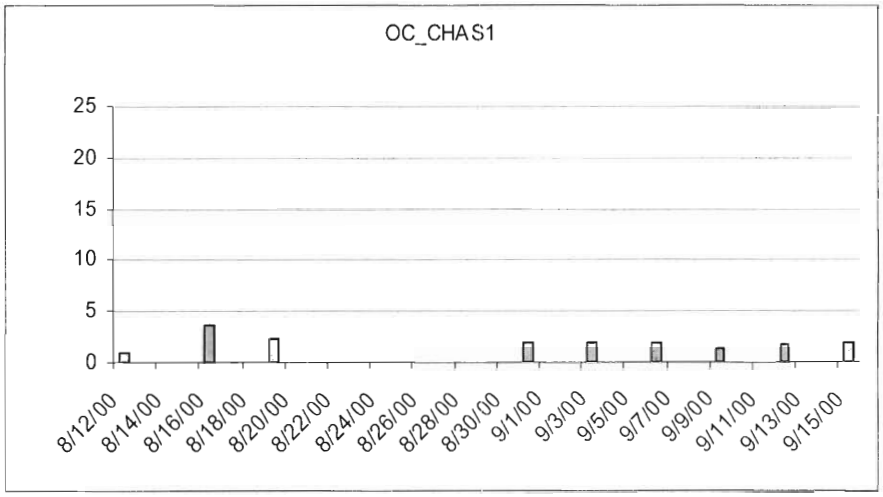

Figure 110. Organic carbon concentration 24-hour averages ($\mu g/m^3$) in Chassahowitzka National Wildlife

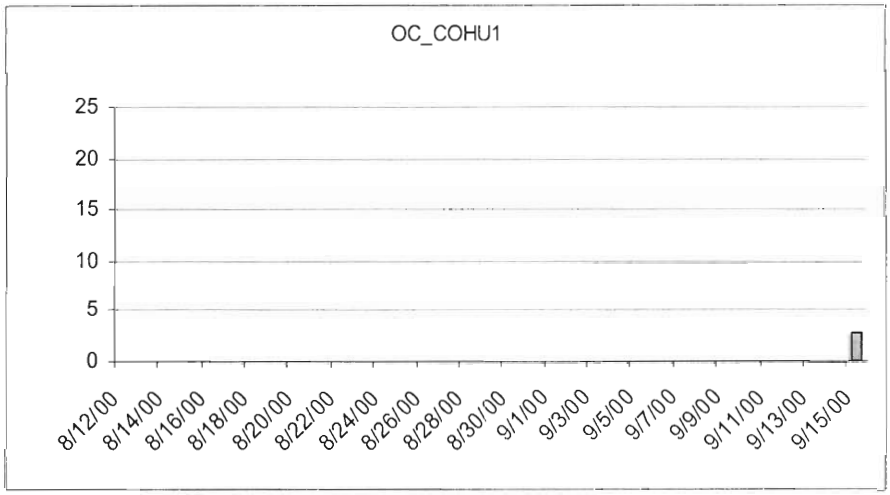

Figure 111. Organic carbon concentration 24-hour averages ($\mu g/m^3$) in Cohutta

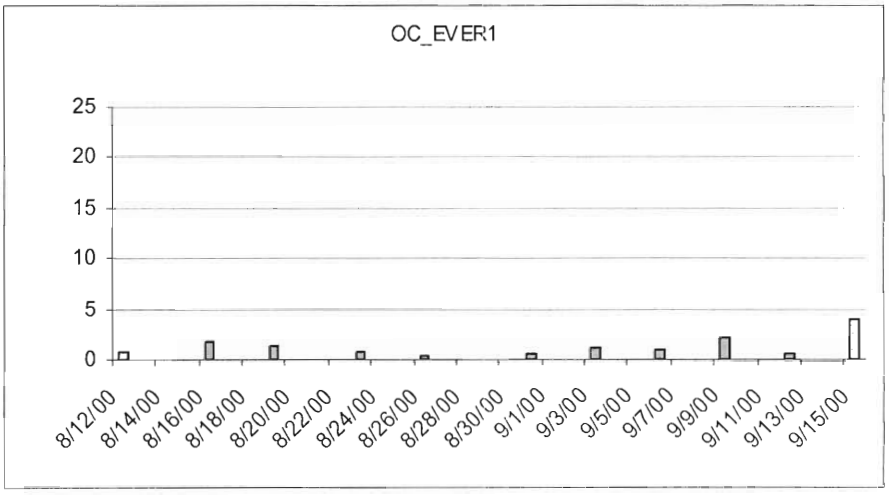

Figure 112. Organic carbon concentration 24-hour averages ($\mu g/m^3$) in Everglades National Park

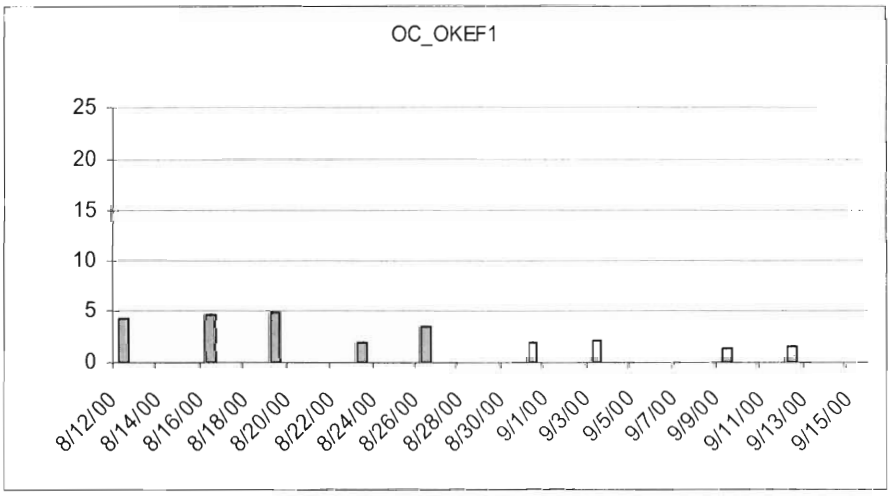

Figure 113. Organic carbon concentration 24-hour averages ($\mu g/m^3$) in Okefenokee National Wildlife Refuge

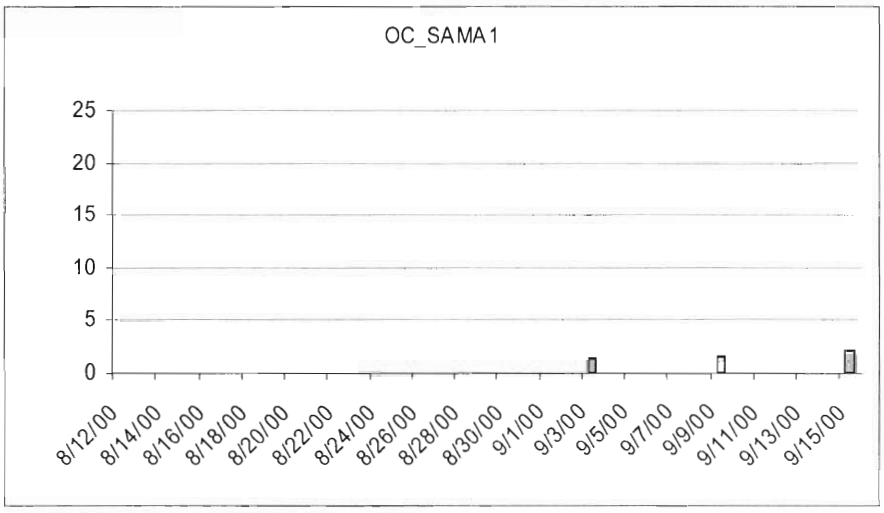

Figure 114. Organic carbon concentration 24-hour averages ($\mu g/m^3$) in St. Marks

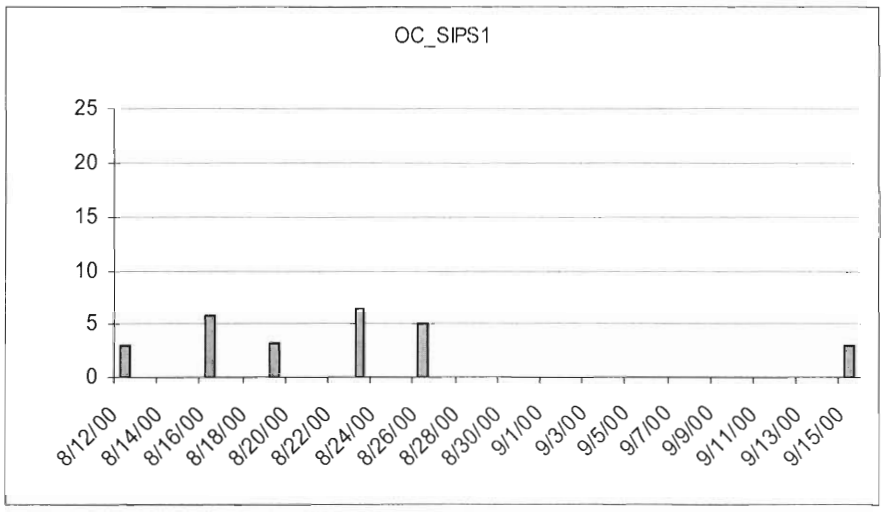

Figure 115. Organic carbon concentration 24-hour averages ($\mu g/m^3$) in Sipsy Wilderness

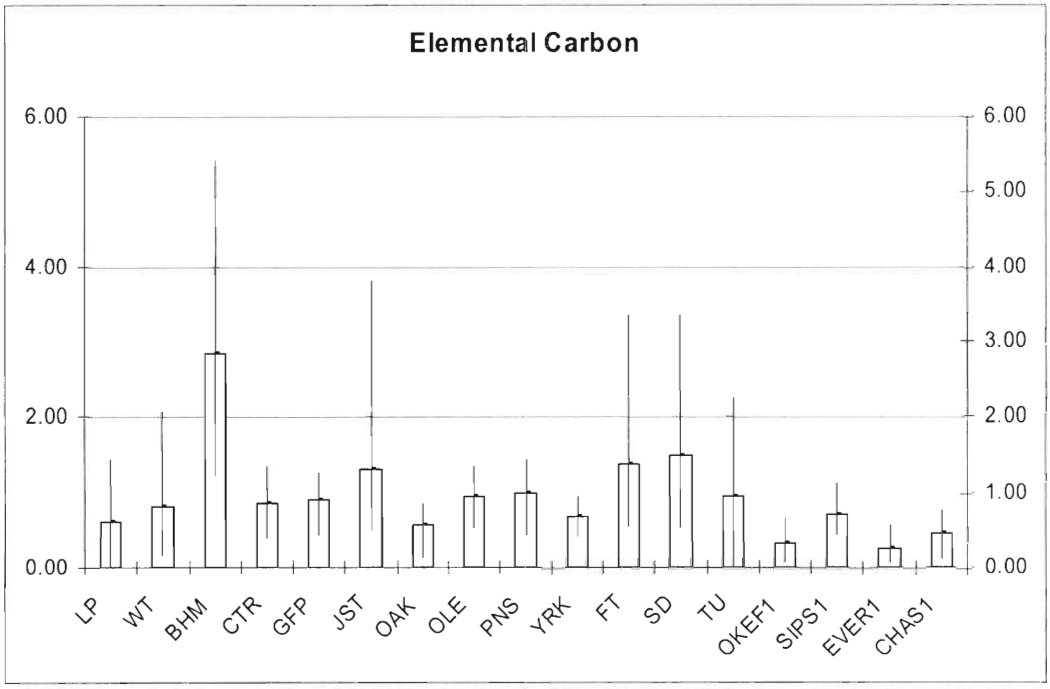

Figure 116. Maximums, minimums and averages of elemental carbon concentrations 24-hour averages ($\mu g/m^3$) from August 12 to September 15, 2000

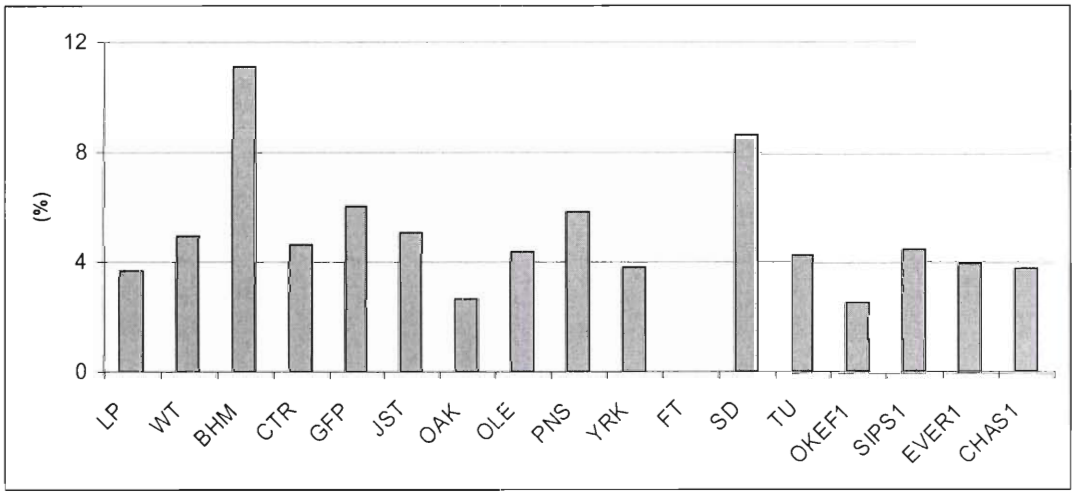

Figure 117. Mass percentage averages of elemental carbon in PM 2.5.

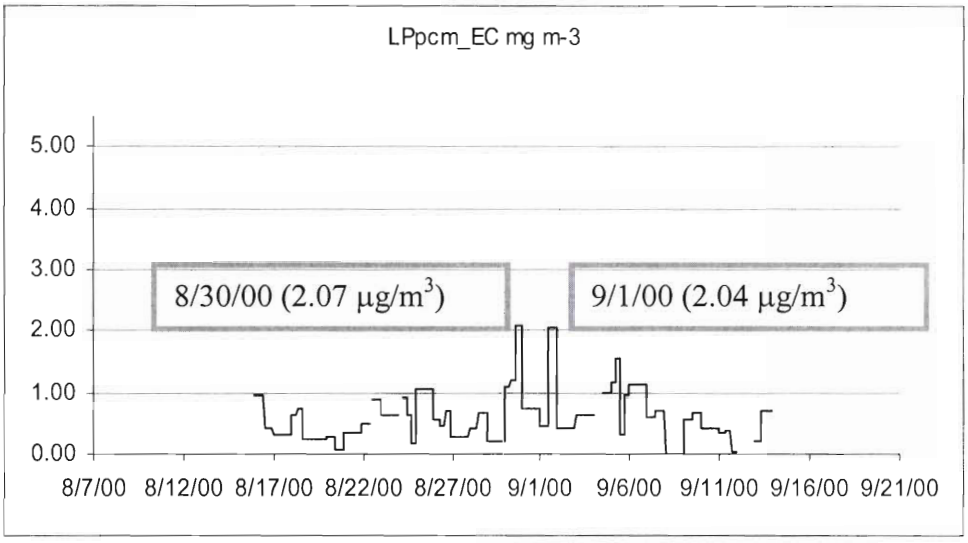

Figure 118. Elemental carbon concentration 30-minute averages ($\mu g/m^3$) in La Porte

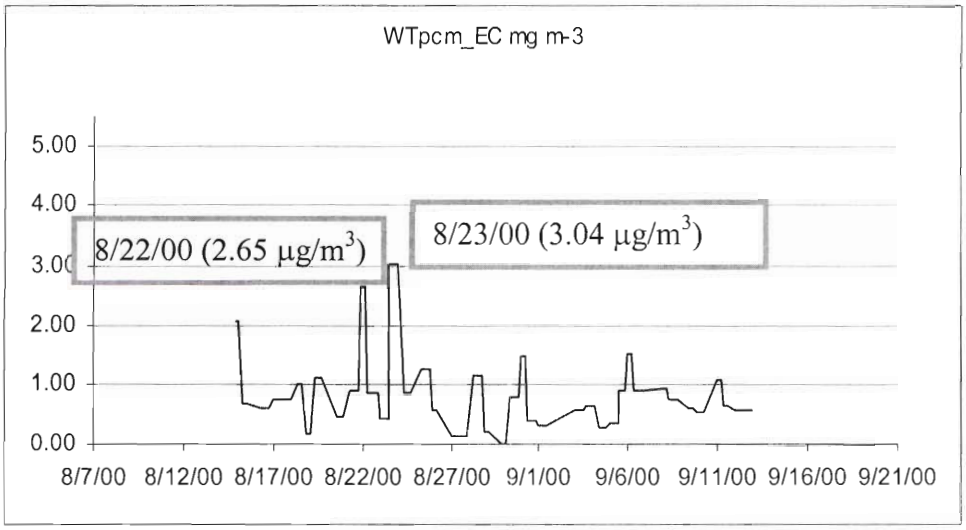

Figure 119. Elemental carbon concentration 30-minute averages ($\mu g/m^3$) in Williams Tower

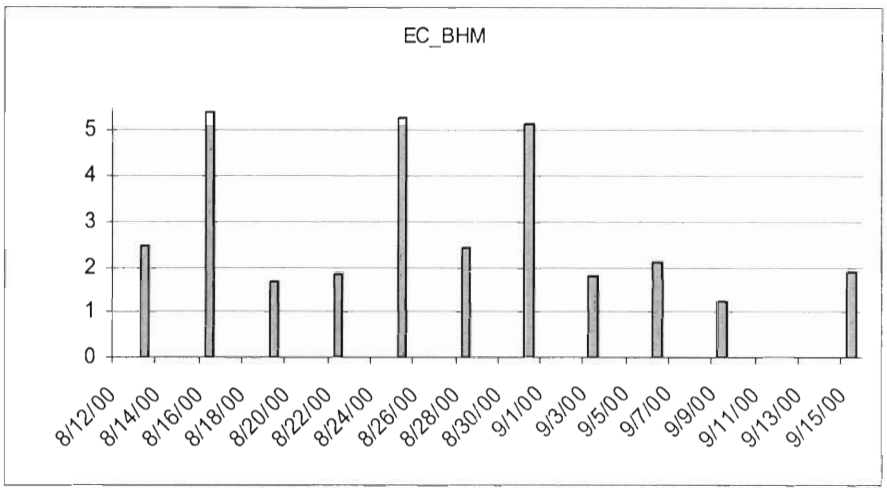

Figure 120. Elemental carbon concentration 24-hour averages ($\mu g/m^3$) in North Birmingham

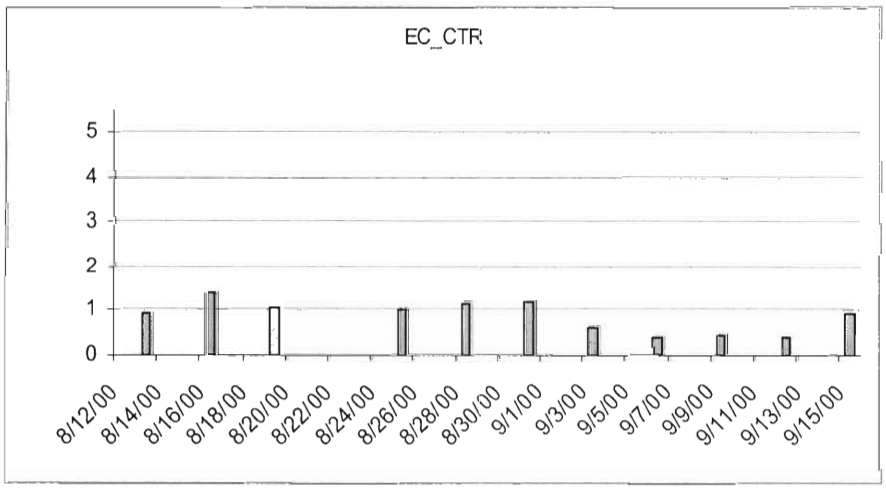

Figure 121. Elemental carbon concentration 24-hour averages ($\mu g/m^3$) in Centreville

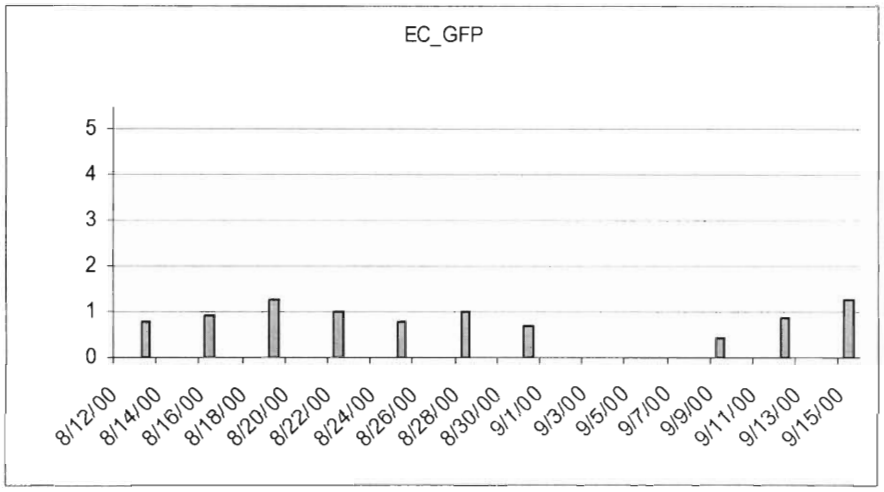

Figure 122. Elemental carbon concentration 24-hour averages ($\mu g/m^3$) in Gulfport

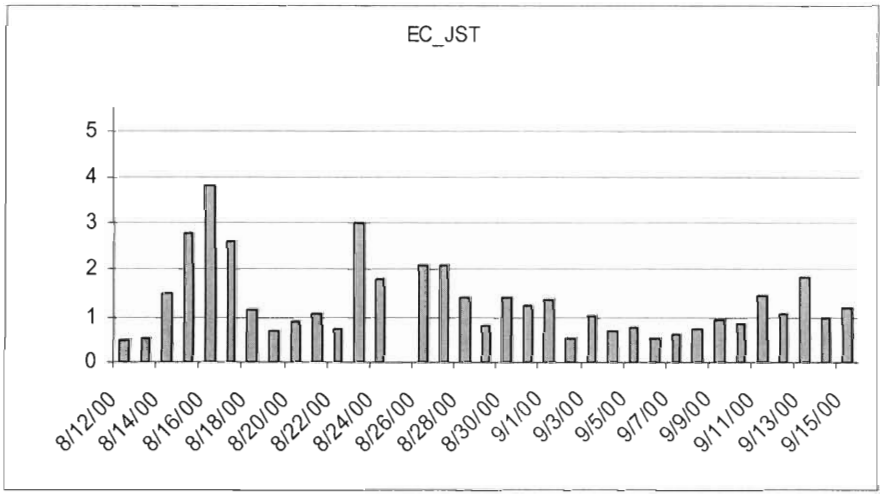

Figure 123. Elemental carbon concentration 24-hour averages ($\mu g/m^3$) in Jefferson Street

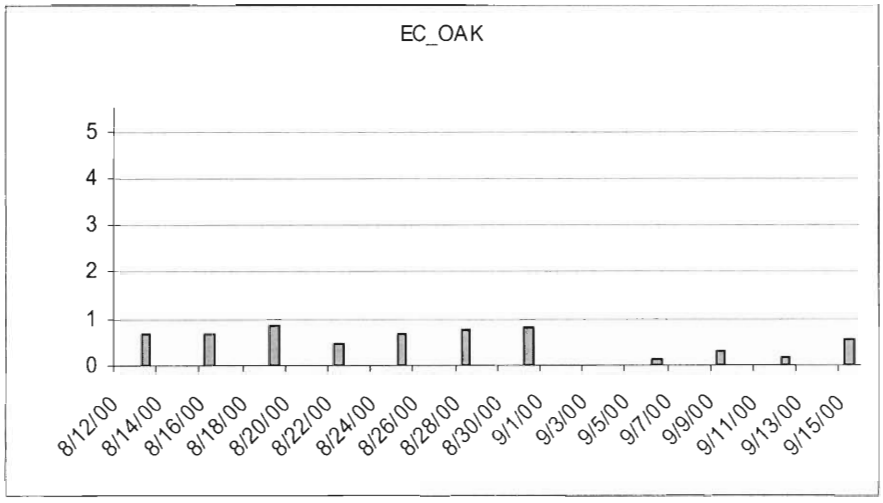

Figure 124. Elemental carbon concentration 24-hour averages ($\mu g/m^3$) in Oak Grove

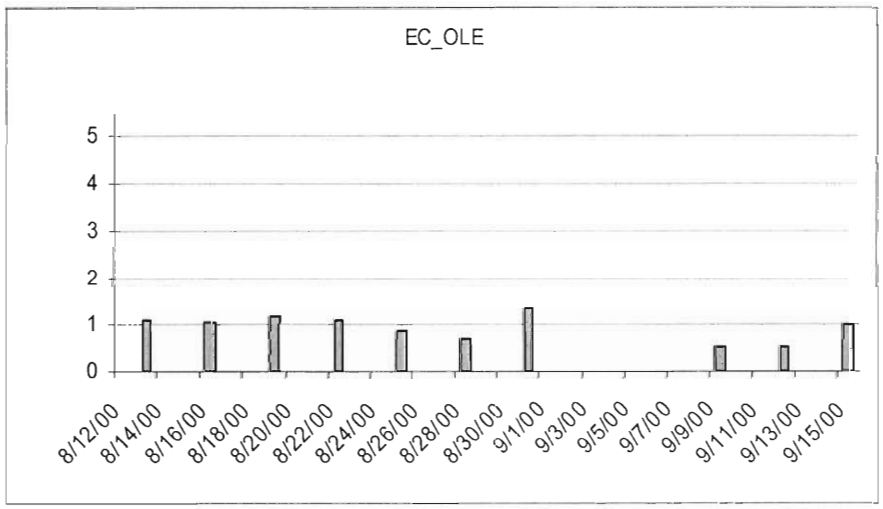

Figure 125. Elemental carbon concentration 24-hour averages ($\mu g/m^3$) in Pensacola (OLE)

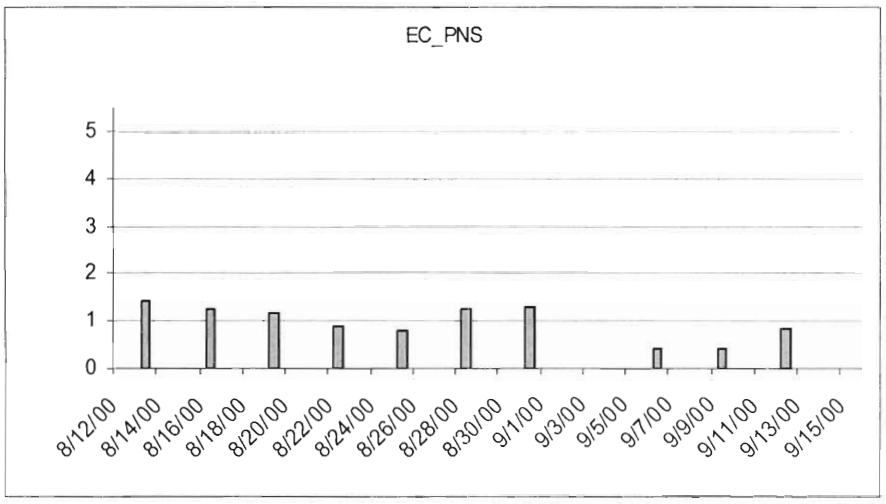

Figure 126. Elemental carbon concentration 24-hour averages ($\mu g/m^3$) in Pensacola (PNS)

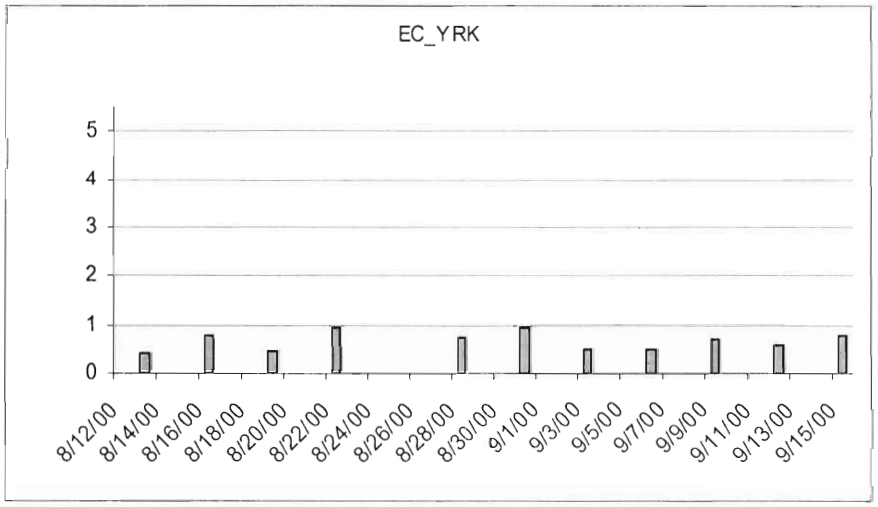

Figure 126. Elemental carbon concentration 24-hour averages ($\mu g/m^3$) in Yorkville

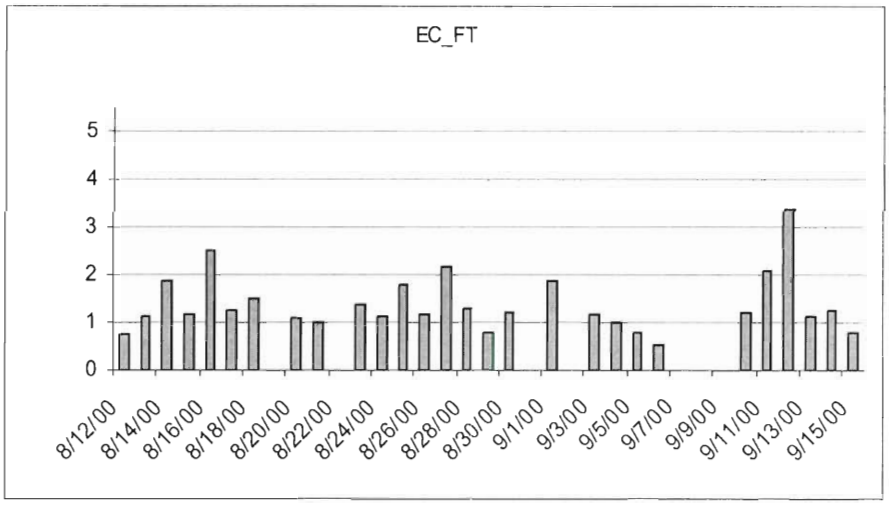

Figure 127. Elemental carbon concentration 24-hour averages ($\mu g/m^3$) in Fort McPherson

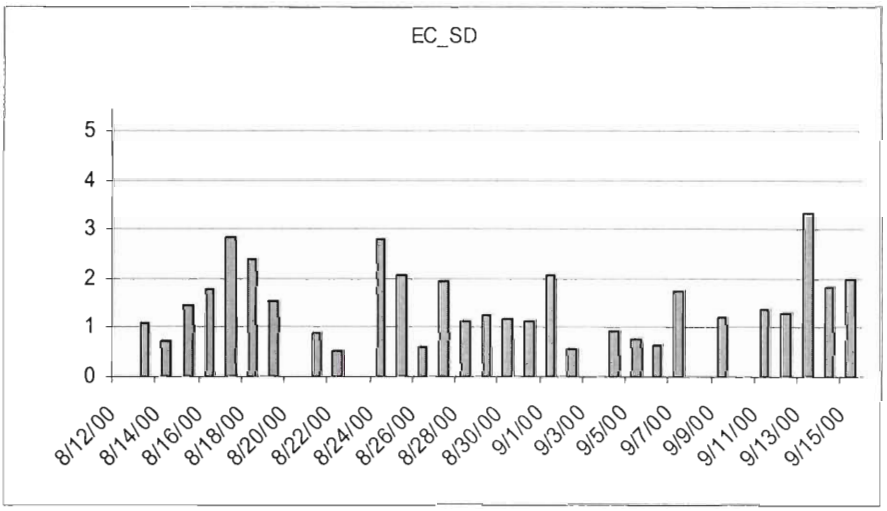

Figure 128. Elemental carbon concentration 24-hour averages ($\mu g/m^3$) in South Dekalb

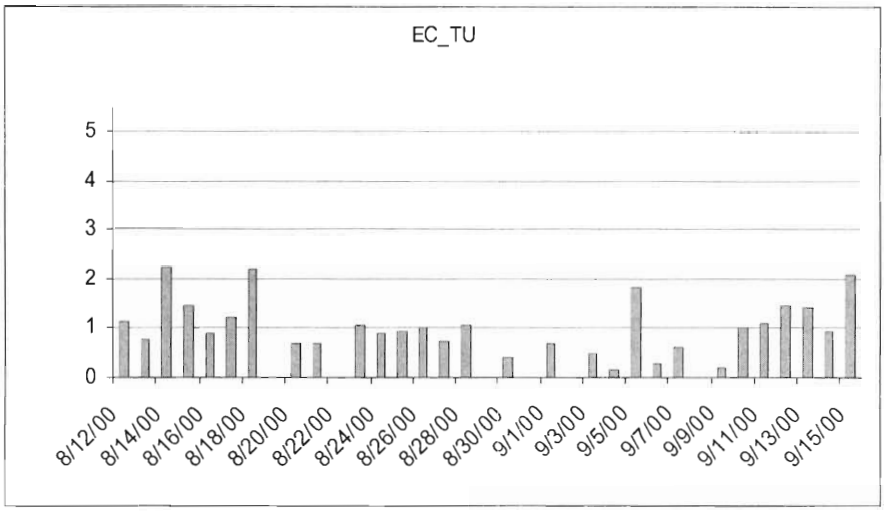

Figure 129. Elemental carbon concentration 24-hour averages ($\mu g/m^3$) in Tucker

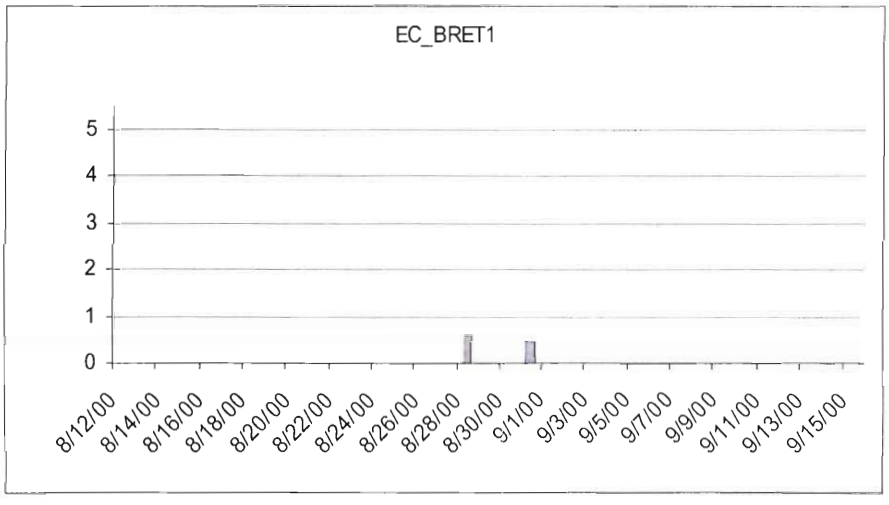

Figure 130. Elemental carbon concentration 24-hour averages ($\mu g/m^3$) in Breton

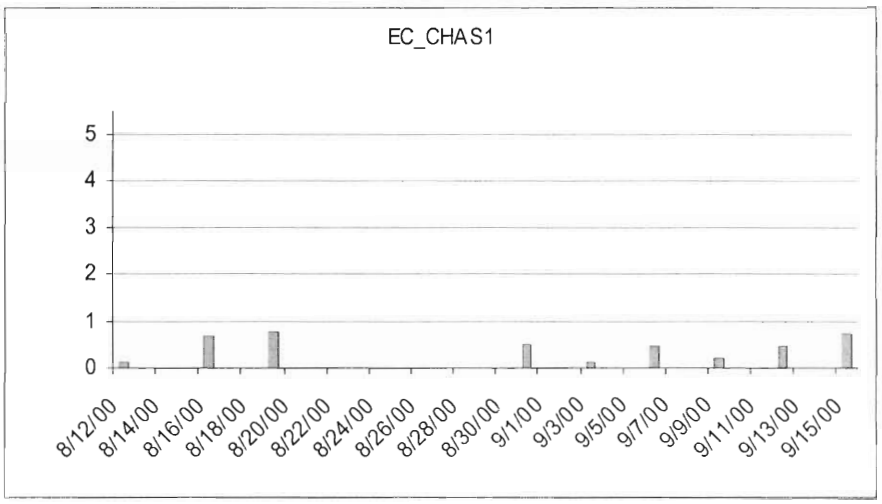

Figure 131. Elemental carbon concentration 24-hour averages ($\mu g/m^3$) in Chassahowitzka National Wildlife

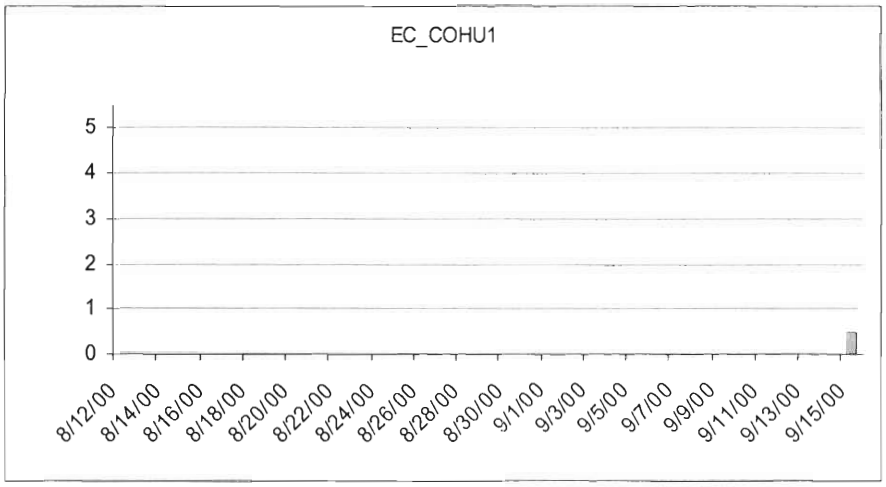

Figure 132. Elemental carbon concentration 24-hour averages ($\mu g/m^3$) in Cohutta

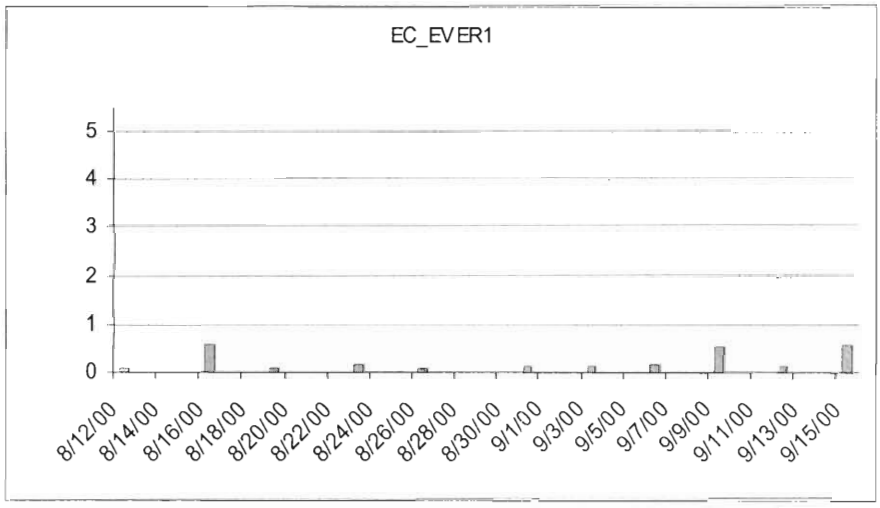

Figure 133. Elemental carbon concentration 24-hour averages ($\mu g/m^3$) in Everglades National Park

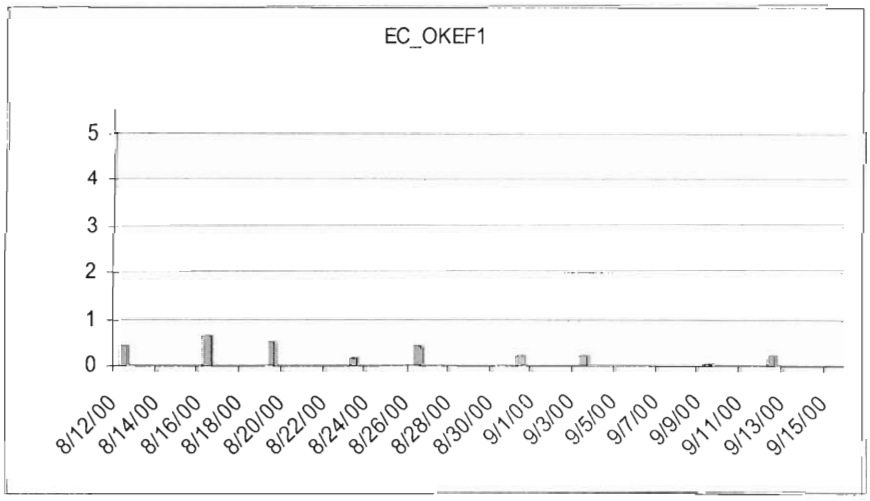

Figure 134. Elemental carbon concentration 24-hour averages ($\mu g/m^3$) in Okefenokee National Wildlife Refuge

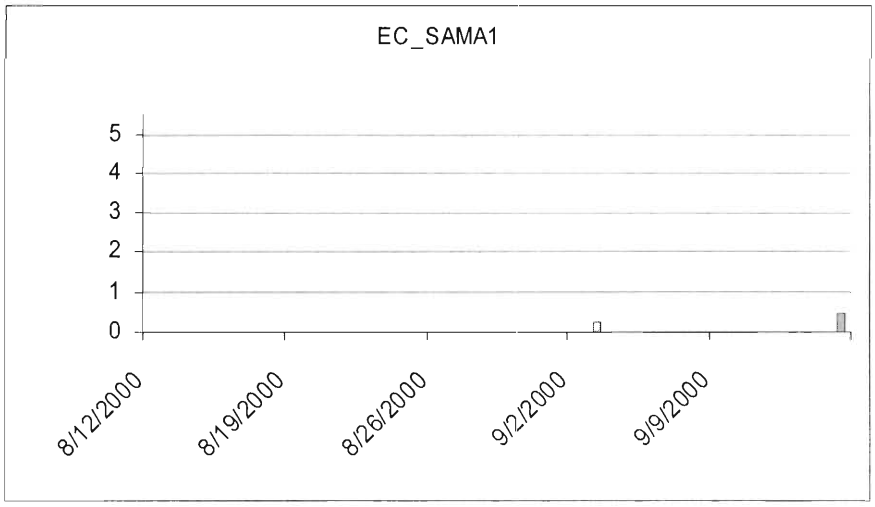

Figure 135. Elemental carbon concentration 24-hour averages ($\mu g/m^3$) in St. Marks

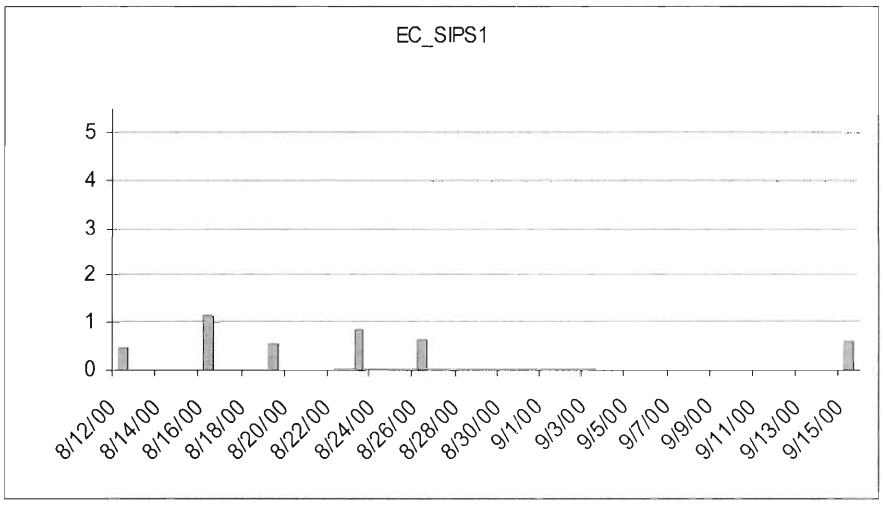

Figure 136. Elemental carbon concentration 24-hour averages ($\mu g/m^3$) in Sipsy Wilderness

Table 1. Measurement stations

ID	Source	x_lon	y_lat	NAME
LP	KB	-95.069	29.671	La_Porte(TX)
WT	KB	-95.475	29.750	Will_Tower(TX)
BHM	SEARCH	-86.815	33.553	North_Birmingham(AL)
CTR	SEARCH	-87.250	32.902	Centreville(AL)
GFP	SEARCH	-89.050	30.391	Gulfport(MS)
JST	SEARCH	-84.413	33.776	Jefferson_St(Atlanta_GA)
OAK	SEARCH	-88.932	30.985	Oak_Grove(MS)
OLE	SEARCH	-87.376	30.550	Pensacola(FL)_OLE
PNS	SEARCH	-87.257	30.437	Pensacola(FL)_PNS
YRK	SEARCH	-85.046	33.931	Yorkville(GA)
FTM	ASACA	-84.443	33.699	Fort_McPherson(Atlanta_GA)
SDK	ASACA	-84.290	33.688	South_Dekalb(Atlanta_GA)
TUC	ASACA	-84.214	33.848	Tucker(Atlanta_GA)
BRET1	IMPROVE	-89.207	29.119	Breton(LA)
CHAS1	IMPROVE	-82.555	28.748	Chassahowitzka_National_Wildlife(FL)
COHU1	IMPROVE	-84.626	34.785	Cohutta(GA)
EVER1	IMPROVE	-80.681	25.391	Everglades_National_Park(FL)
OKEF1	IMPROVE	-82.128	30.740	Okefenokee_National_Wildlife_Refuge(GA)
SAMA1	IMPROVE	-84.161	30.093	St_Marks(FL)
SIPS1	IMPROVE	-87.339	34.343	Sipsy_Wilderness(AL)

Table 2. Number of exceeding the ozone standard for each station from August 12 to September 15, 2000

	Sample Size	LP	WT	BHM	CTR	GFP	JST	OAK	OLF	PNS	YRK
1-hour standard	840	19	4	4	3	0	9	0	3	3	0
8-hour standard	105	7	2	3	8	3	4	6	14	12	8

Table 3.1. Correlation coefficients (r) of ozone concentrations 1-hour averages

Ozone (1hr)	LP	WT	BHM	CTR	GFP	JST	OAK	OLE	PNS	YRK
LP	1.00	0.77	0.58	0.52	0.59	0.44	0.58	0.50	0.50	0.30
WT		1.00	0.41	0.42	0.48	0.41	0.48	0.42	0.33	0.25
BHM			1.00	0.77	0.56	0.69	0.73	0.61	0.68	0.71
CTR				1.00	0.67	0.68	0.76	0.70	0.72	0.71
GFP					1.00	0.55	0.81	0.72	0.71	0.40
JST						1.00	0.60	0.58	0.62	0.73
OAK							1.00	0.86	0.80	0.63
OLE								1.00	0.88	0.63
PNS									1.00	0.61
YRK										1.00

Table 3.2. Correlation coefficients (r) of ozone concentrations 24-hour averages

Ozone (24hr)	LP	WT	BHM	CTR	GFP	JST	OAK	OLE	PNS	YRK
LP	1.00	0.87	0.18	0.26	0.66	0.03	0.38	0.35	0.25	-0.21
WT		1.00	0.09	0.16	0.51	0.07	0.34	0.24	0.12	-0.09
BHM			1.00	0.84	0.43	0.63	0.67	0.47	0.64	0.64
CTR				1.00	0.64	0.65	0.84	0.73	0.78	0.67
GFP					1.00	0.22	0.87	0.85	0.74	0.19
JST						1.00	0.64	0.56	0.65	0.79
OAK							1.00	0.91	0.89	0.62
OLE								1.00	0.93	0.76
PNS									1.00	0.72
YRK										1.00

Table 4. Correlation coefficients (r) of PM 2.5 concentrations 24-hour averages

PM2.5	LP	WT	BHM	CTR	GFP	JST	OAK	OLE	PNS	YRK	FT	SD	TU	OKEF1	SIPS1	EVER1	CHAS1
LP	1.00	0.91	-0.01	-0.17	0.60	-0.17	0.36	0.49	-0.05	-0.06		0.33	-0.70	0.60	-0.24	-0.03	-0.04
WT		1.00	0.24	0.12	0.72	0.04	0.41	0.51	0.00	0.09		0.28	-0.64	0.65	0.40	0.16	0.17
BHM			1.00	0.77	0.51	0.65	0.02	-0.08	0.11	0.64		0.32	0.61	-0.38	0.65	-0.13	0.01
CTR				1.00	0.73	0.67	0.15	0.17	0.78	0.66		0.46	0.97	0.06	0.66	0.33	0.77
GFP					1.00	0.68	0.90	0.91	0.97	0.74		0.74	1.00	0.68	-0.67	0.18	0.69
JST						1.00	0.48	0.25	0.70	0.87		0.89	1.00	0.03	0.58	0.26	0.79
OAK							1.00	0.89	0.92	0.44		0.54	0.09	0.57	-0.04	-0.28	0.77
OLE								1.00	0.97	0.30		0.20		0.68	-0.33	-0.29	0.66
PNS									1.00	0.55		0.43	0.93	0.44	0.71	0.25	0.91
YRK										1.00		0.74	0.94	-0.18	0.42	0.07	0.59
FT																	
SD												1.00		0.29	0.91	0.04	0.71
TU													1.00				
OKEF1														1.00	-0.31	0.43	0.64
SIPS1															1.00	0.12	0.94
EVER1																1.00	0.52
CHAS1																	1.00

Table 5. Correlation coefficients (r) of sulfate concentrations 24-hour averages

SO4	LP	WT	BHM	CTR	GFP	JST	OAK	OLE	PNS	YRK	FT	SD	TU	OKEF1	SIPS1	EVER1	CHAS1
LP	1.00	0.88	-0.07	-0.26	0.82	0.15	0.36	0.79	0.68	0.18	0.49	0.16	0.26	0.50	0.43	-0.25	0.20
WT		1.00	-0.09	-0.41	0.70	0.08	0.24	0.72	0.50	0.14	0.31	0.29	-0.07	0.33	0.69	-0.24	0.11
BHM			1.00	0.92	-0.01	0.06	0.44	0.23	0.11	0.58	-0.56	0.30	-0.05	-0.70	0.99	-0.13	-0.07
CTR				1.00	0.25	0.02	0.61	0.37	0.33	0.03	0.53	0.03	-0.06	-0.10	1.00	0.54	0.02
GFP					1.00	0.83	0.93	0.95	0.95	0.45	0.19	0.55	0.76	0.69	1.00	-0.08	0.83
JST						1.00	0.78	0.80	0.81	0.85	0.60	0.69	0.78	0.09	0.57	-0.52	0.62
OAK							1.00	0.92	0.92	0.66	0.13	0.55	0.66	0.52	1.00	-0.05	0.73
OLE								1.00	1.00	0.62	0.33	0.55	0.56	0.73	0.99	0.07	0.89
PNS									1.00	0.45	0.34	0.59	0.80	0.67	1.00	0.06	0.78
YRK										1.00	-0.06	0.91	0.87	0.63	1.00	0.18	0.86
FT											1.00	0.31	0.39	0.79	0.79	0.79	0.85
SD												1.00	0.22	-0.30	0.85	-0.14	0.33
TU													1.00	0.80	-0.31	0.69	0.81
OKEF1														1.00	-0.24	0.57	0.84
SIPS1															1.00	-0.18	0.68
EVER1																1.00	0.43
CHAS1																	1.00

Table 6. Correlation coefficients (r) of ammonium concentration 24-hour averages

NH4	LP	WT	BHM	CTR	GFP	JST	OAK	OLE	PNS	YRK	FT	SD	TU	OKEF1	SIPS1	EVER1	CHAS1
LP	1.00	0.85	-0.37	-0.22	0.76	0.10	0.22	0.79	0.59	0.18	0.45	0.01	0.22				
WT		1.00	-0.42	-0.31	0.70	-0.03	0.04	0.71	0.46	-0.04	0.09	-0.04	-0.11				
BHM			1.00	0.63	0.02	0.07	0.45	0.20	0.18	0.12	0.48	-0.02	0.10				
CTR				1.00	0.52	0.18	0.82	0.59	0.72	0.46	0.79	0.33	-0.19				
GFP					1.00	0.47	0.94	0.95	0.94	0.24	0.90	0.78	0.75				
JST						1.00	0.58	0.47	0.59	0.60	0.57	0.90	0.67				
OAK							1.00	0.96	0.96	0.47	0.95	0.84	0.72				
OLE								1.00	0.99	0.40	0.84	0.88	0.70				
PNS									1.00	0.24	0.96	0.74	0.82				
YRK										1.00	0.17	0.79	0.68				
FT											1.00	0.82	0.29				
SD												1.00	0.62				
TU													1.00				
OKEF1																	
SIPS1																	
EVER1																	
CHAS1																	

Table 7. Correlation coefficients (r) of nitrate concentrations 24-hour averages

NO3	LP	WT	BHM	CTR	GFP	JST	OAK	OLE	PNS	YRK	FT	SD	TU	OKEF1	SIPS1	EVER1	CHAS1
LP	1.00	0.83	-0.47	0.77	0.10	-0.17	0.27	0.10	0.17	-0.27	-0.15	0.26	-0.35	-0.26	-0.40	0.36	-0.10
WT		1.00	-0.29	0.67	-0.08	-0.06	0.31	-0.18	0.00	-0.26	0.01	0.28	-0.30	-0.26	-0.46	0.40	0.06
BHM			1.00	-0.25	0.12	0.57	0.11	-0.24	-0.36	0.57	0.20	0.43	0.51	-0.22	-0.68	0.49	-0.01
CTR				1.00	0.69	0.00	0.71	0.74	0.68	-0.13	0.49	-0.59	-0.40	-0.05	1.00	-0.08	0.10
GFP					1.00	0.36	0.26	0.35	0.46	0.61	0.52	0.10	0.69	-0.39	0.30	0.34	-0.01
JST						1.00	0.73	-0.10	0.11	0.48	0.64	0.44	0.53	0.33	0.30	0.35	0.73
OAK							1.00	0.50	0.20	0.13	0.82	0.69	0.38	-0.72	-0.14	0.44	0.05
OLE								1.00	0.95	-0.04	0.11	-0.02	0.73	-0.37	1.00	-0.30	-0.38
PNS									1.00	-0.28	0.91	0.44	0.48	-0.08	1.00	0.06	0.31
YRK										1.00	-0.09	0.29	0.48	-0.20	0.25	0.35	0.01
FT											1.00	0.66	0.73	-0.34	0.20	0.70	0.37
SD												1.00	0.23	-0.18	0.16	0.35	0.20
TU													1.00	0.15	0.90	0.08	0.57
OKEF1														1.00	0.02	0.26	0.51
SIPS1															1.00	-0.31	-0.15
EVER1																1.00	0.51
CHAS1																	1.00

Table 8. Correlation coefficients (r) of organic carbon concentrations 24-hour averages

OC	LP	WT	BHM	CTR	GFP	JST	OAK	OLE	PNS	YRK	FT	SD	TU	OKEF1	SIPS1	EVER1	CHAS1
LP	1.00	0.85	-0.54	-0.50	0.17	-0.43	-0.38	0.27	-0.46	-0.70	-0.21	-0.27	-0.15	-0.17	-0.42	-0.10	-0.24
WT		1.00	-0.47	-0.43	0.27	-0.39	-0.34	0.48	-0.39	-0.63	-0.06	0.18	-0.21	0.02	-0.51	-0.04	-0.18
BHM			1.00	0.78	-0.20	0.45	0.48	-0.20	0.49	0.53	0.62	-0.23	-0.03	0.32	1.00	-0.35	0.56
CTR				1.00	0.47	0.74	0.81	0.44	0.77	0.57	0.91	-0.11	0.31	0.71	0.96	0.07	0.86
GFP					1.00	0.30	0.62	0.70	0.61	-0.25	0.67	0.34	0.64	0.67	-0.33	0.15	0.51
JST						1.00	0.40	0.23	0.46	0.42	0.59	0.17	0.09	0.00	0.87	-0.07	0.82
OAK							1.00	0.48	0.69	0.45	0.97	0.29	0.58	0.82	0.28	0.00	0.59
OLE								1.00	0.78	-0.47	0.72	-0.07	0.25	0.47	-0.50	0.38	0.45
PNS									1.00	0.25	0.64	0.00	0.39	0.78	1.00	0.00	0.72
YRK										1.00	0.29	0.09	0.21	-0.02	0.80	0.25	0.35
FT											1.00	0.24	0.39	0.52	0.57	0.78	0.93
SD												1.00	0.25	0.30	-0.64	-0.34	-0.46
TU													1.00	-0.24	-0.35	0.66	0.26
OKEF1														1.00	0.04	-0.44	0.39
SIPS1															1.00	-0.41	0.88
EVER1																1.00	0.16
CHAS1																	1.00

Table 9. Correlation coefficients (r) of elemental carbon concentrations 24-hour averages

EC	LP	WT	BHM	CTR	GFP	JST	OAK	OLE	PNS	YRK	FT	SD	TU	OKEF1	SIPS1	EVER1	CHAS1
LP	1.00	0.13	0.39	0.02	-0.42	0.07	-0.12	0.23	-0.38	0.18	-0.24	-0.13	-0.24	-0.12	0.78	0.16	-0.26
WT		1.00	-0.04	0.14	0.39	0.18	0.04	0.22	-0.15	0.20	-0.03	-0.23	0.43	-0.17	0.06	-0.20	0.33
BHM			1.00	0.67	-0.23	0.72	0.43	0.35	0.36	0.44	0.89	0.60	0.21	0.47	1.00	0.06	0.31
CTR				1.00	0.38	0.57	0.92	0.74	0.80	0.47	0.01	0.49	0.06	0.77	0.97	0.22	0.63
GFP					1.00	0.01	0.35	0.32	0.44	-0.11	-0.43	0.02	0.71	0.76	-1.00	-0.11	0.93
JST						1.00	0.28	0.04	0.30	0.36	0.38	0.43	0.21	0.35	0.96	0.36	0.38
OAK							1.00	0.70	0.80	0.19	-0.13	0.45	-0.02	0.63	-0.09	0.01	0.66
OLE								1.00	0.67	0.21	-0.59	-0.08	-0.49	0.53	-0.35	-0.24	0.65
PNS									1.00	0.07	0.12	0.21	0.21	0.70	1.00	-0.16	0.74
YRK										1.00	0.22	-0.15	-0.26	-0.04	0.56	0.46	0.18
FT											1.00	0.13	0.23	0.04	0.97	0.14	0.28
SD												1.00	0.20	0.45	0.56	0.51	0.57
TU													1.00	0.35	-0.89	-0.23	0.01
OKEF1														1.00	0.26	0.04	0.60
SIPS1															1.00	0.55	0.38
EVER1																1.00	0.28
CHAS1																	1.00

Air Quality in Houston

(August 11 ~ 20, 2007)

Sun-Kyoung Park and Armistead G. Russell

Georgia Institute of Technology, Atlanta GA

Tables of Contents

List of Figures

List of Tables

1. INTRODUCTION

The Houston area is among non-attainment areas, where pollutant levels are higher than the National Ambient Air Quality Standard (NAAQS). Thus, EPA provided a control strategy over the Houston area. We examined how effectively the control strategy would reduce pollutant concentrations over the Houston area using Community Multiscale Air Quality (CMAQ) modeling system.

We modeled two episodes. One is from August 11 to 20, 2000, and the other is from August 11 to 20, 2007. First, we collected an emission inventory in 2000, and modeled an air quality from August 11 to 20, 2000. In addition, we evaluated the simulated result by comparing the measured concentrations. Then, we prepared an emission inventory in 2007 by applying a federal control strategy and EGAS (Economic Growth Analysis System) growth factors based on the emission inventory in 2000. Finally, we modeled the air quality in Houston from August 11 to 20, 2007 using the emission inventory in 2007.

We used a SAPRC-99 chemical mechanism in simulation. The projection of the model grid is a Lambert conformal conic projection with a center of (40 N, 90 W) and standard parallels of 30 N and 60 N. An origin of the model domain is (-1,188,000 m, –

1,620,000 m) and the size of each grid is (36,000 m, 36,000 m). Figure 1 represented the model domain and grids.

Section 2 showed the evaluation of modeling result from August 11 to 20, 2000. Section 3 described the changes of emission inventory from 2000 to 2007. Section 4 compared pollutant concentrations in 2000 and in 2007.

Figure 1. Model domain. Lambert conformal conic projection with a center of (40 N, 90 W) and standard parallels of 30 N and 60 N. An origin of the model domain is (-1,188,000 m, – 1,620,000 m) and the size of each grid is (36,000 m, 36,000 m). The Houston area is inside a green rectangle.

2. Model Evaluation

We compared simulated pollutant concentrations with measured concentrations from August 11 to 20, 2000. Table 1 illustrated measured pollutant species and simulated species we compared with. Figure 2 showed the measurement stations over the Houston area and Table 2 described those stations in detail. Table 3 illustrates statistics representing differences of measured and simulated ozone concentrations only when concentrations were higher than 40 ppb. Figures 3 through 14 showed time series plots of the measured and simulated pollutants concentrations.

Table 1. Comparable simulated pollutants to measured pollutants

Measured Pollutants	**Simulated Pollutants (SAPRC-99)**
Ammonium	ANH4J, ANH4I
Nitrate	ANO3J, ANO3I
Sulfate	ASO4J, ASO4I
Organic Carbon	AORGAJ, AORGAI, AORGPAJ, AORGPAI, APRGBJ, AORGBI
Elemental Carbon	AECJ, AECI
PM 2.5	ASO4J, ASO4I, ANH4J, ANH4I, ANO3J, ANO3I, AORGAJ, AORGAI, AORGPAJ, AORGPAI, APRGBJ, AORGBI, AECJ, AECI, A25J, A25I
Ozone	O3
Carbon Monoxide	CO
Sulfur Dioxide	SO2
Nitric Oxide	NO
NOx	NO, NO2
NOy	NO, NO2, NO3, N2O5, HNO3, HNO4, HONO, RNO3, RO2_N, BZNO2-O, PAN, PAN2 and MA_PAN

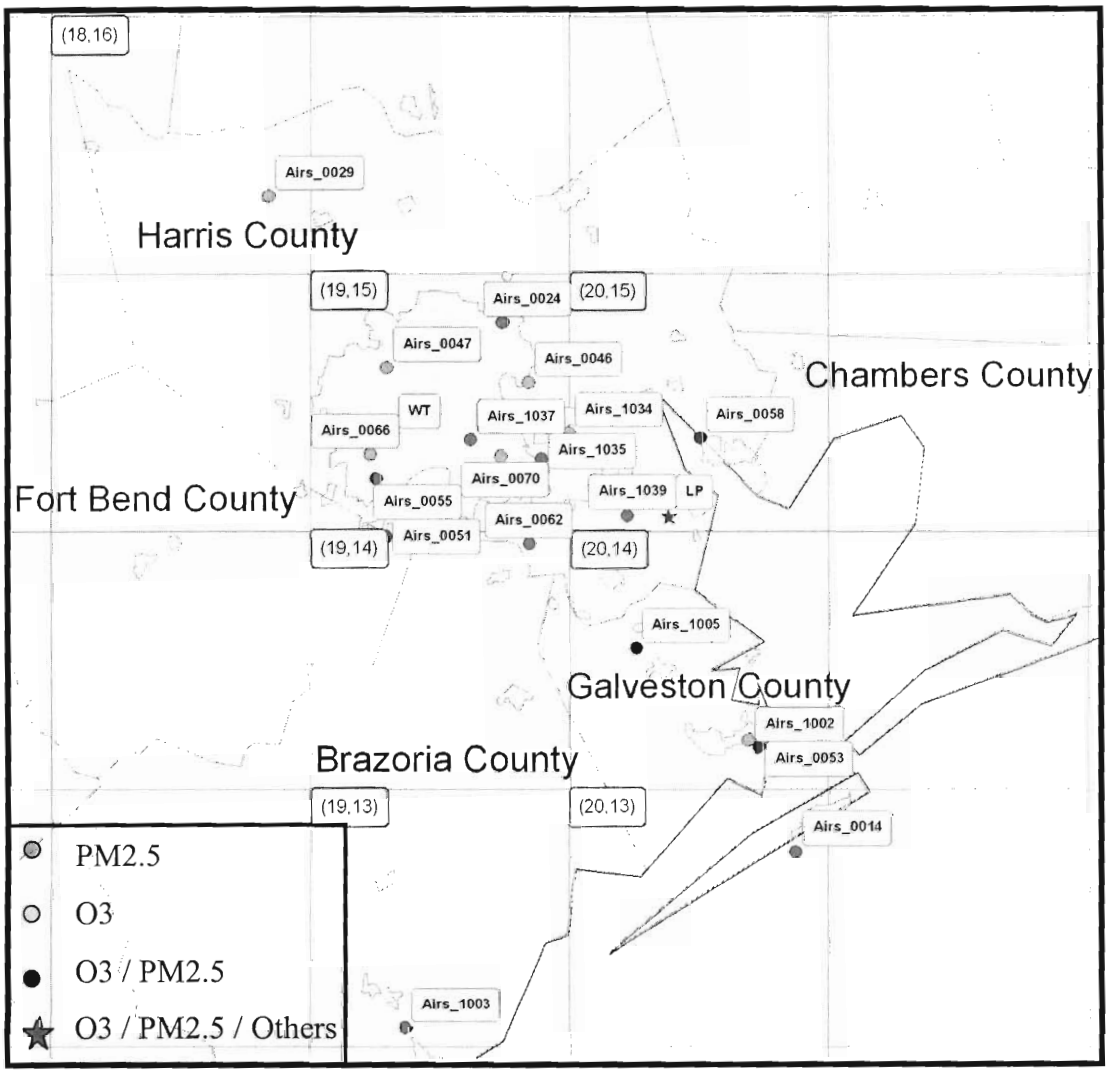

Figure 2. Measurement stations in the Houston area over plotted by model grids. Numbers with a yellow background are a column and a row of each grids.

Table 2. Measurement stations with their coordinates.

SiteID	State ID	Cnty ID	Pollutants	Lon	Lat	Street
AIRS_0014	48	167	O3 / PM25	-94.856	29.263	8715 CESSNA STREET
AIRS_0024	48	201	O3 / PM25	-95.327	29.901	4510 1/2 ALDINE MAIL RD.
AIRS_0026	48	201	PM25	-95.125	29.803	1405 SHELDON ROAD
AIRS_0029	48	201	O3	-95.675	30.039	16822 KITZMAN
AIRS_0046	48	201	O3	-95.284	29.828	7330 1/2 NORTH WAYSIDE
AIRS_0047	48	201	O3	-95.489	29.835	4401 1/2 LANG RD.
AIRS_0051	48	201	O3 / PM25	-95.474	29.624	13826 1/2 CROQUET
AIRS_0053	48	167	PM25	-94.919	29.390	17TH & 5TH AVE. N. PUMPHOUSE ROOF
AIRS_0055	48	201	O3 / PM25	-95.494	29.695	6400 BISSONNET STREET
AIRS_0058	48	201	PM25	-95.031	29.772	7210 1/2 BAYWAY DRIVE
AIRS_0062	48	201	O3 / PM25	-95.268	29.626	9726 1/2 MONROE
AIRS_0066	48	201	O3	-95.504	29.725	3333 1/2 HWY 6 SOUTH
AIRS_0070	48	201	O3	-95.317	29.733	5425 POLK AVE., SUITE H
AIRS_0803	48	201	PM25	-95.181	29.748	1504 HADEN ROAD
AIRS_1002	48	167	O3	-94.933	29.399	2701 13TH AVE NORTH AT LOGAN
AIRS_1003	48	39	O3 / PM25	-95.398	29.011	426 COMMERCE STREET
AIRS_1005	48	167	PM25	-95.104	29.504	171 CALDER DRIVE
AIRS_1034	48	201	O3	-95.221	29.768	1262 1/2 MAE DRIVE
AIRS_1035	48	201	O3 / PM25	-95.257	29.733	9525 CLINTON DR
AIRS_1037	48	201	O3 / PM25	-95.361	29.751	1307 1/2 CRAWFORD ST.
AIRS_1039	48	201	O3 / PM25	-95.128	29.669	5414 1\2 DURANT ST.
LP	48	201	O3 / PM25 / Others	-95.069	29.671	La Porte
WT	48	201	O3 / PM25 / Others	-95.475	29.750	Williams Tower (254 m above ground level)

Table 3. Statistics of ozone concentration from August 11 to August 20, 2000.
(cut off value: 40 ppb)

Site ID	Model (col, row)	MBE (ppb)	MNB (%)	RMSE (ppb)	MNE (%)
AIRS_0014	(20,13)	16.349	17.859	29.83	25.18
AIRS_0024	(19,15)	25.395	32.176	40.074	50.07
AIRS_0029	(18,16)	8.077	11.571	20.447	26.7
AIRS_0046	(19,15)	20.756	29.477	34.886	45.553
AIRS_0047	(19,15)	13.063	20.22	33.868	50.229
AIRS_0051	(19,14)	14.743	16.756	27.935	28.852
AIRS_0055	(19,15)	23.834	31.986	38.98	47.586
AIRS_0062	(19,14)	17.105	18.639	32.334	32.594
AIRS_0066	(19,15)	20.129	28.487	36.513	46.281
AIRS_0070	(19,15)	21.149	32.518	33.31	44.436
AIRS_1002	(20,14)	8.519	8.813	26.67	32.346
AIRS_1003	(19,13)	2.184	-1.33	17.78	22.850
AIRS_1034	(19,15)	21.935	29.762	37.683	49.221
AIRS_1035	(19,15)	18.873	26.743	35.152	48.000
AIRS_1037	(19,15)	20.453	31.411	34.793	47.600
AIRS_1039	(20,15)	23.846	30.611	39.0	45.54
LP	(20,15)	-3.487	-30.288	16.431	42.593
WT	(19,15) 5th layer	6.215	5.086	17.604	21.137

(a)

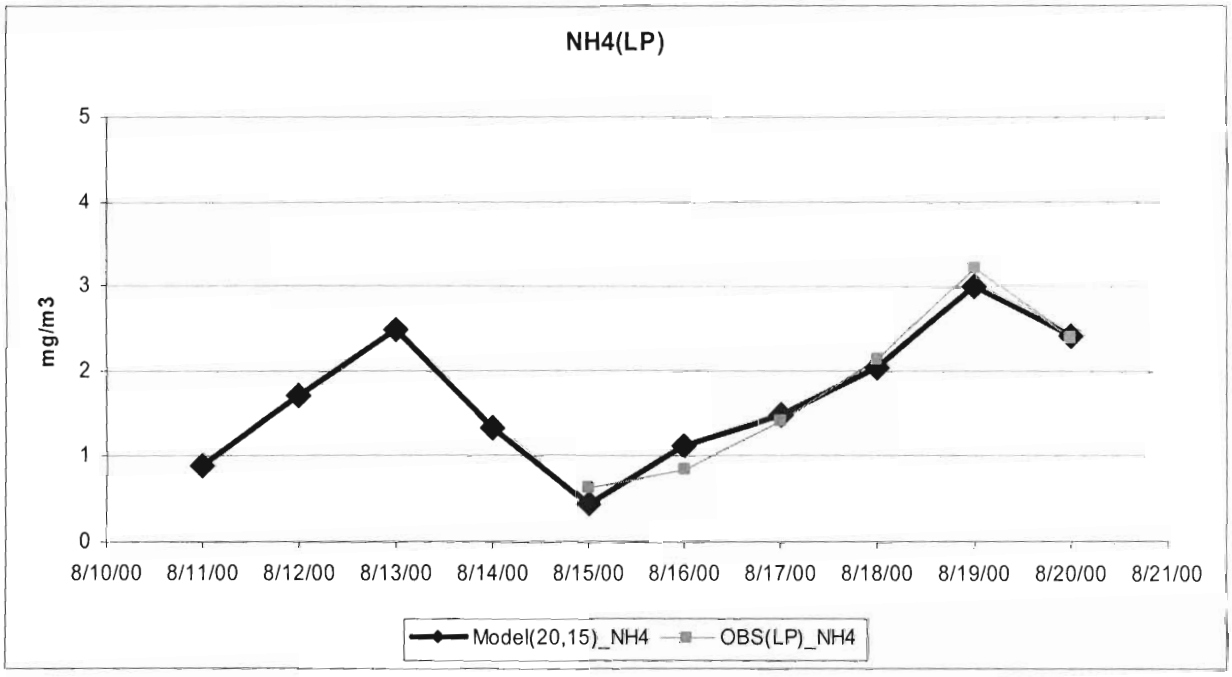

(b)

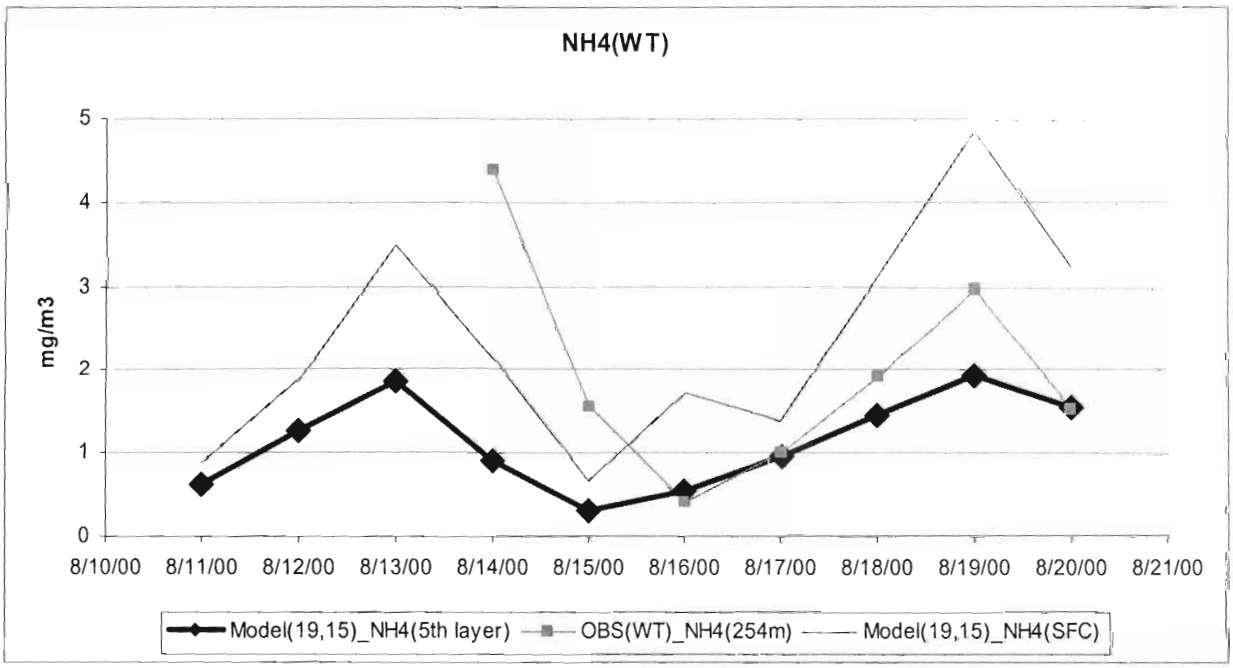

Figure 3. Comparisons of measured and simulated daily ammonium concentrations. (a) is for the LP station and (b) is for the WT station

(a)

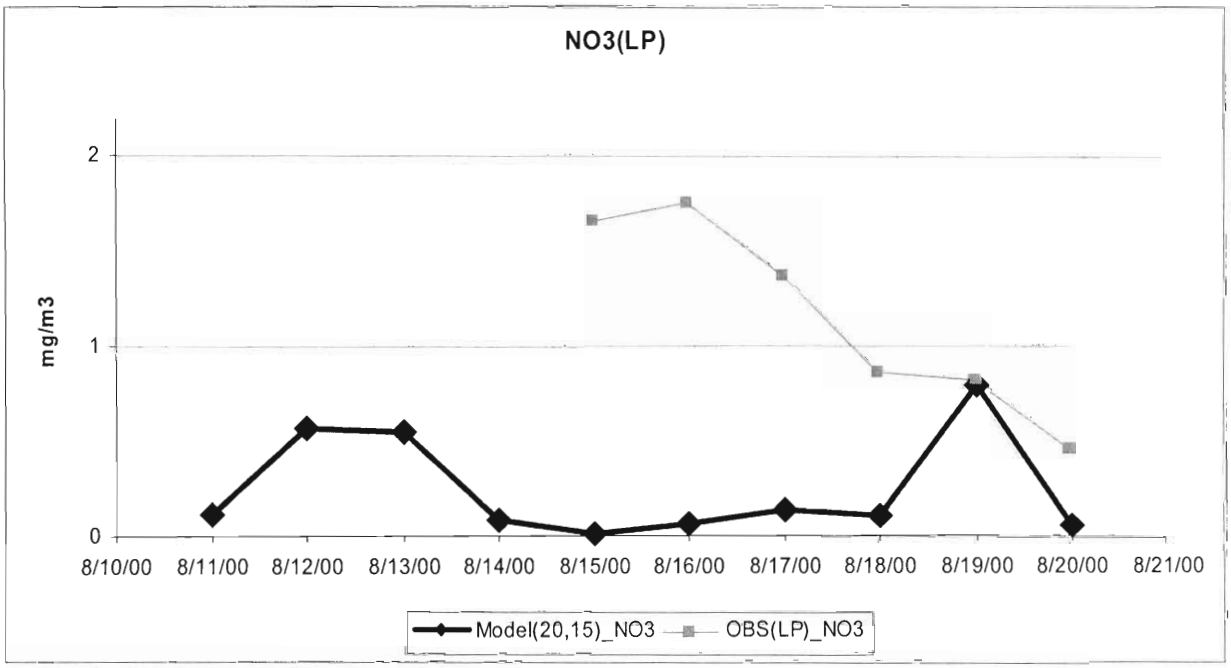

(b)

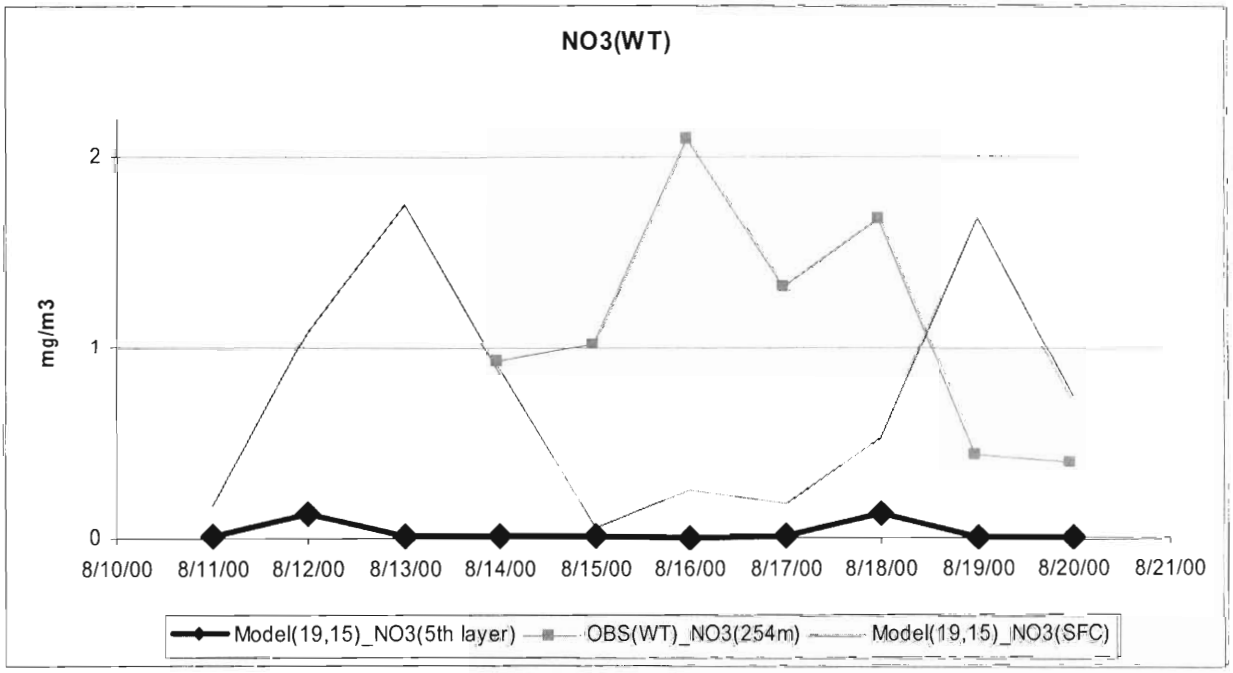

Figure 4. Comparisons of measured and simulated daily nitrate concentrations. (a) is for the LP station and (b) is for the WT station

(a)

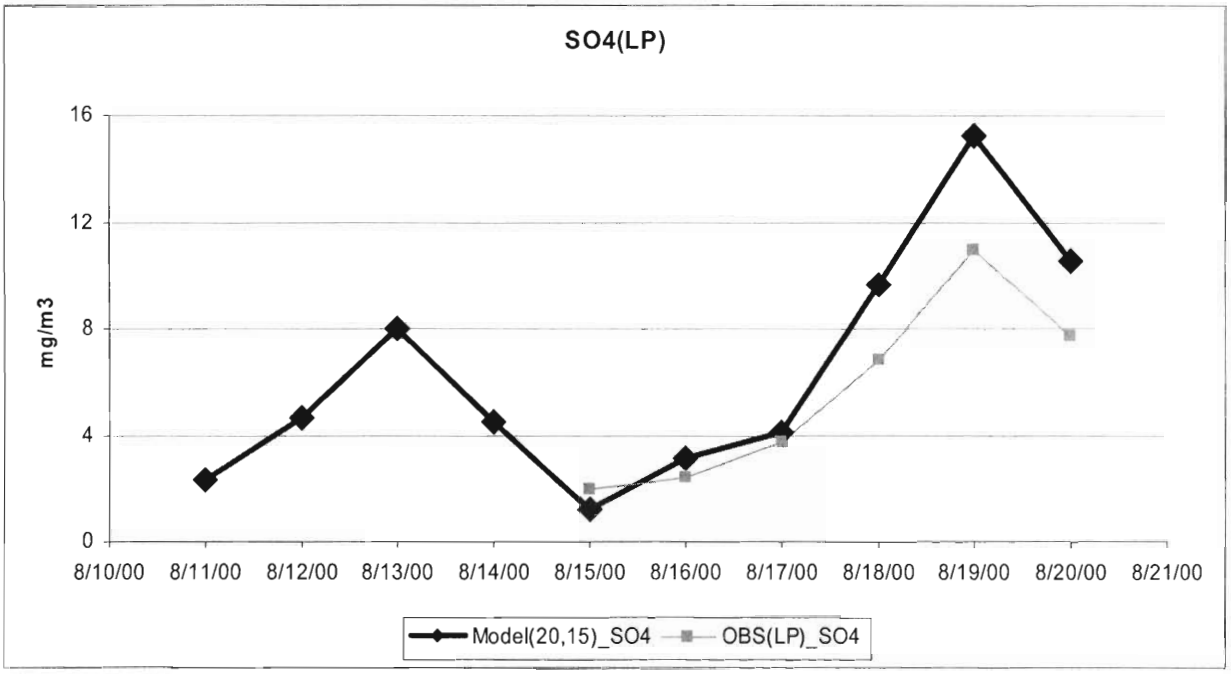

(b)

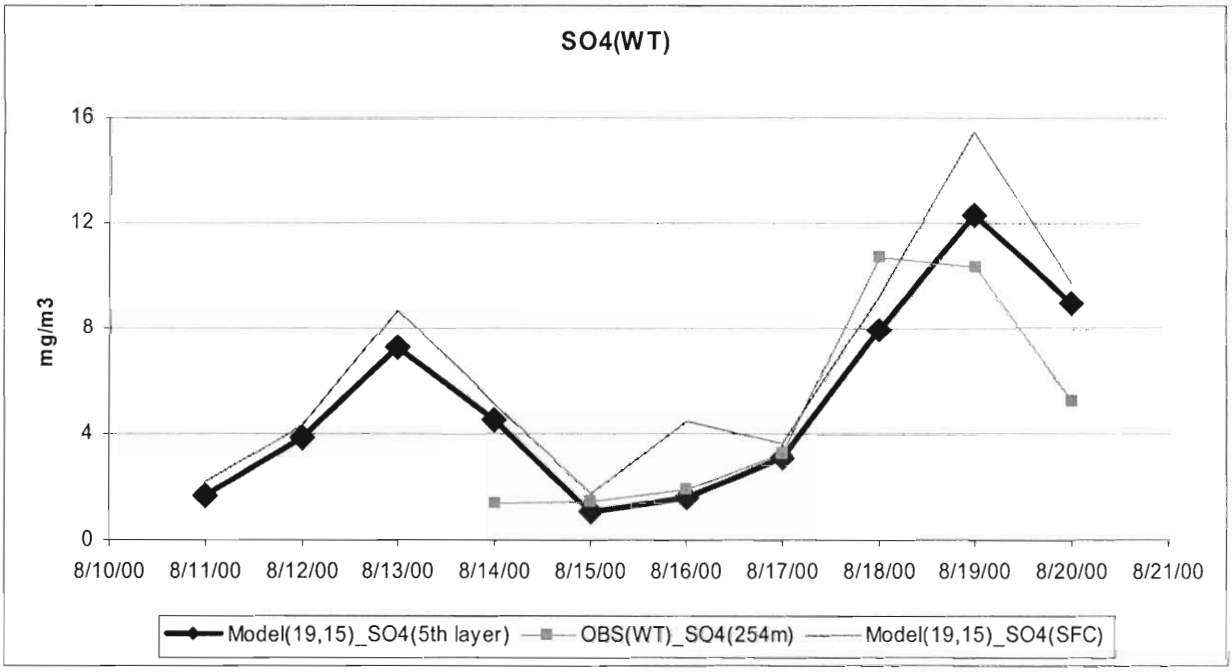

Figure 5. Comparisons measured and simulated daily sulfate concentrations. (a) is for the LP station and (b) is for the WT station

(a)

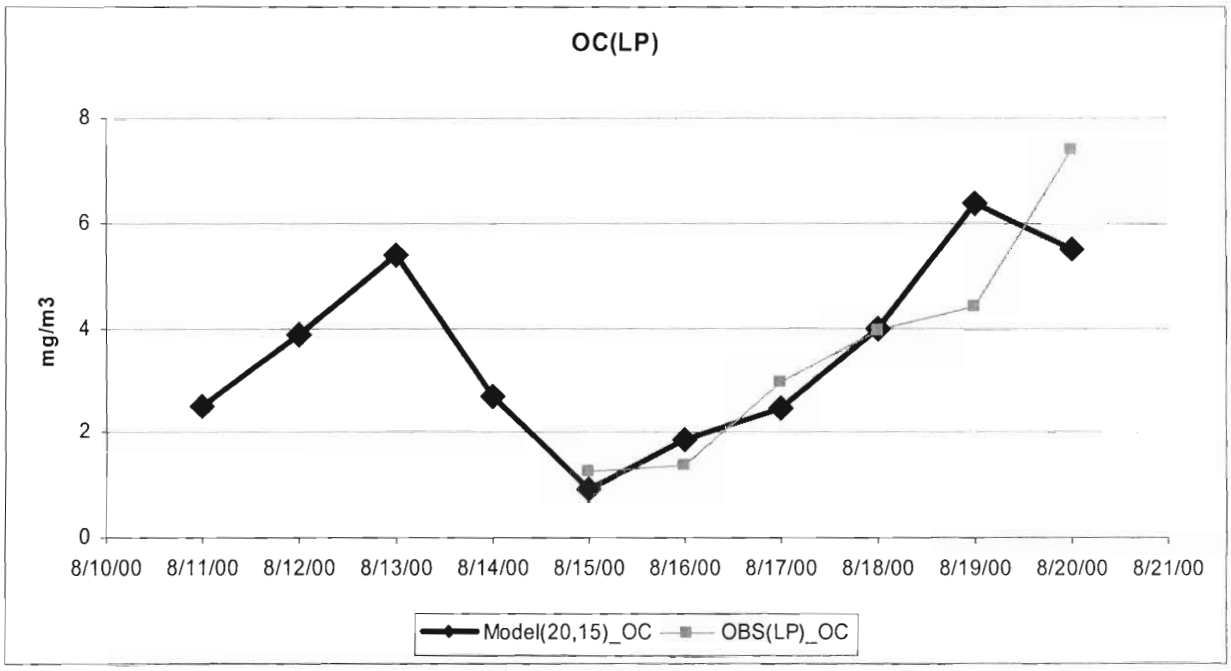

(b)

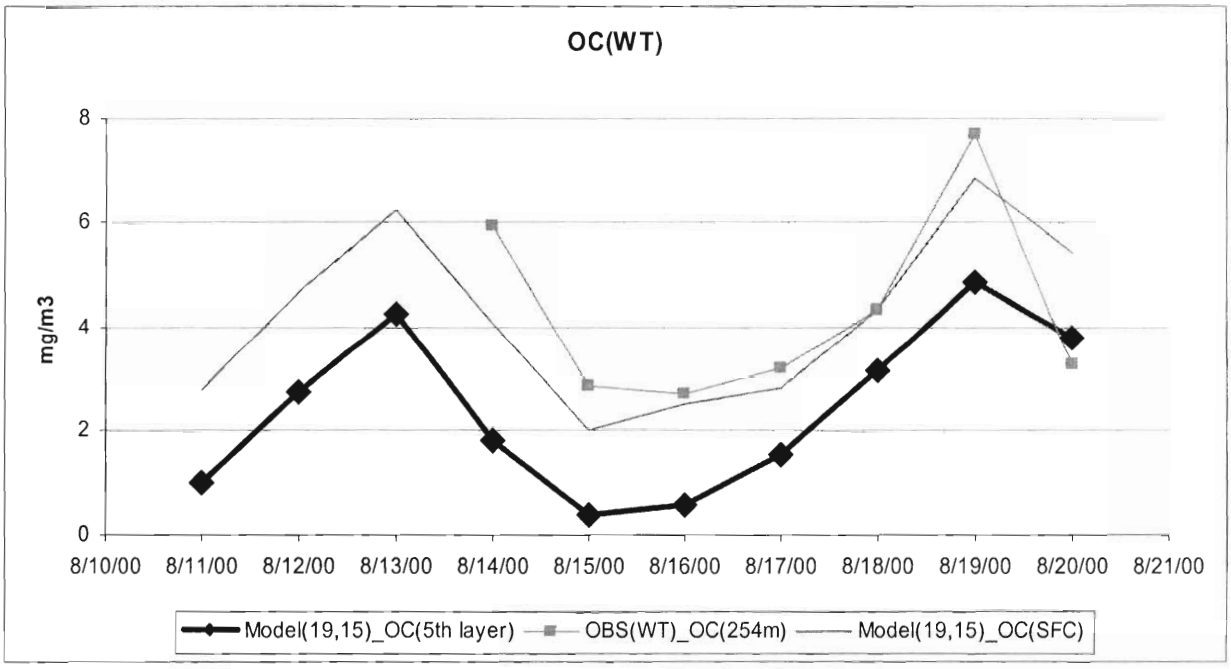

Figure 6. Comparisons of measured and simulated daily organic carbon concentrations. (a) is for the LP station and (b) is for the WT station.

(a)

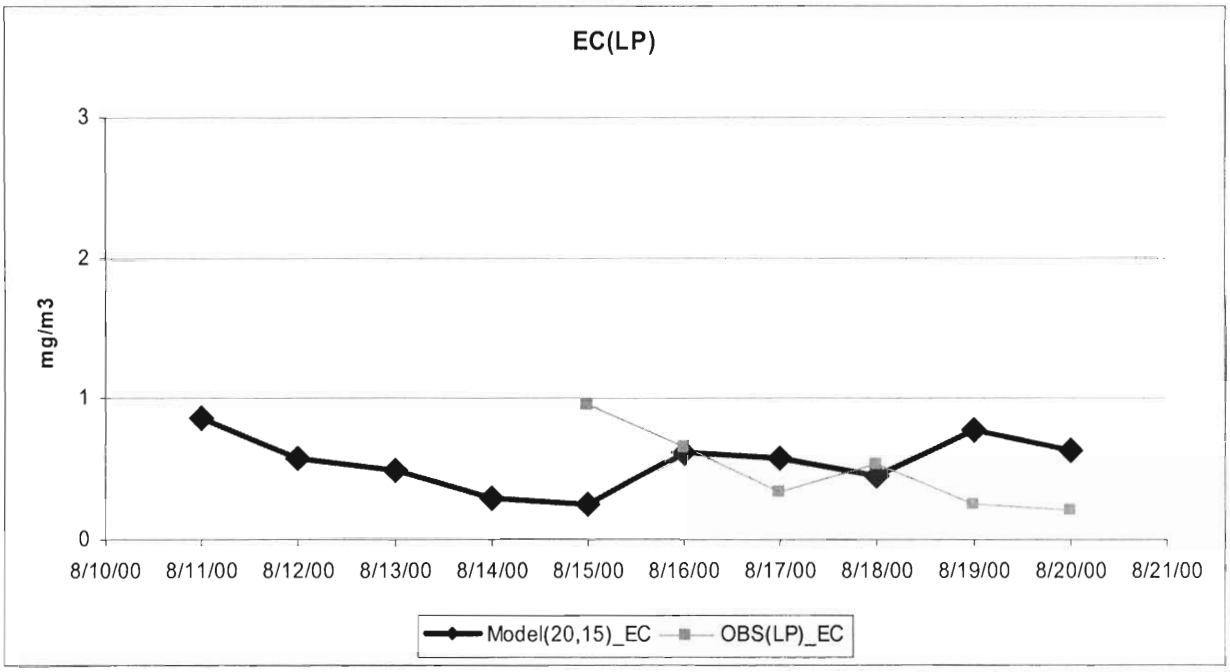

(b)

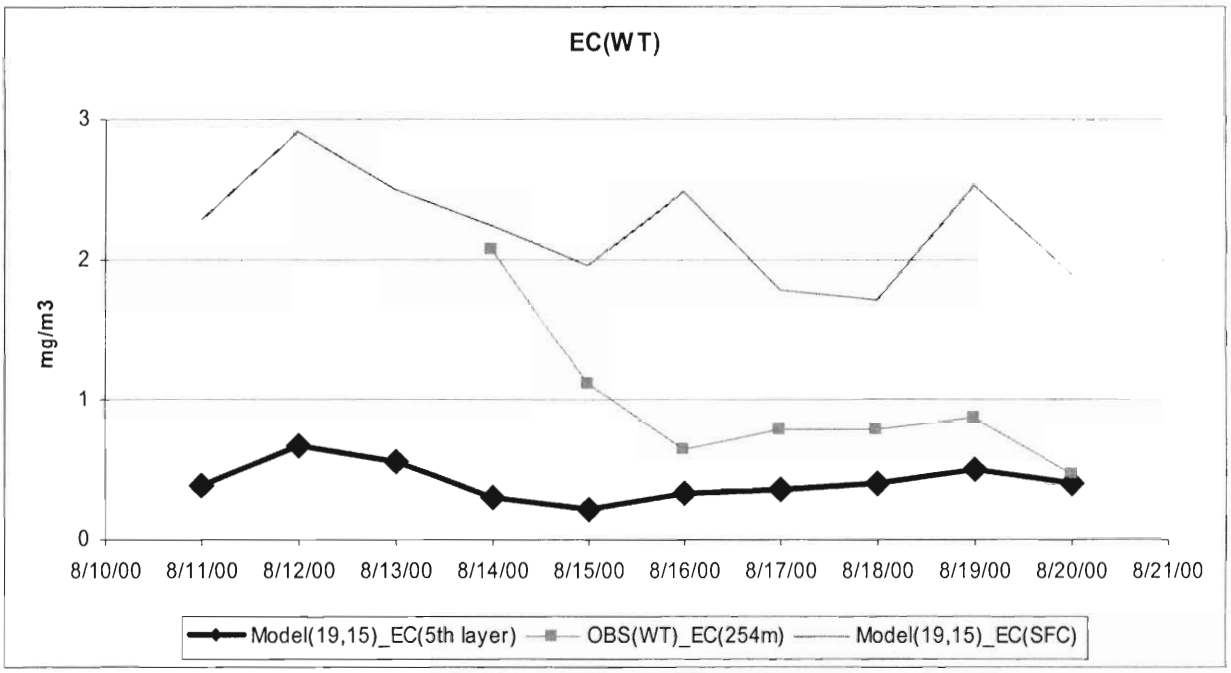

Figure 7. Comparisons of measured and simulated daily elemental carbon concentrations. (a) is for the LP station and (b) is for the WT station

(a)

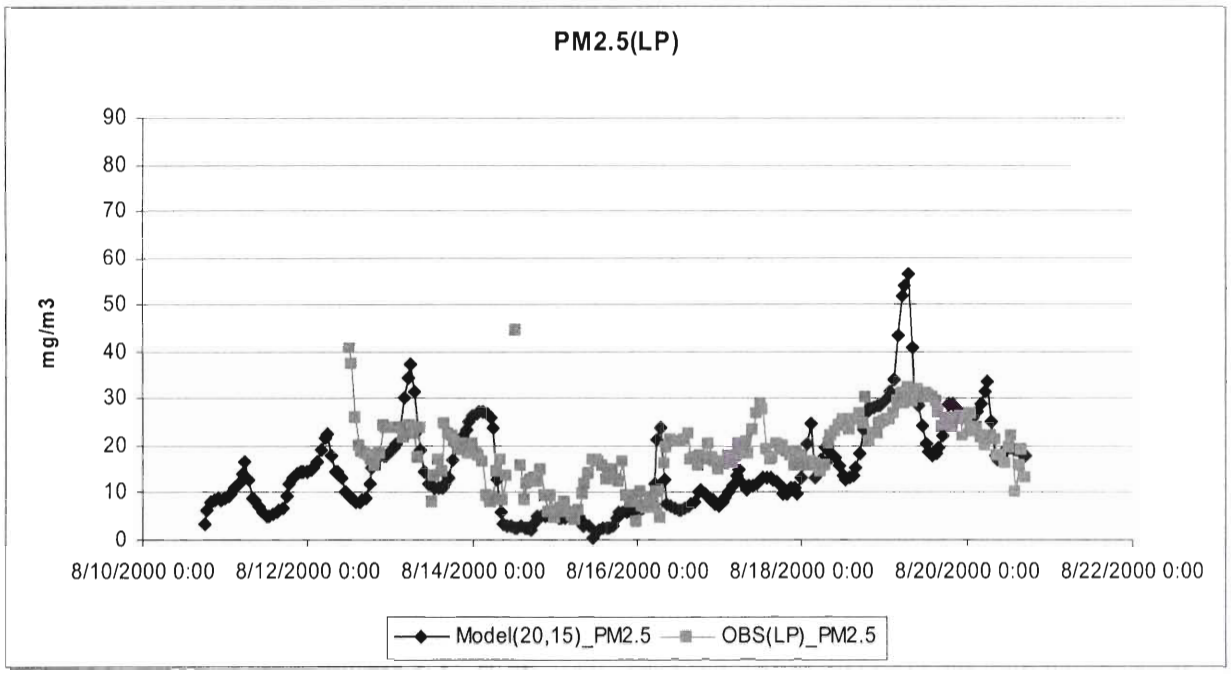

(b)

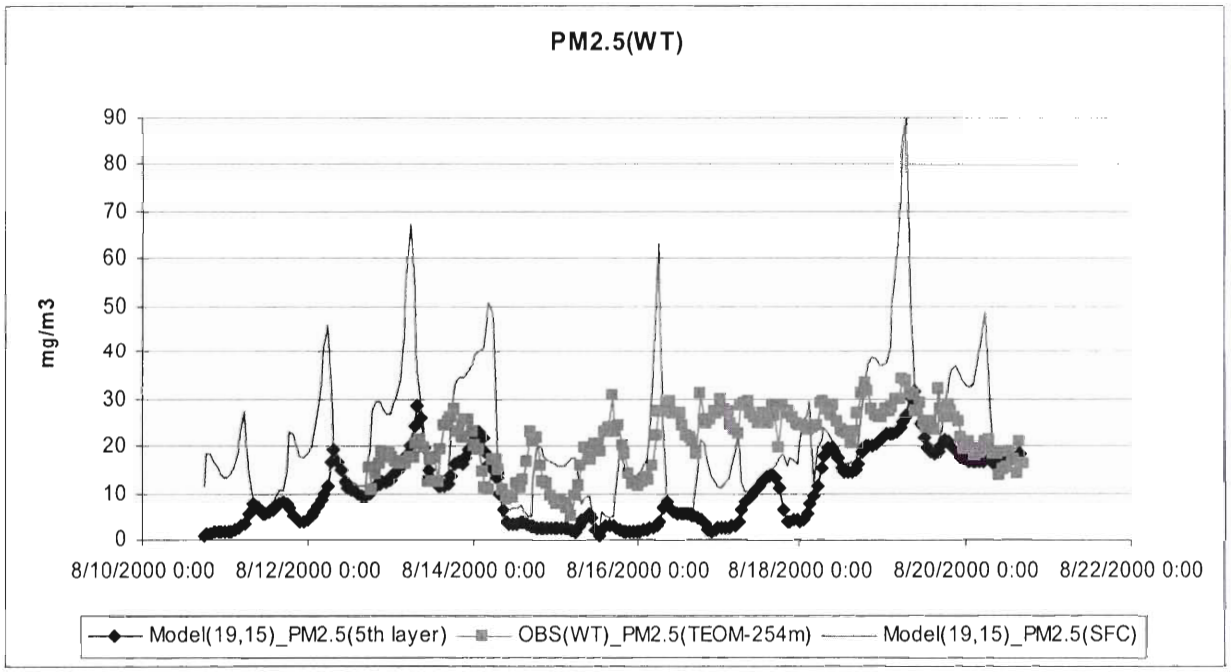

Figure 8. Comparisons of measured and simulated hourly PM 2.5 concentrations. (a) is for the LP station, and (b) is for the WT station.

(a)

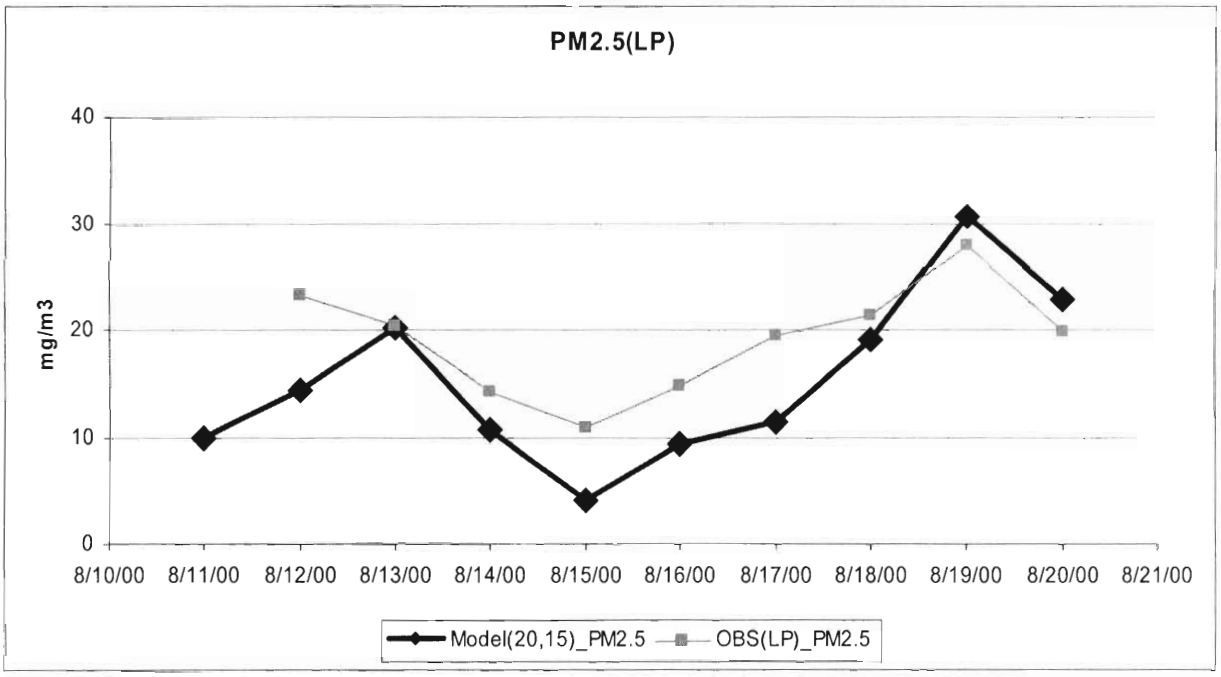

(b)

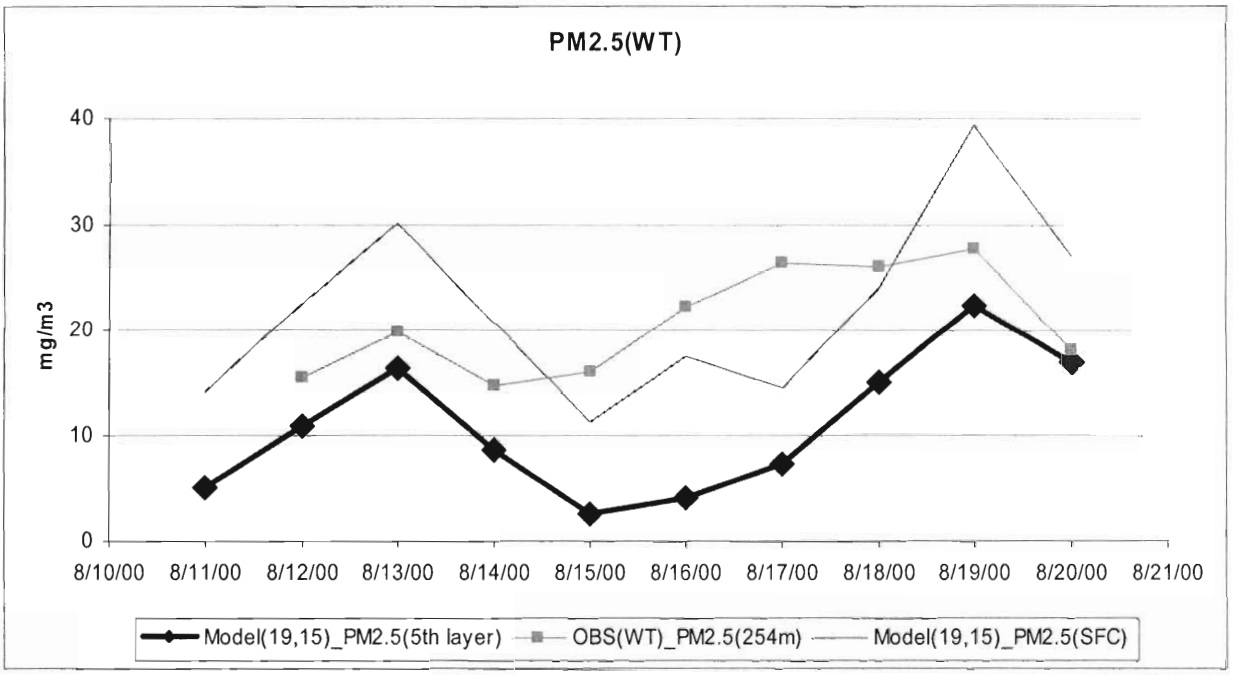

Figure 9. Comparisons of measured and simulated daily PM 2.5 concentrations. (a) is for the LP station, and (b) is for the WT station.

(c)

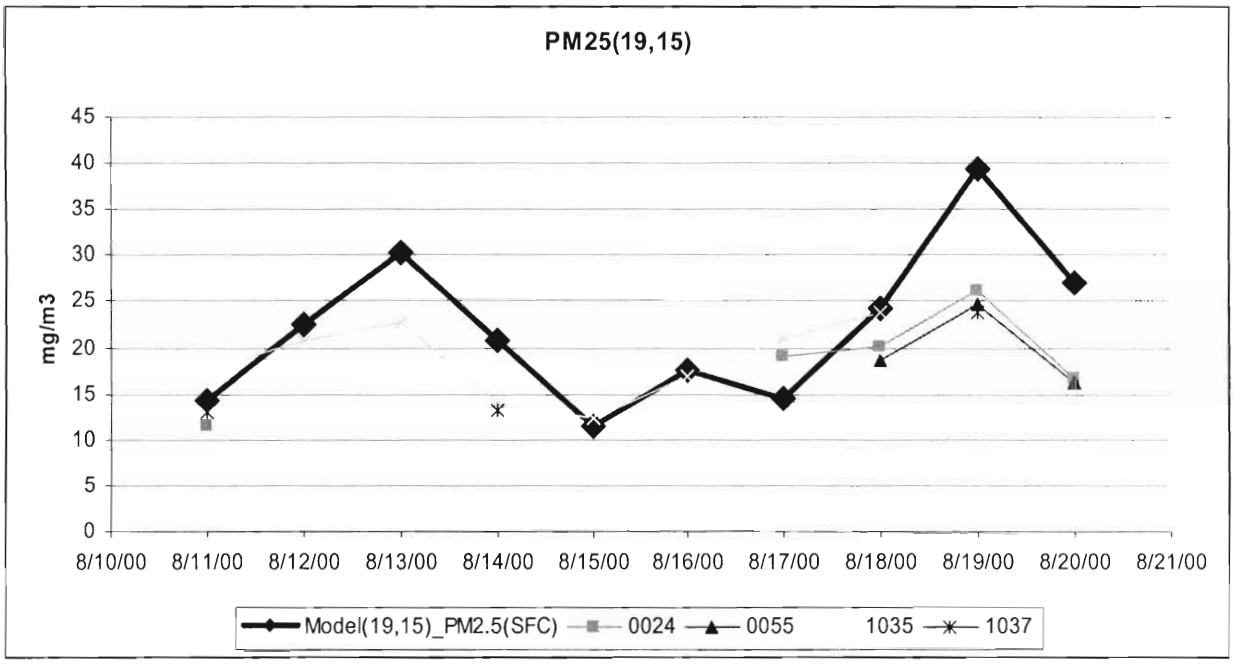

(d)

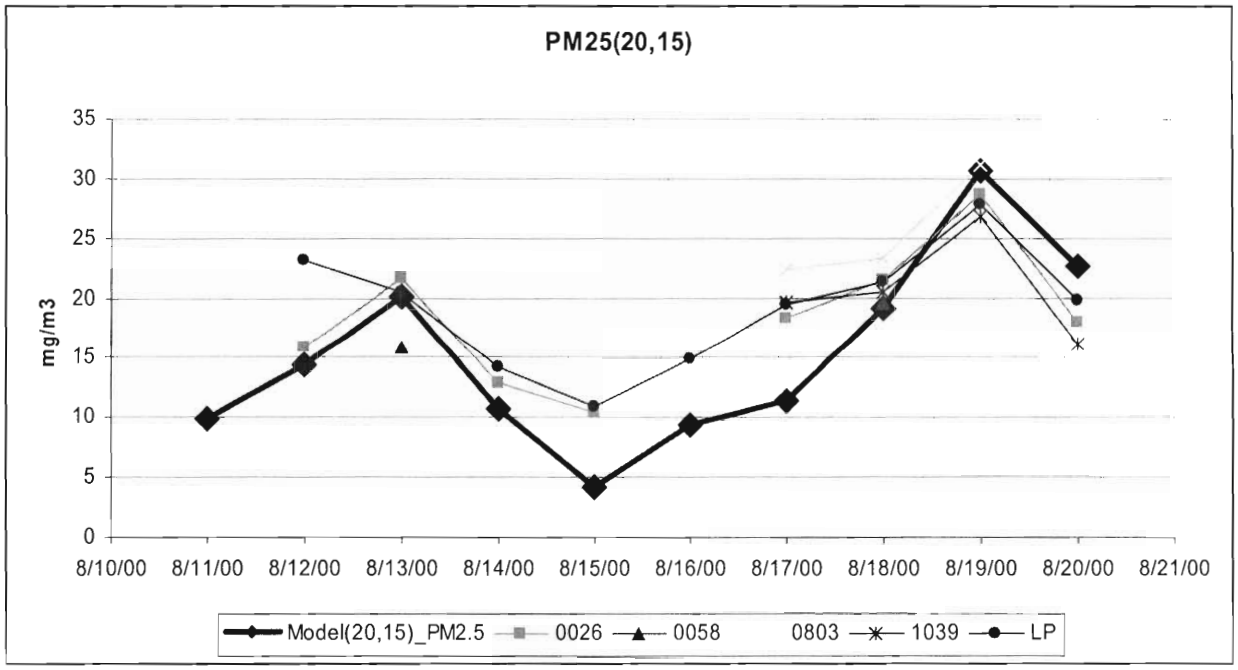

Figure 9. Continued. (c) is for the 0024, 0055, 1035, and 1037 stations, and (d) is for the 0026, 0058, 0803, 1039, and LP stations.

(e)

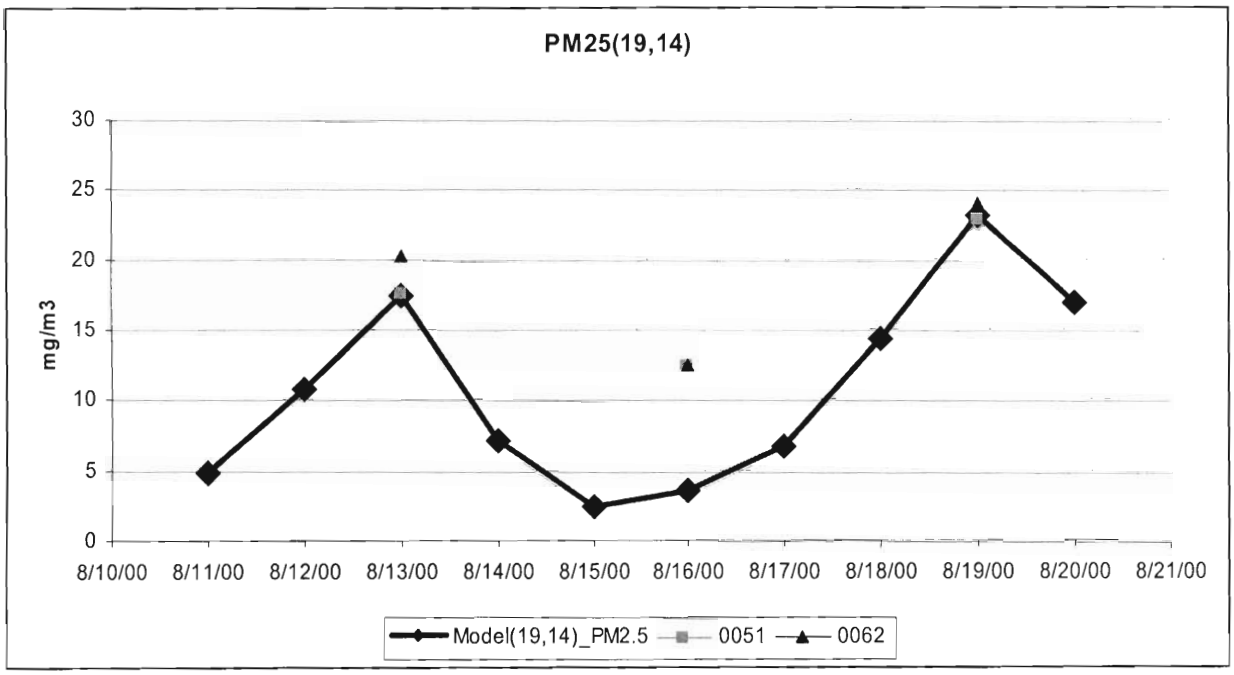

(f)

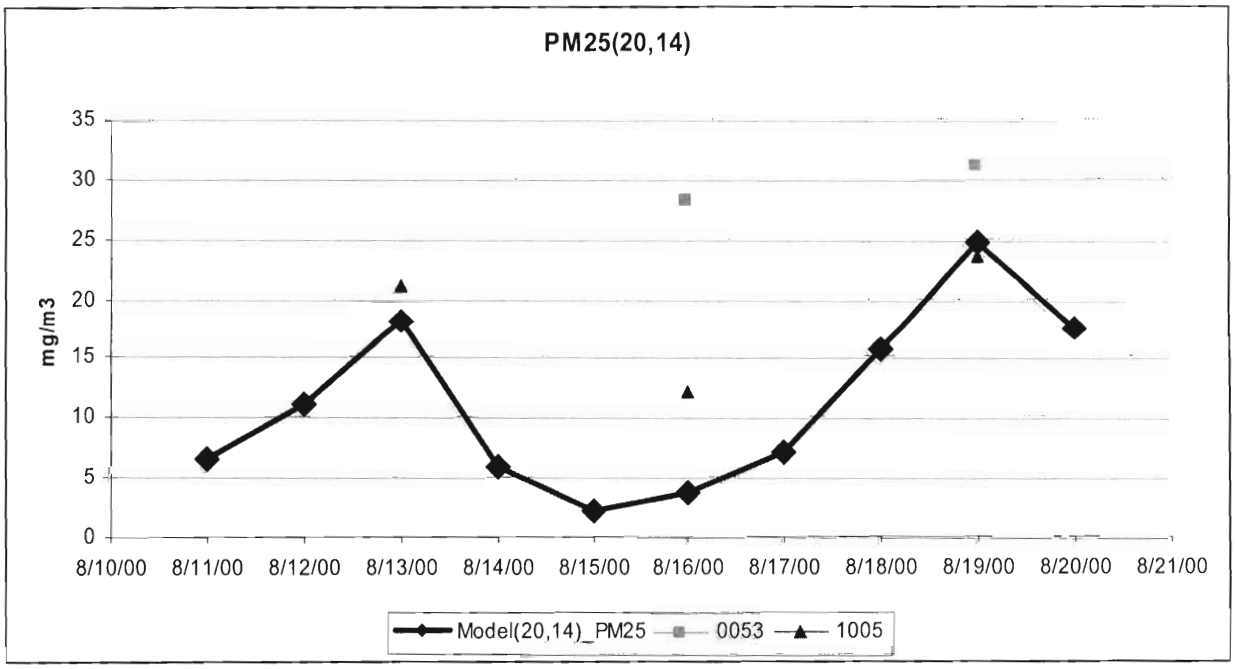

Figure 9. Continued. (e) is for the 0051and 0062 stations, and (f) is for the 0053 and 1005 stations.

(g)

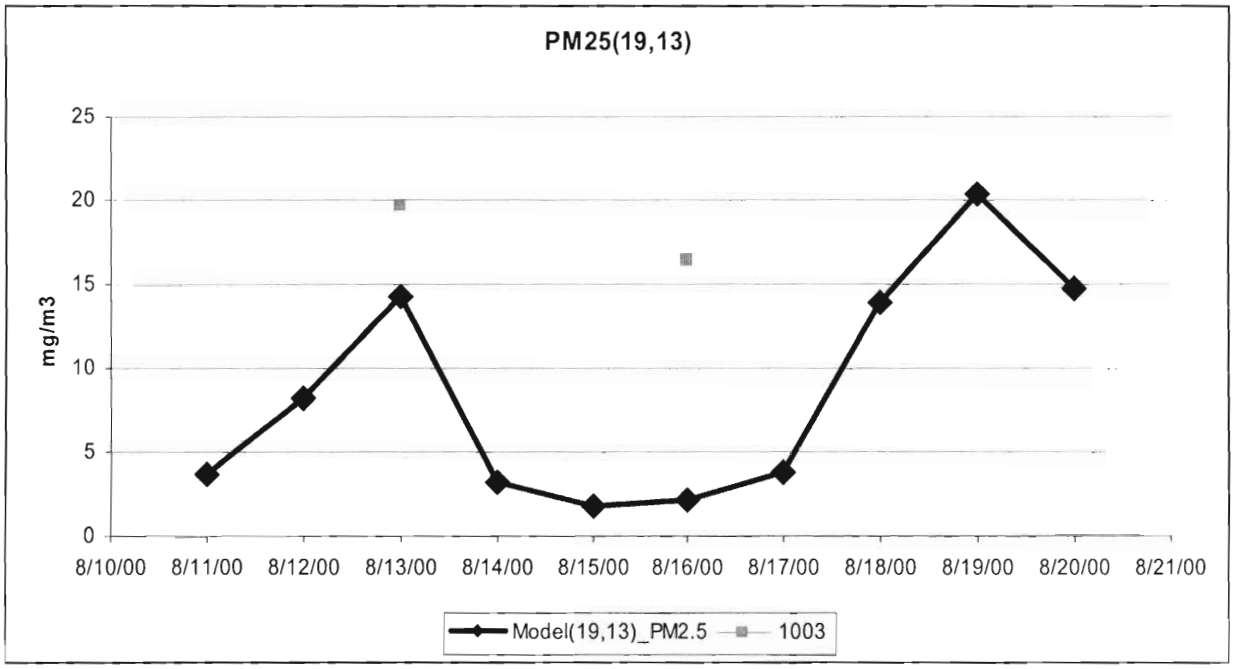

(h)

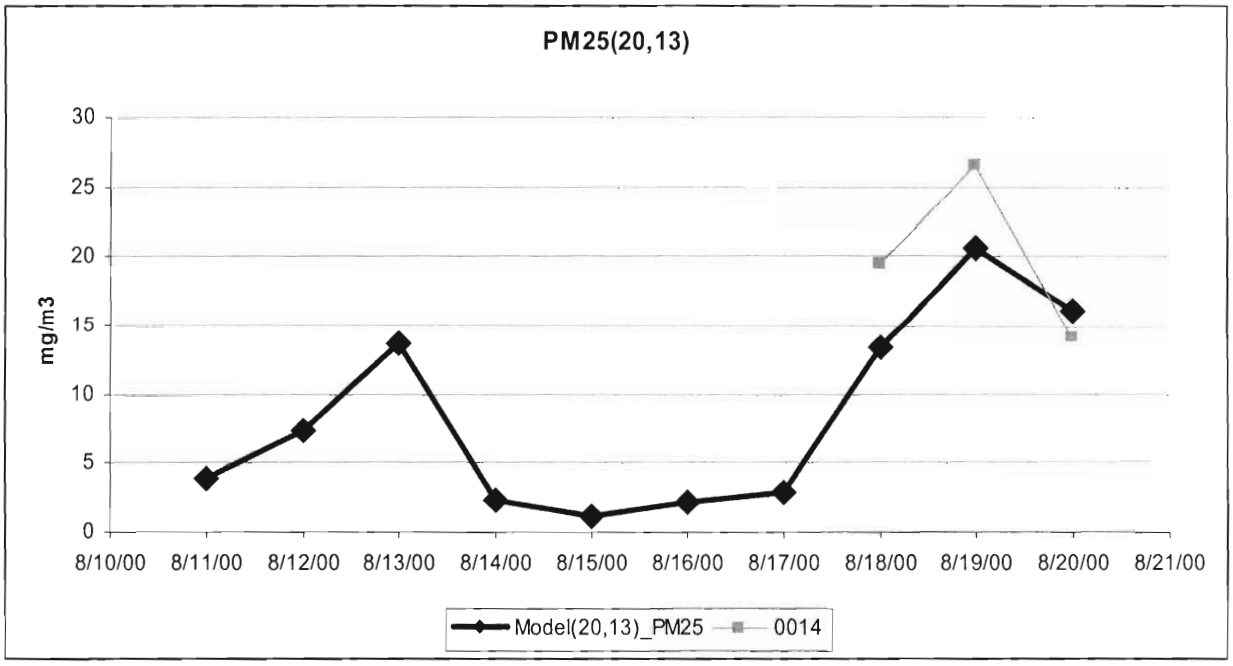

Figure 9. Continued. (g) is for the 1003 station, and (h) is for the 0014 station.

(a)

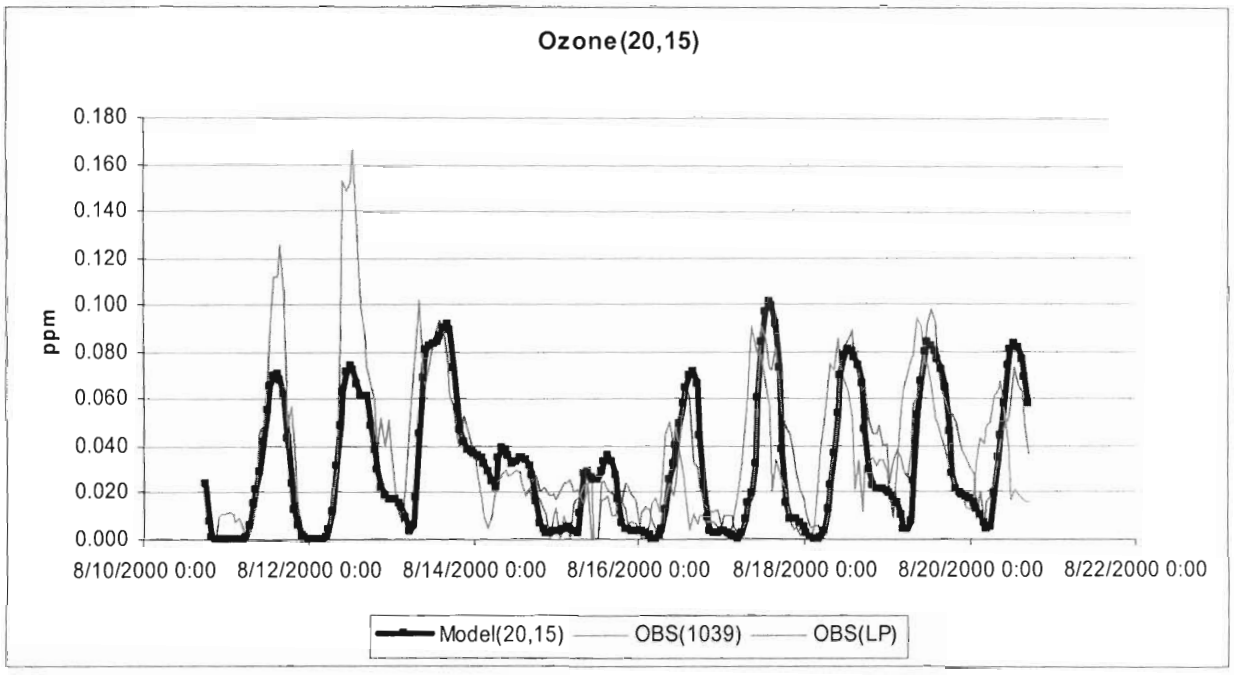

(b)

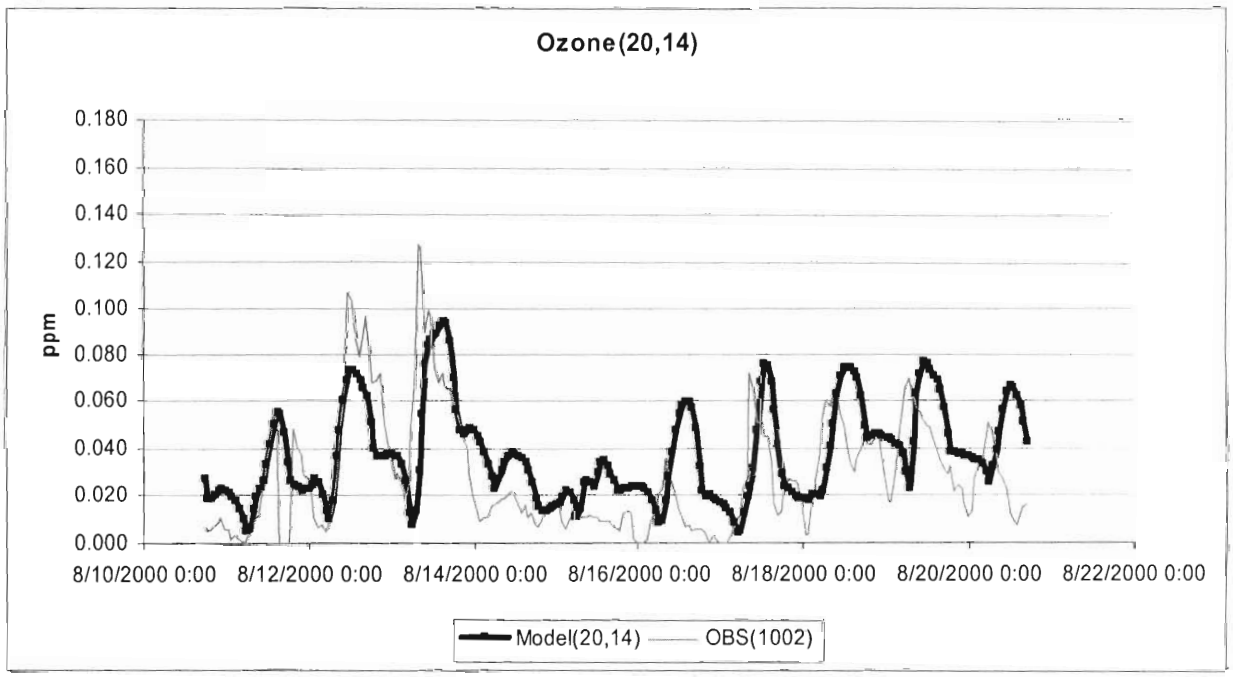

Figure 10. Comparisons of measured and simulated hourly ozone concentrations. (a) is for the LP station, and (b) is for the WT station.

(c)

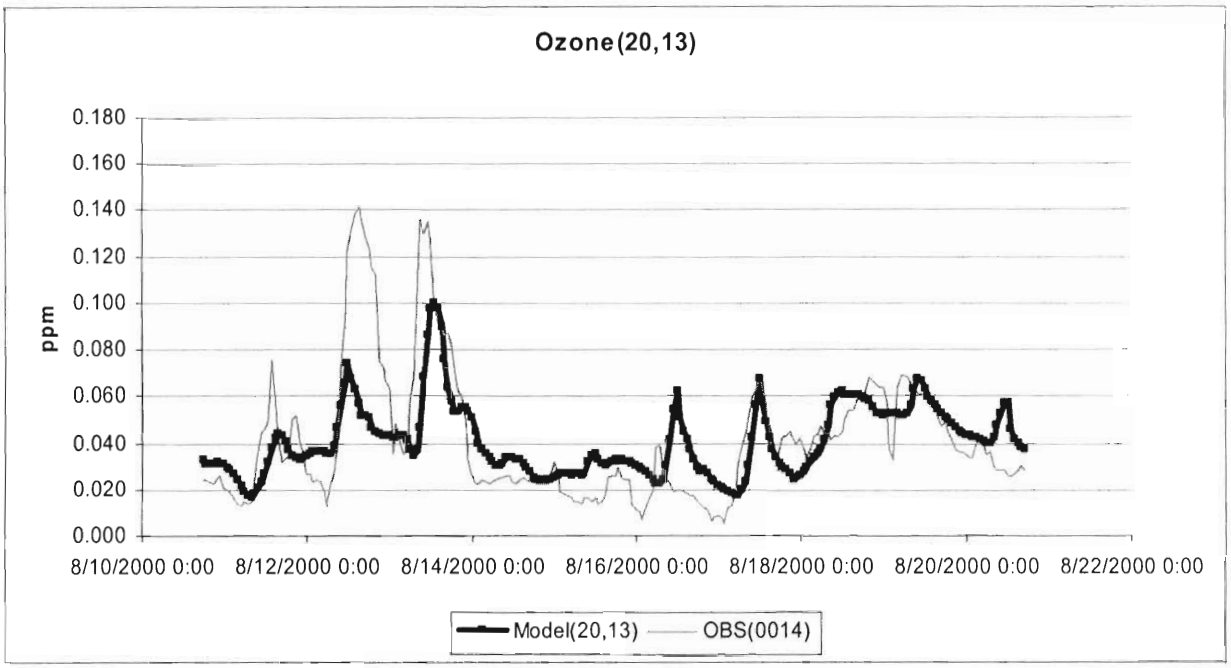

(d)

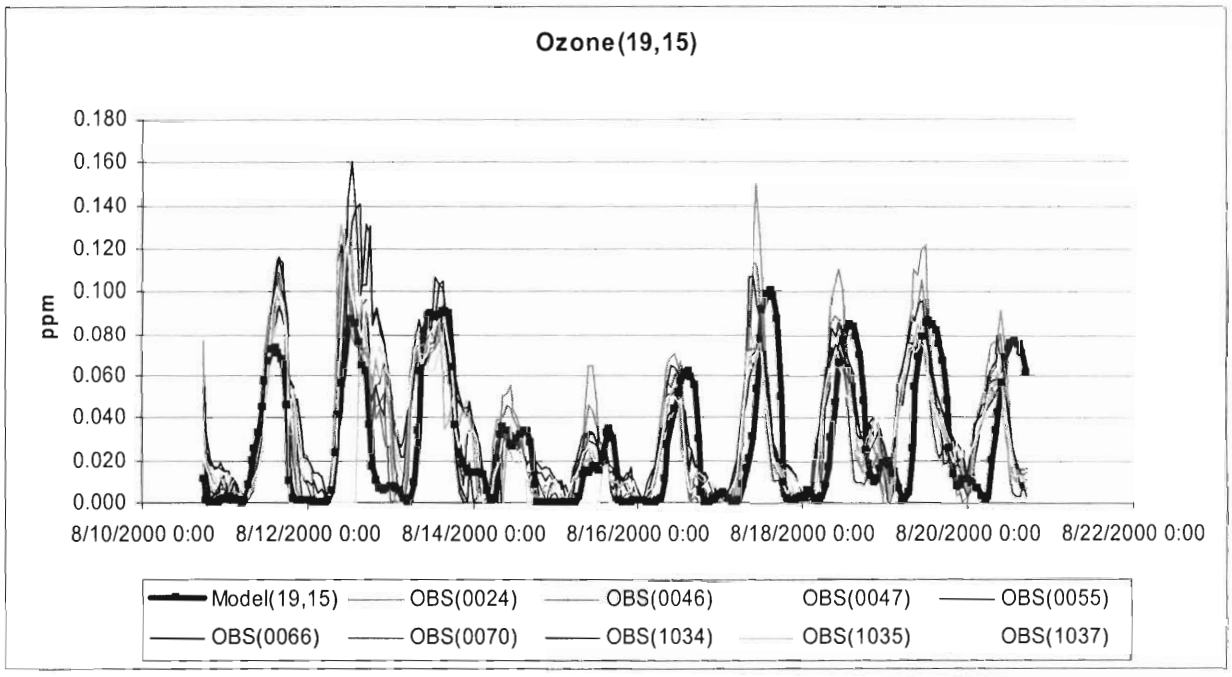

Figure 10. Continued. (c) is for the 0014 station, and (d) is for the 0024, 0046, 0047, 0055, 0066, 0070, 1034, 1035 and 1037 stations.

(e)

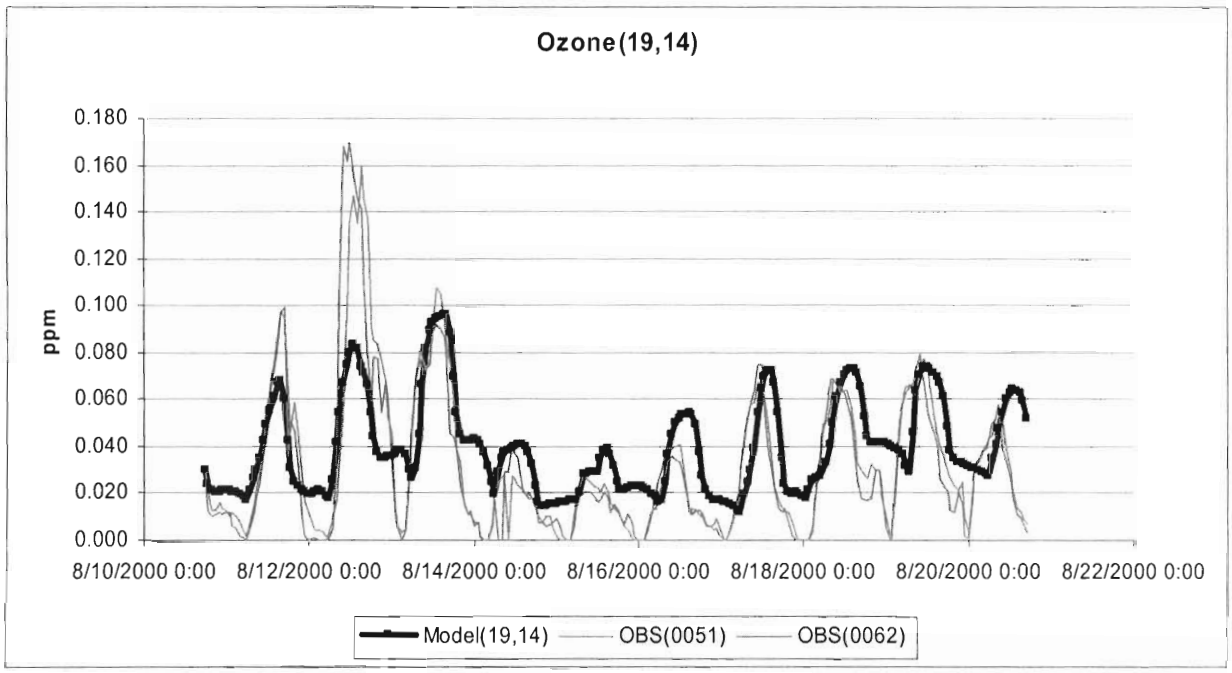

(f)

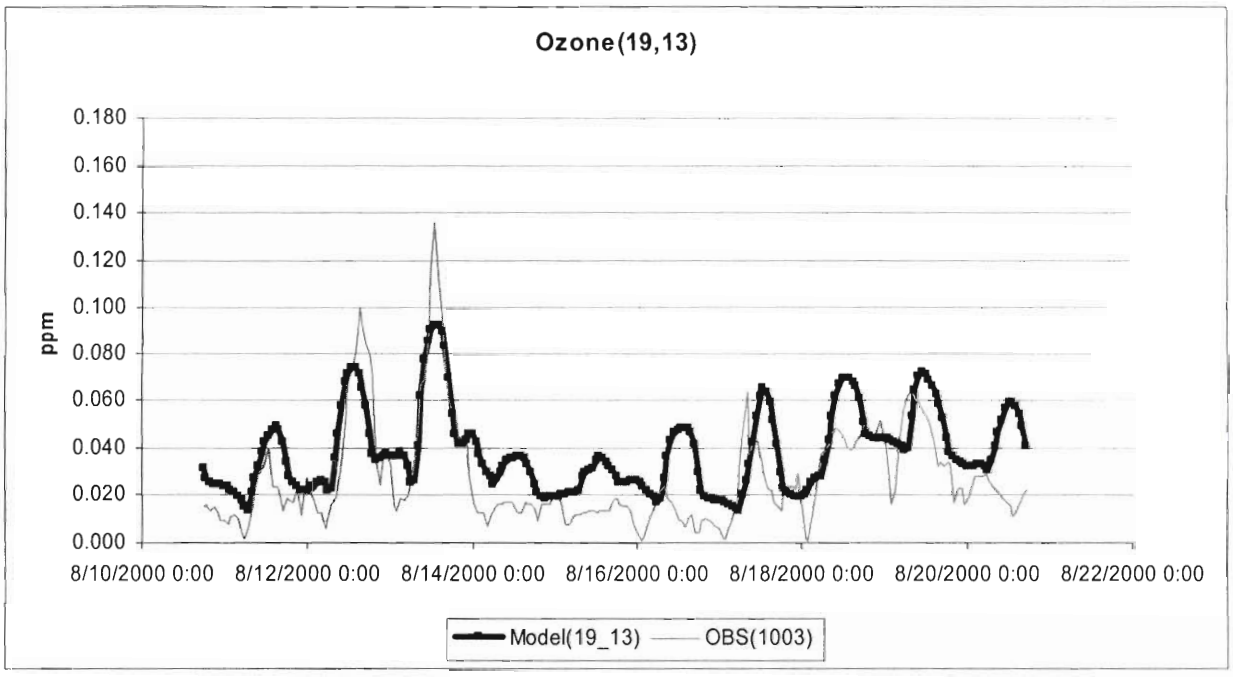

Figure 10. Continued. (e) is for the 0051, 0062 stations, and (f) is for the 1003 station.

(g)

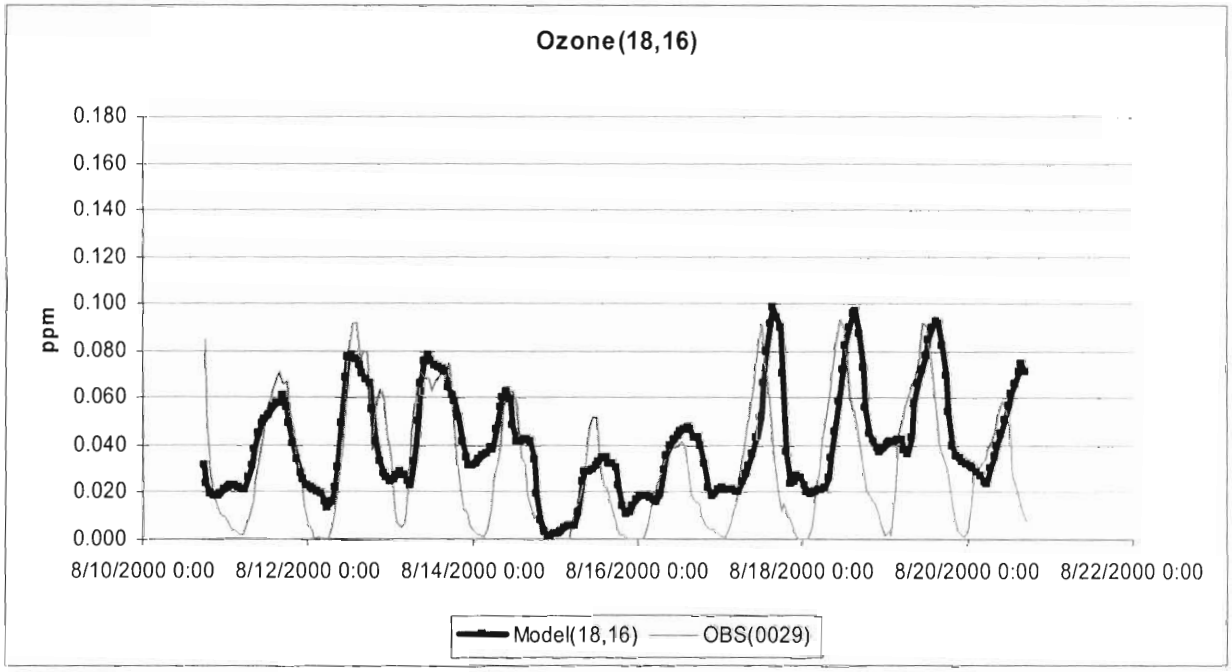

(h)

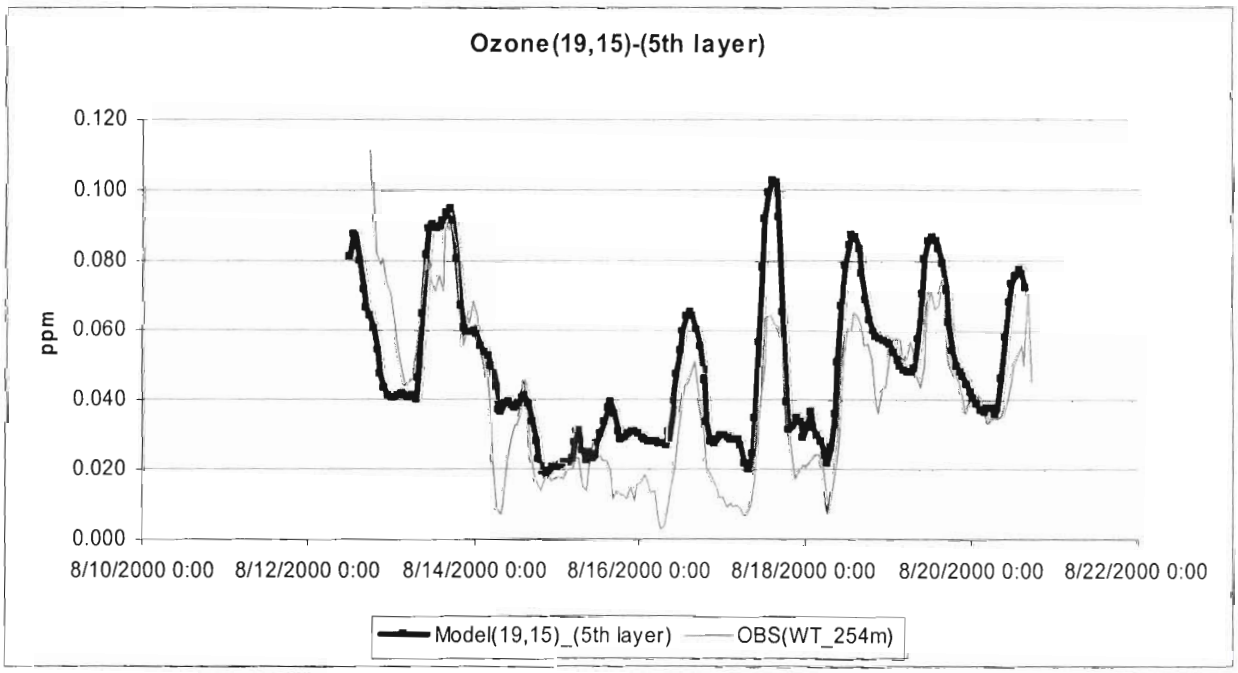

Figure 10. Continued. (g) is for the 0029 station, and (h) is for the WT station.

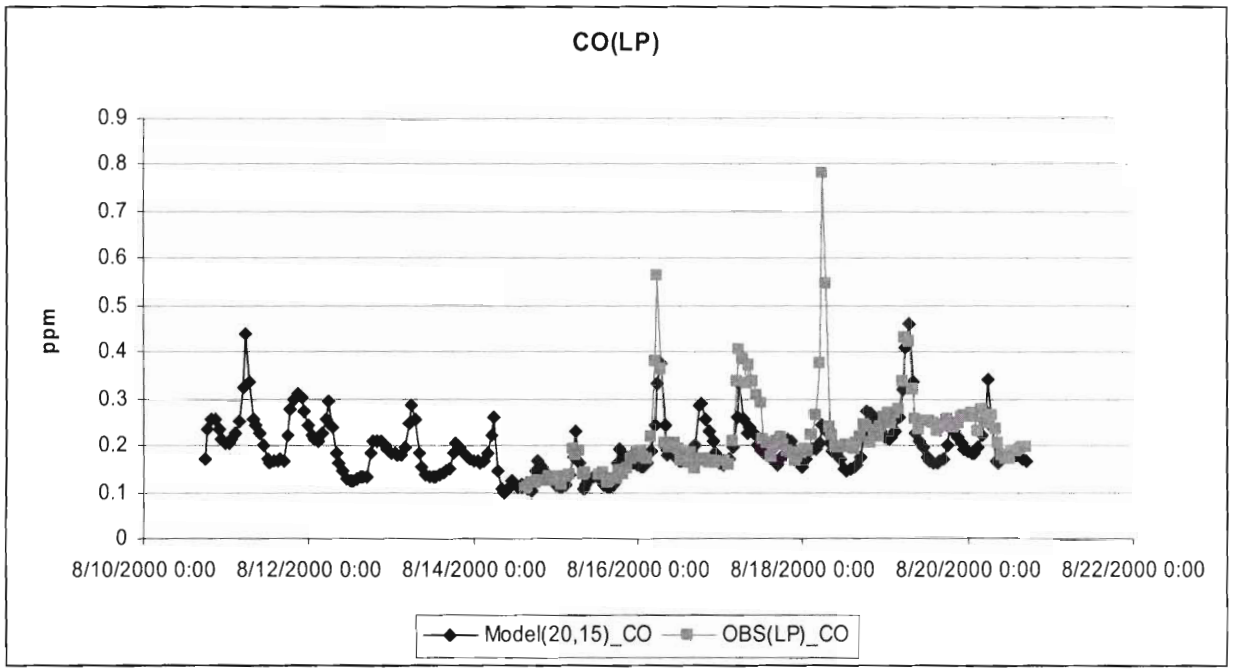

Figure 11. Comparison of measured and simulated hourly carbon monoxide concentrations for the LP station.

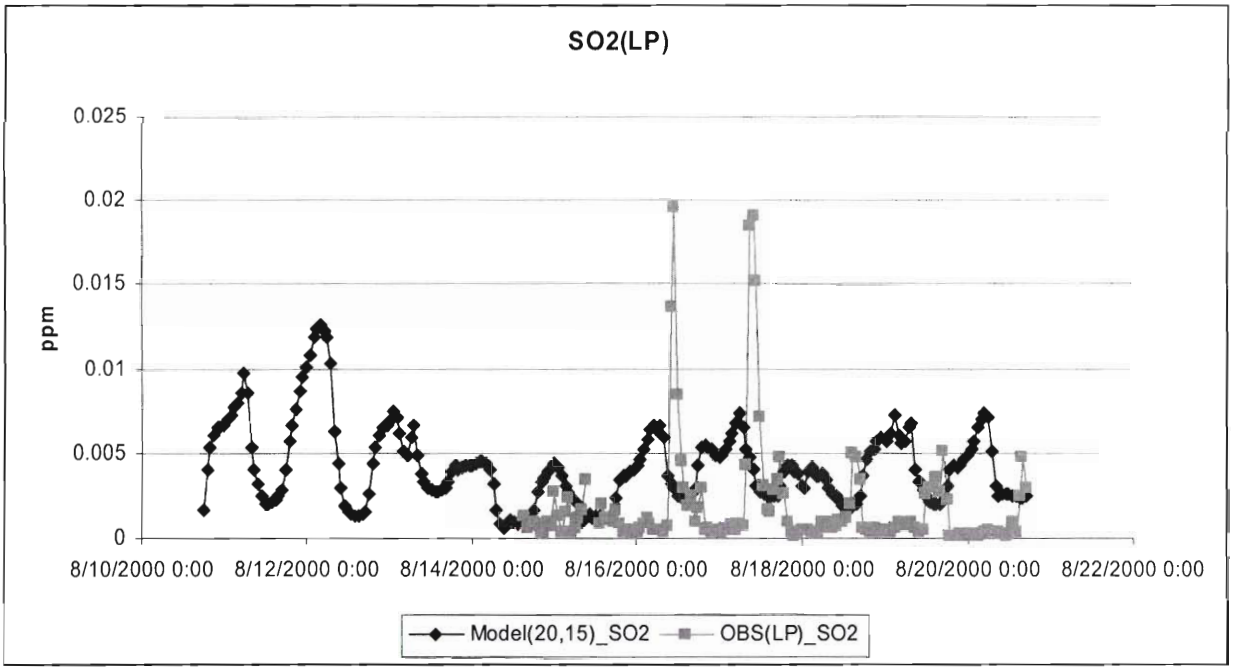

Figure 12. Comparison of measured and simulated hourly sulfur dioxide concentrations for the LP station.

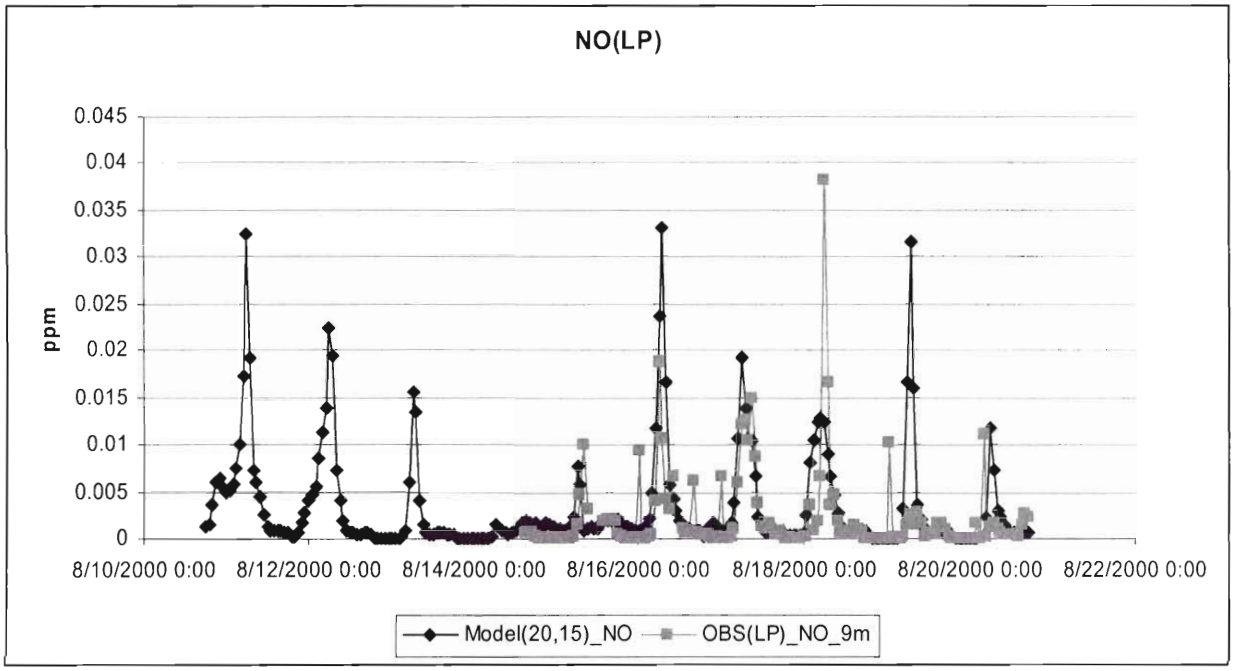

Figure 13. Comparison of measured and simulated hourly nitric oxide concentrations for the LP station.

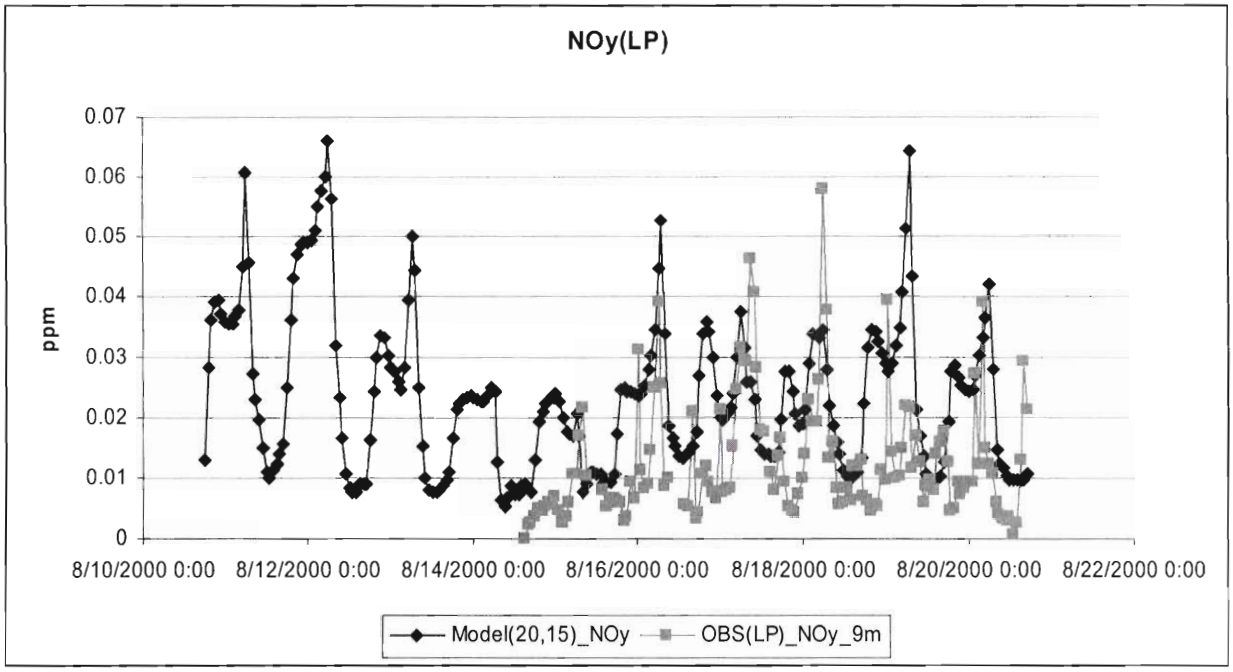

Figure 14. Comparison of measured and simulated hourly NOy concentrations for the LP station.

3. Emissions in 2000 and in 2007

We examined changes in an emission inventory from 2000 to 2007. We collected an emission inventory in 2000. Then, we prepared an emission inventory in 2007 by applying a federal control strategy and EGAS (Economic Growth Analysis System) growth factors. We plotted the emission of criteria pollutants: ammonium, carbon monoxide, volatile organic carbon, sulfur dioxide, PM 2.5, PM 10, and NOx in 2000 and 2007. Figure 15 showed sum of area, nonroad, mobile, point, and biogenic sources of emission. Figures 16 through 23 illustrated emissions of each source.

(a)

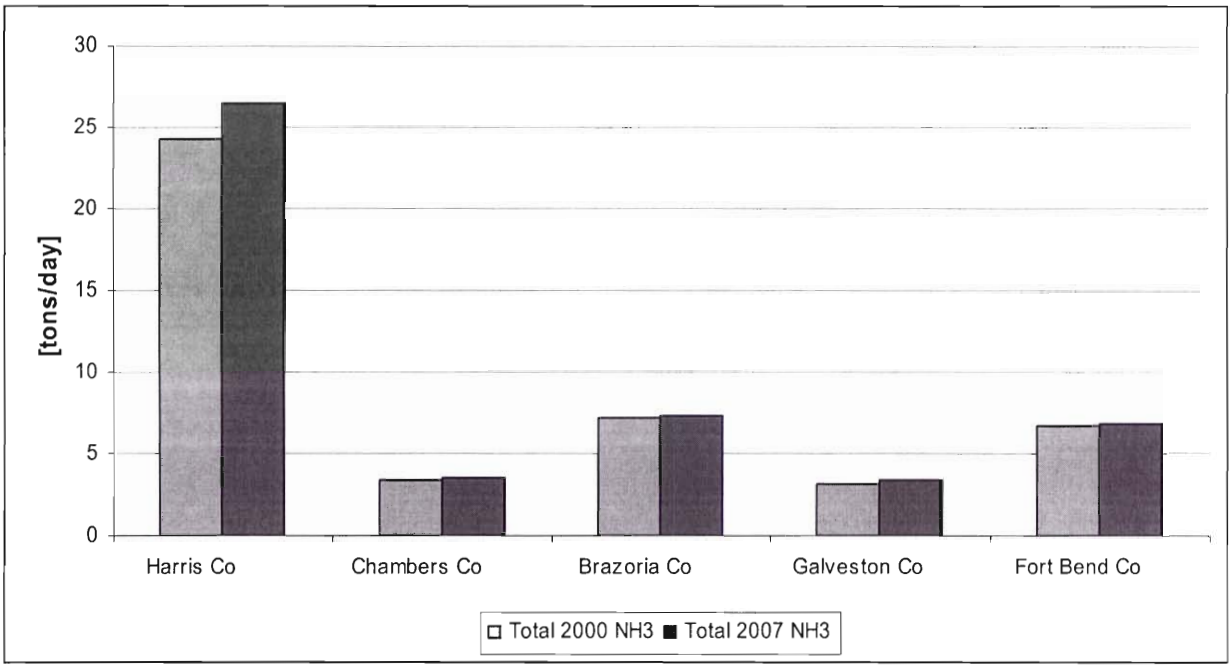

(b)

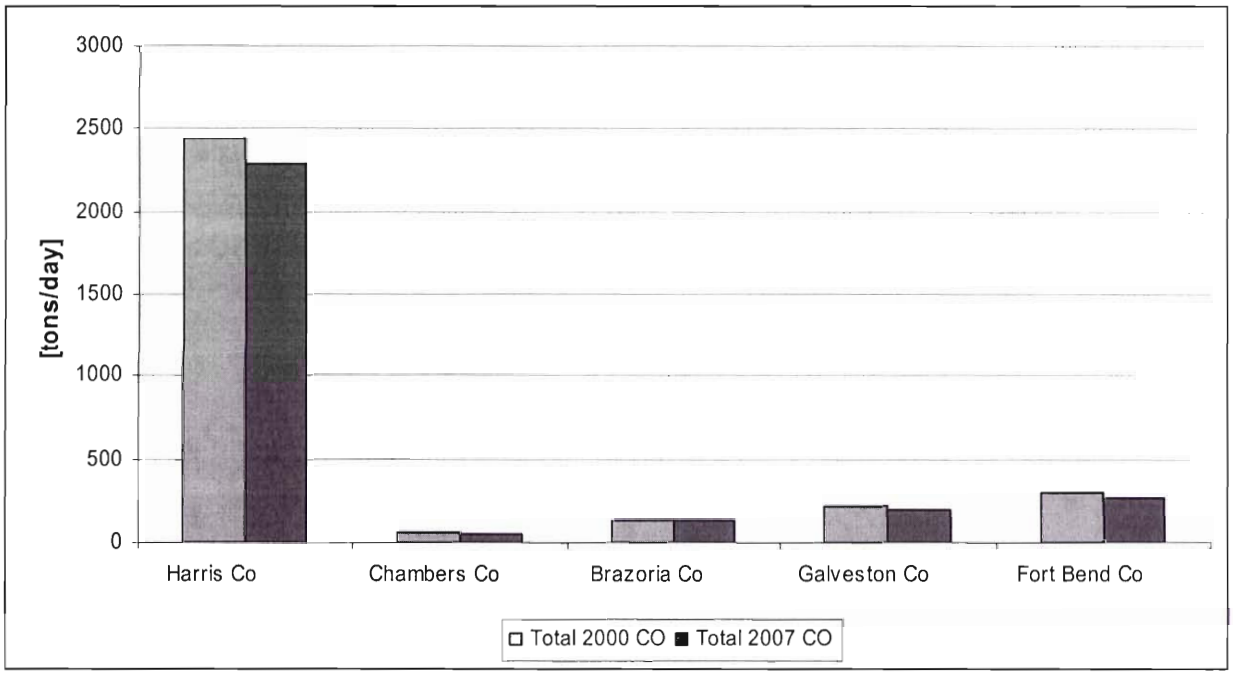

Figure 15. Total emission in 2000 and in 2007. (a) is for ammonium emission, and (b) is for carbon monoxide emission.

(c)

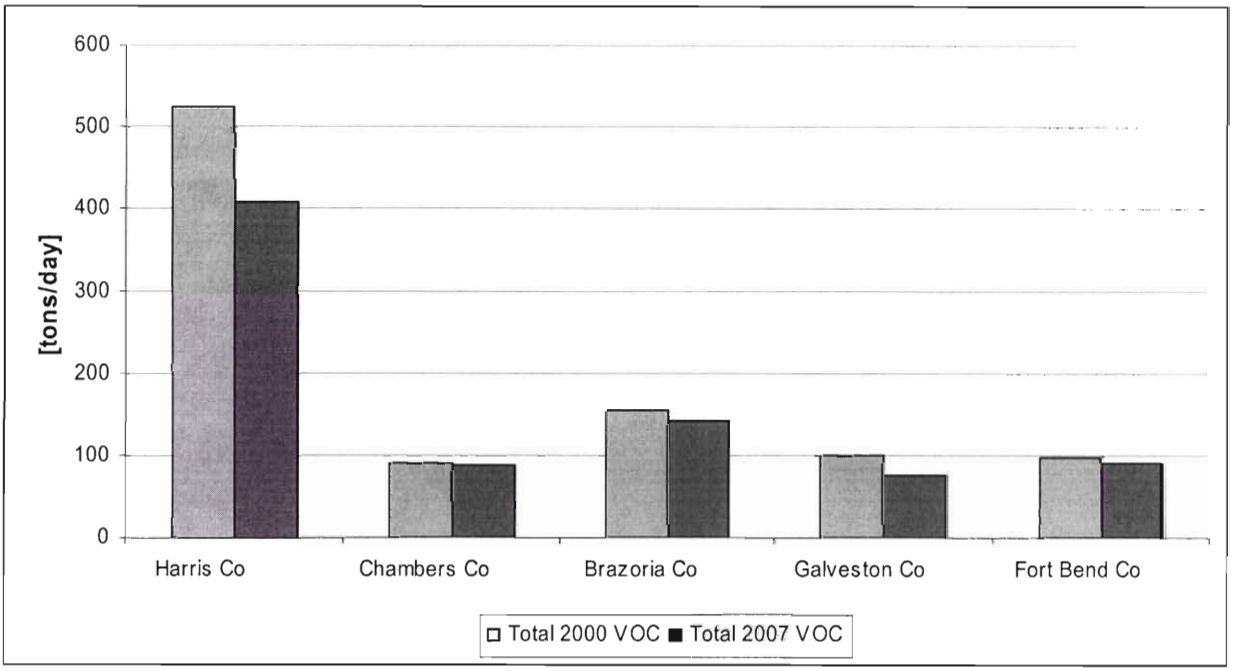

(d)

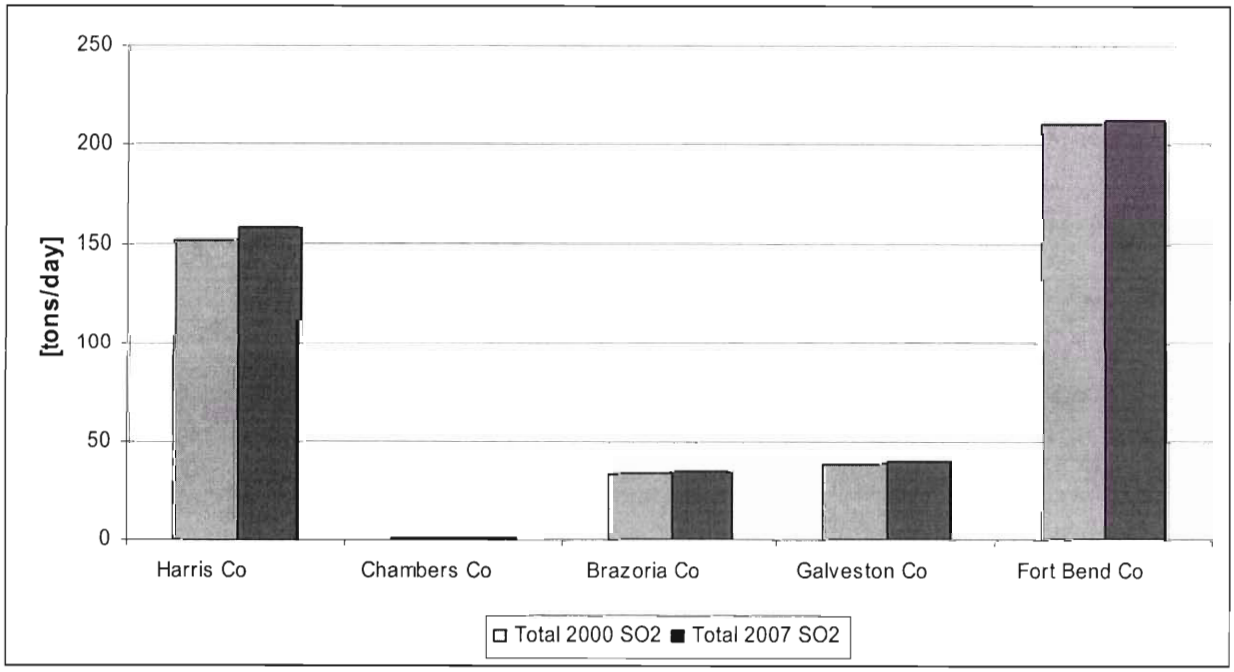

Figure 15. Continued. (c) is for volatile organic carbon emission, and (b) is for sulfur dioxide emission.

(e)

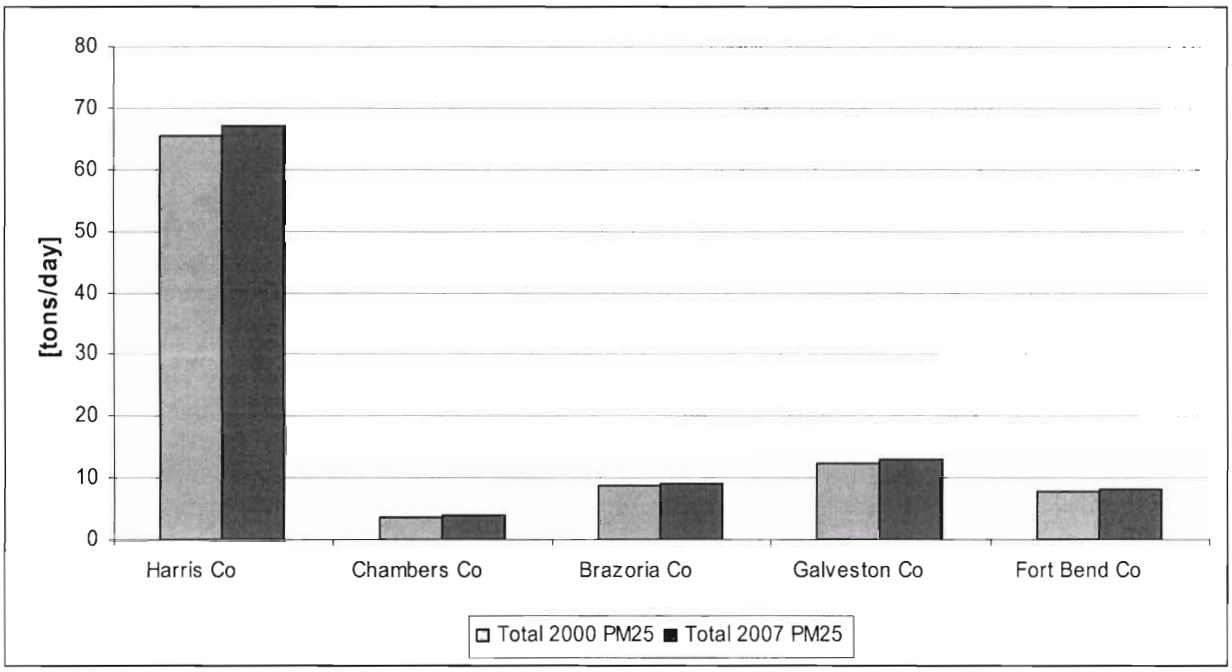

(f)

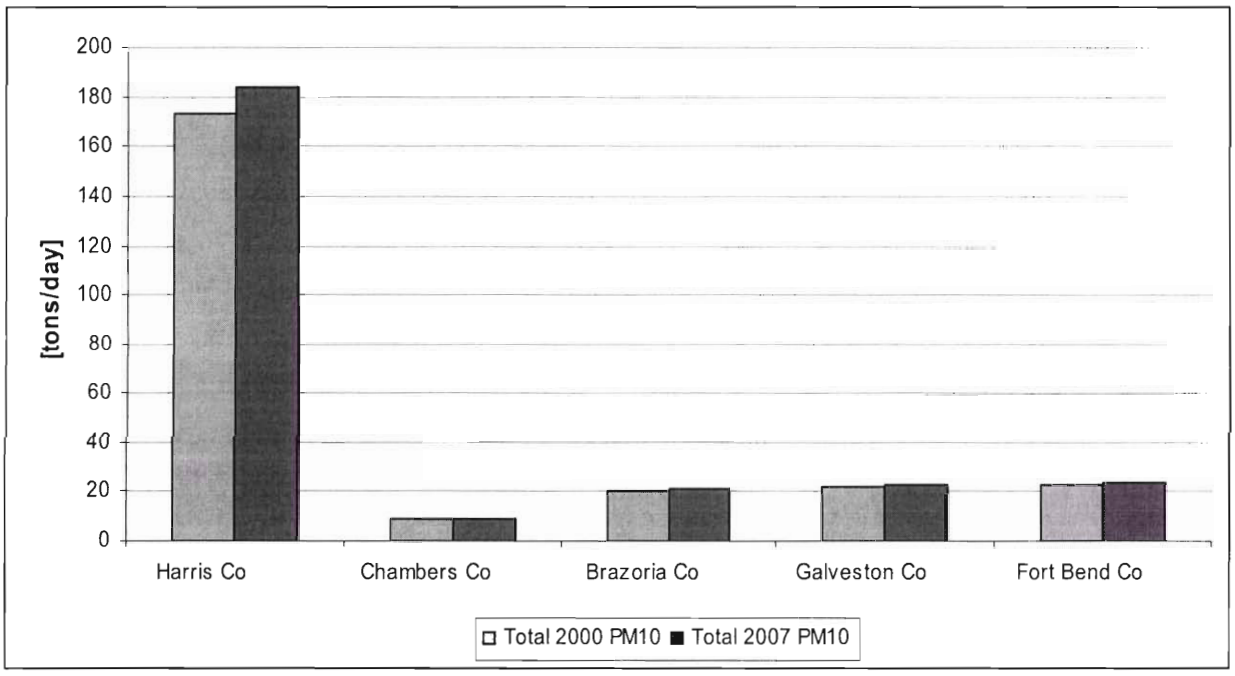

Figure 15. Continued. (e) is for PM 2.5, and (f) is for PM 10 emission.

(g)

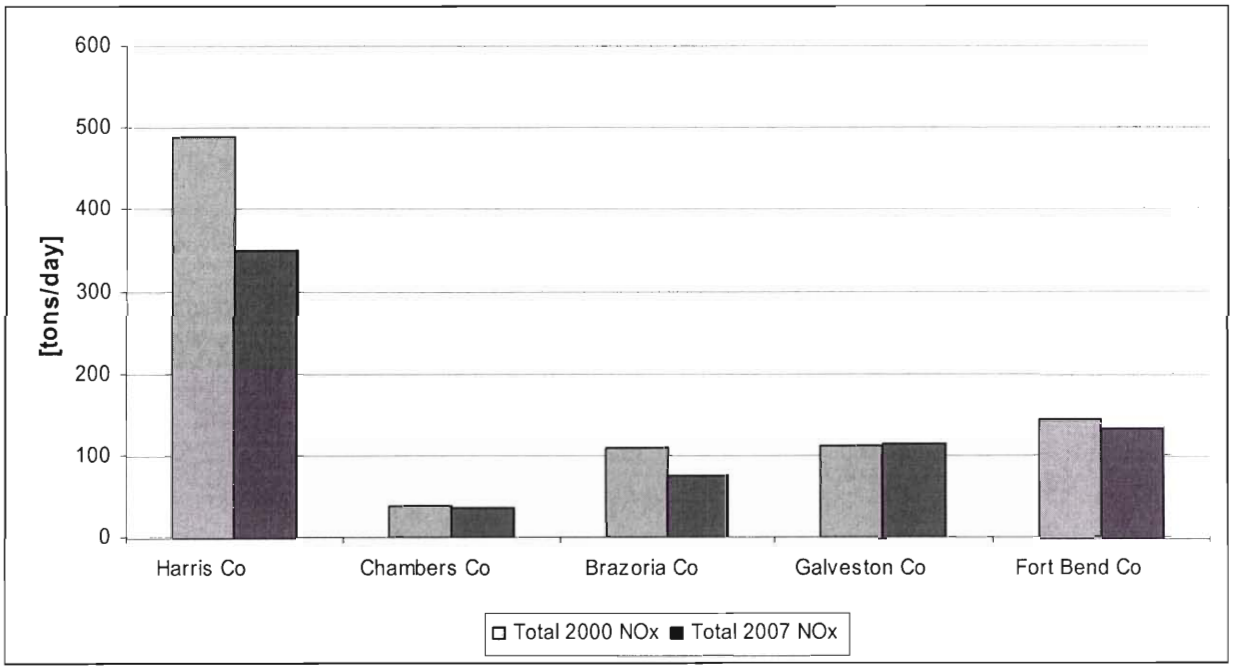

Figure 15. Continued. (g) is for NOx emission.

(a)

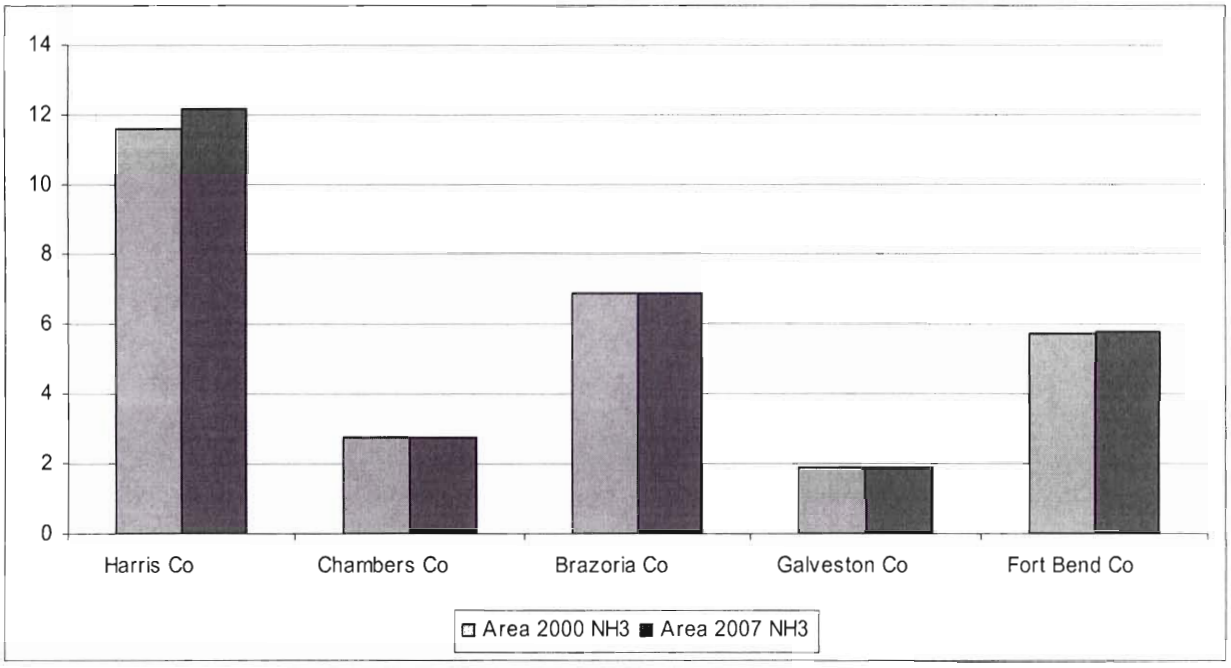

(b)

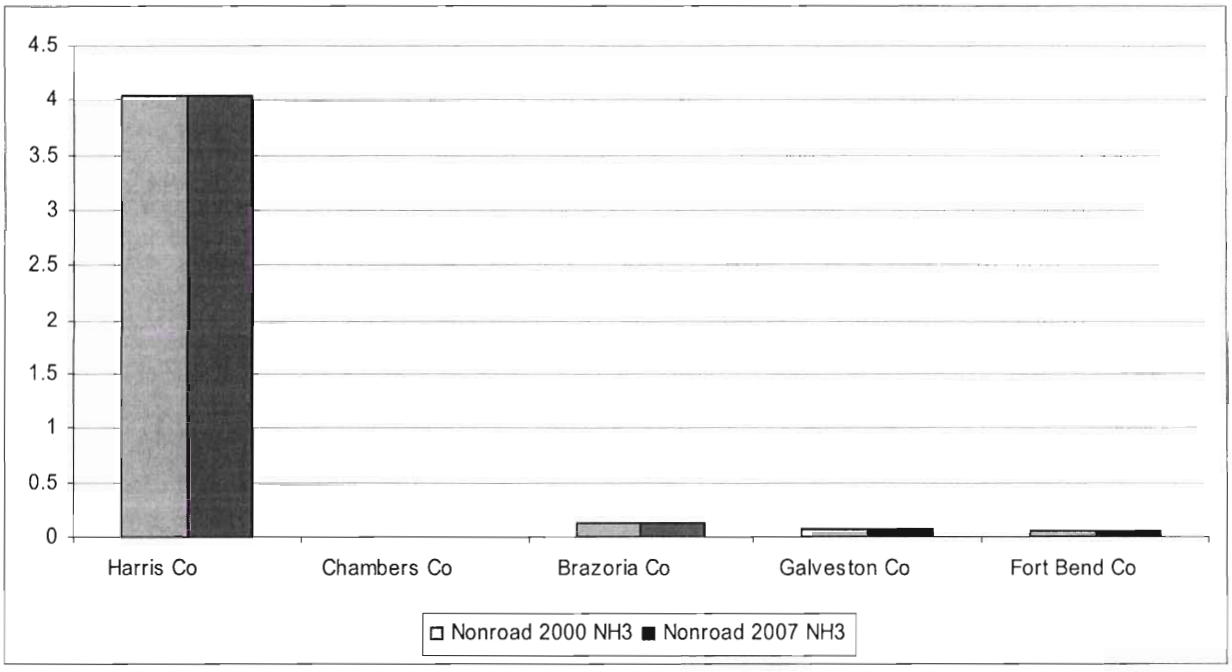

Figure 16. Ammonium emission in 2000 and in 2007 [tons/day]. (a) is area source emission, and (b) is nonroad source emission.

(c)

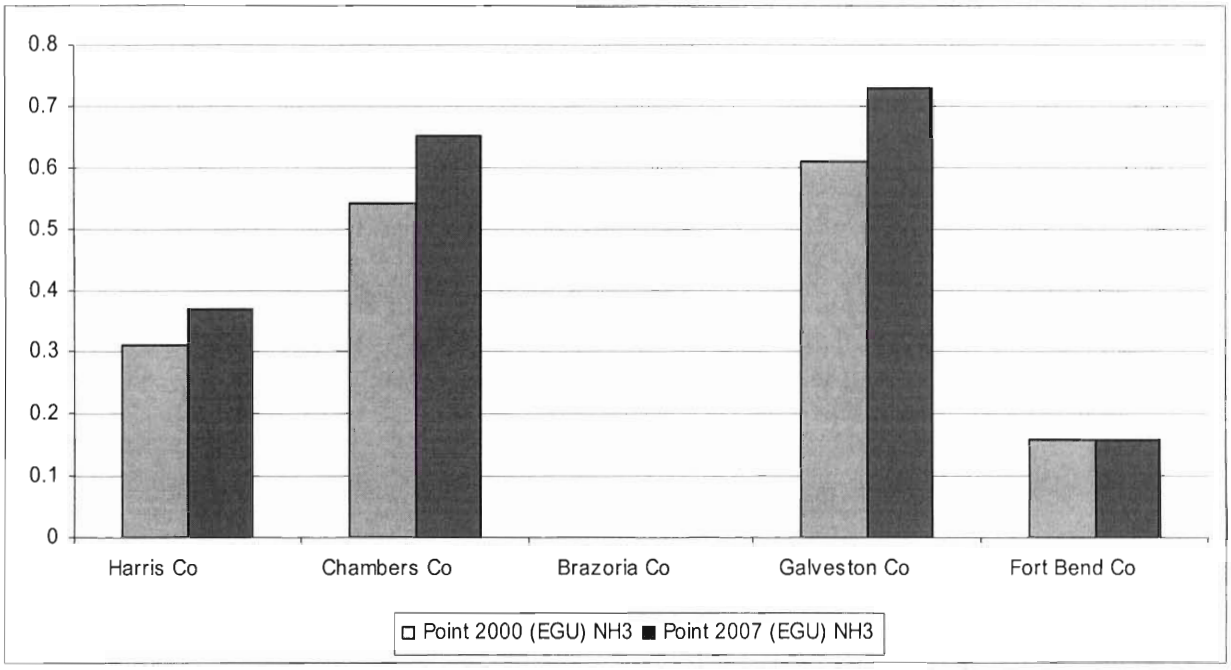

(d)

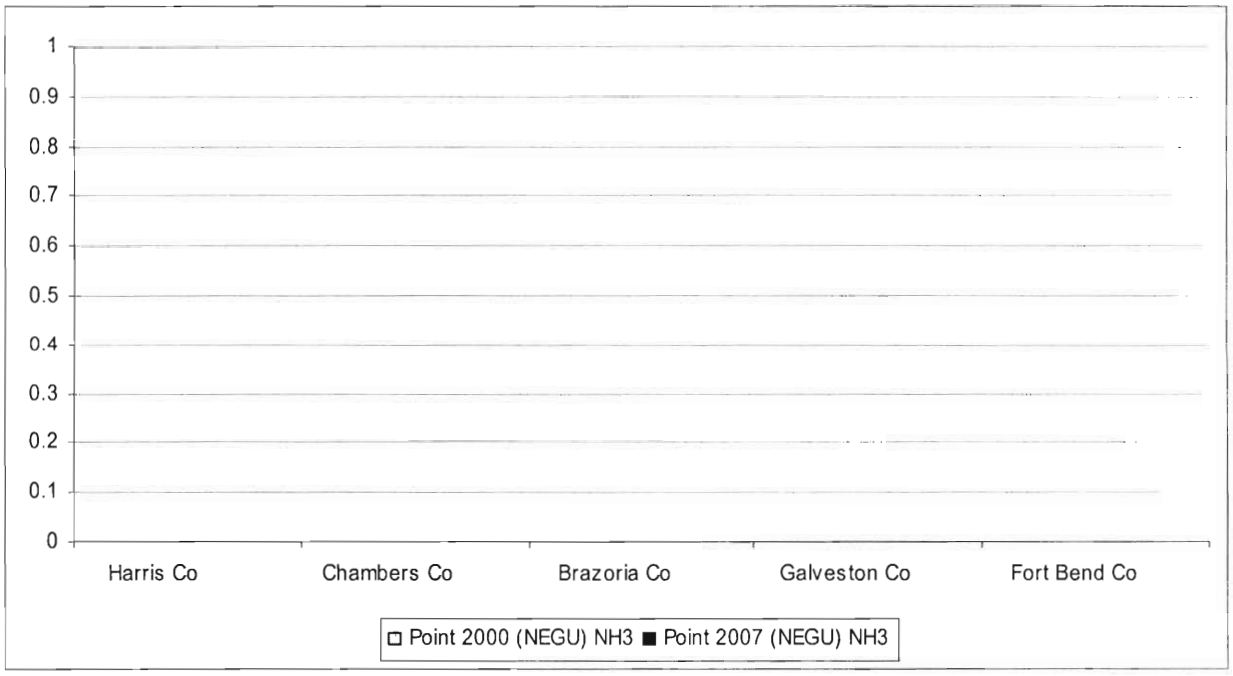

Figure 16. Continued. (c) is point source (electricity generating units) emission, and (d) is point source (non-electricity generating units) emission.

(e)

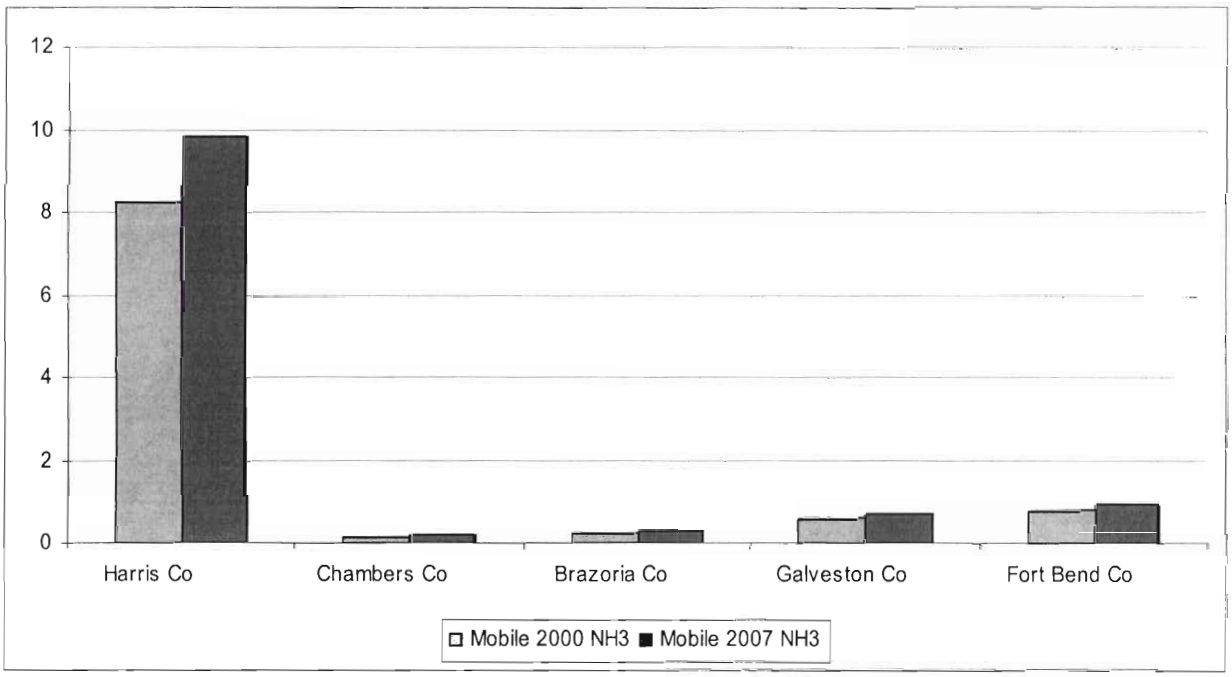

Figure 16. Continued. (e) is mobile source emission

(a)

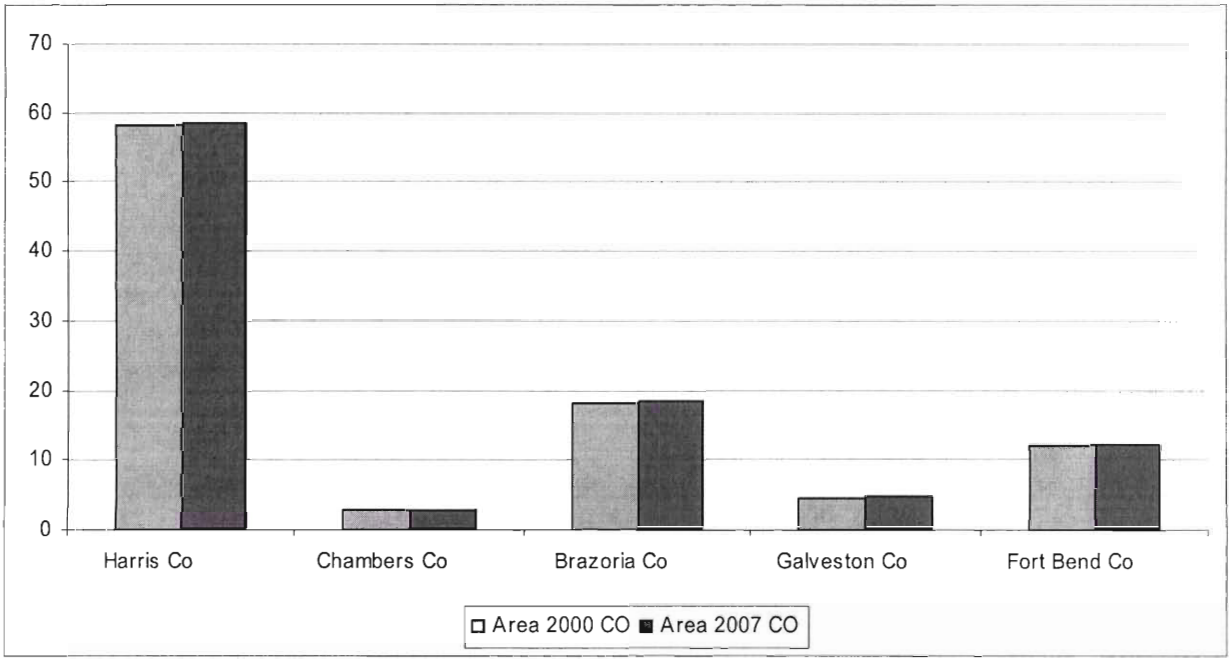

(b)

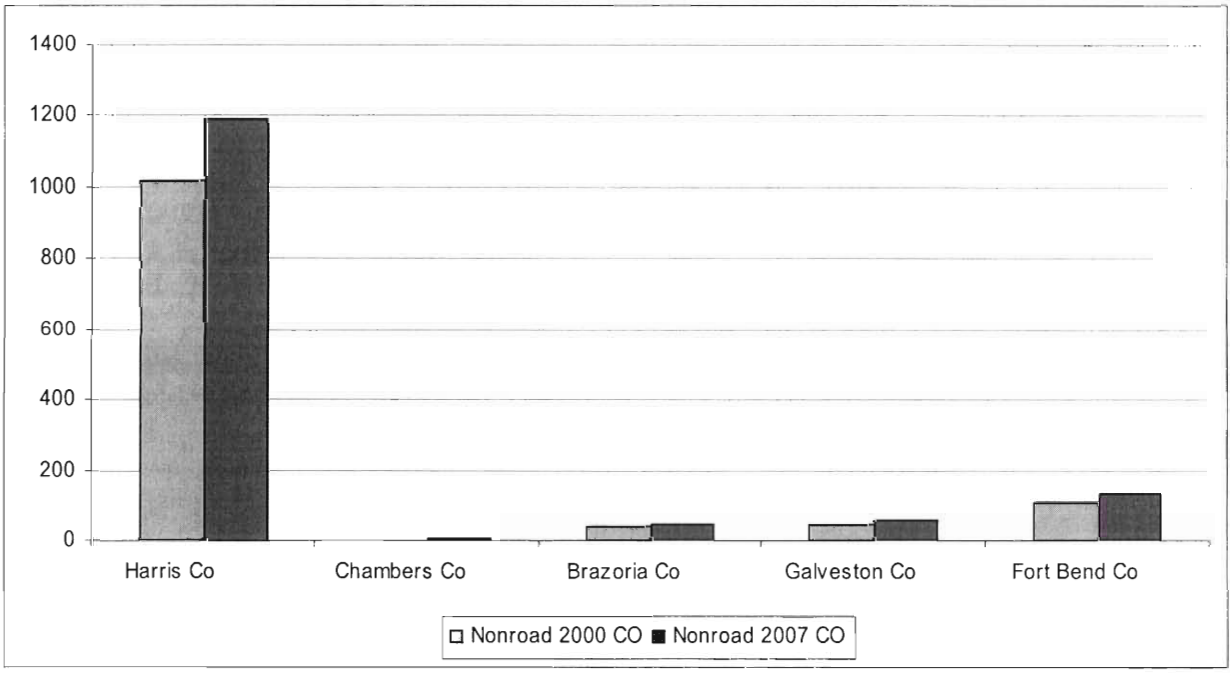

Figure 17. Carbon monoxide emission in 2000 and in 2007 [tons/day]. (a) is area source emission, and (b) is nonroad source emission.

(c)

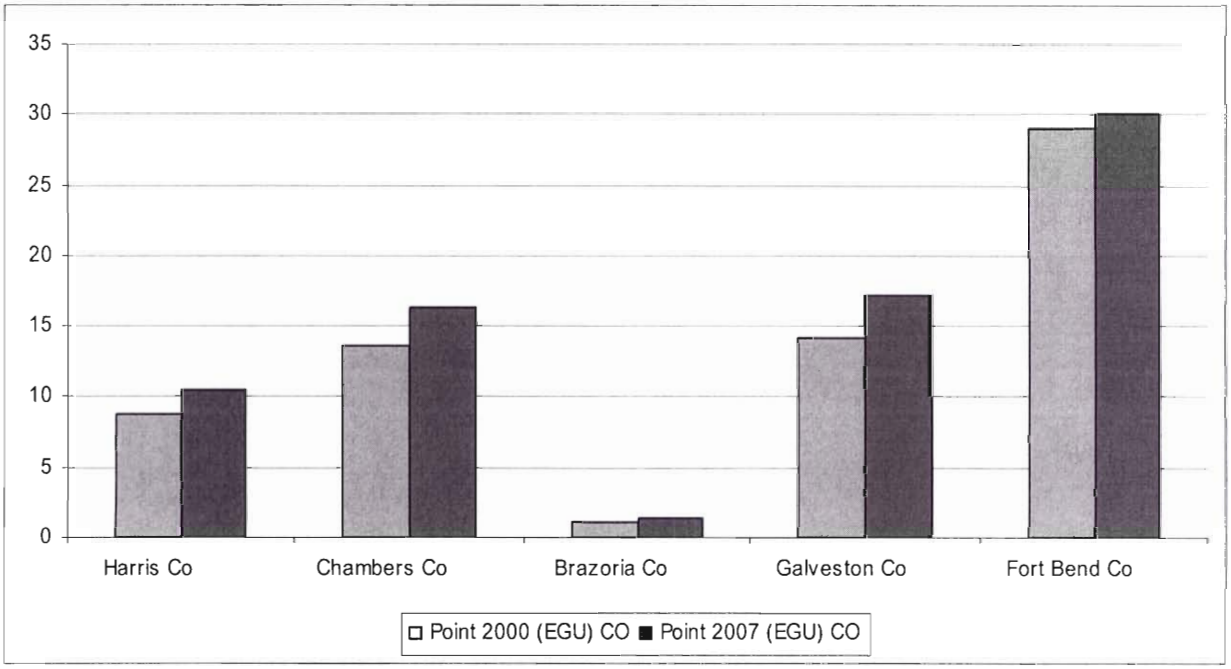

(d)

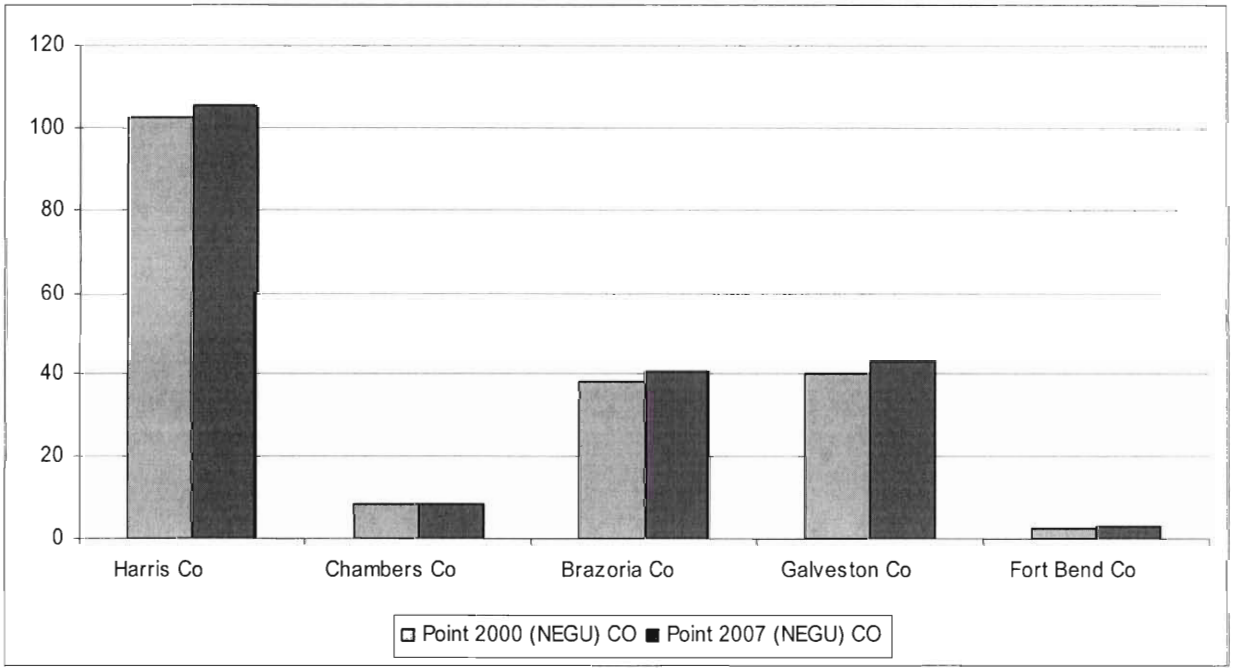

Figure 17. Continued. (c) is point source (electricity generating units) emission, and (d) is point source (non-electricity generating units) emission.

(e)

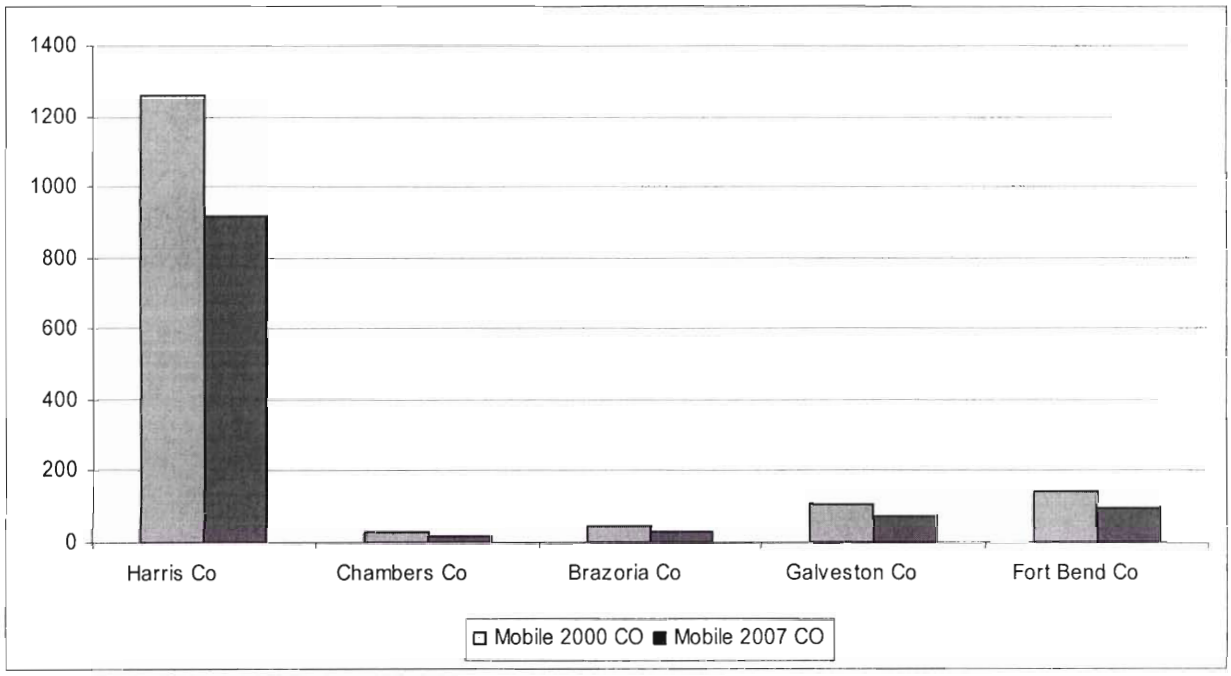

Figure 17. Continued. (e) is mobile source emission

(a)

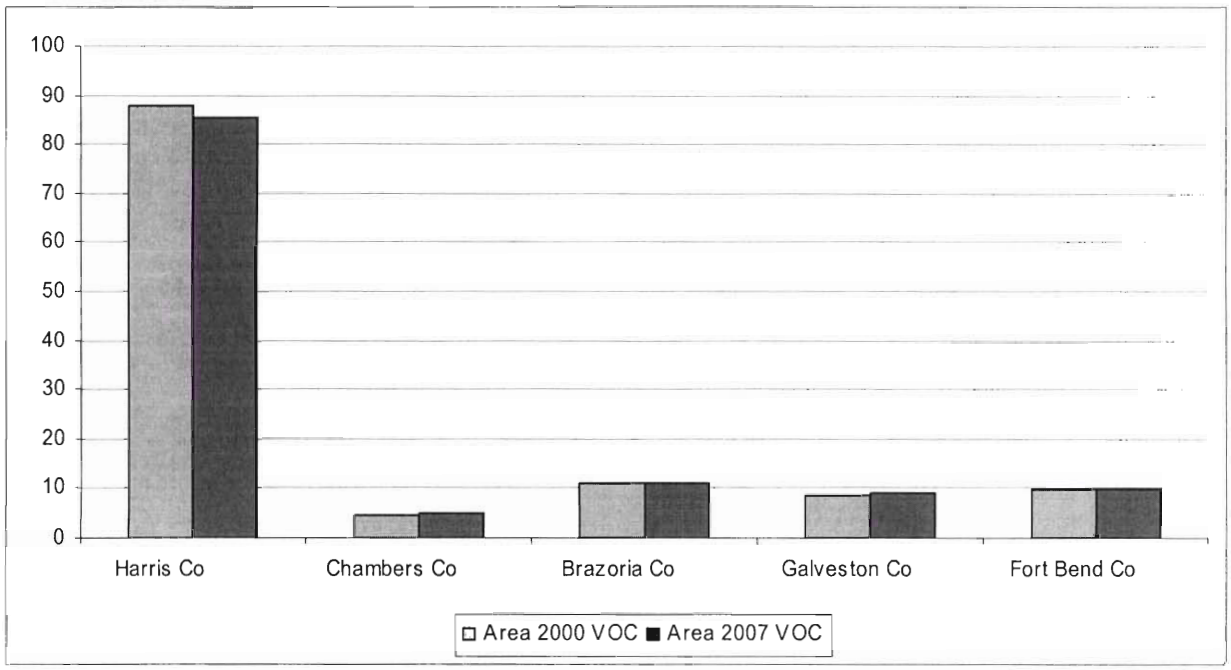

(b)

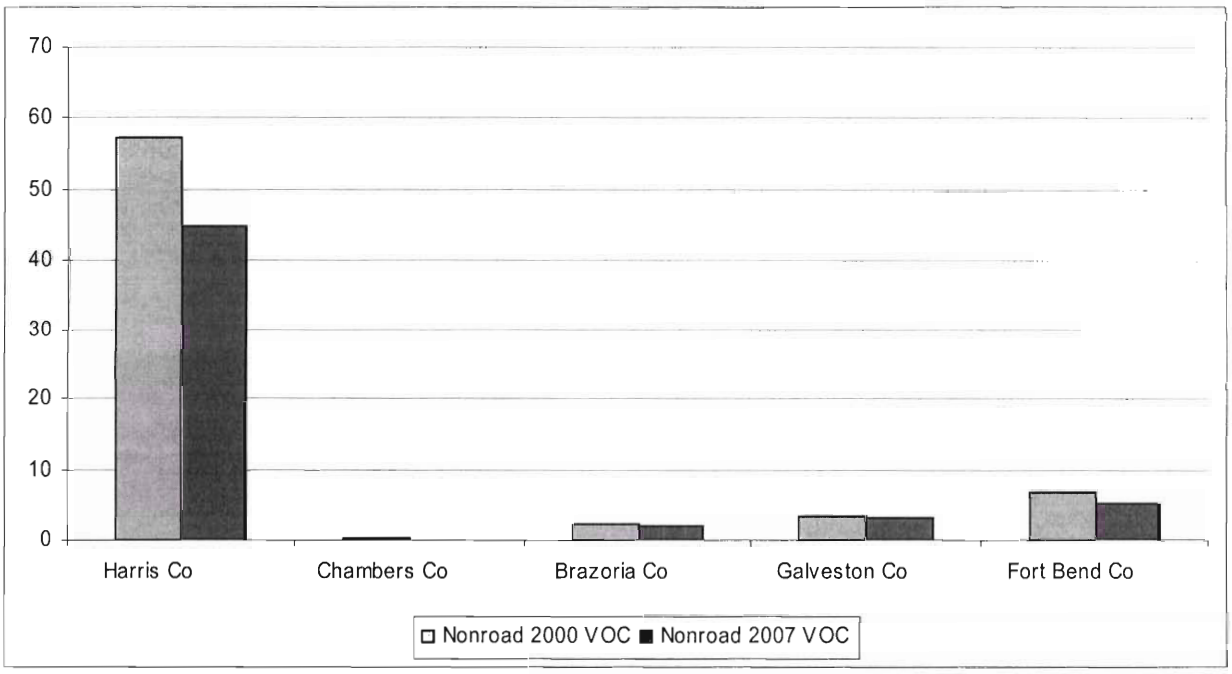

Figure 18. Volatile organic carbon emission in 2000 and in 2007 [tons/day]. (a) is area source emission, and (b) is nonroad source emission.

(c)

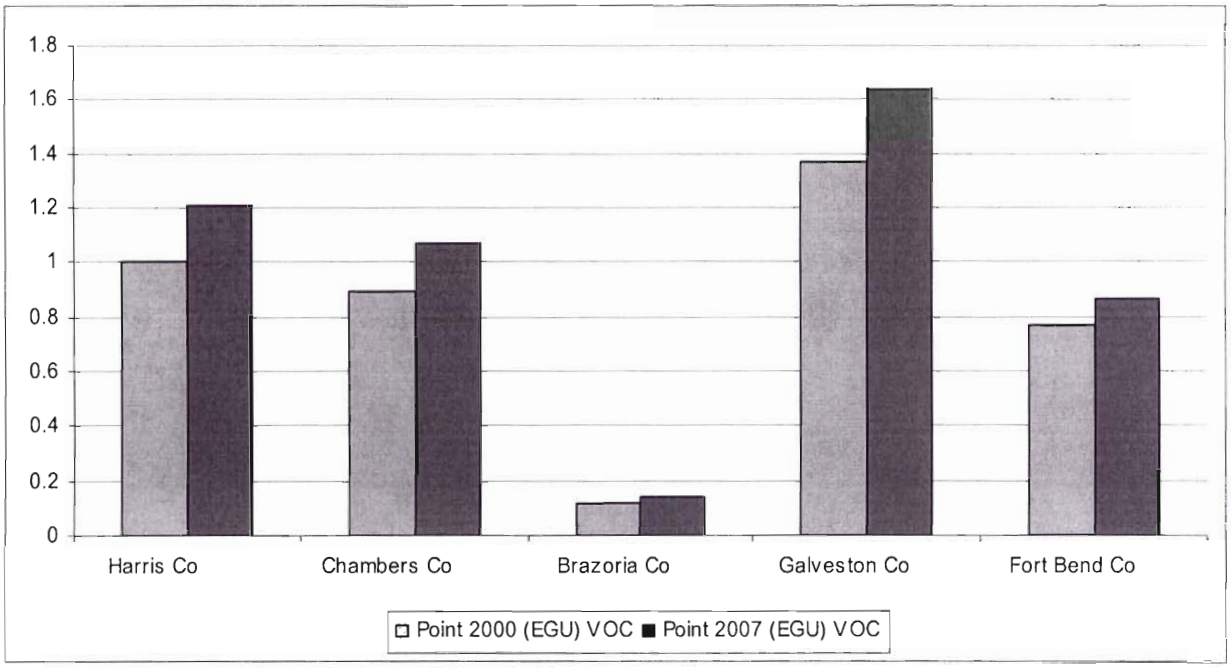

(d)

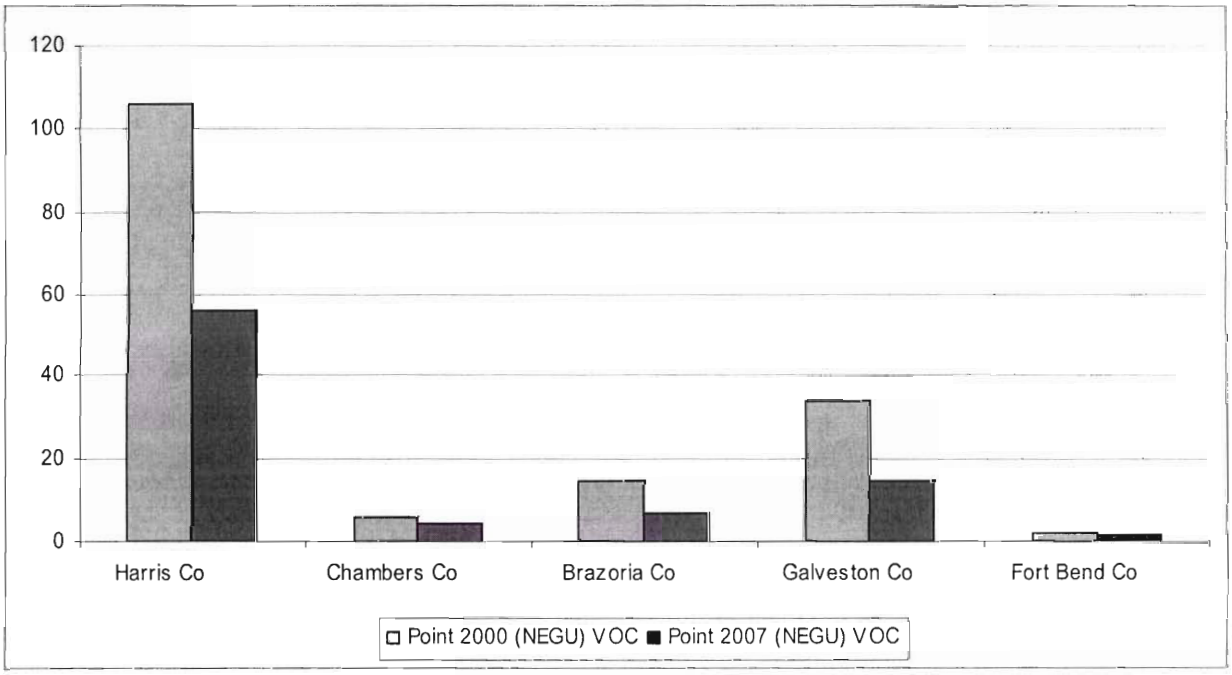

Figure 18. Continued. (c) is point source (electricity generating units) emission, and (d) is point source (non-electricity generating units) emission.

(e)

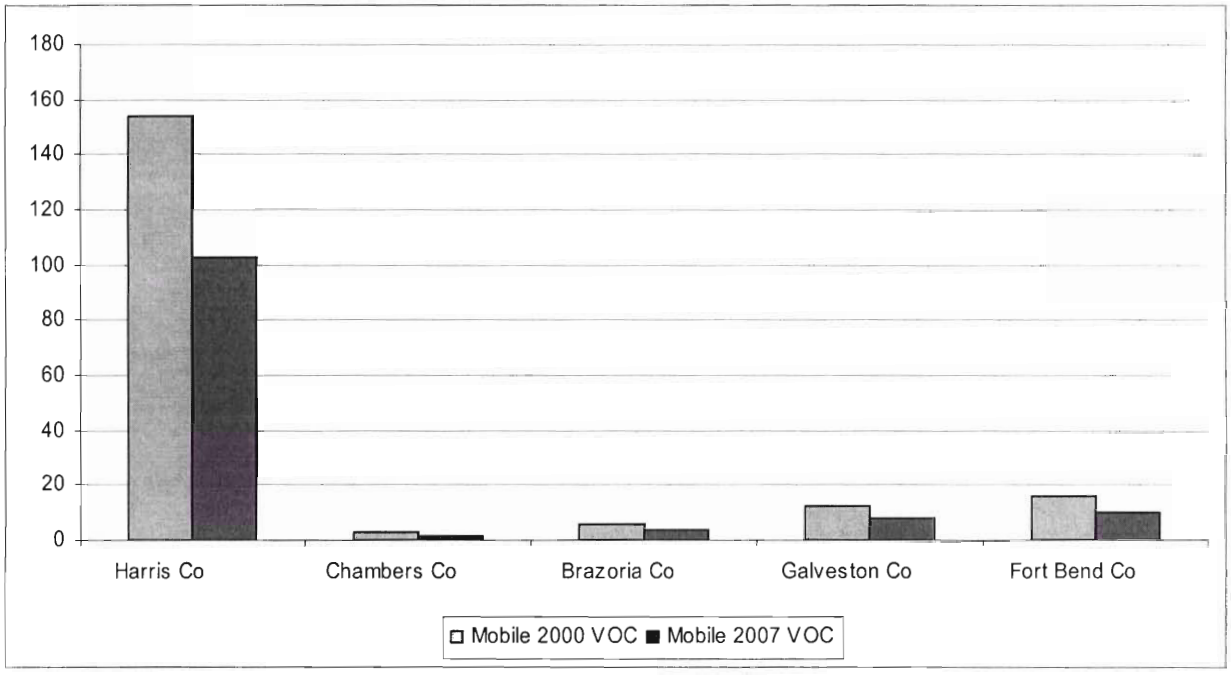

(f)

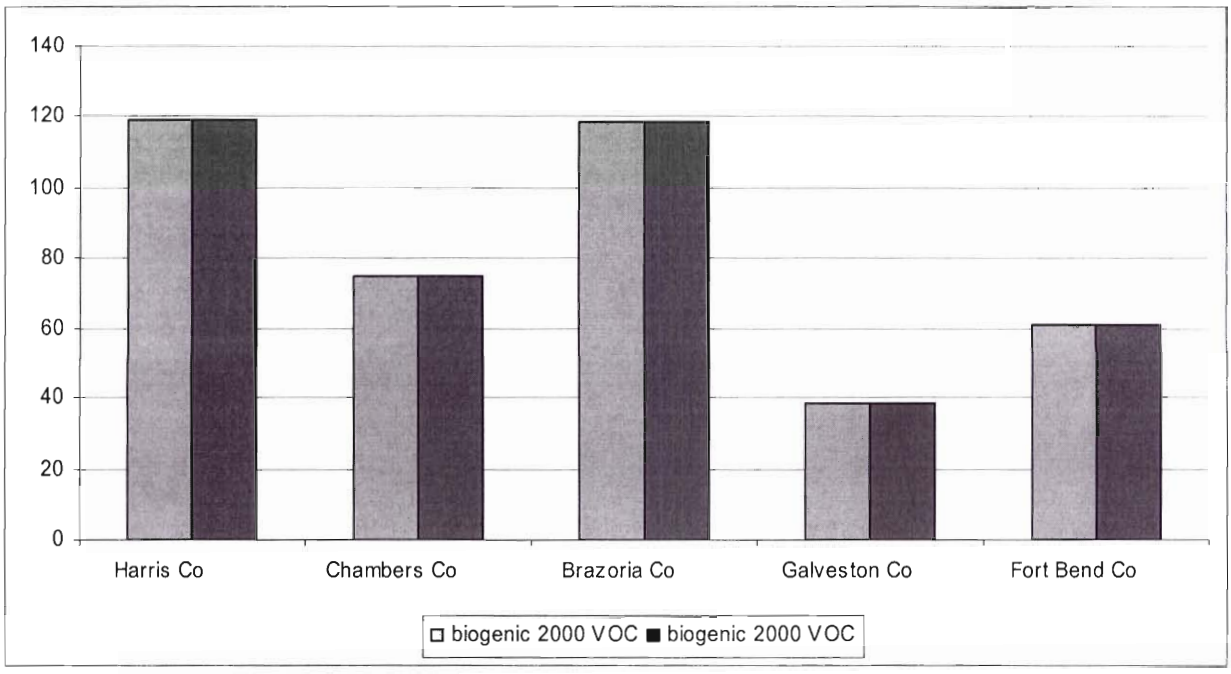

Figure 18. Continued. (e) is mobile source emission, and (f) is biogenic emission.

(a)

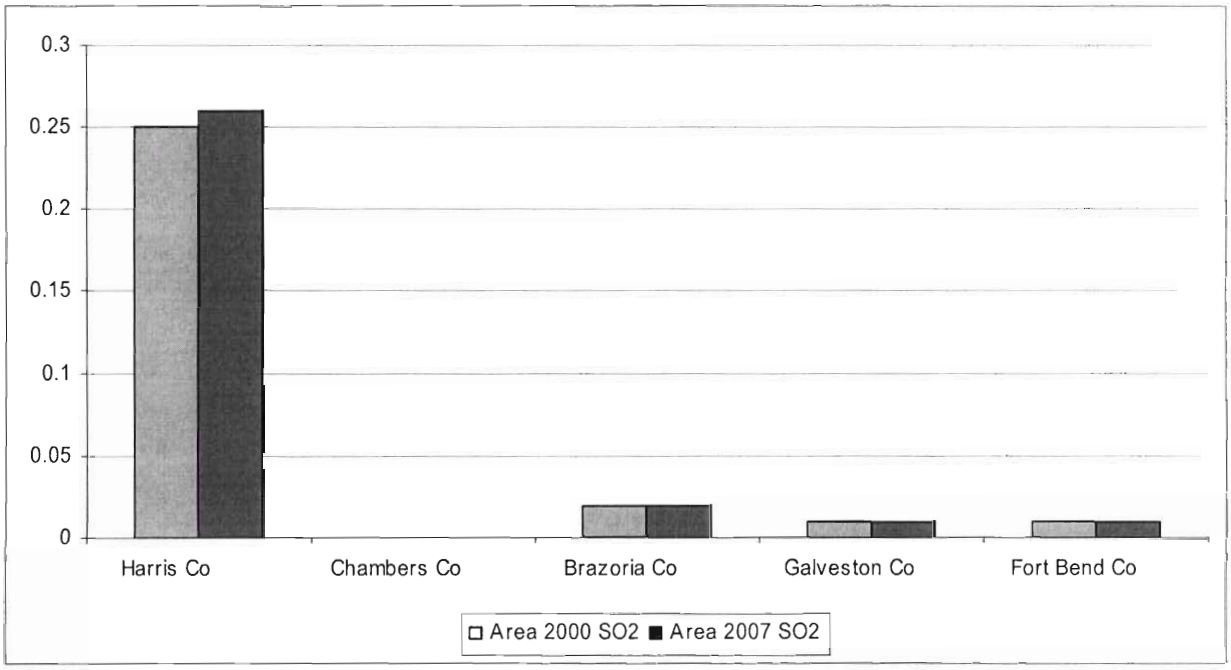

(b)

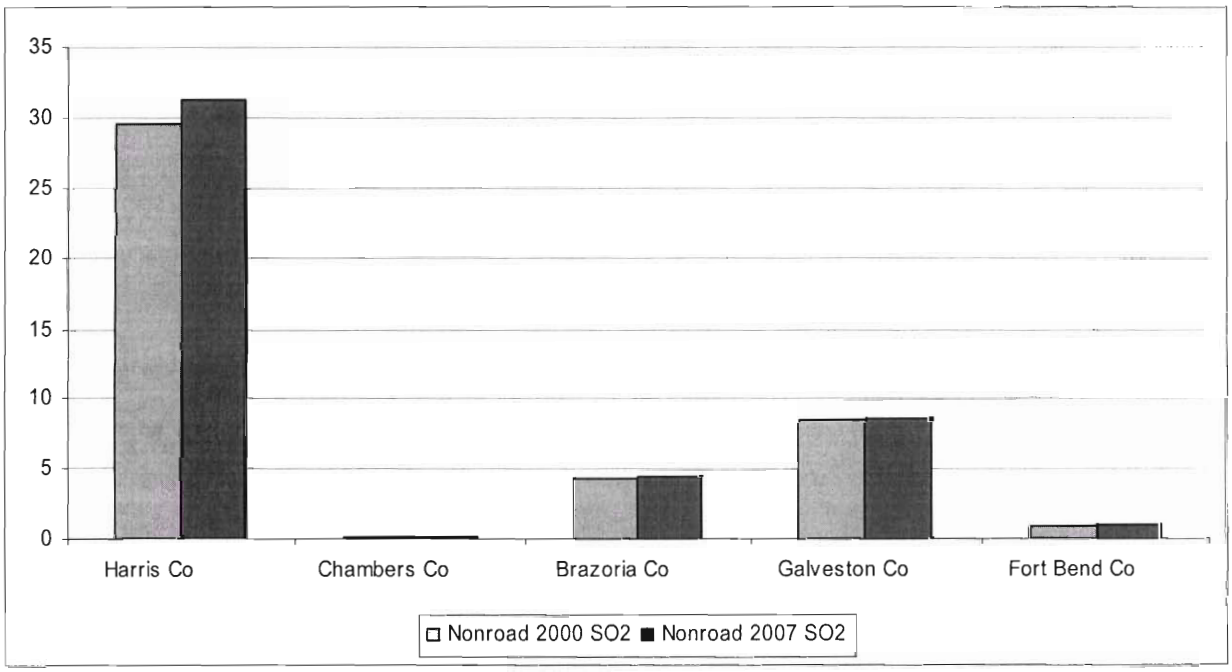

Figure 19. Sulfur dioxide emission in 2000 and in 2007 [tons/day]. (a) is area source emission, and (b) is nonroad source emission.

(c)

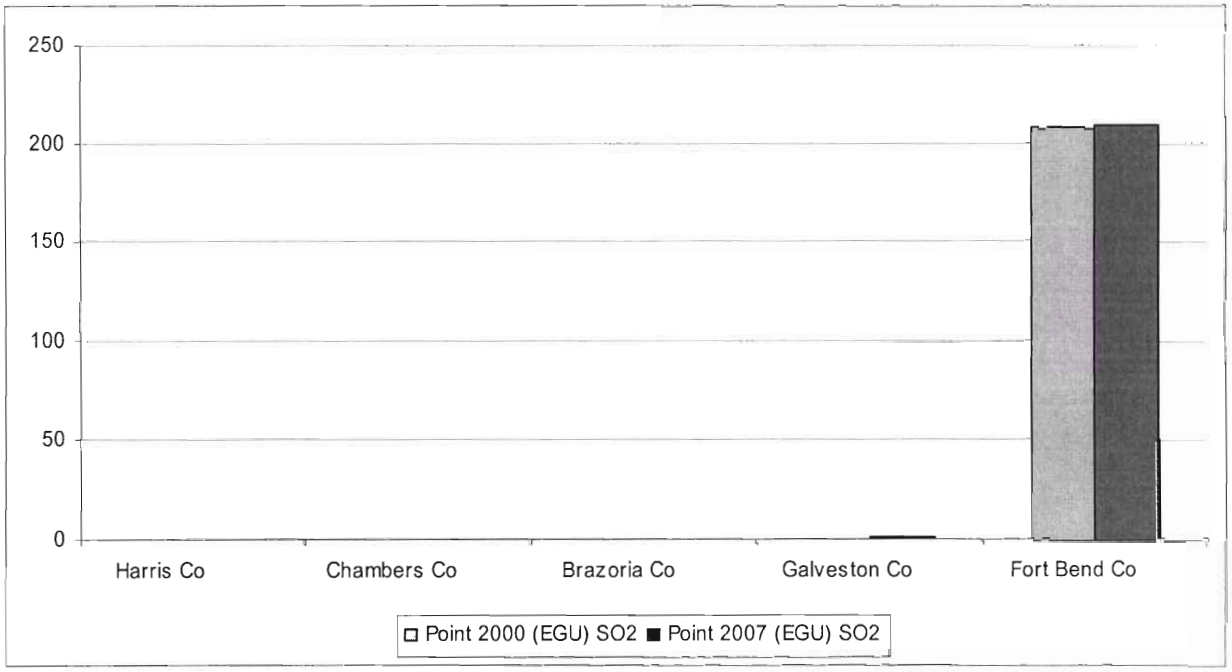

(d)

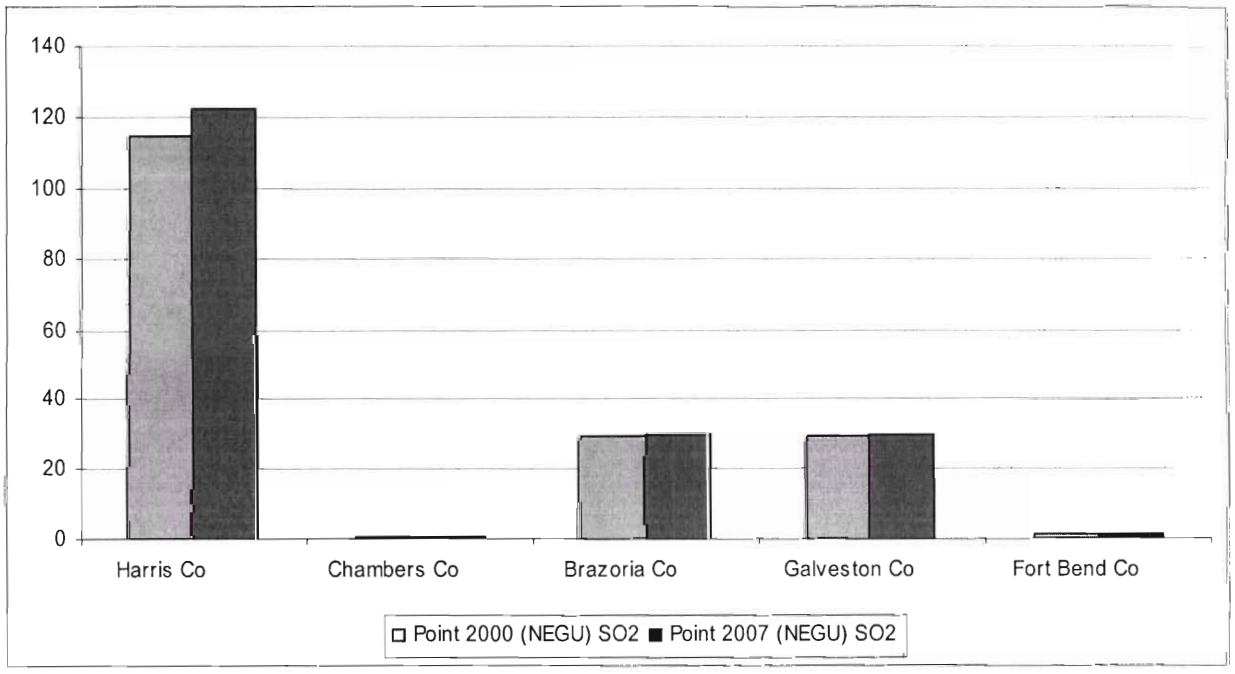

Figure 19. Continued. (c) is point source (electricity generating units) emission, and (d) is point source (non-electricity generating units) emission.

(e)

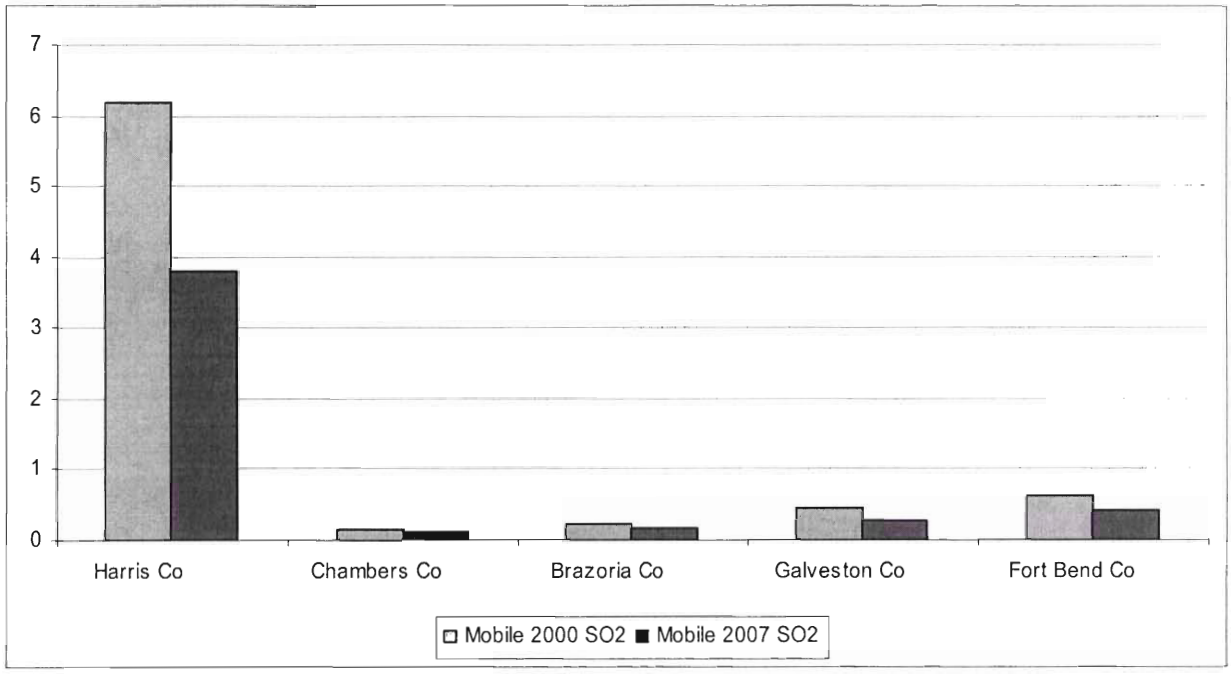

Figure 19. Continued. (e) is mobile source emission

(a)

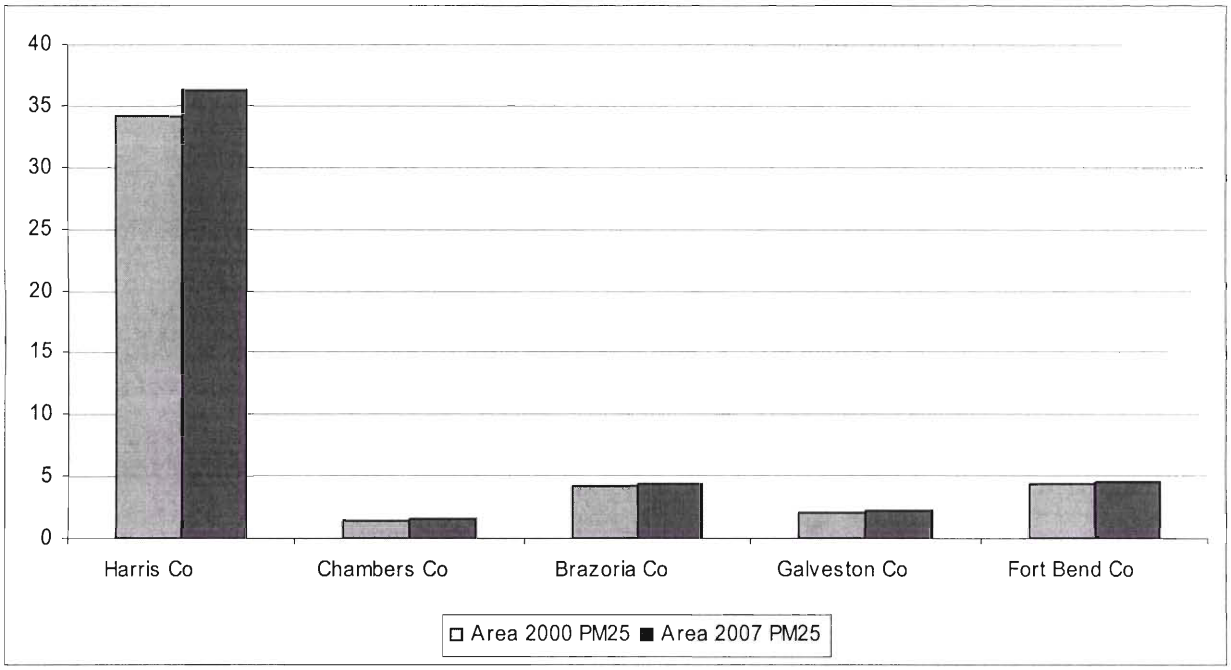

(b)

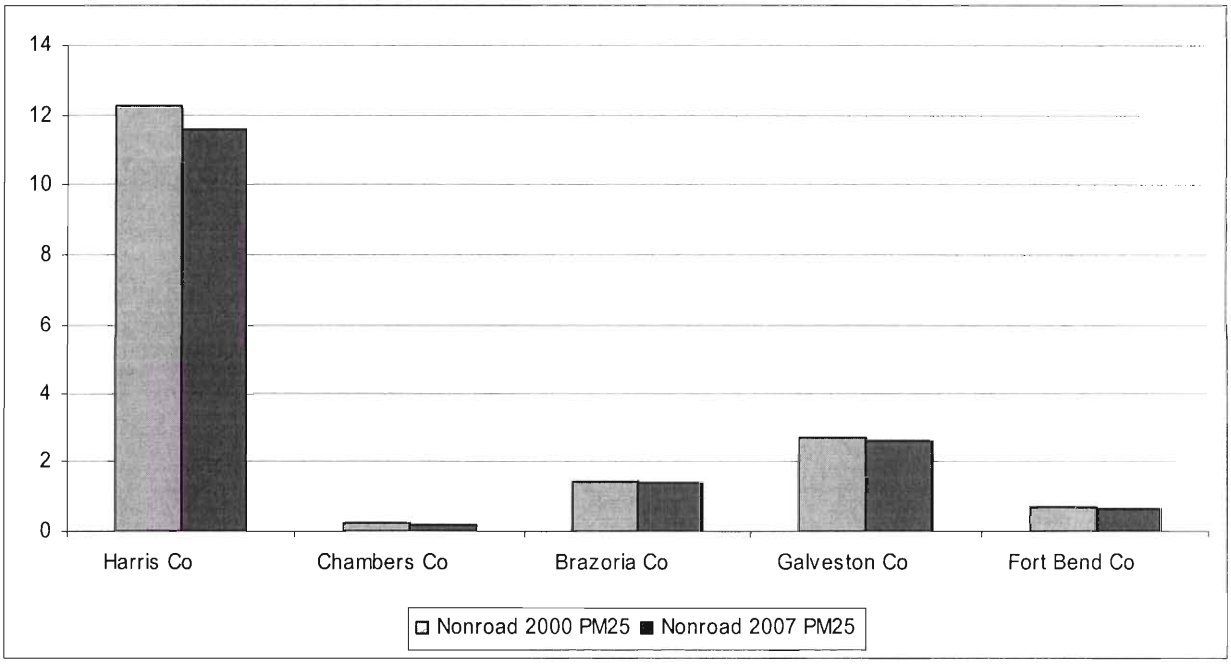

Figure 20. PM 2.5 emission in 2000 and in 2007 [tons/day]. (a) is area source emission, and (b) is nonroad source emission.

(c)

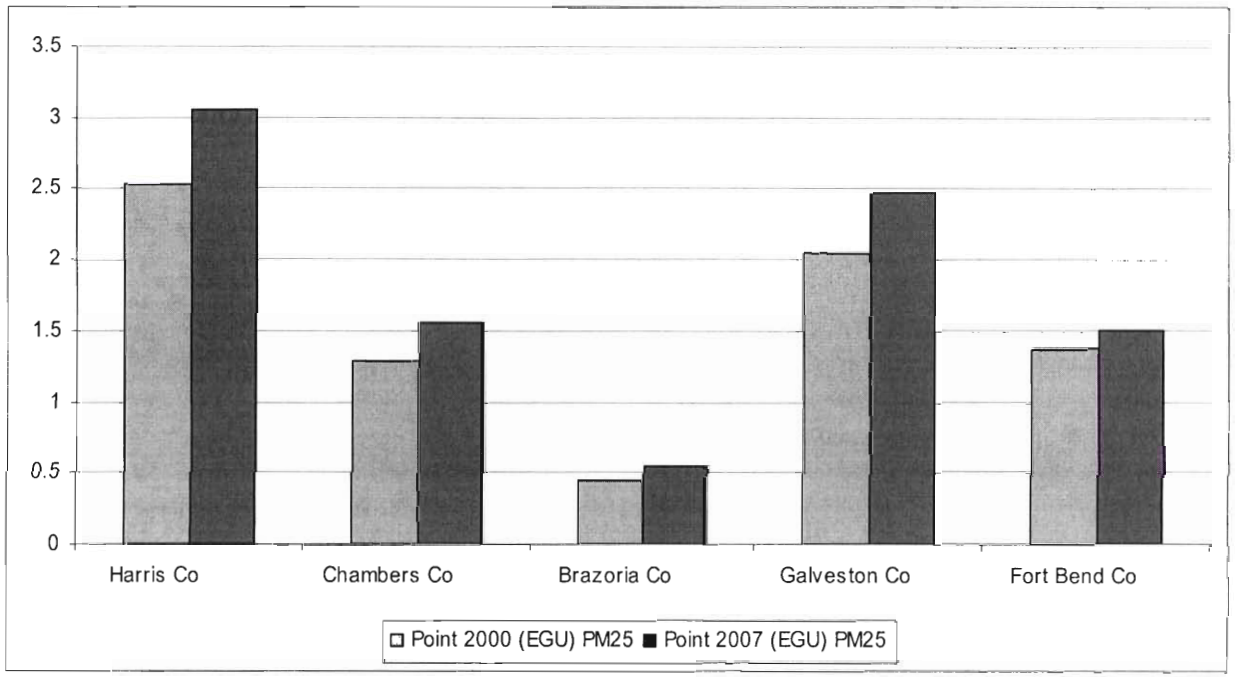

(d)

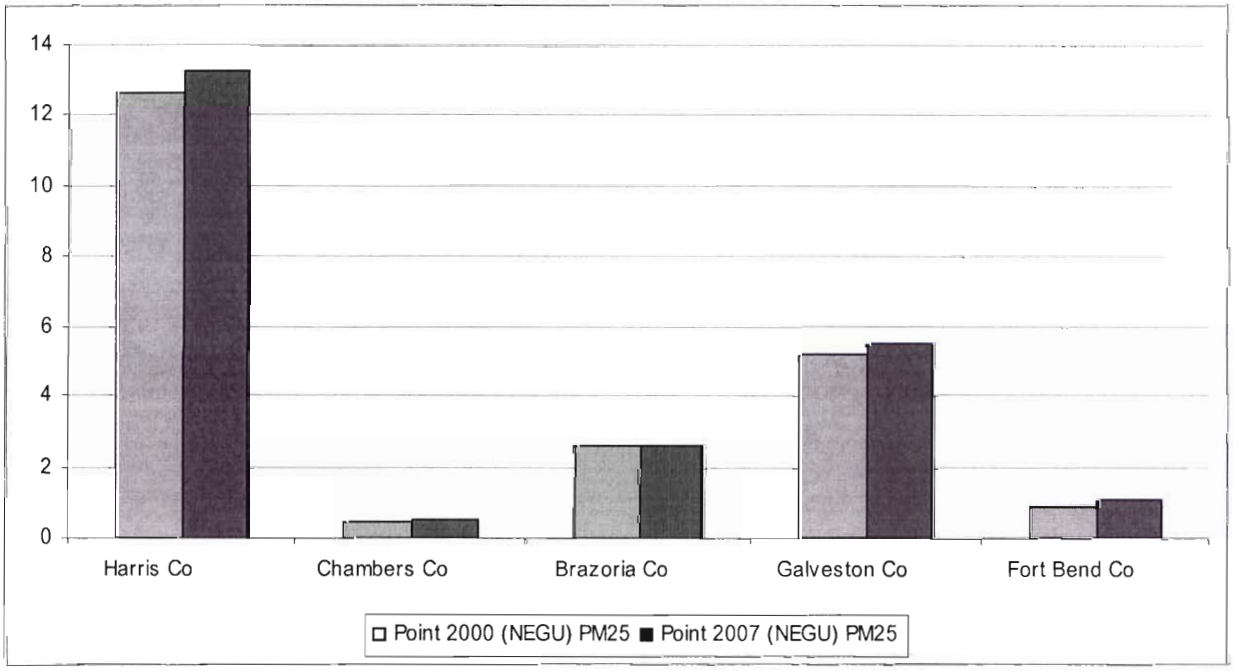

Figure 20. Continued. (c) is point source (electricity generating units) emission, and (d) is point source (non-electricity generating units) emission.

(e)

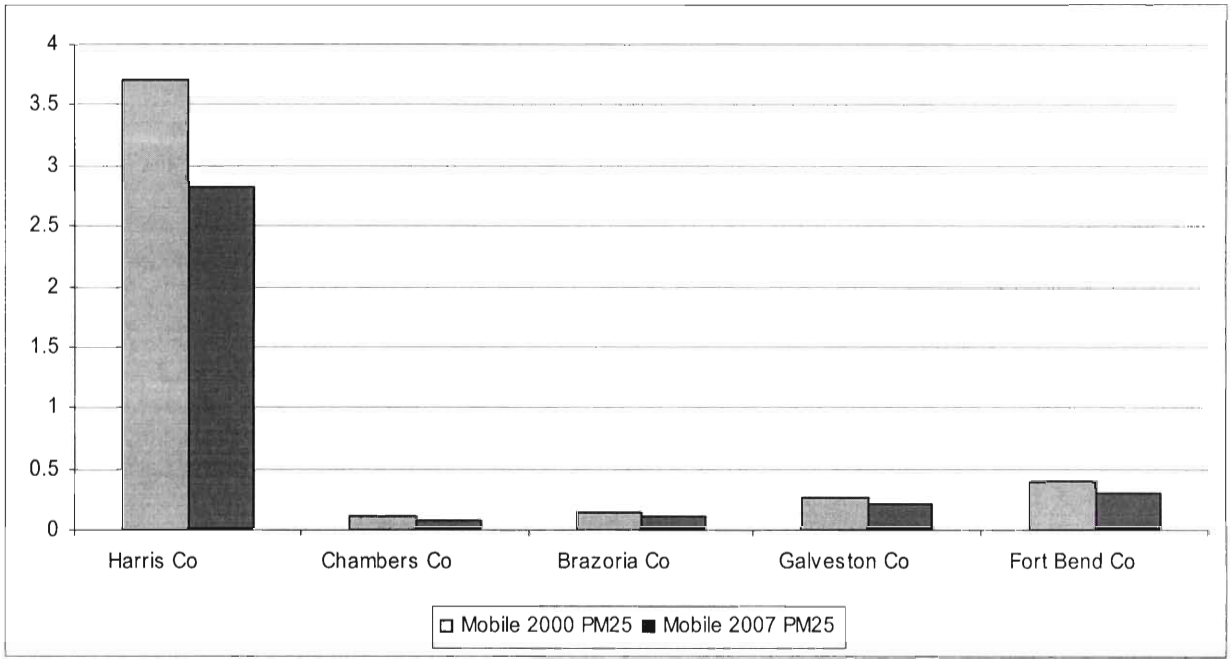

Figure 20. Continued. (e) is mobile source emission

(a)

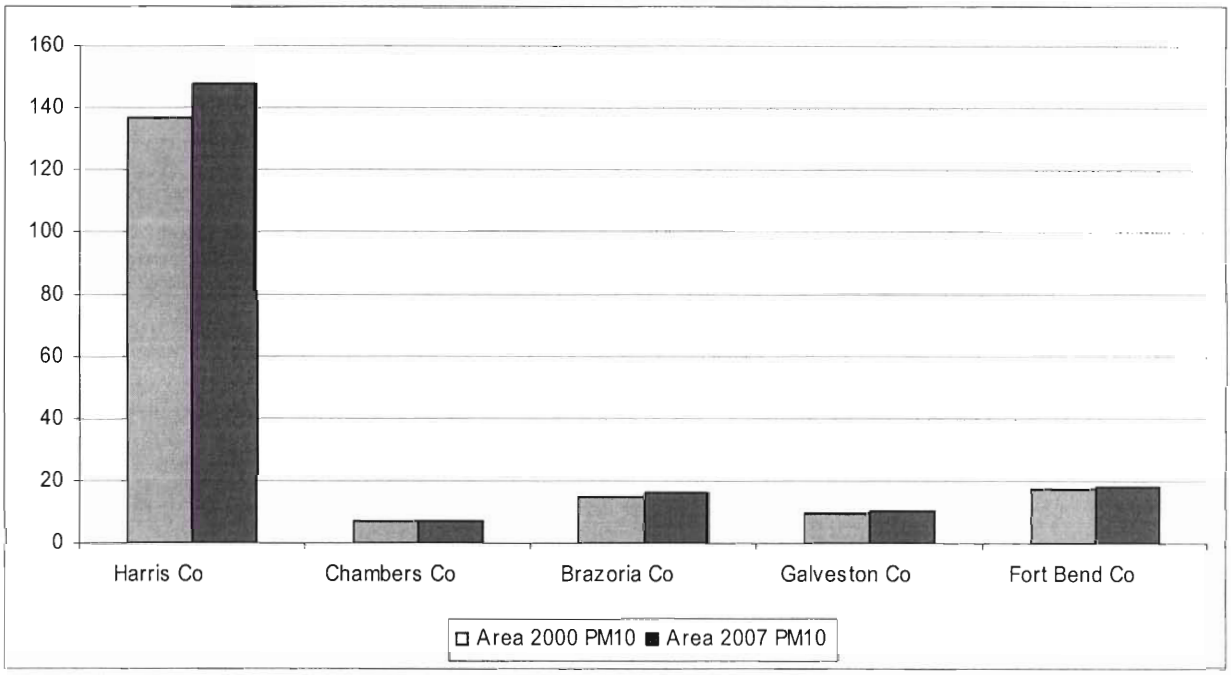

(b)

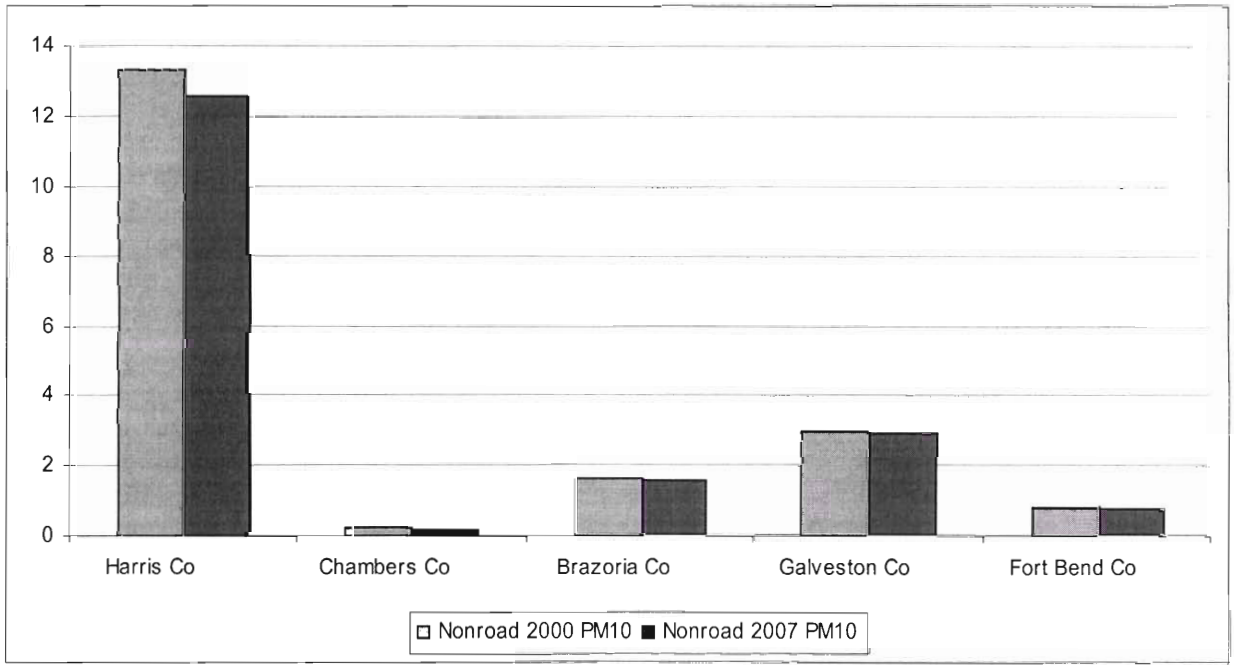

Figure 21. PM 10 emission in 2000 and in 2007 [tons/day]. (a) is area source emission, and (b) is nonroad source emission.

(c)

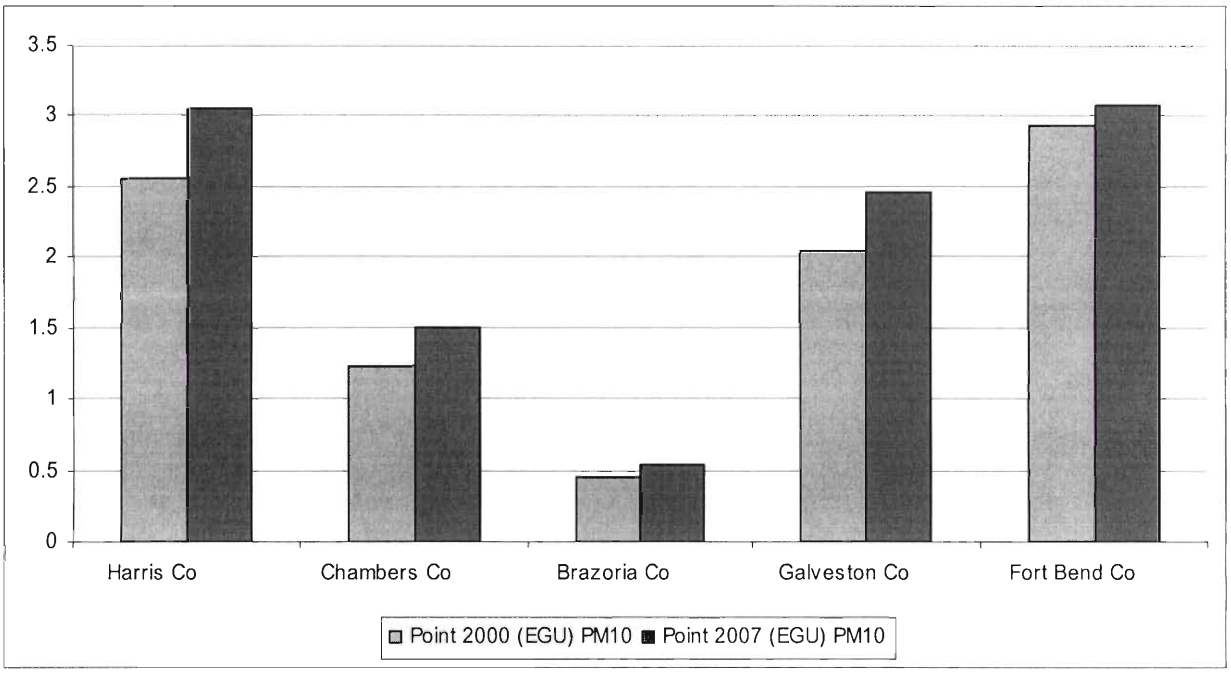

(d)

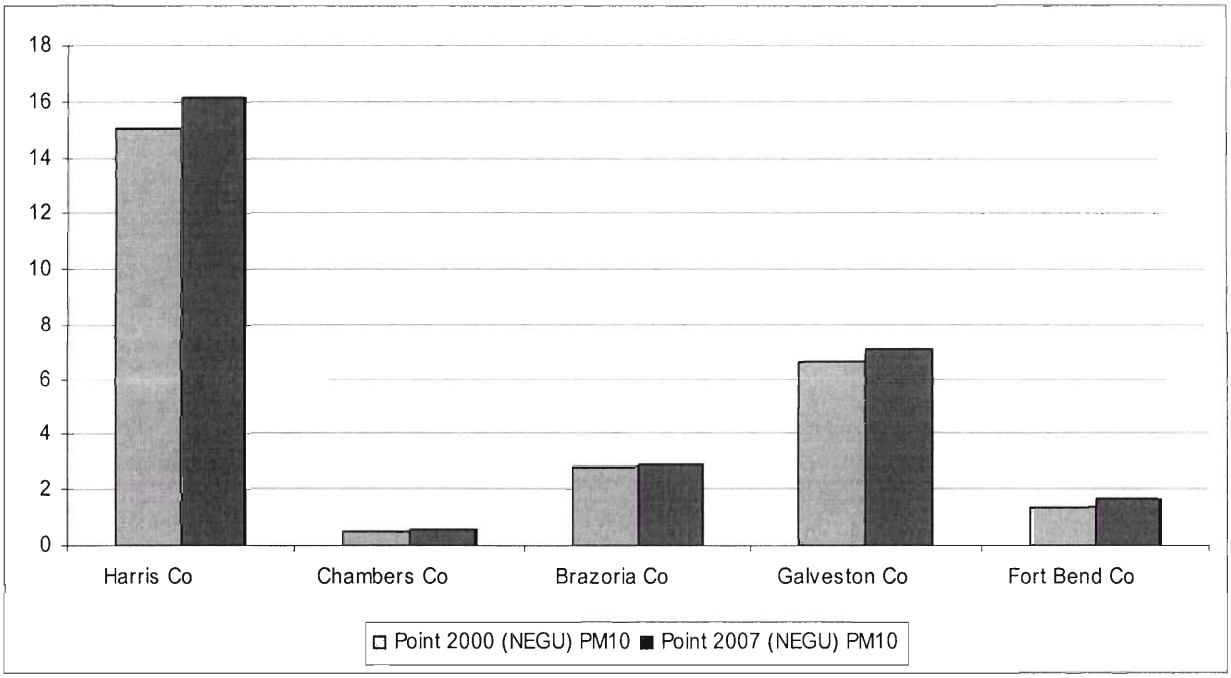

Figure 21. Continued. (c) is point source (electricity generating units) emission, and (d) is point source (non-electricity generating units) emission.

(e)

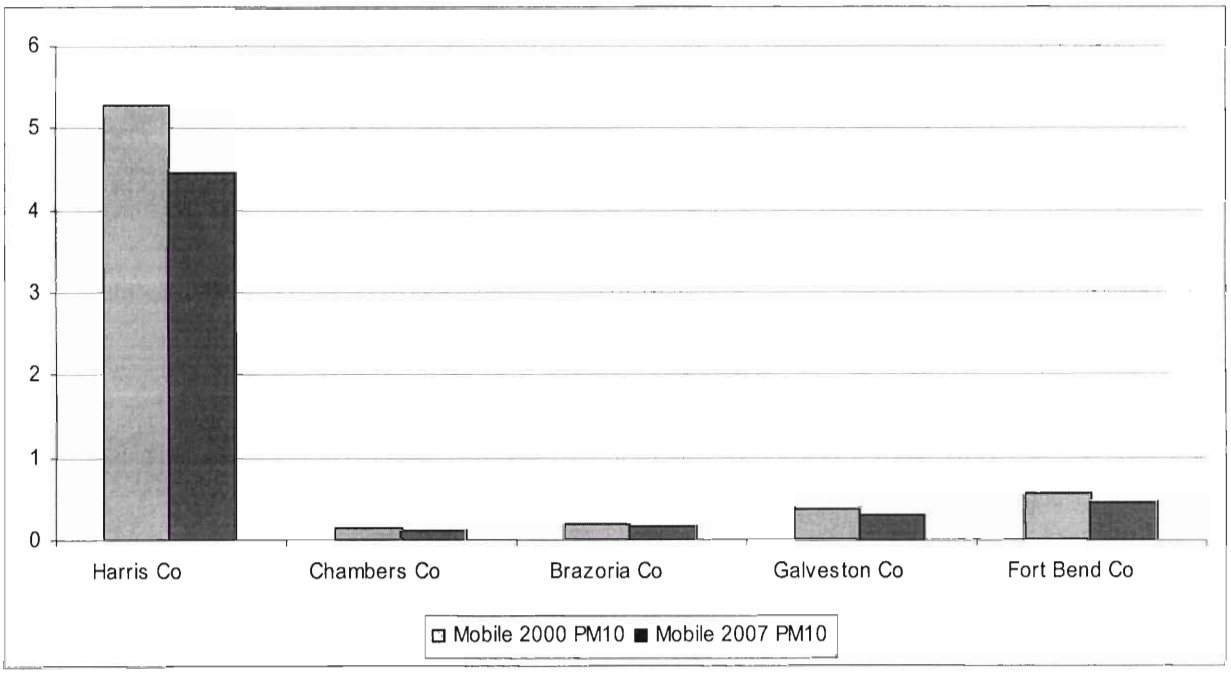

Figure 21. Continued. (e) is mobile source emission

(a)

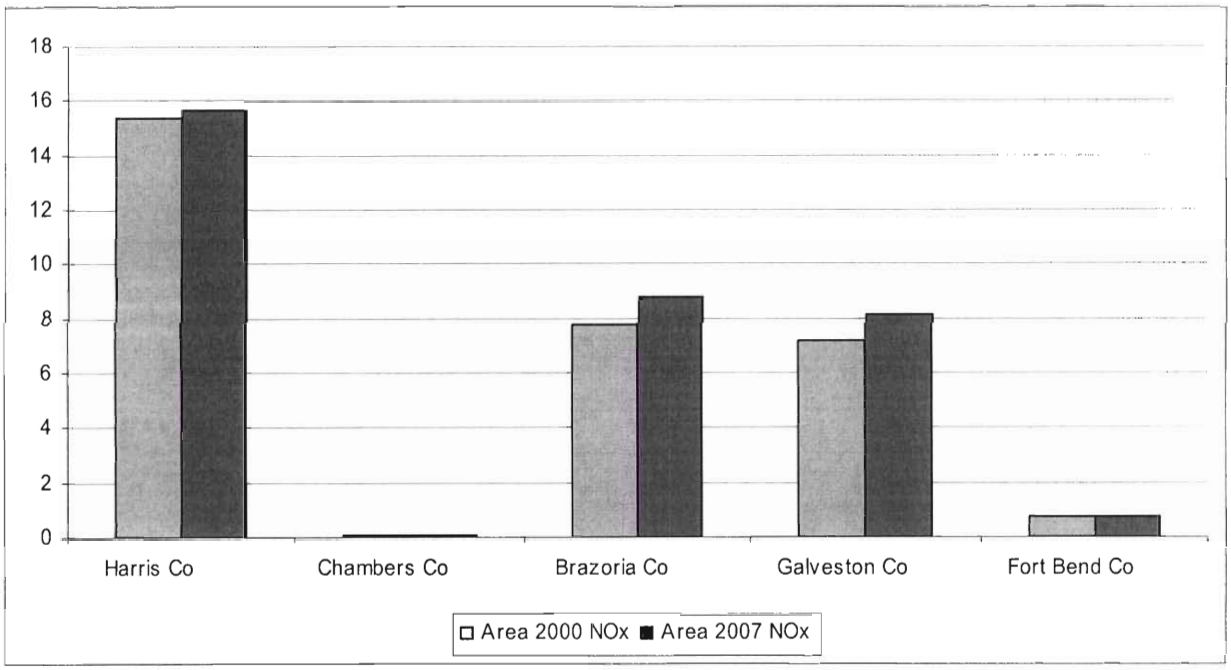

(b)

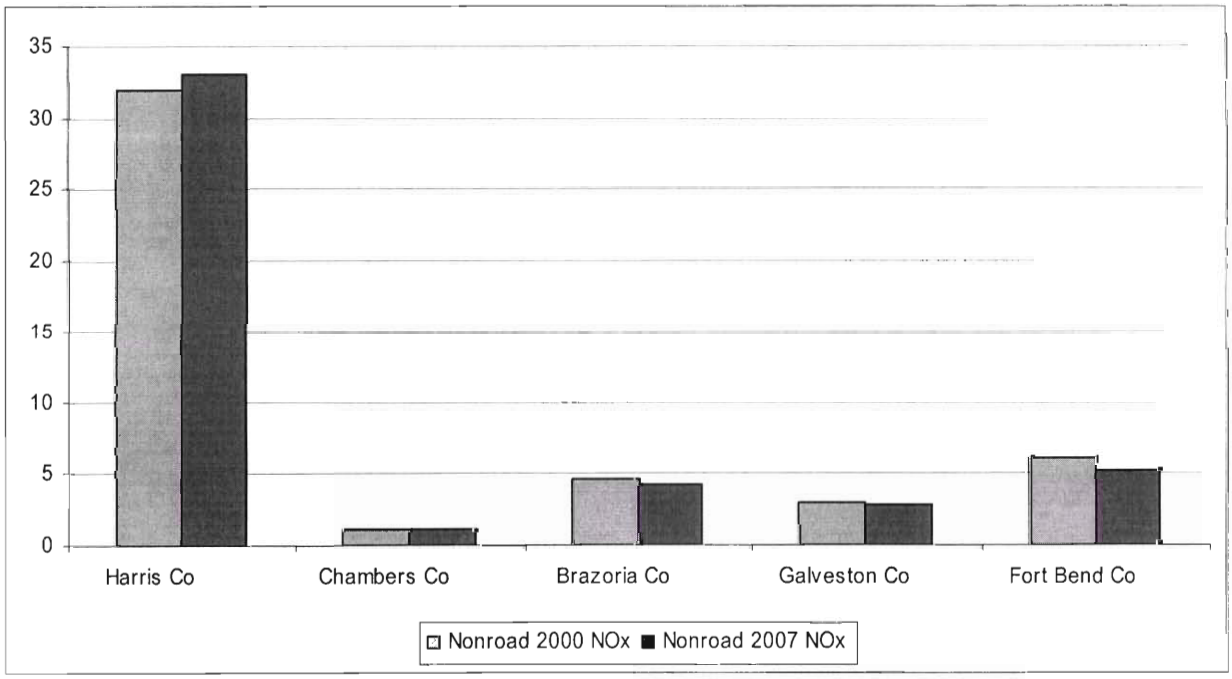

Figure 22. NOx emission in 2000 and in 2007 [tons/day]. (a) is area source emission, and (b) is nonroad source emission.

(c)

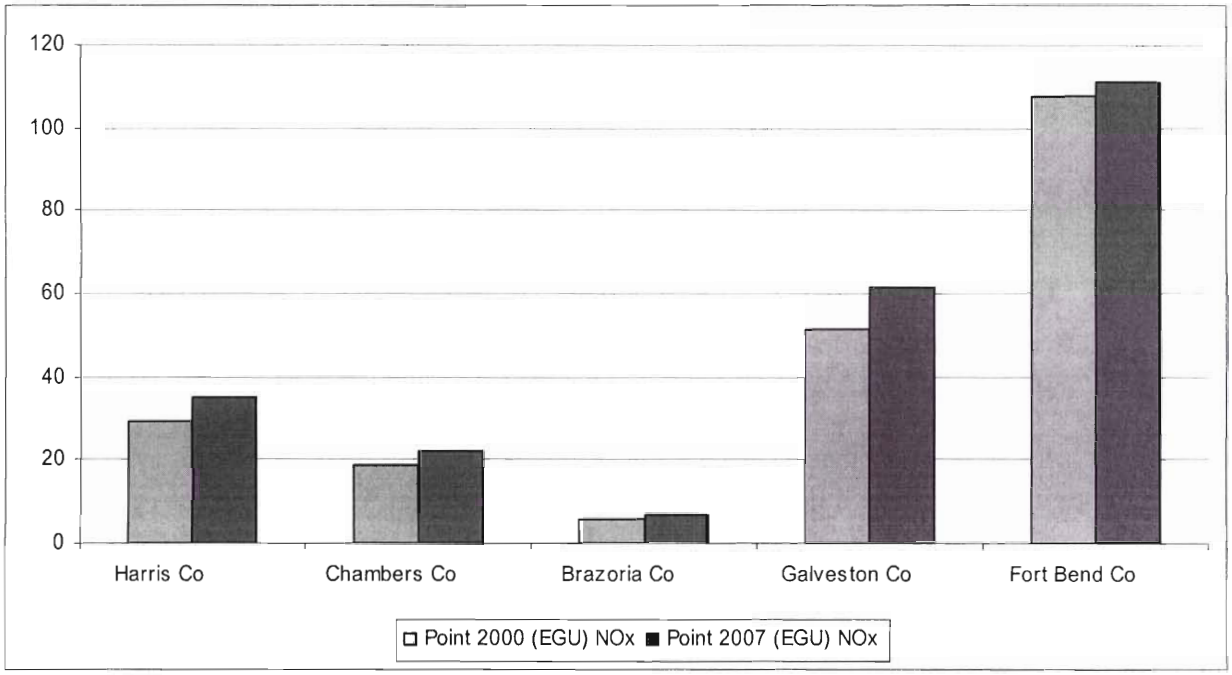

(d)

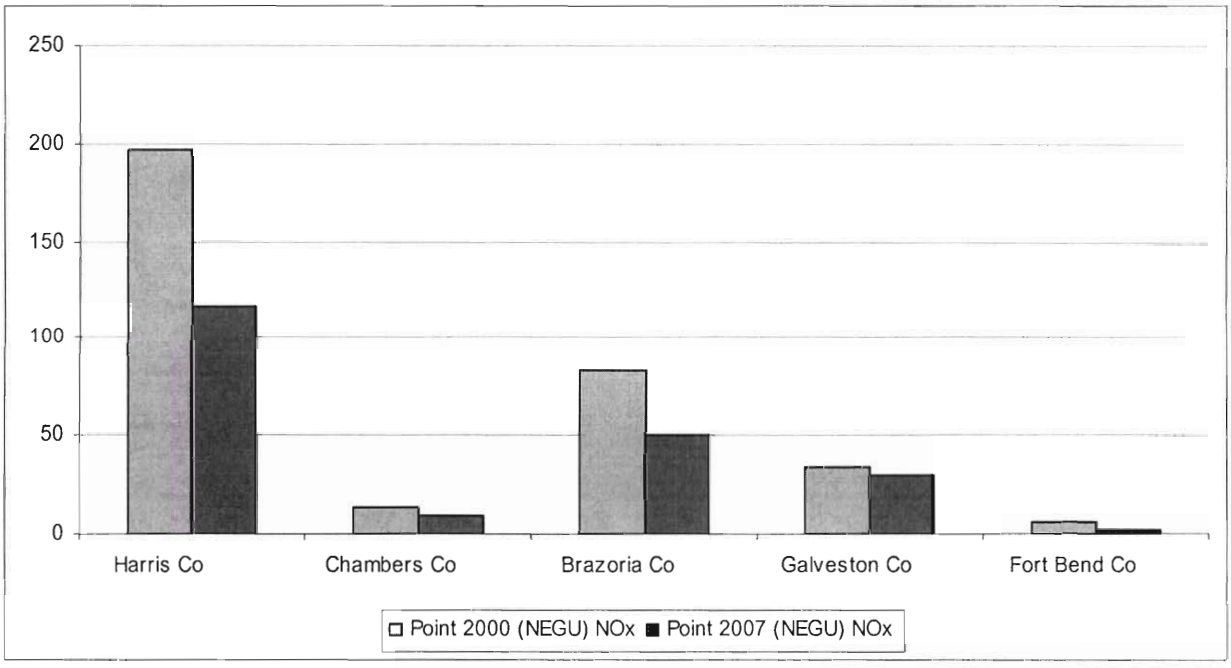

Figure 22. Continued. (c) is point source (electricity generating units) emission, and (d) is point source (non-electricity generating units) emission.

(e)

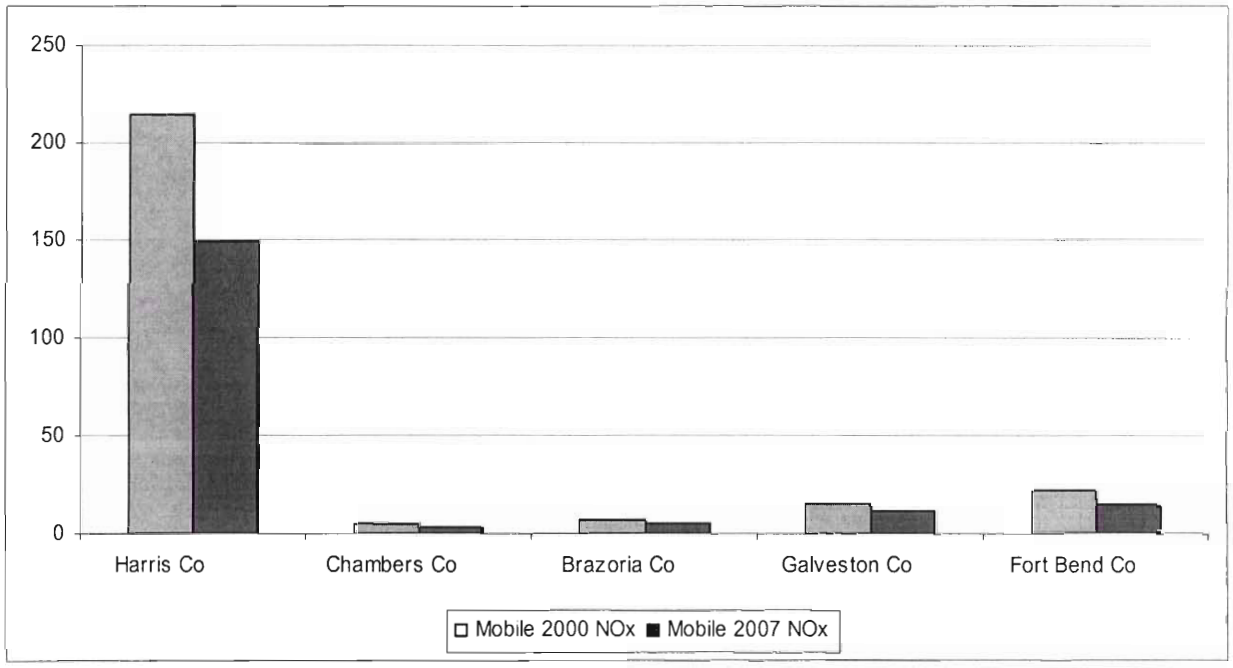

Figure 22. Continued. (e) is mobile source emission

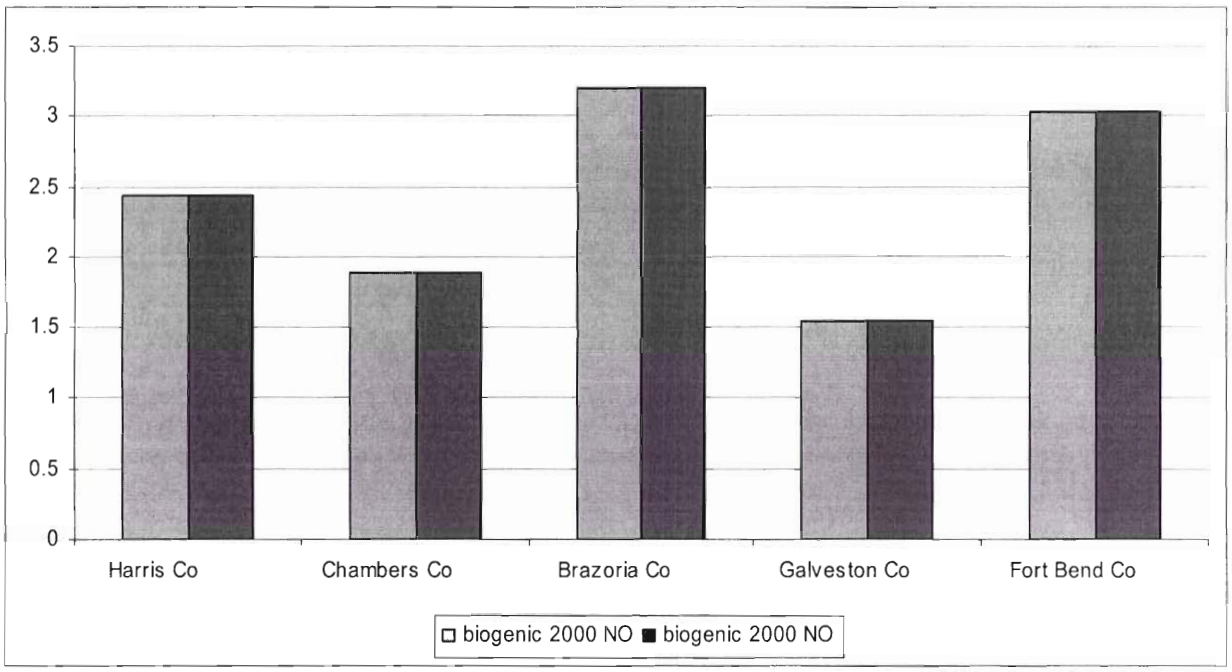

Figure 23. Biogenic NO emission in 2000 and in 2007 [tons/day].

4. Air Quality in Houston

We simulated an air quality in the Houston area from August 11 to 20, 2000 and from August 20, 2007. Then, we compared hourly pollutant concentrations in 2000 and in 2007 in Figures 24 through 47. Those compared pollutants are ammonium, nitrate, sulfate, organic carbon, elemental carbon, PM 2.5, ozone, carbon monoxide, sulfur dioxide, nitric oxide, NOx and NOy.

(a)

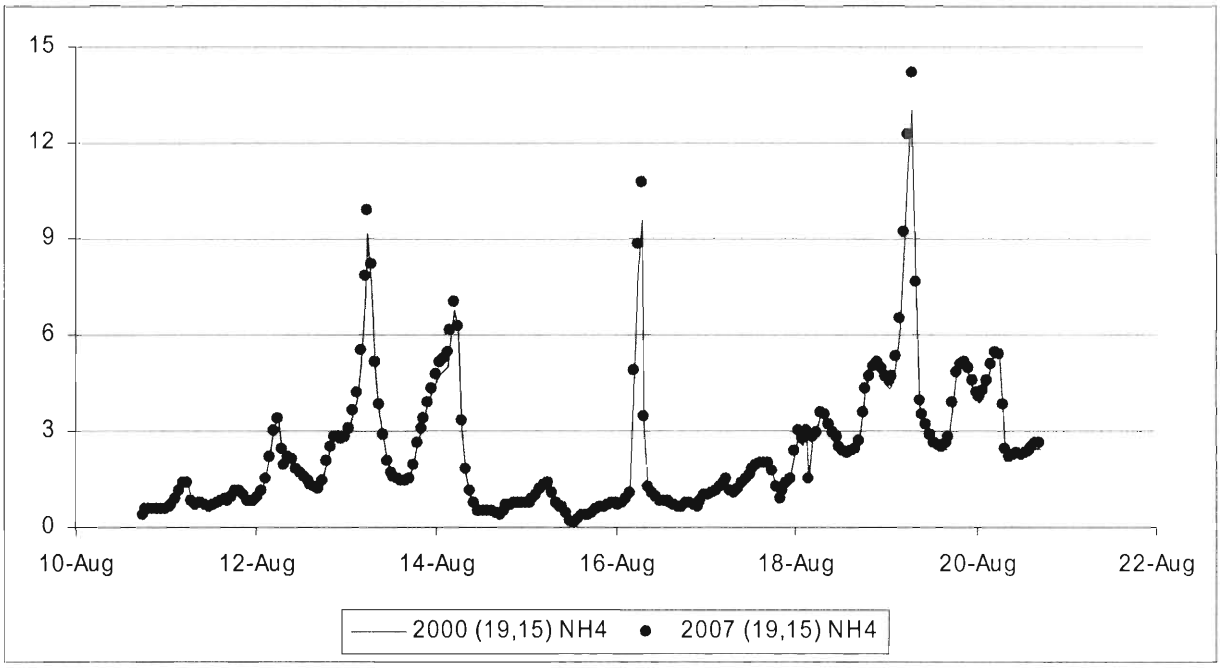

(b)

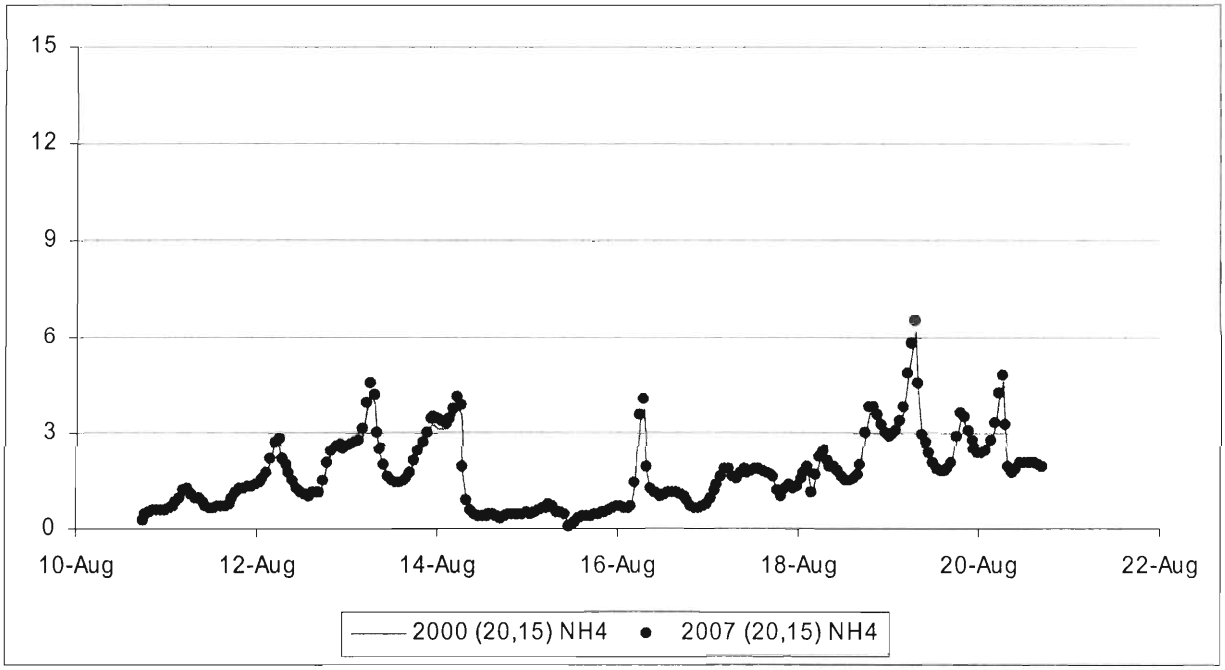

Figure 24. Comparison of the simulated hourly ammonium concentrations in 2000 and in 2007. (a) is for the 19th column and the 15th row of grids and (b) is for the 20th column and the 15th row.

(c)

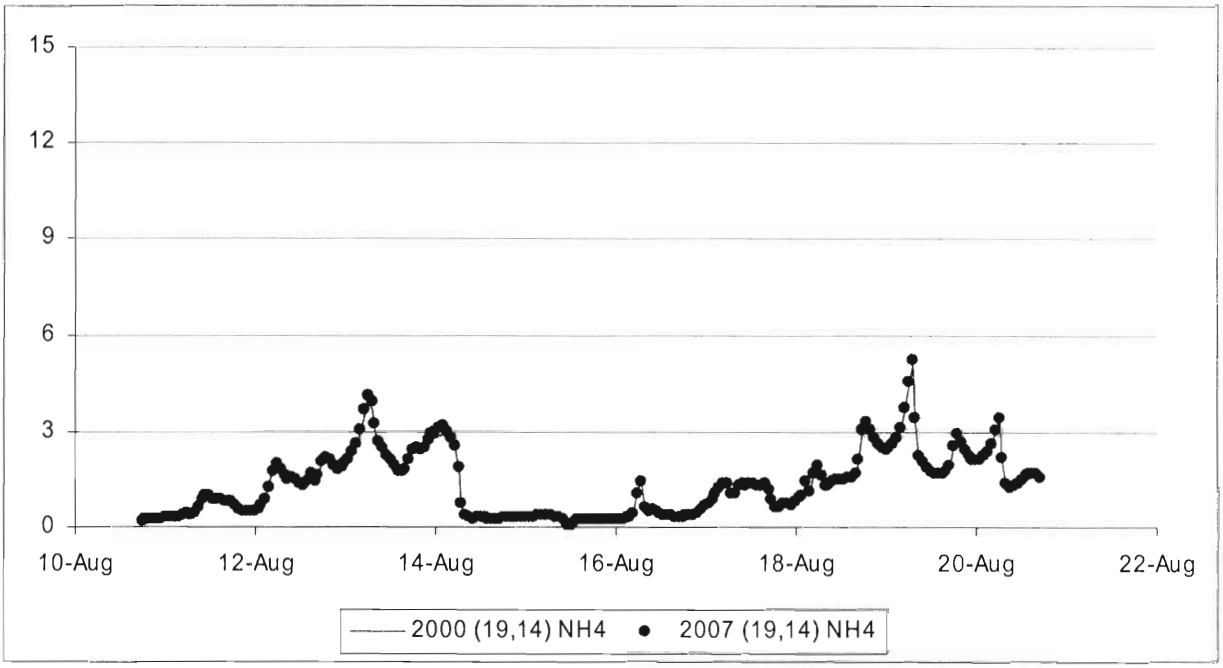

(d)

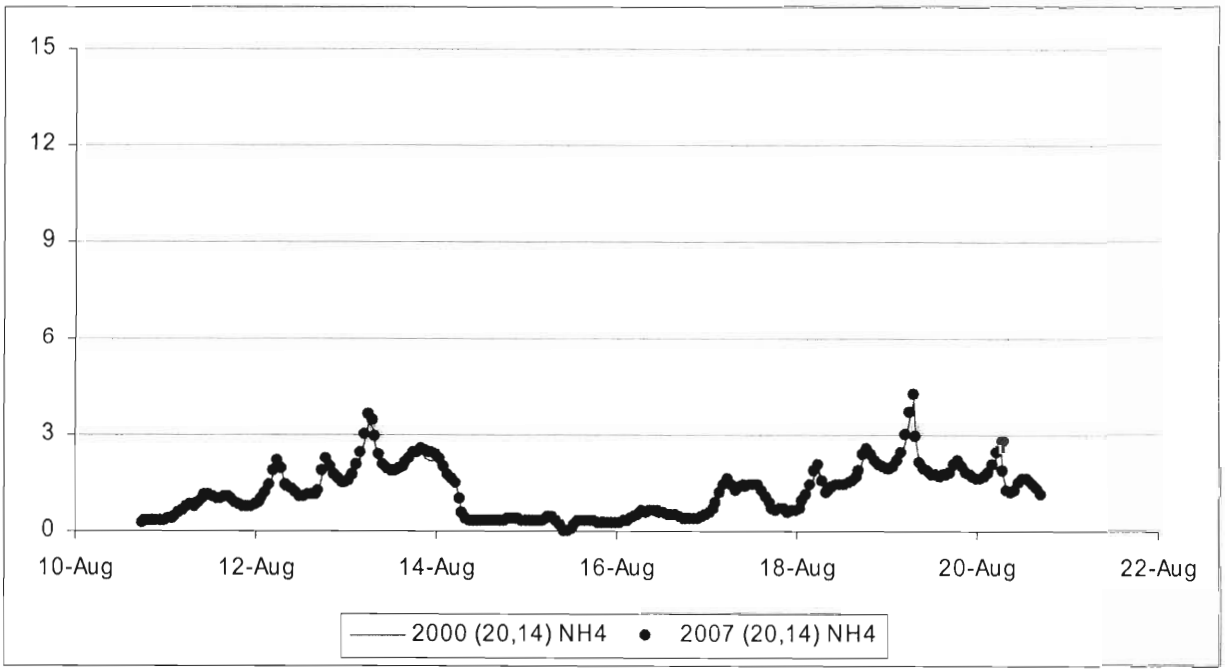

Figure 24. Continued. (c) is for the 19th column and the 14th row of grids and (d) is for the 20th column and the 14th row.

(e)

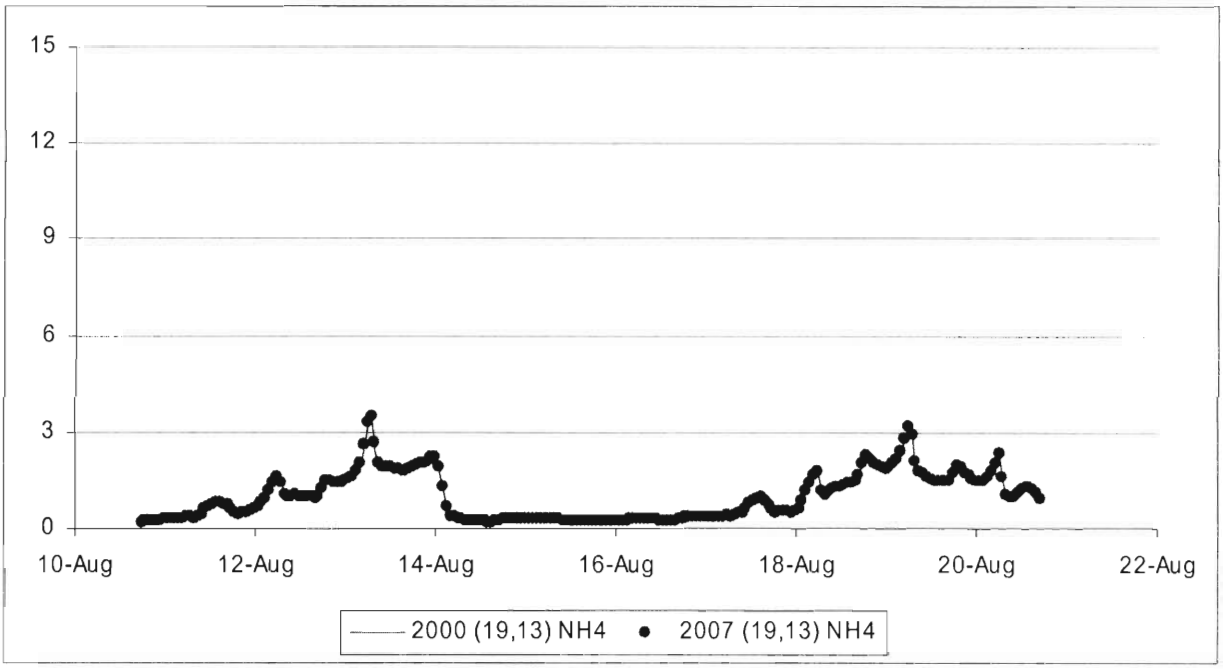

(f)

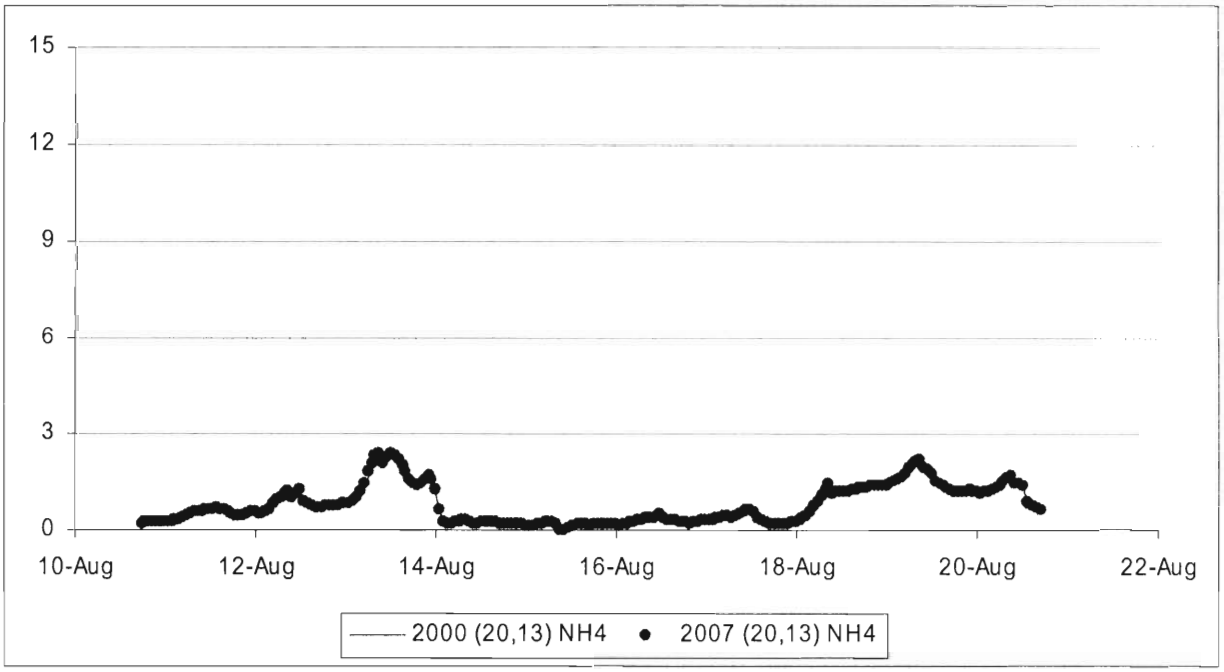

Figure 24. Continued. (e) is for the 19th column and the 13th row of grids and (f) is for the 20th column and the 13th row.

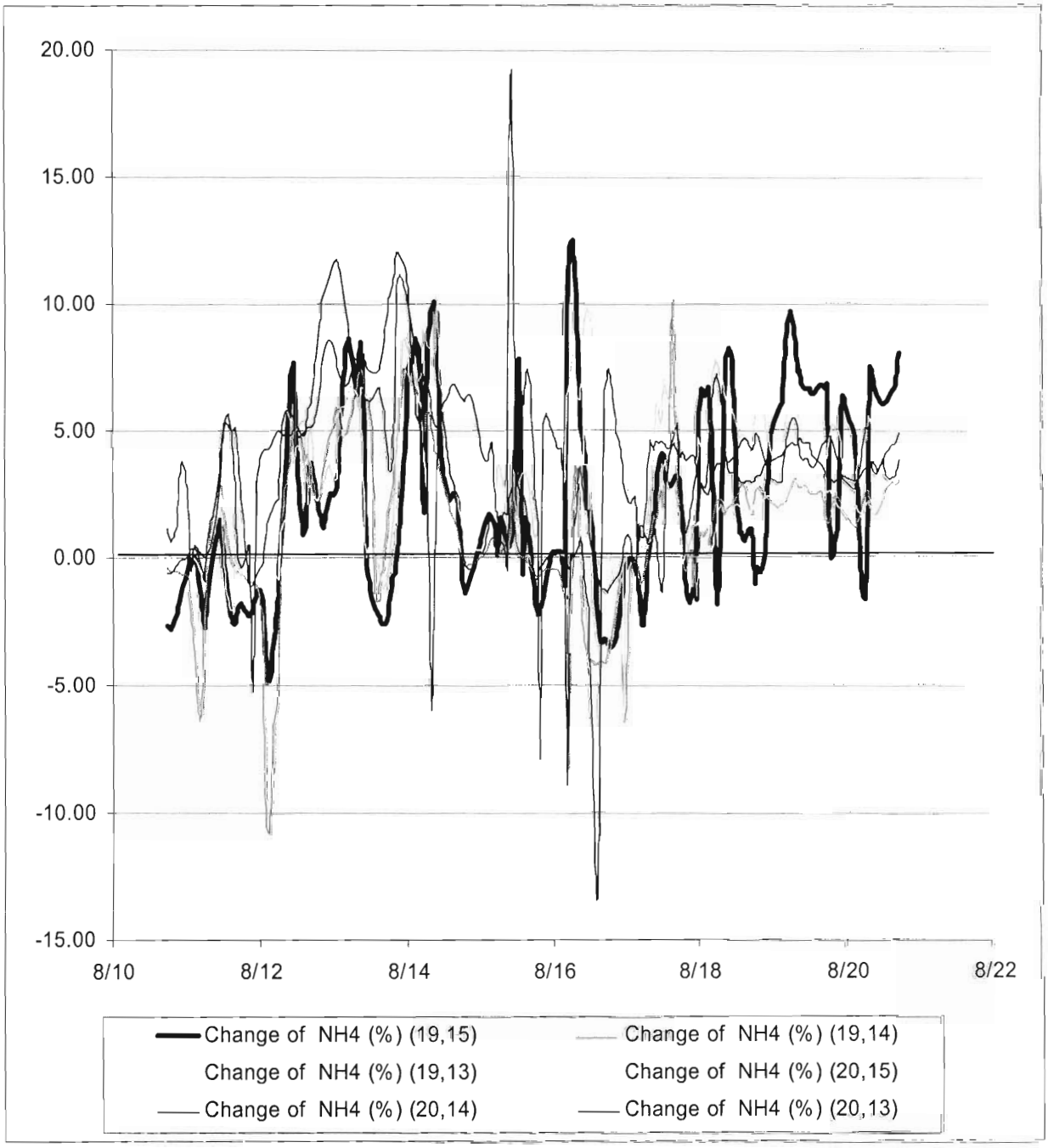

Figure 25. Changes (%) of ammonium concentrations from the 2000 year to the 2007 year.

(a)

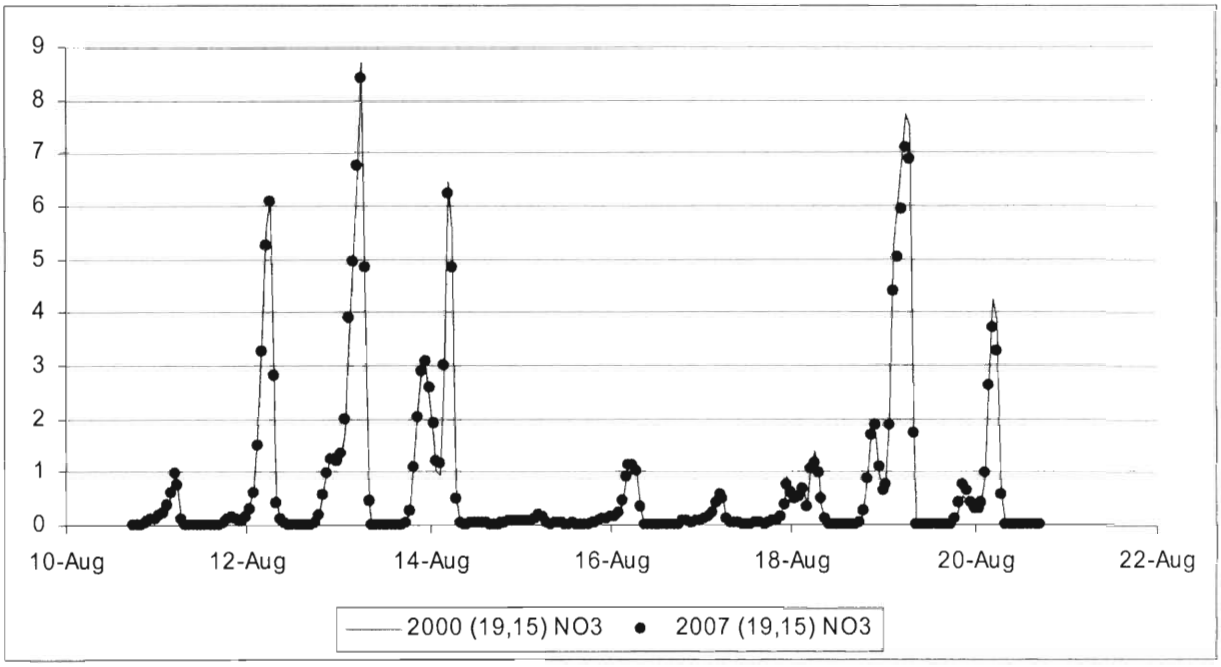

(b)

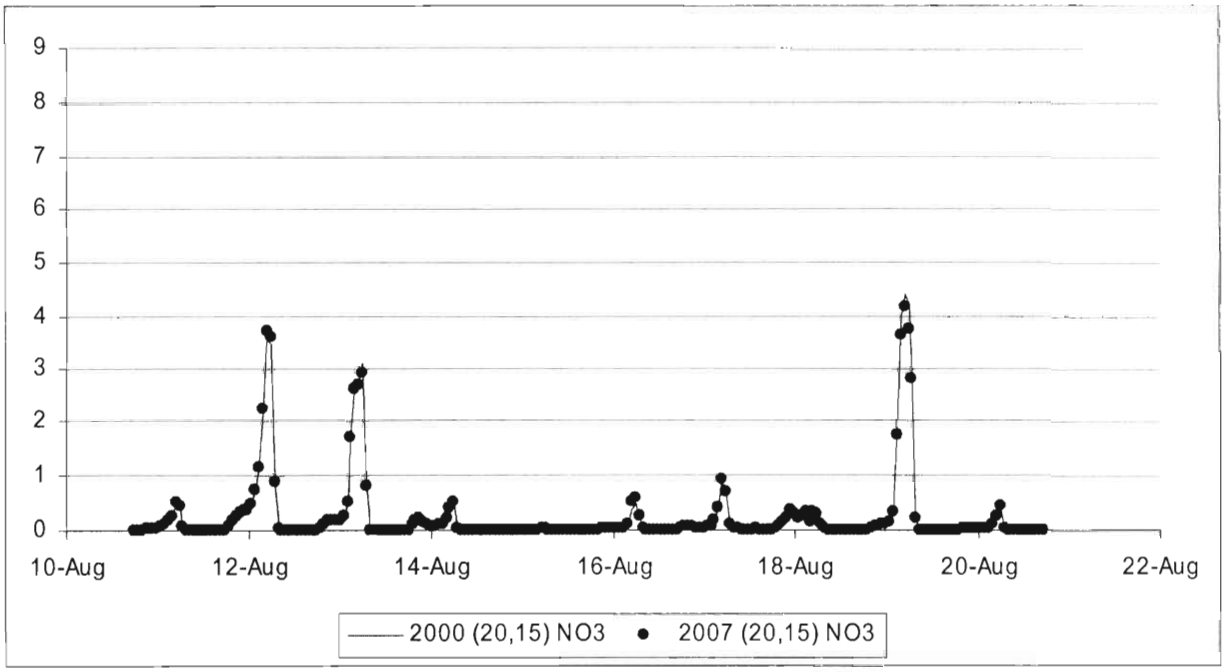

Figure 26. Comparison of the simulated hourly nitrate concentrations in 2000 and in 2007. (a) is for the 19th column and the 15th row of grids and (b) is for the 20th column and the 15th row.

(a)

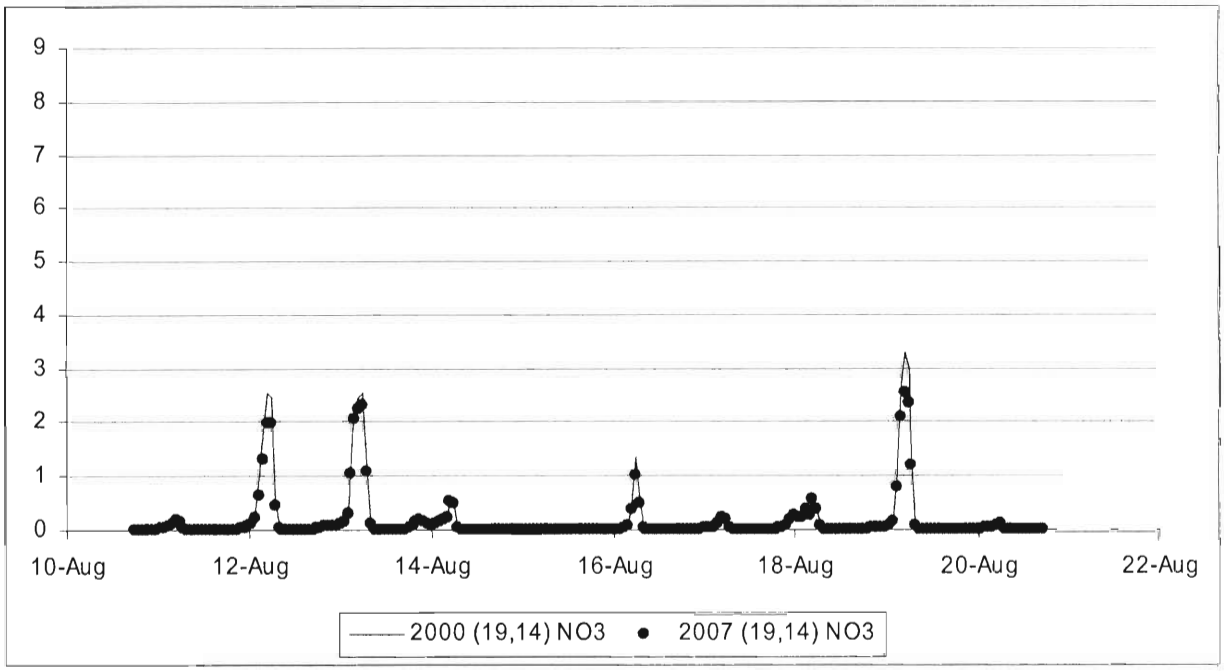

(b)

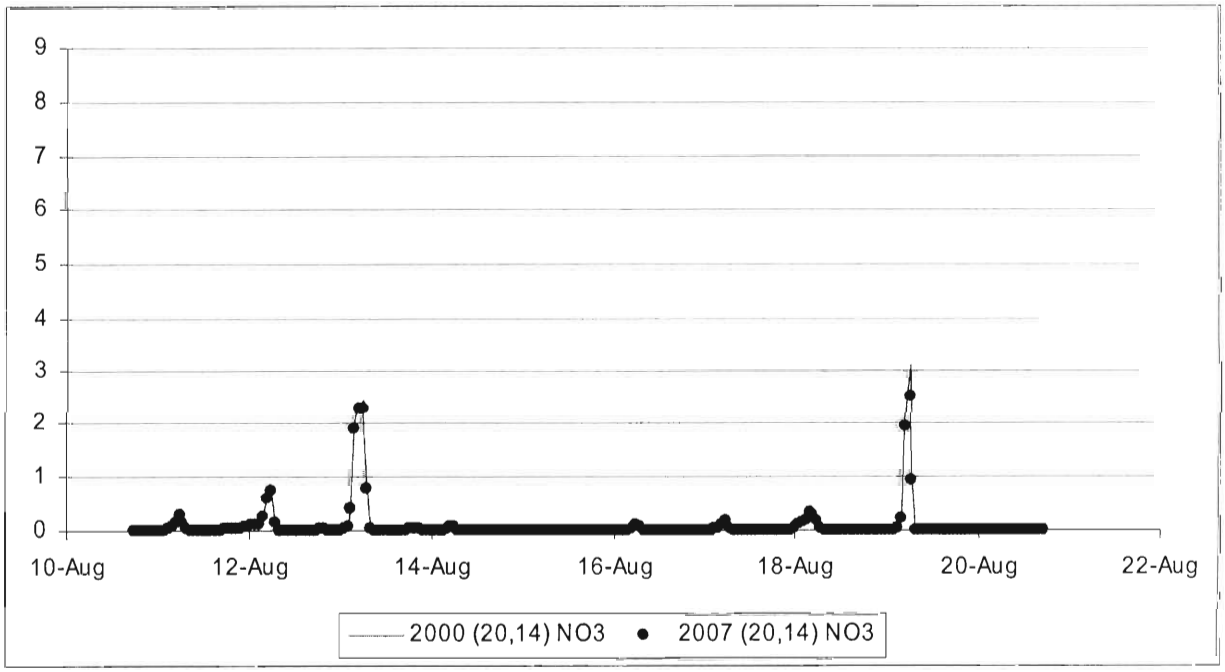

Figure 26. Continued. (c) is for the 19th column and the 14th row of grids and (d) is for the 20th column and the 14th row.

(a)

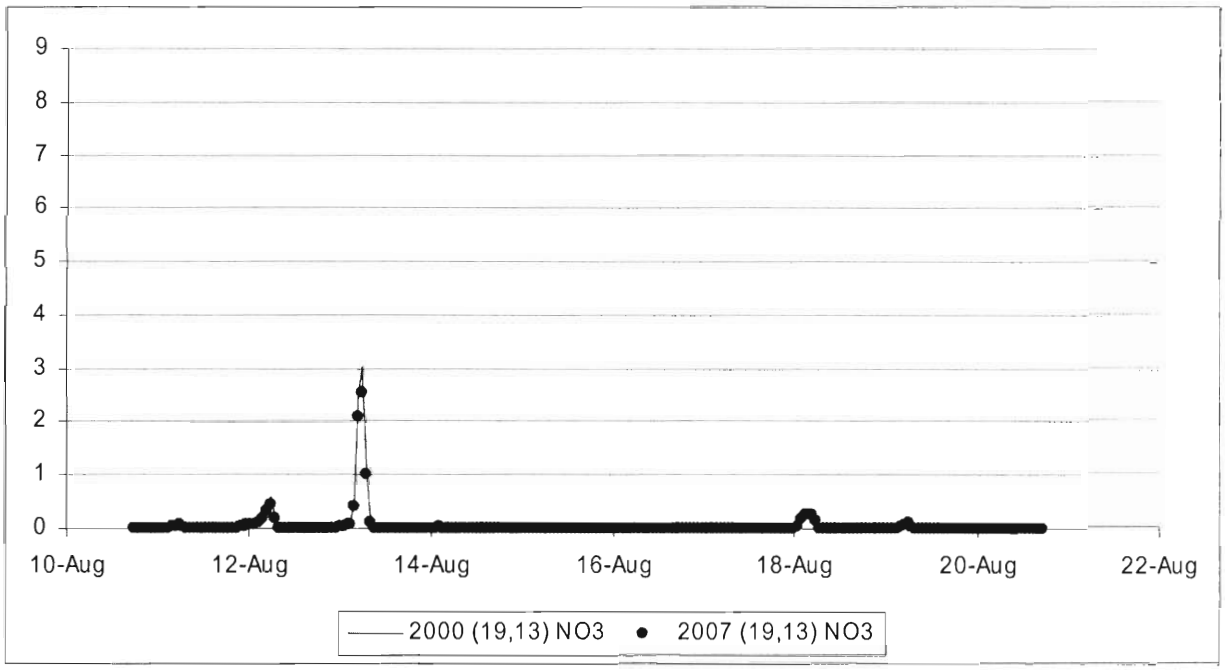

(b)

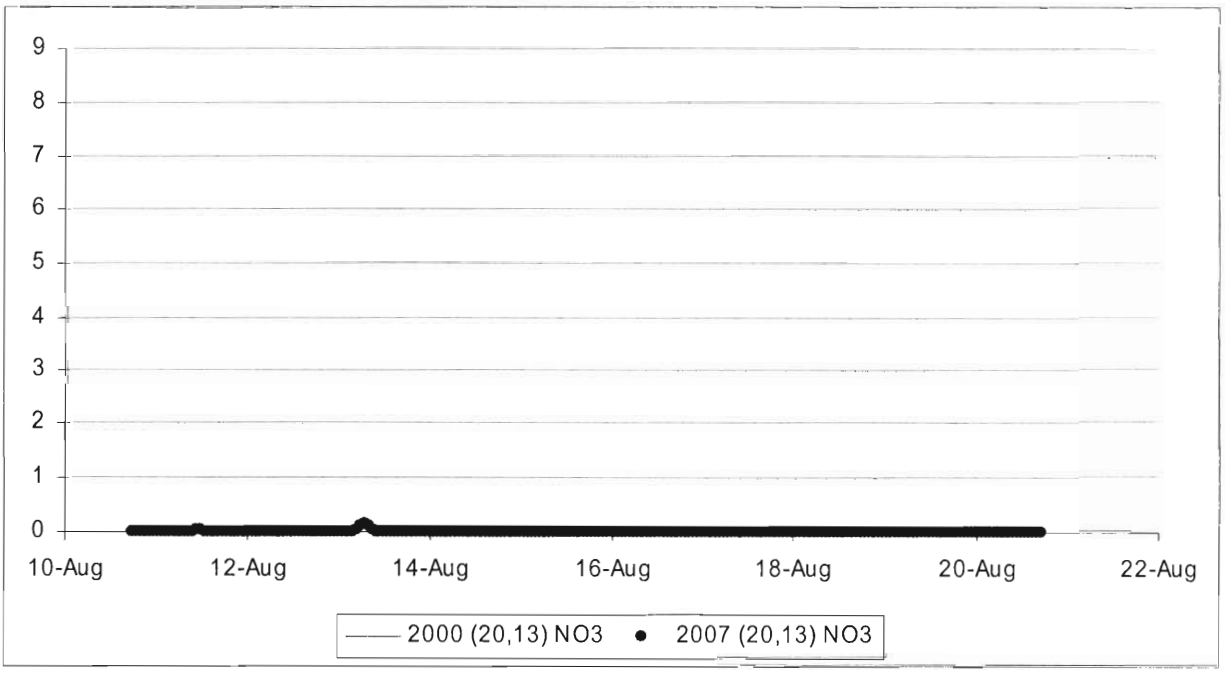

Figure 26. Continued. (e) is for the 19th column and the 13th row of grids and (f) is for the 20th column and the 13th row.

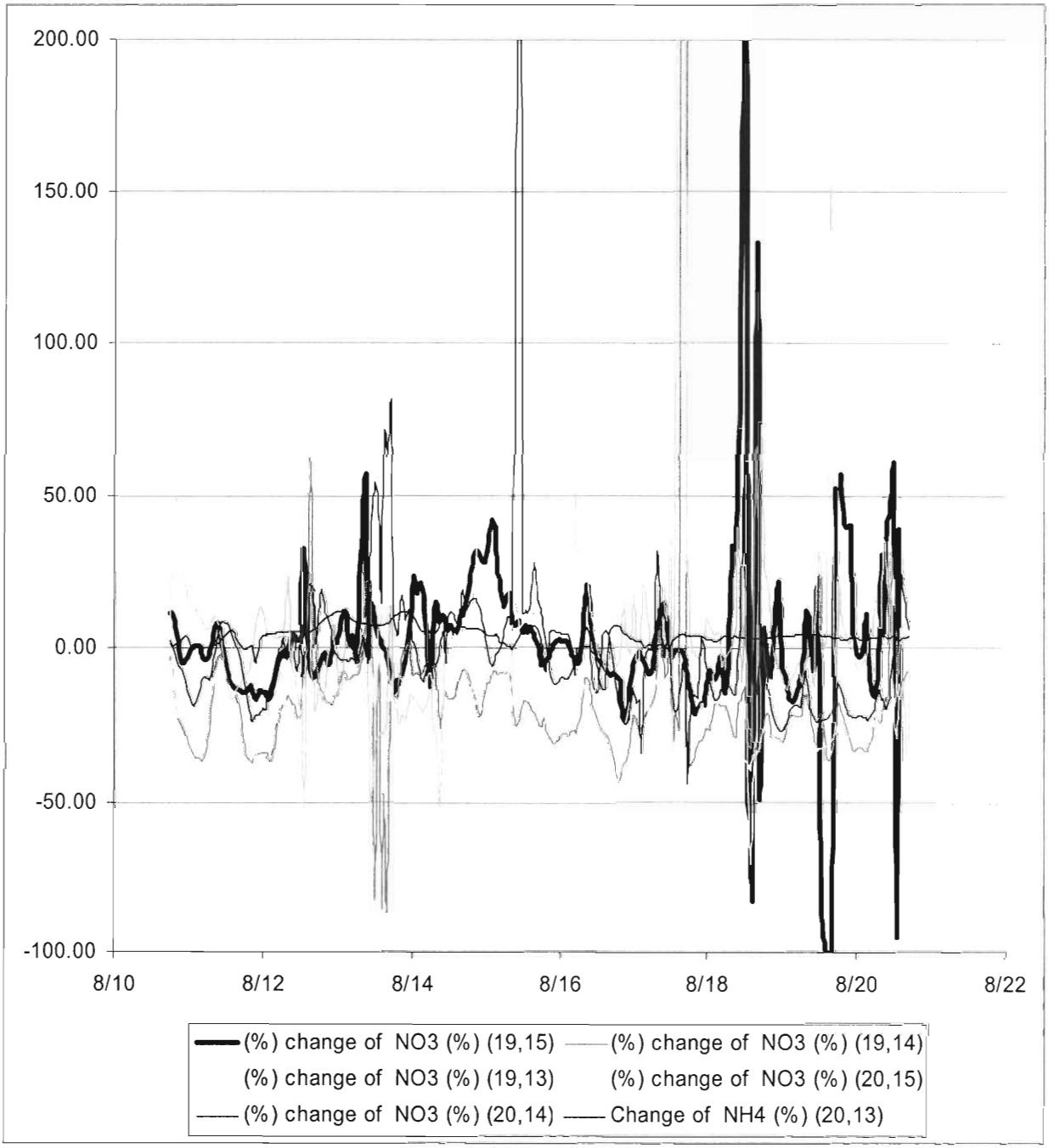

Figure 27. Changes (%) of nitrate concentrations from the 2000 year to the 2007 year.

(a)

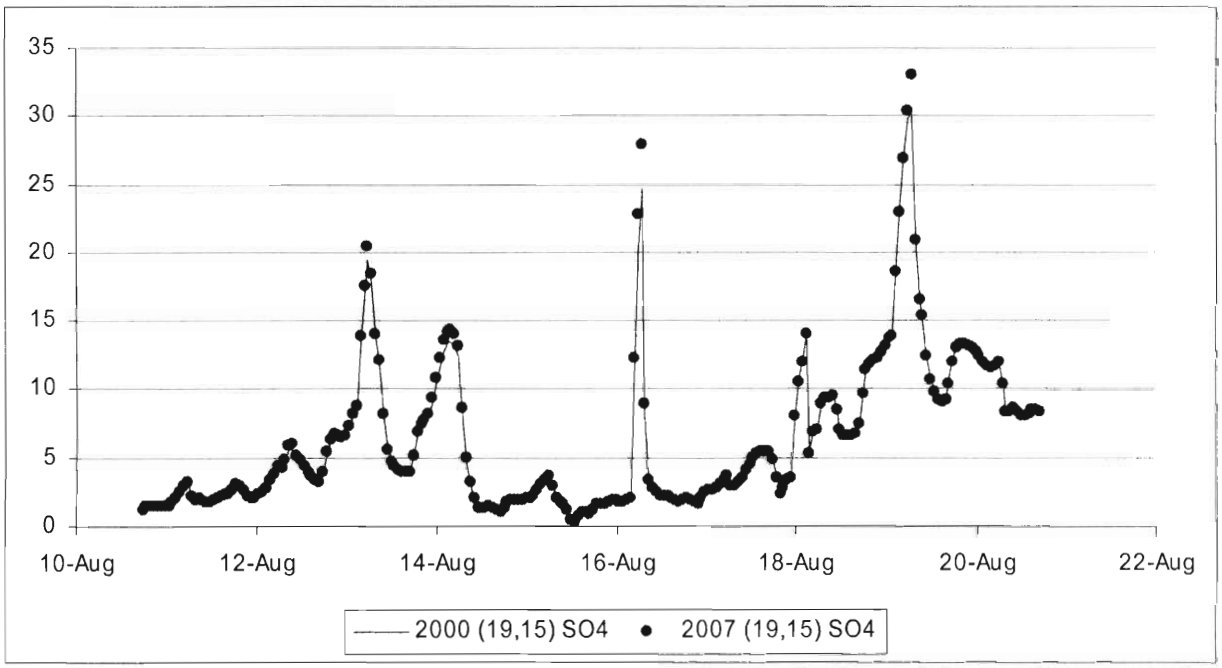

(b)

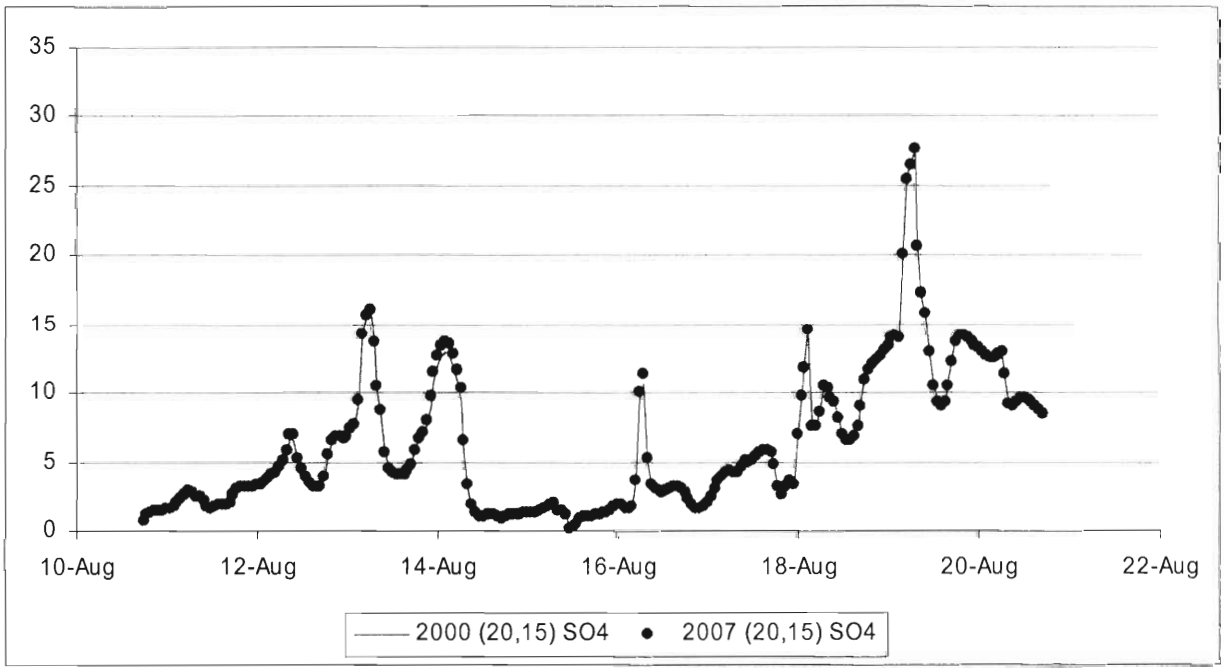

Figure 28. Comparison of the simulated hourly sulfate concentrations in 2000 and in 2007. (a) is for the 19th column and the 15th row of grids and (b) is for the 20th column and the 15th row.

(c)

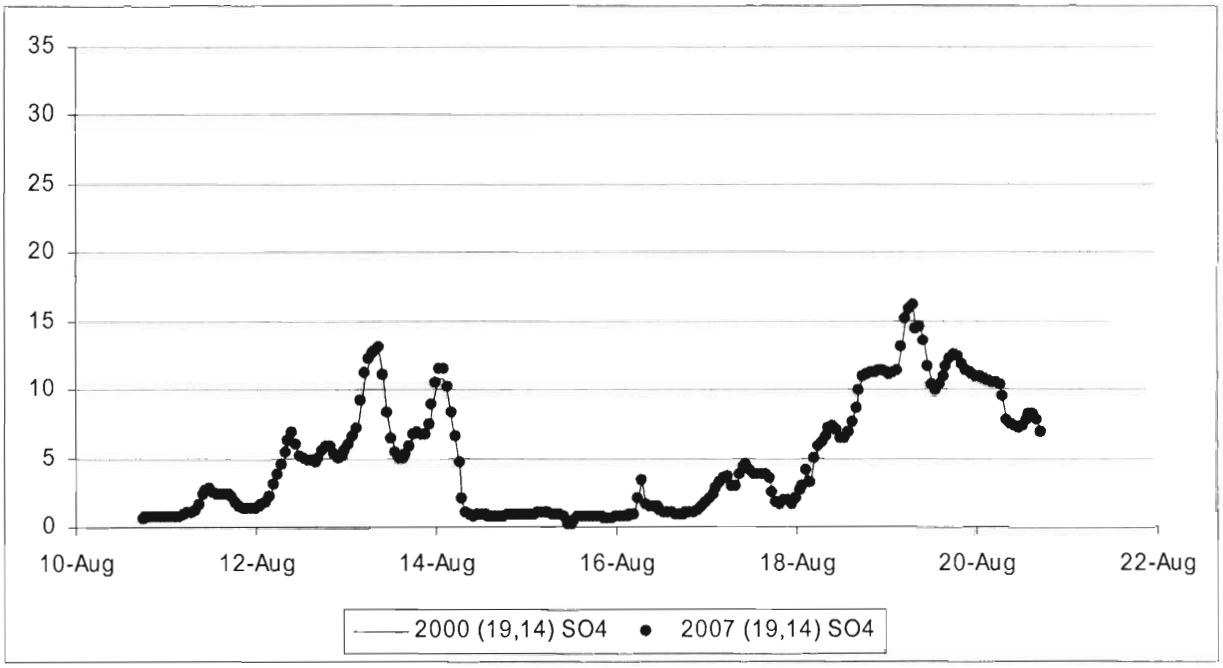

(d)

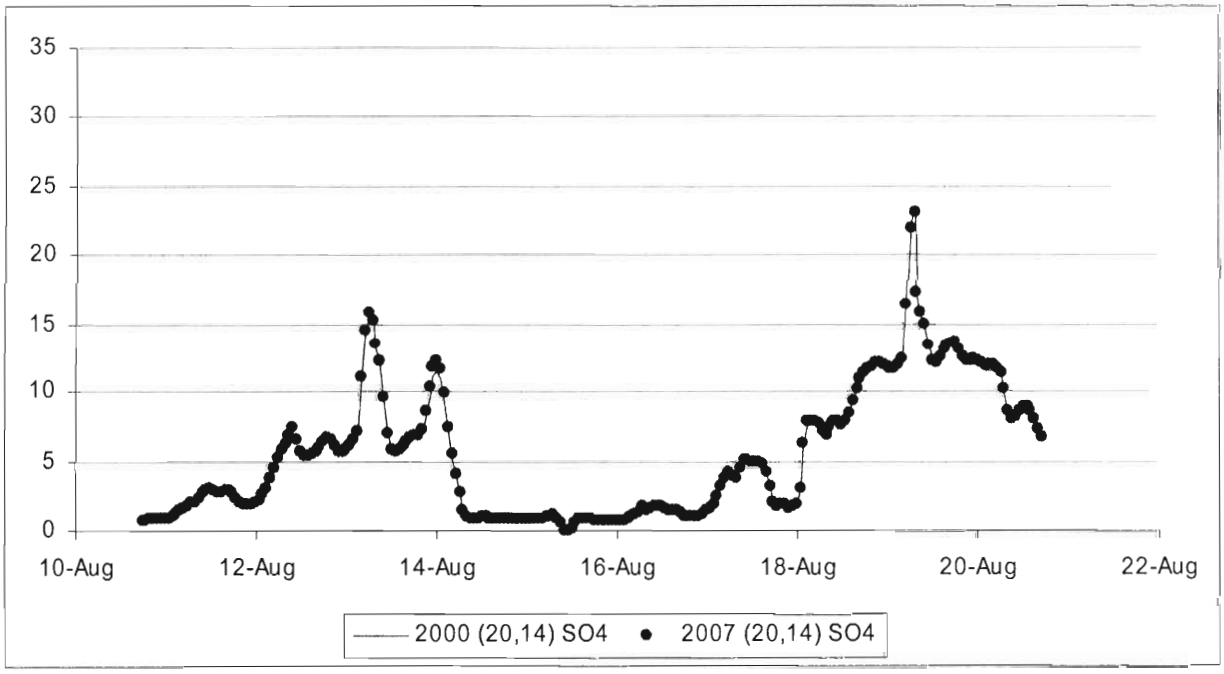

Figure 28. Continued. (c) is for the 19th column and the 14th row of grids and (d) is for the 20th column and the 14th row.

(e)

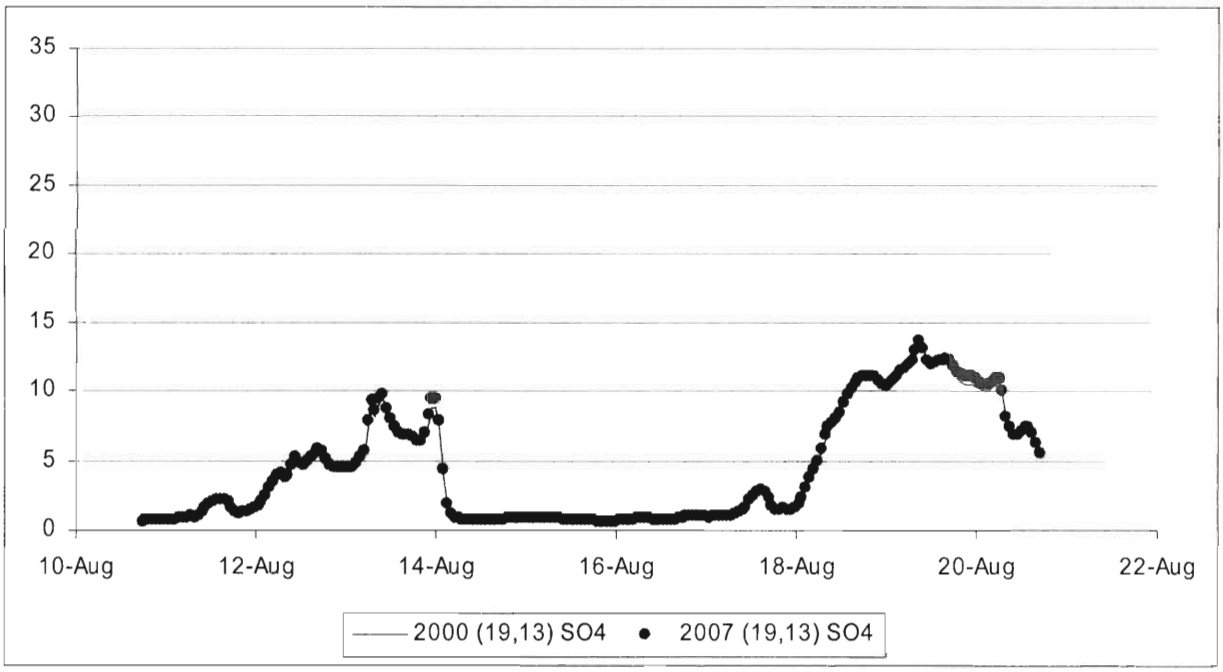

(f)

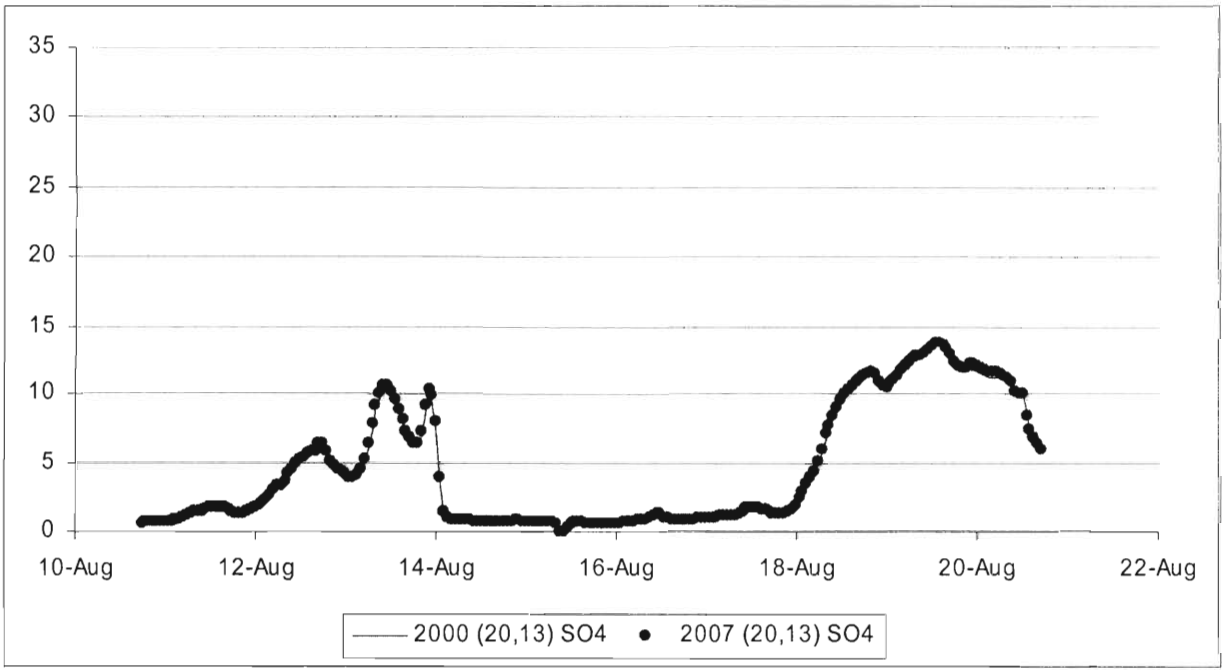

Figure 28. Continued. (e) is for the 19th column and the 13th row of grids and (f) is for the 20th column and the 13th row.

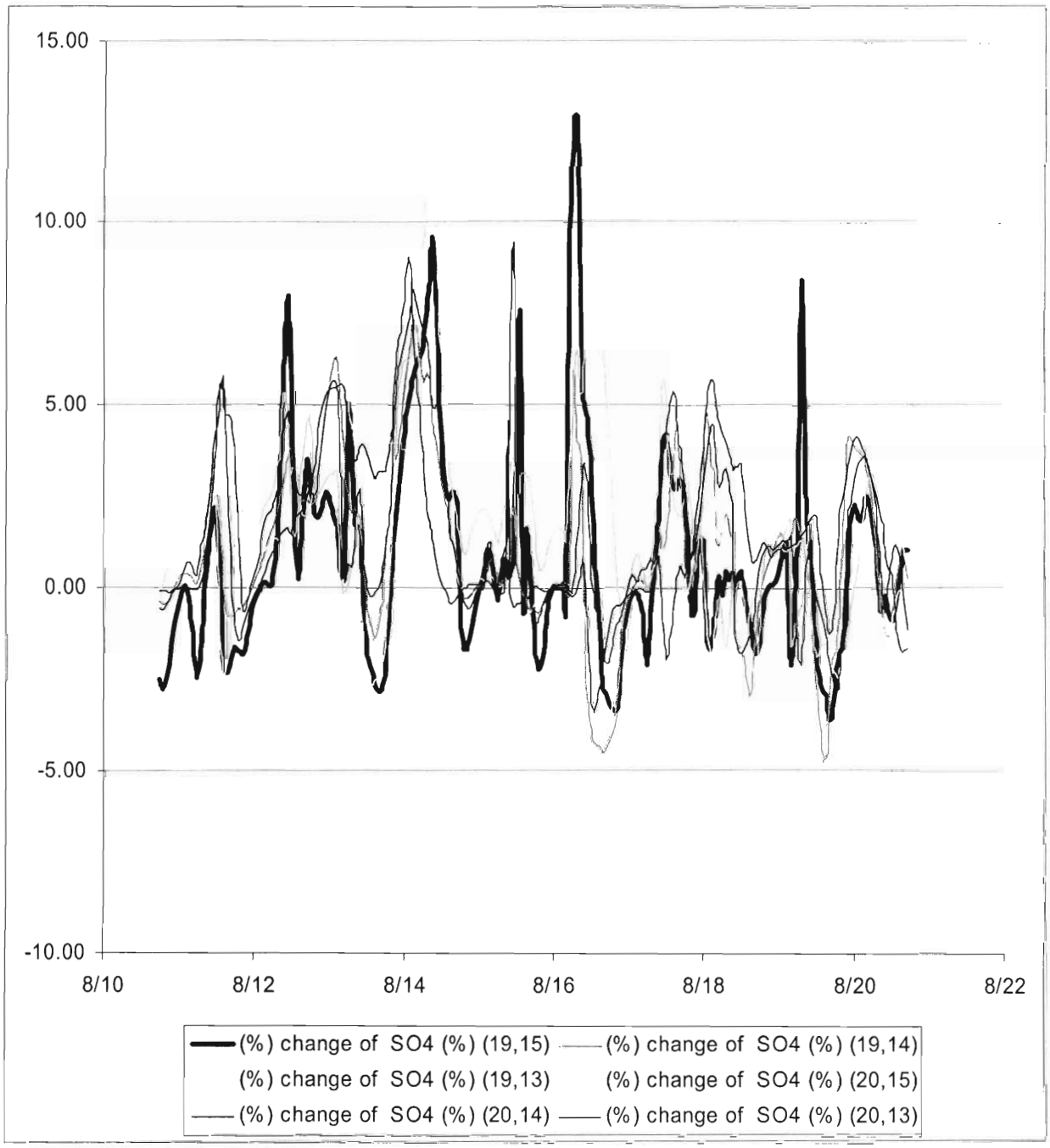

Figure 29. Changes (%) of sulfate concentrations from the 2000 year to the 2007 year.

(a)

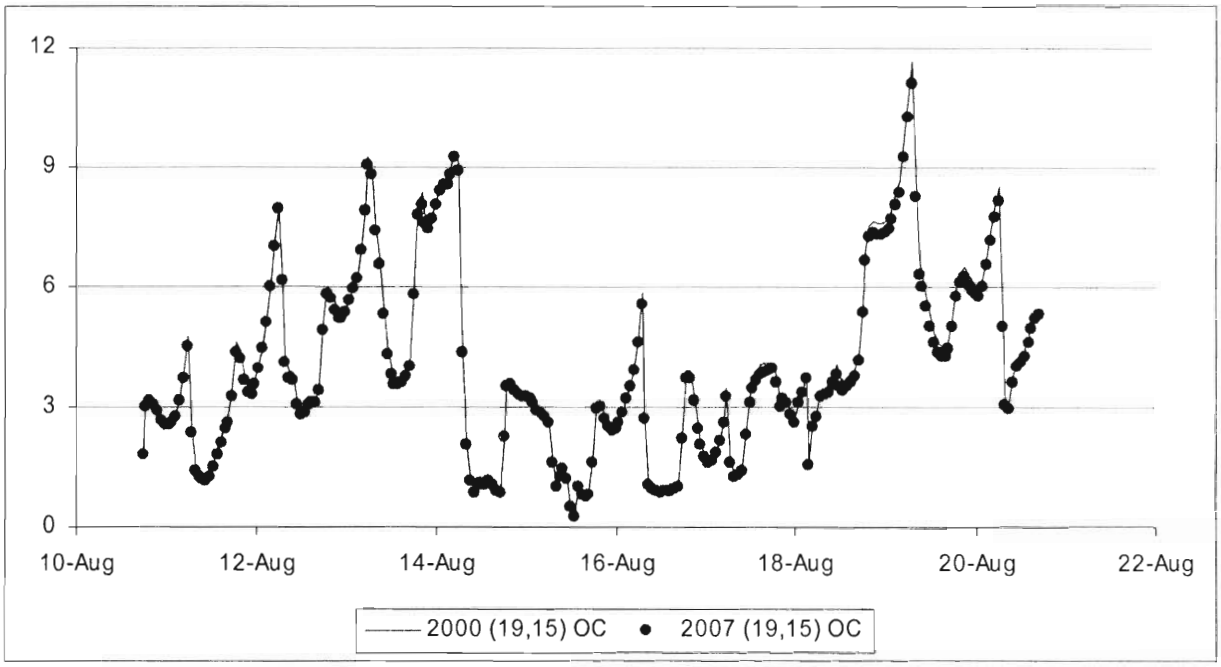

(b)

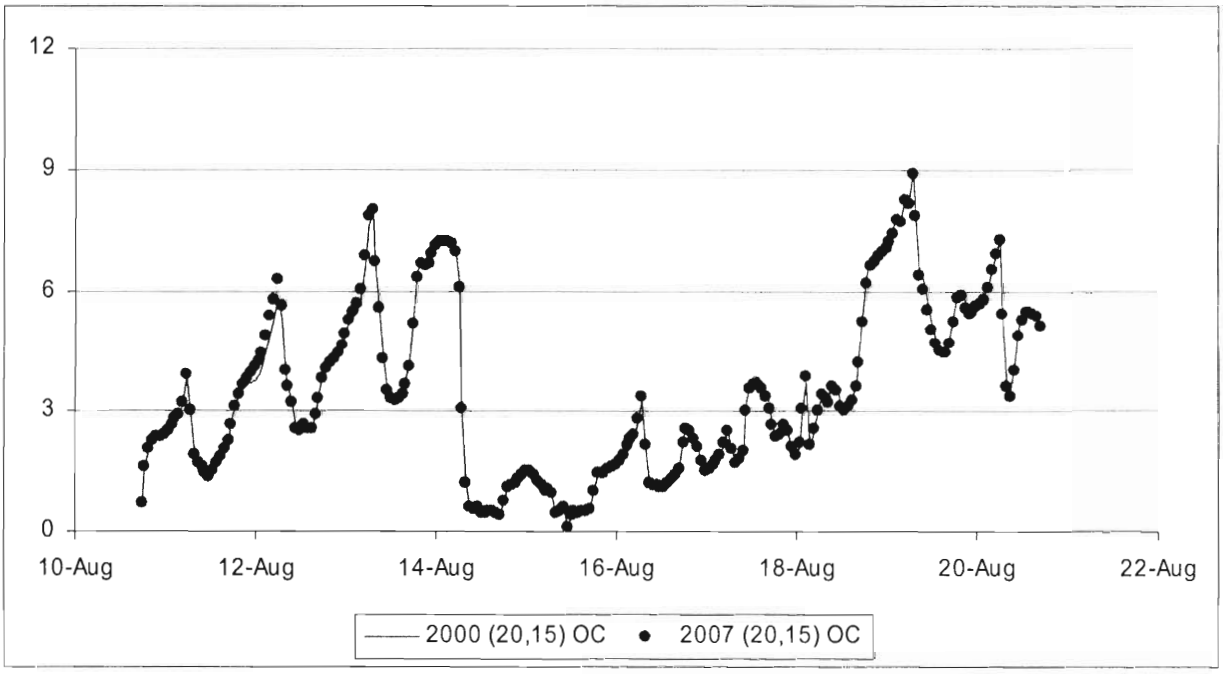

Figure 30. Comparison of the simulated hourly organic carbon concentrations in 2000 and in 2007. (a) is for the 19th column and the 15th row of grids and (b) is for the 20th column and the 15th row.

(c)

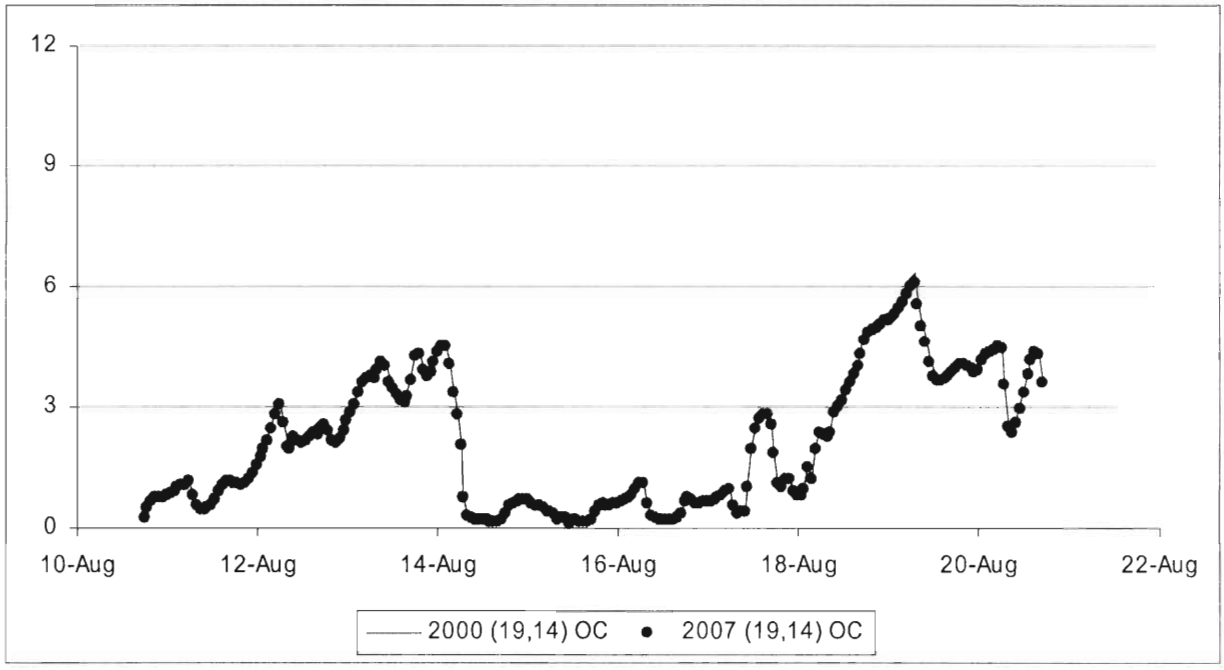

(d)

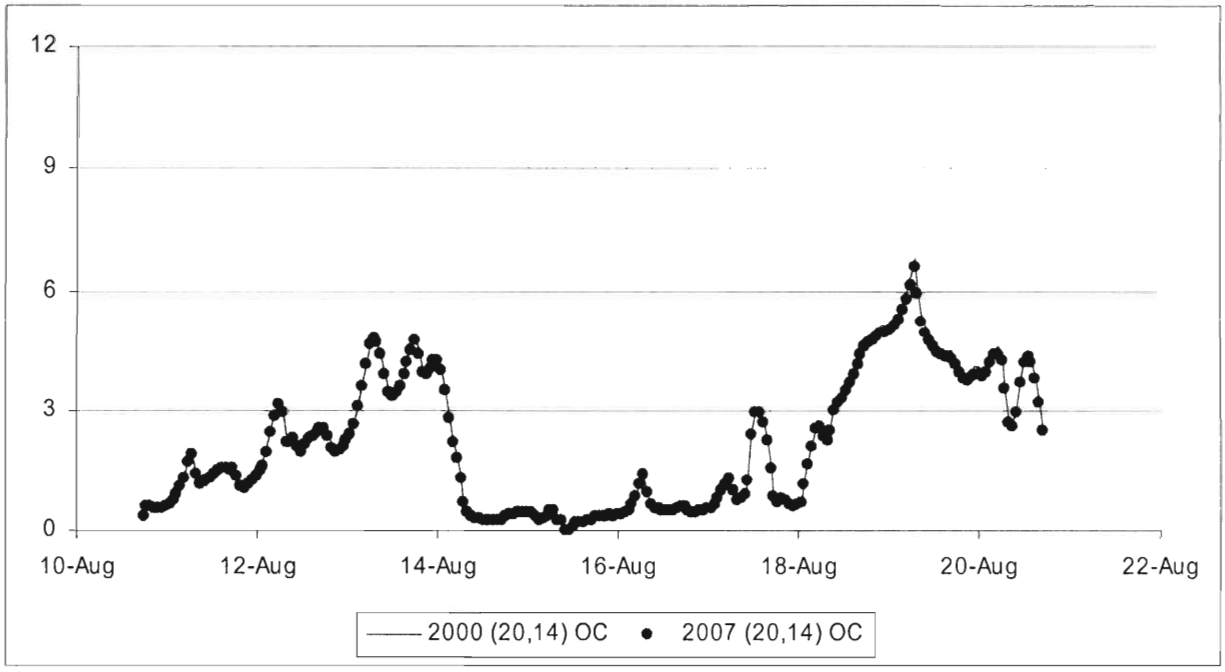

Figure 30. Continued. (c) is for the 19th column and the 14th row of grids and (d) is for the 20th column and the 14th row.

(e)

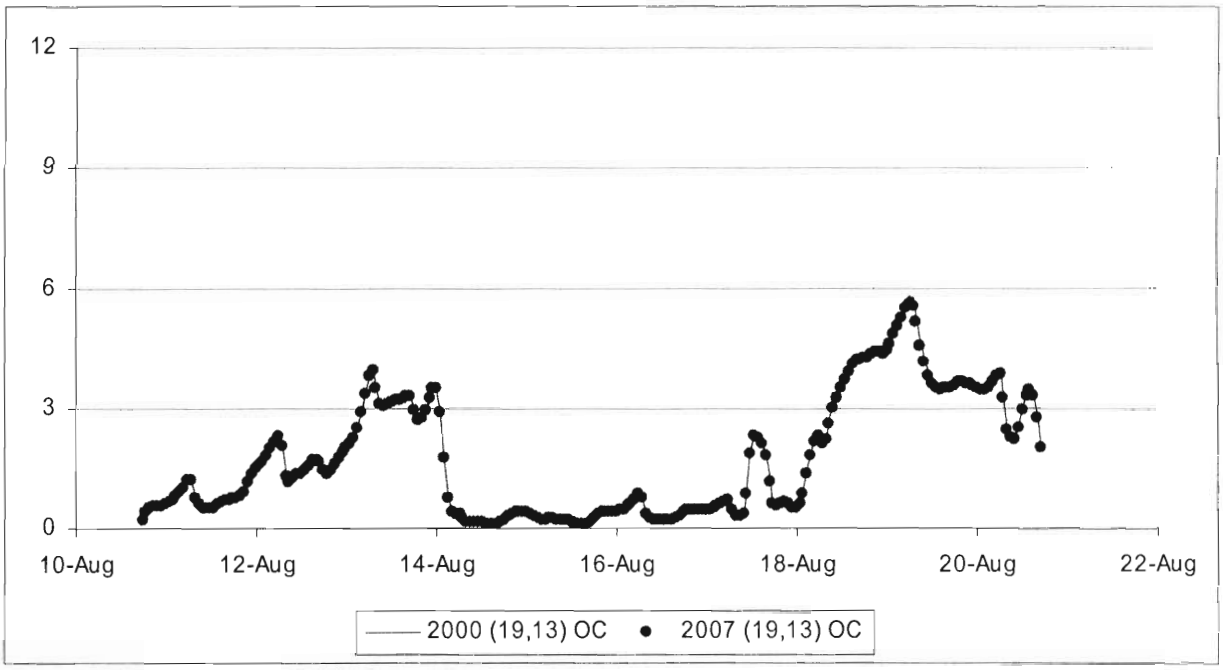

(f)

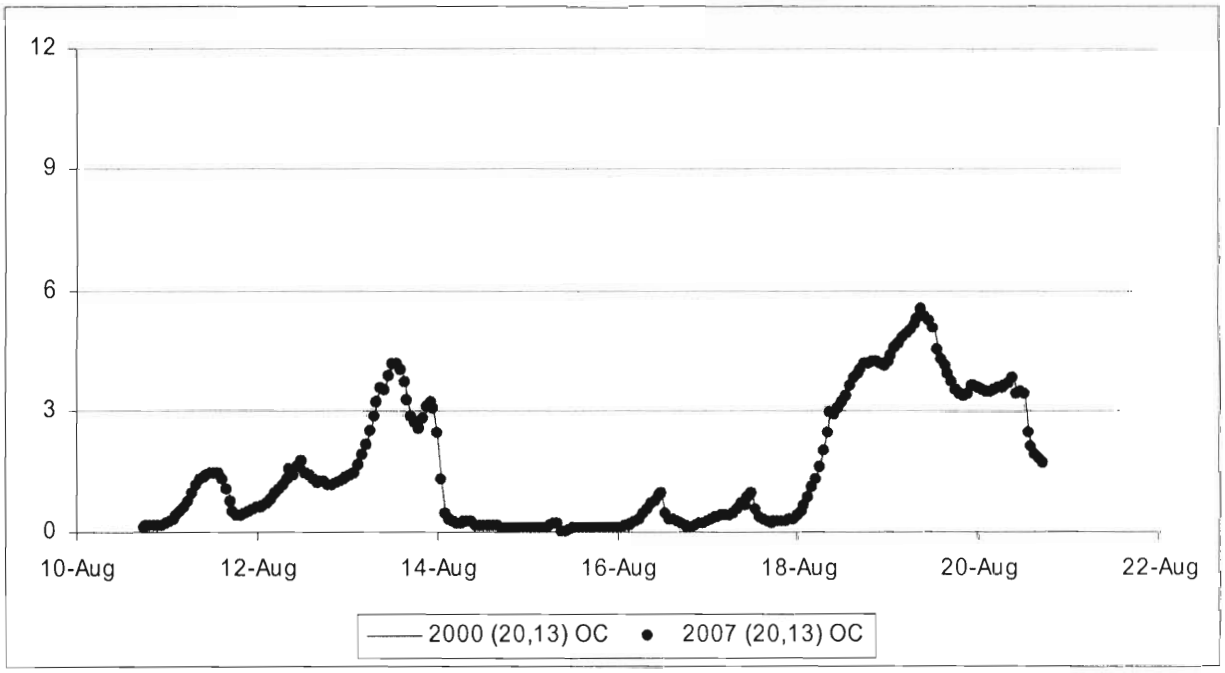

Figure 30. Continued. (e) is for the 19th column and the 13th row of grids and (f) is for the 20th column and the 13th row.

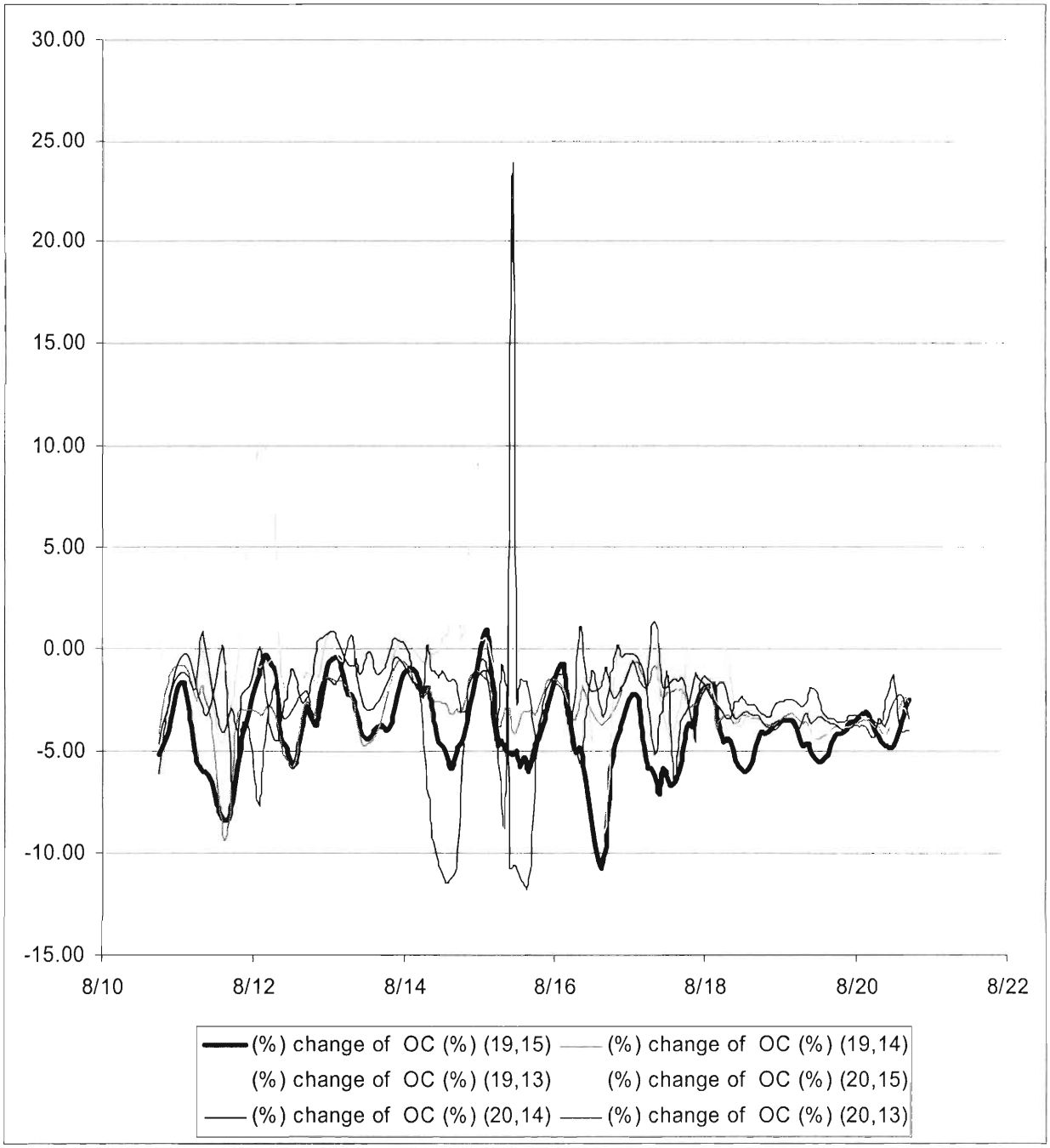

Figure 31. Changes (%) of organic carbon concentrations from the 2000 year to the 2007 year.

(a)

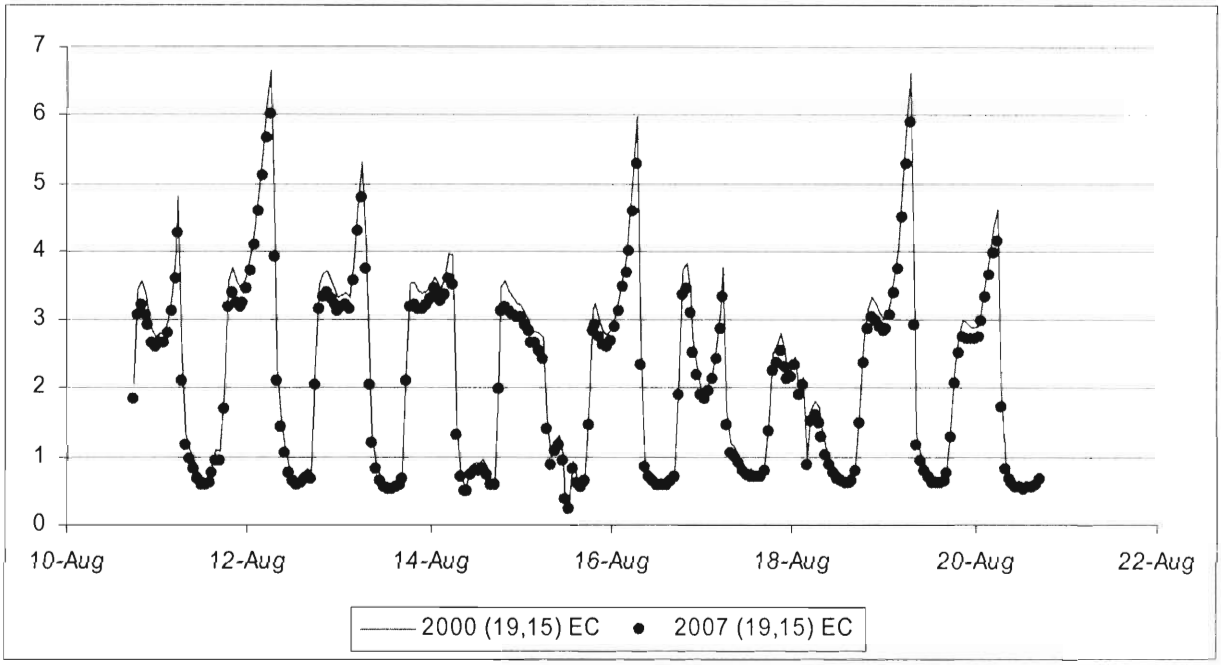

(b)

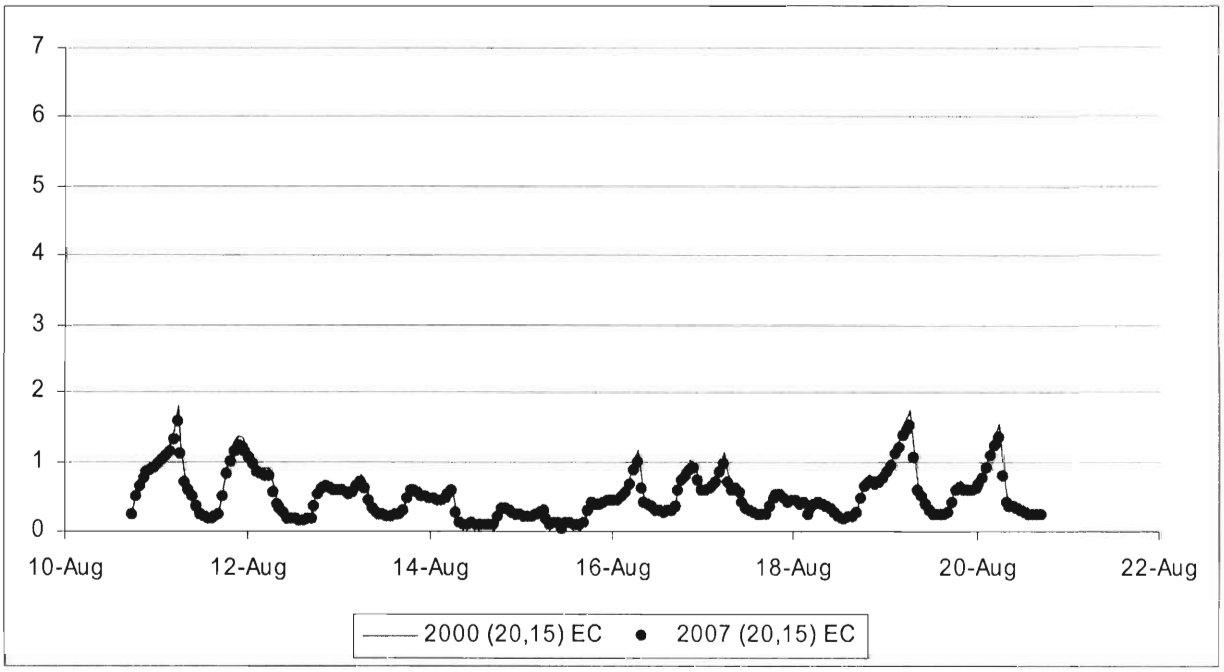

Figure 32. Comparison of the simulated hourly elemental carbon concentrations in 2000 and in 2007. (a) is for the 19th column and the 15th row of grids and (b) is for the 20th column and the 15th row.

(c)

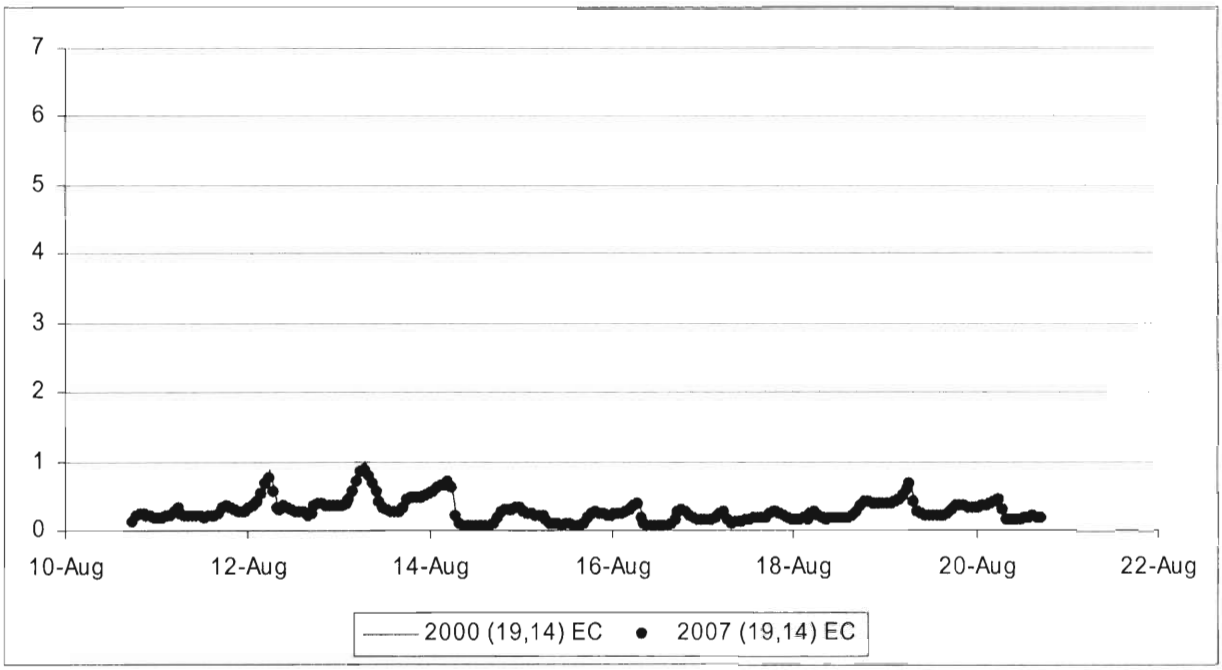

(d)

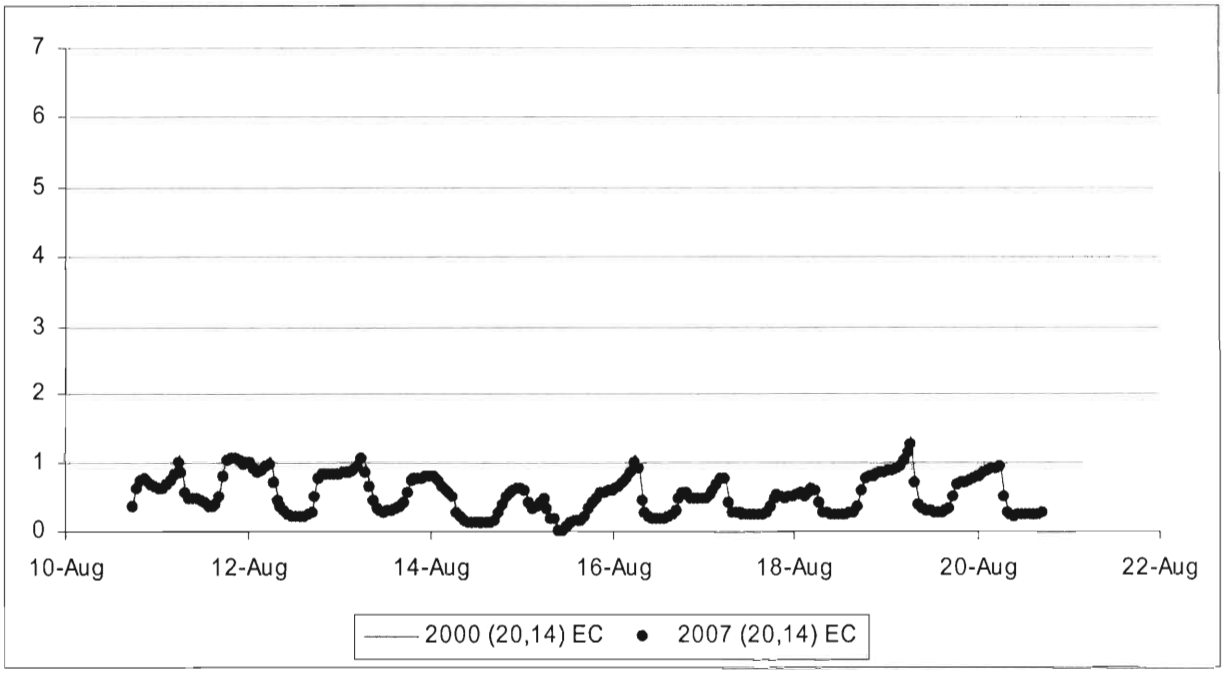

Figure 32. Continued. (c) is for the 19th column and the 14th row of grids and (d) is for the 20th column and the 14th row.

(e)

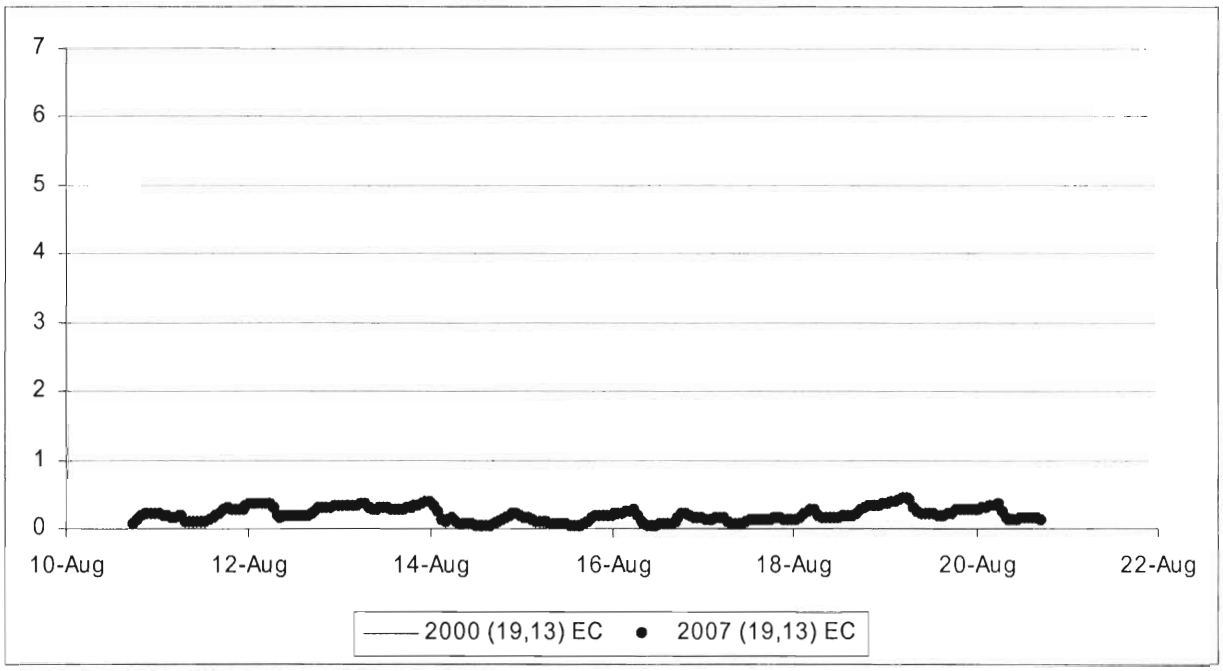

(f)

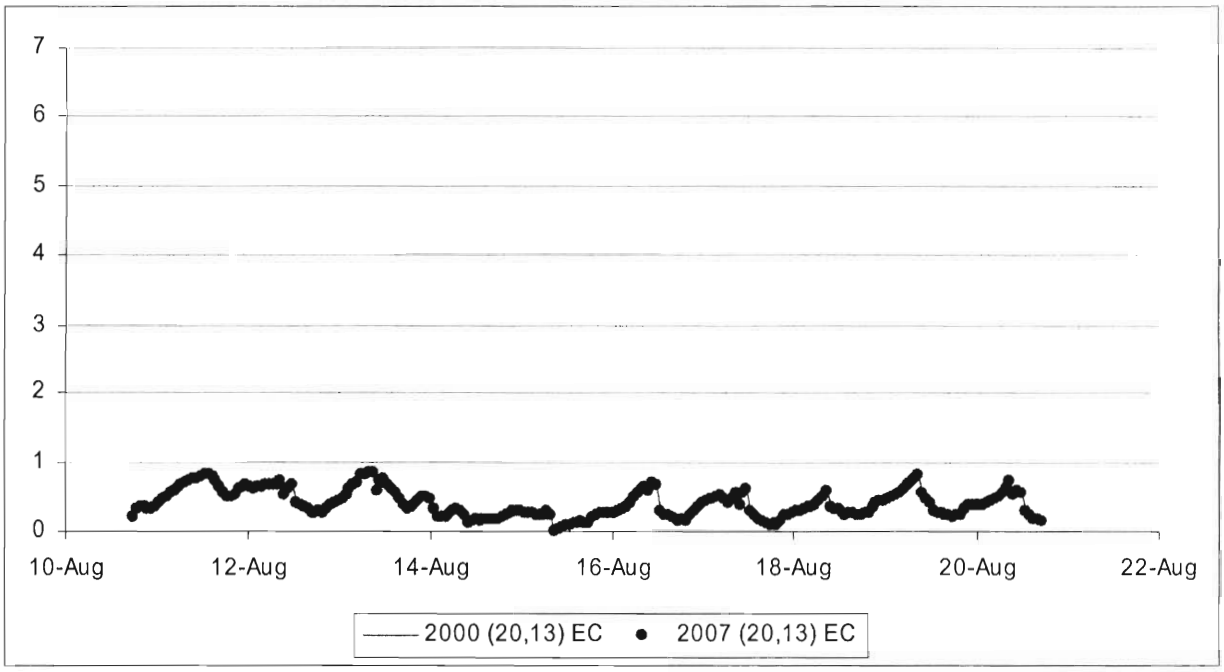

Figure 32. Continued. (e) is for the 19th column and the 13th row of grids and (f) is for the 20th column and the 13th row.

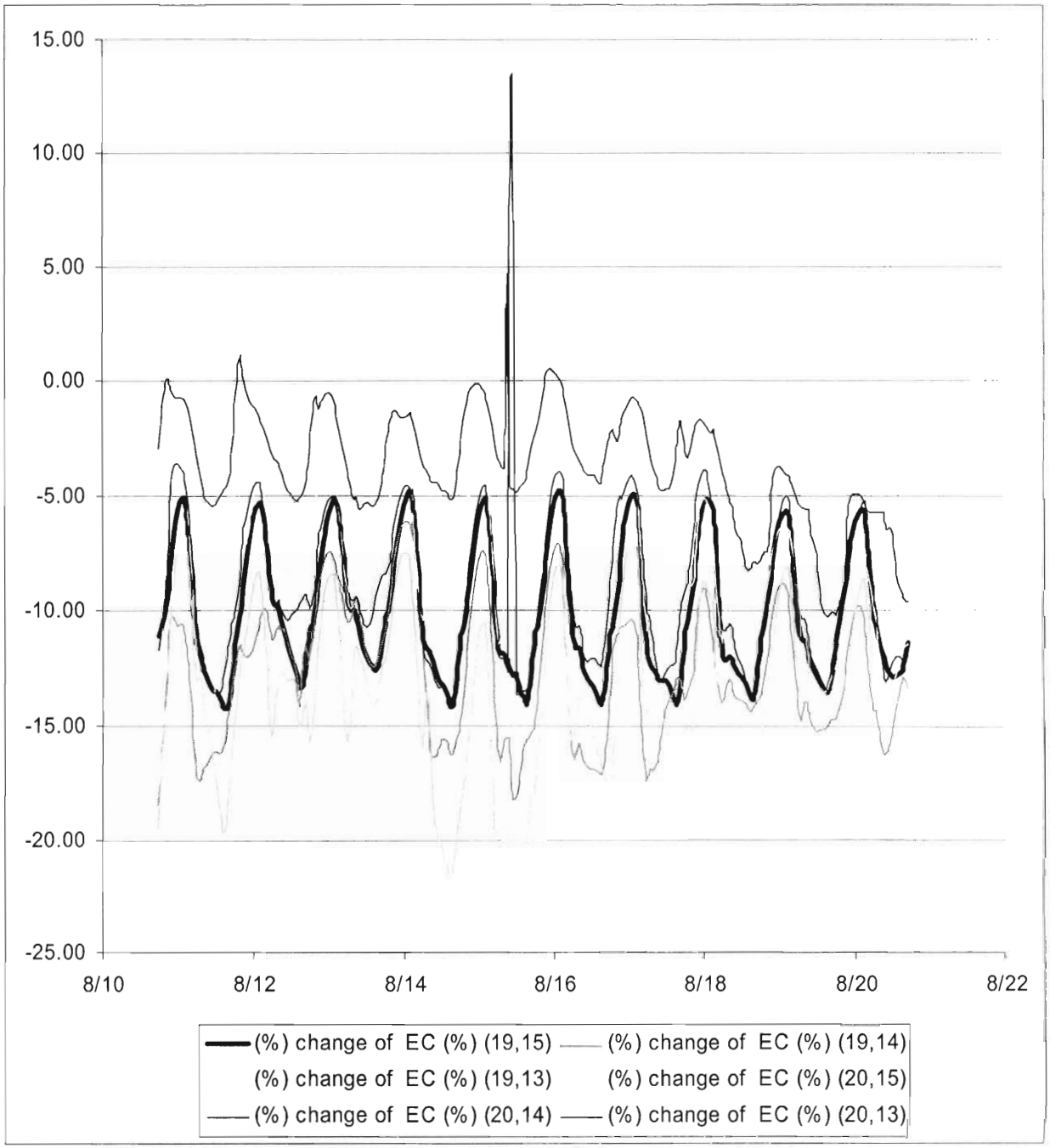

Figure 33. Changes (%) of elemental carbon concentrations from the 2000 year to the 2007 year.

(a)

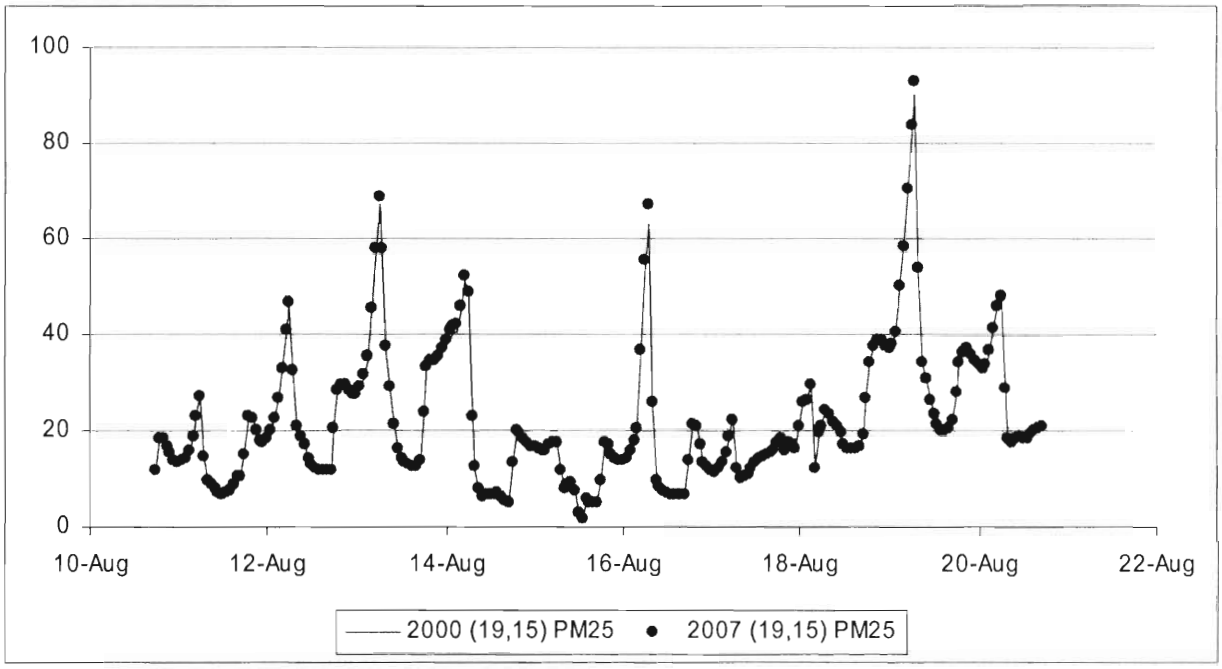

(b)

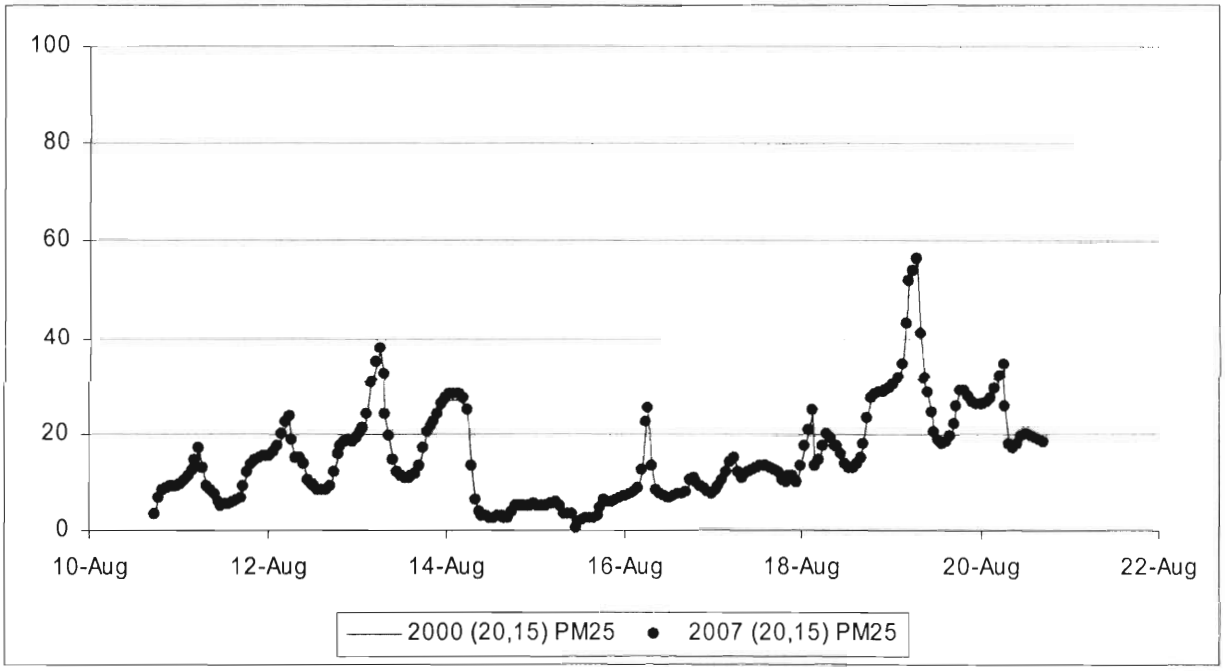

Figure 34. Comparison of the simulated hourly PM 2.5 concentrations in 2000 and in 2007. (a) is for the 19th column and the 15th row of grids and (b) is for the 20th column and the 15th row.

(c)

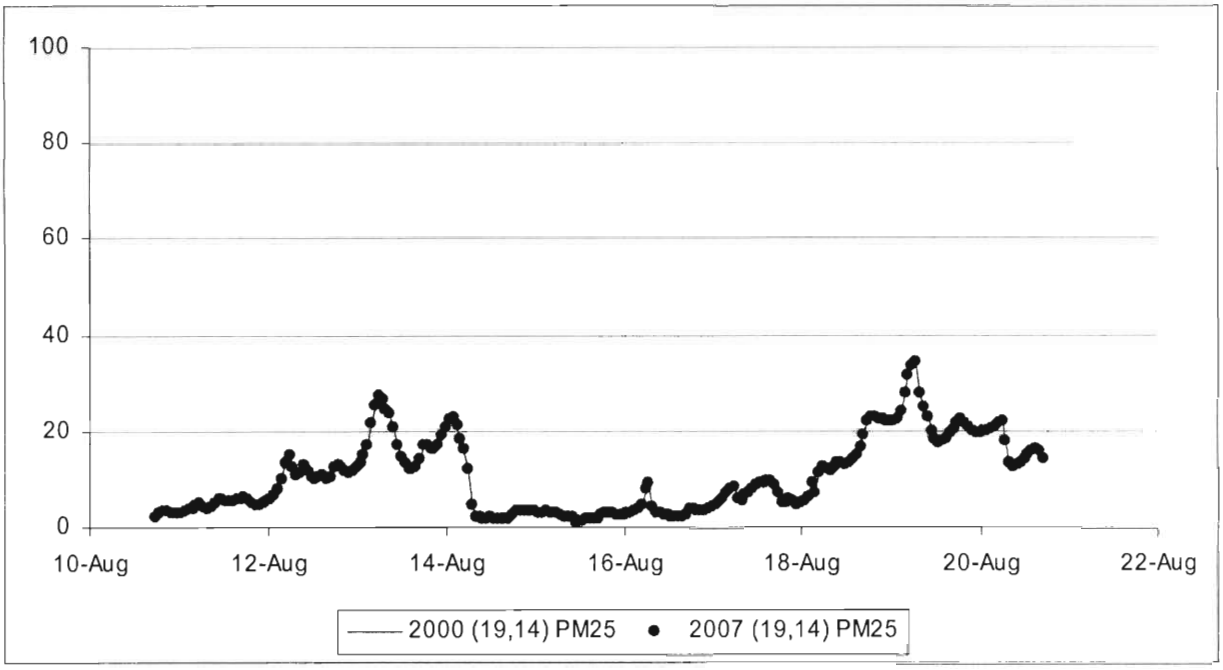

(d)

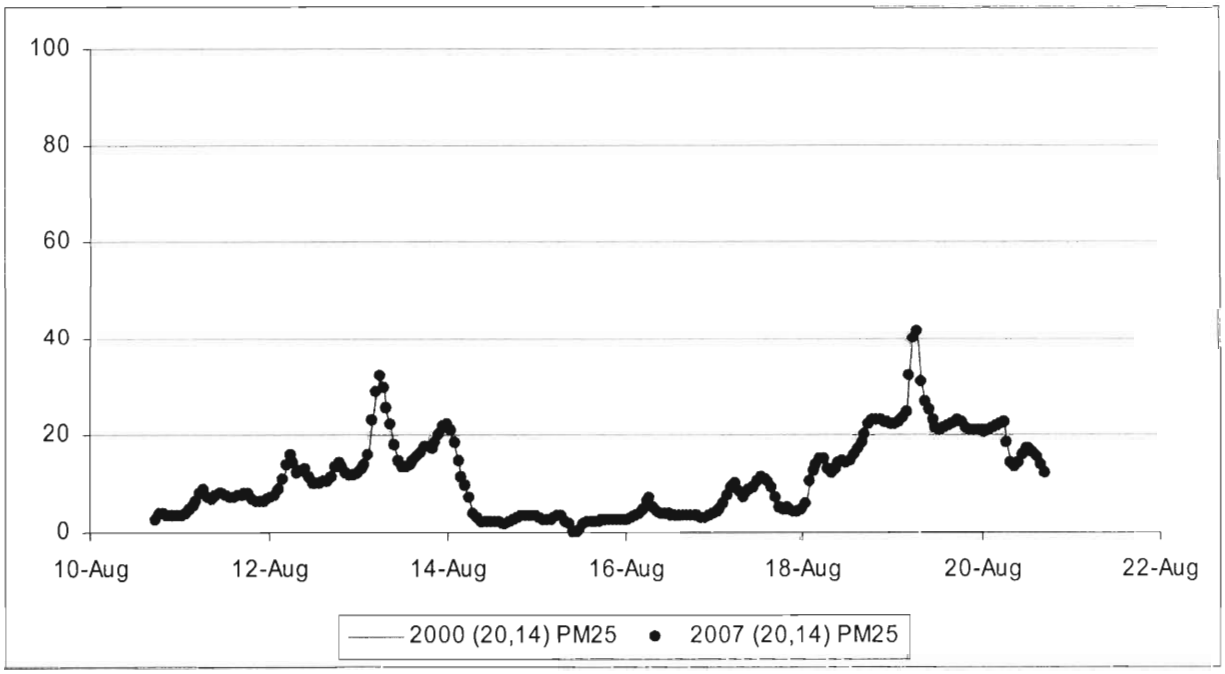

Figure 34. Continued. (c) is for the 19th column and the 14th row of grids and (d) is for the 20th column and the 14th row.

(e)

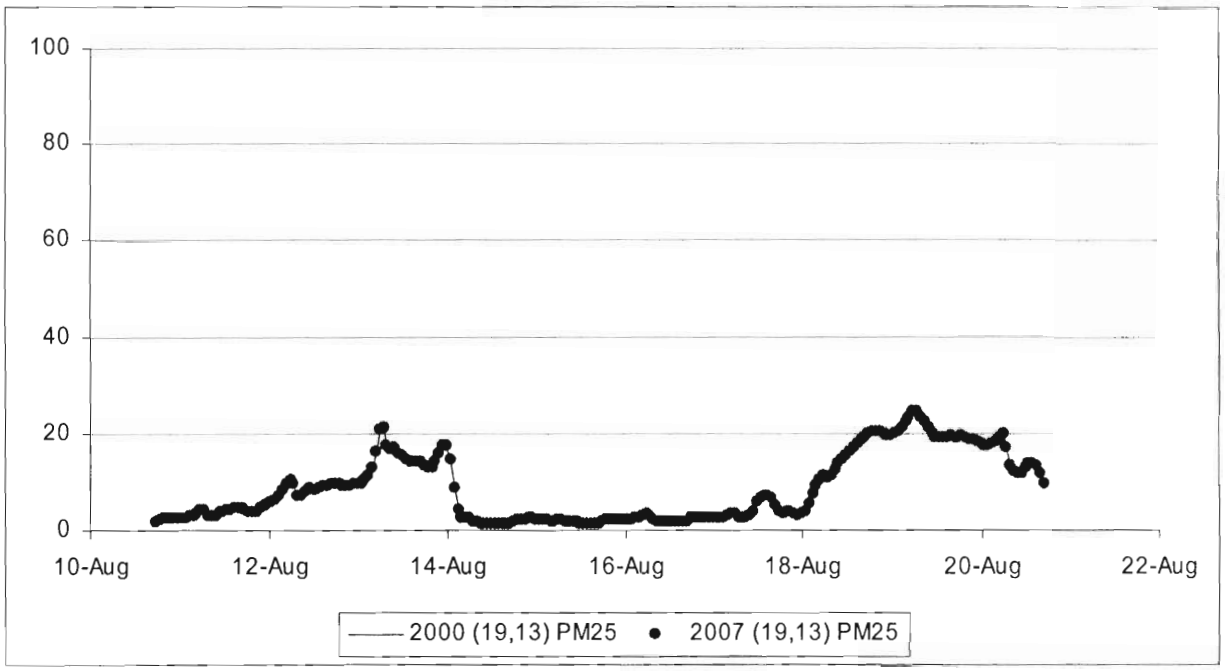

(f)

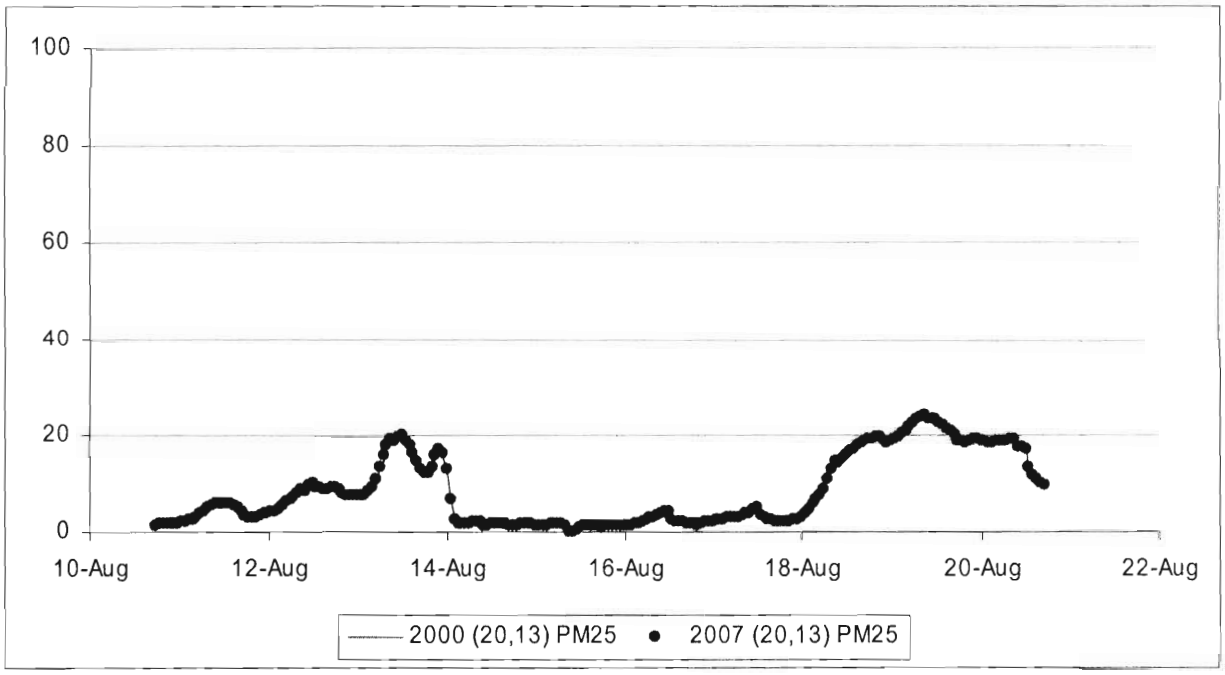

Figure 34. Continued. (e) is for the 19th column and the 13th row of grids and (f) is for the 20th column and the 13th row.

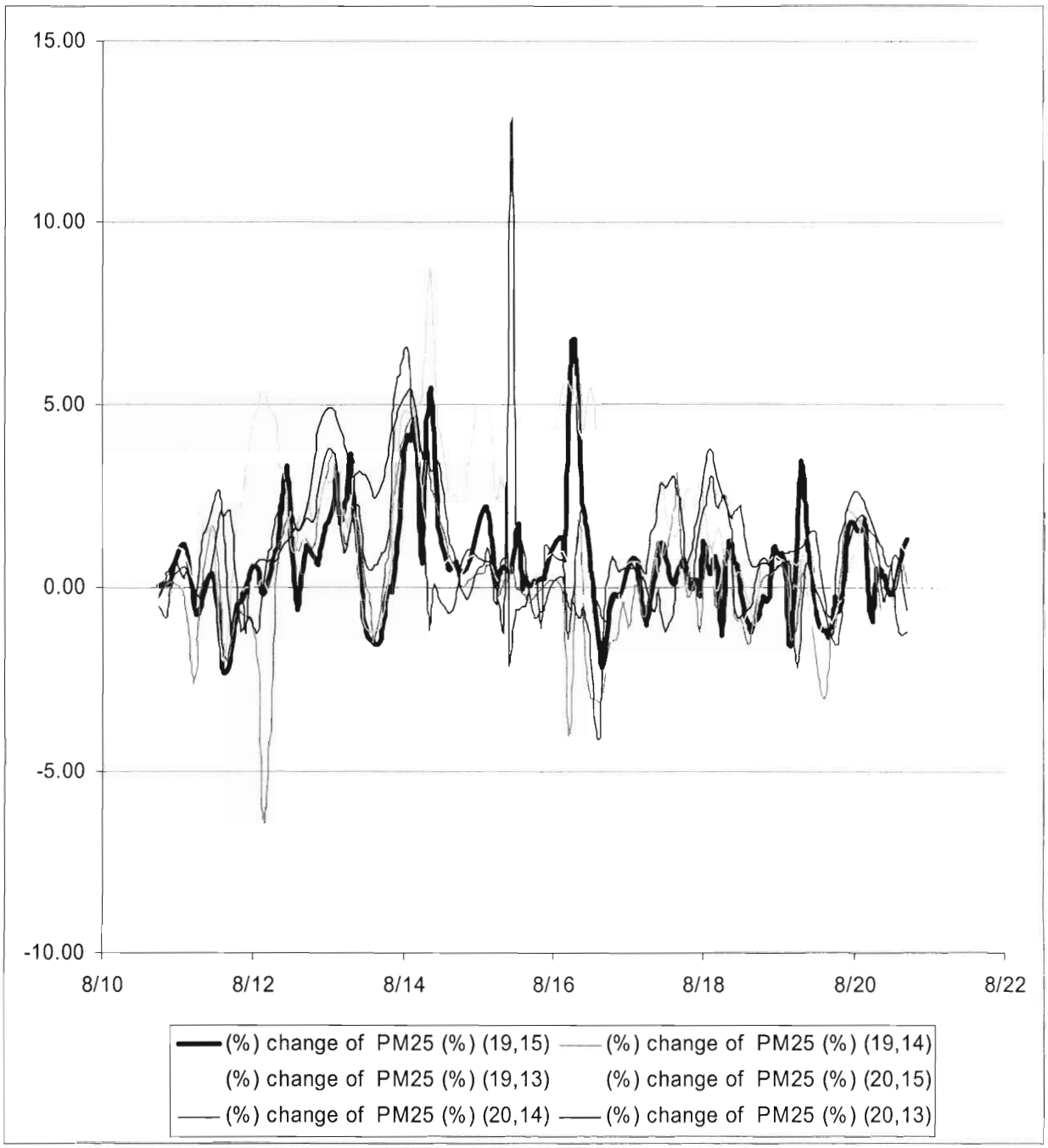

Figure 35. Changes (%) of PM 2.5 concentrations from the 2000 year to the 2007 year.

(a)

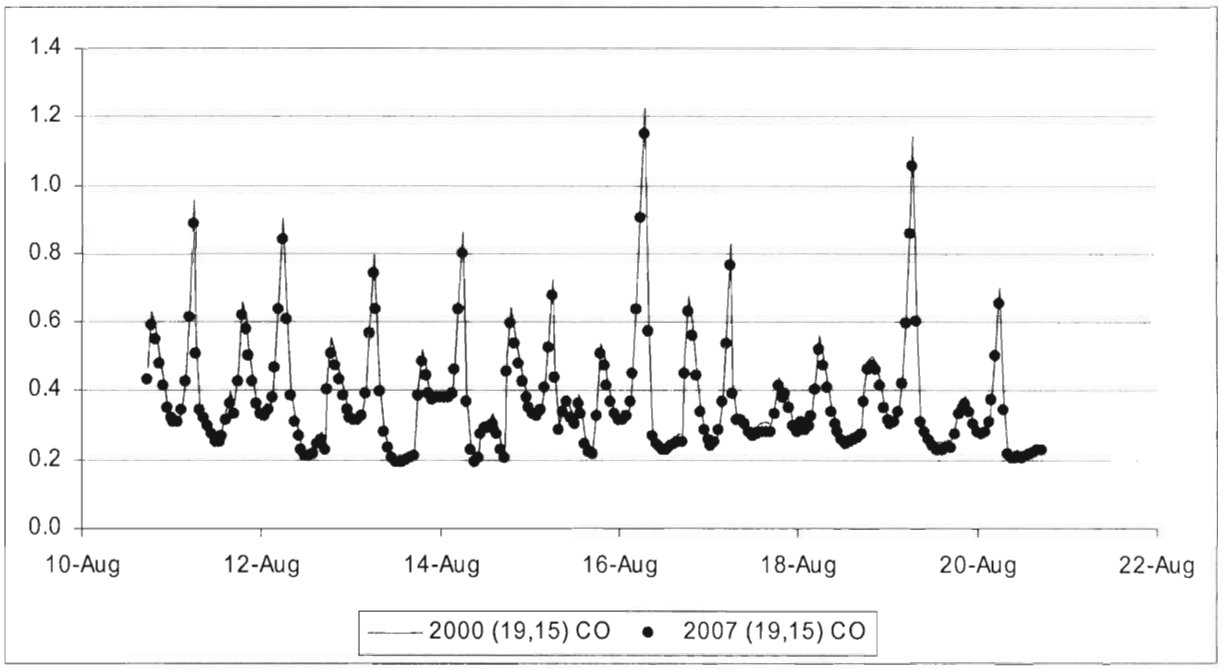

(b)

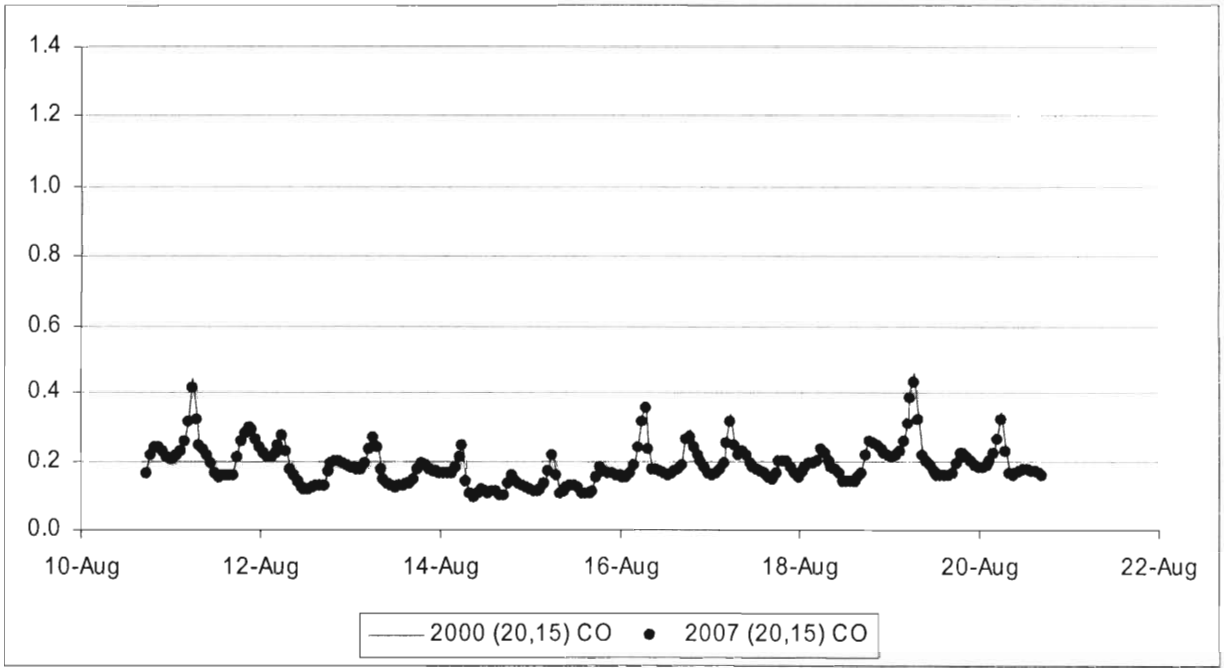

Figure 36. Comparison of the simulated hourly carbon monoxide concentrations in 2000 and in 2007. (a) is for the 19th column and the 15th row of grids and (b) is for the 20th column and the 15th row.

(c)

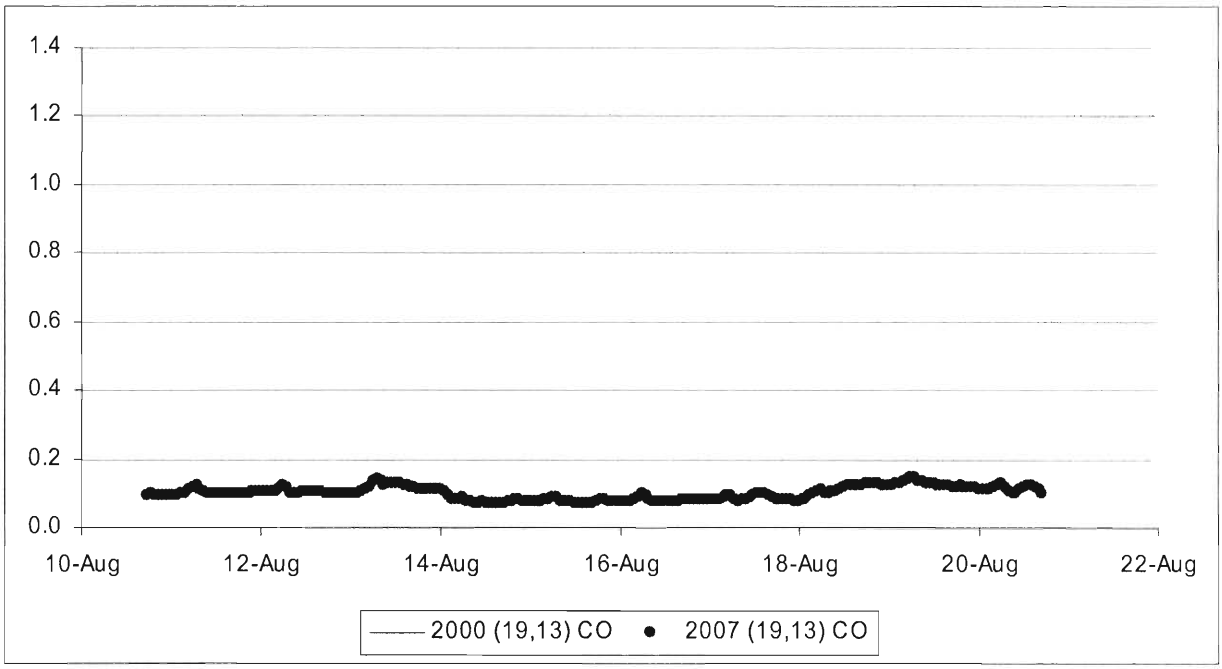

(d)

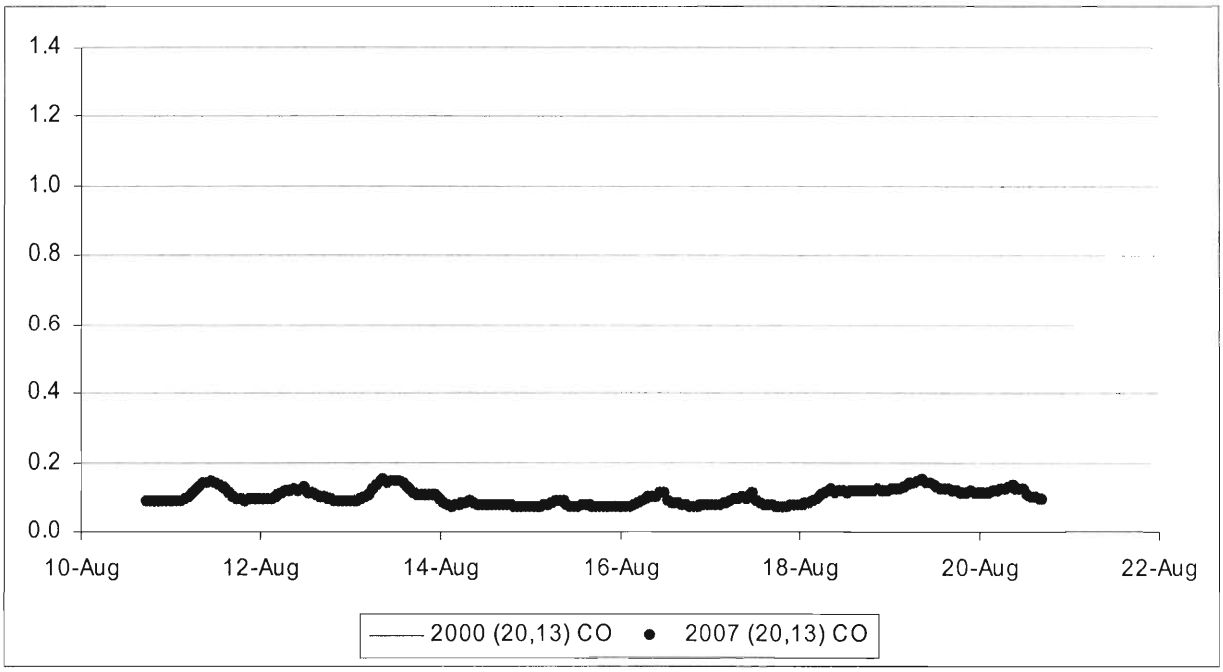

Figure 36. Continued. (e) is for the 19th column and the 13th row of grids and (f) is for the 20th column and the 13th row.

(e)

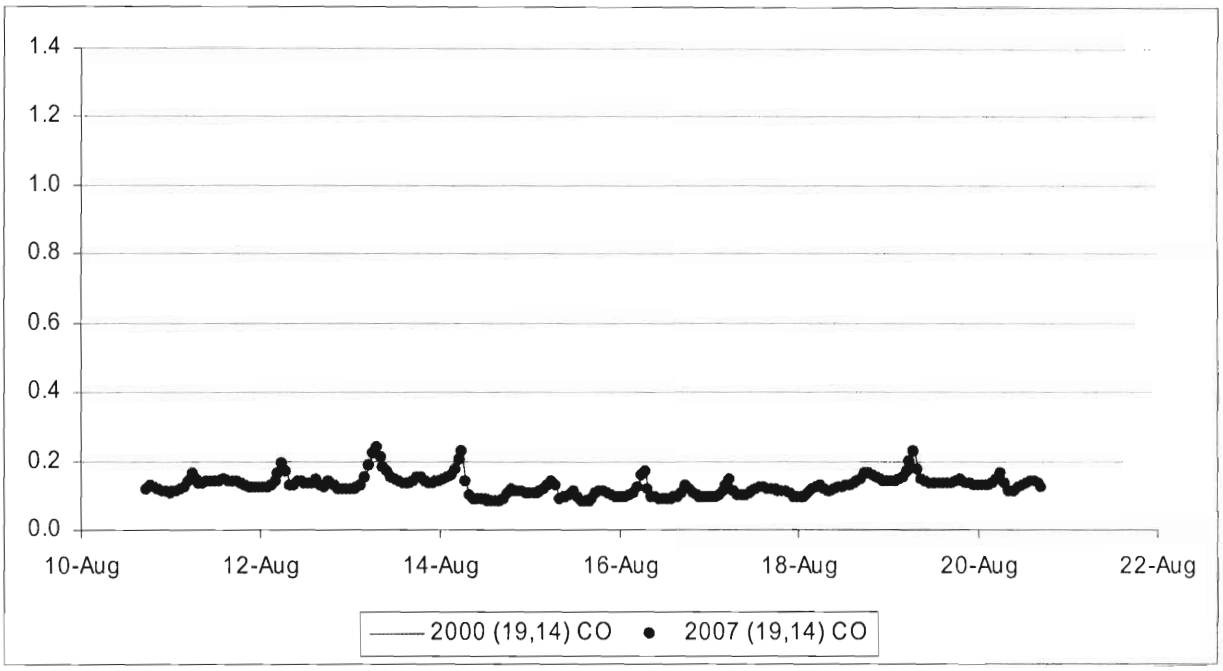

(f)

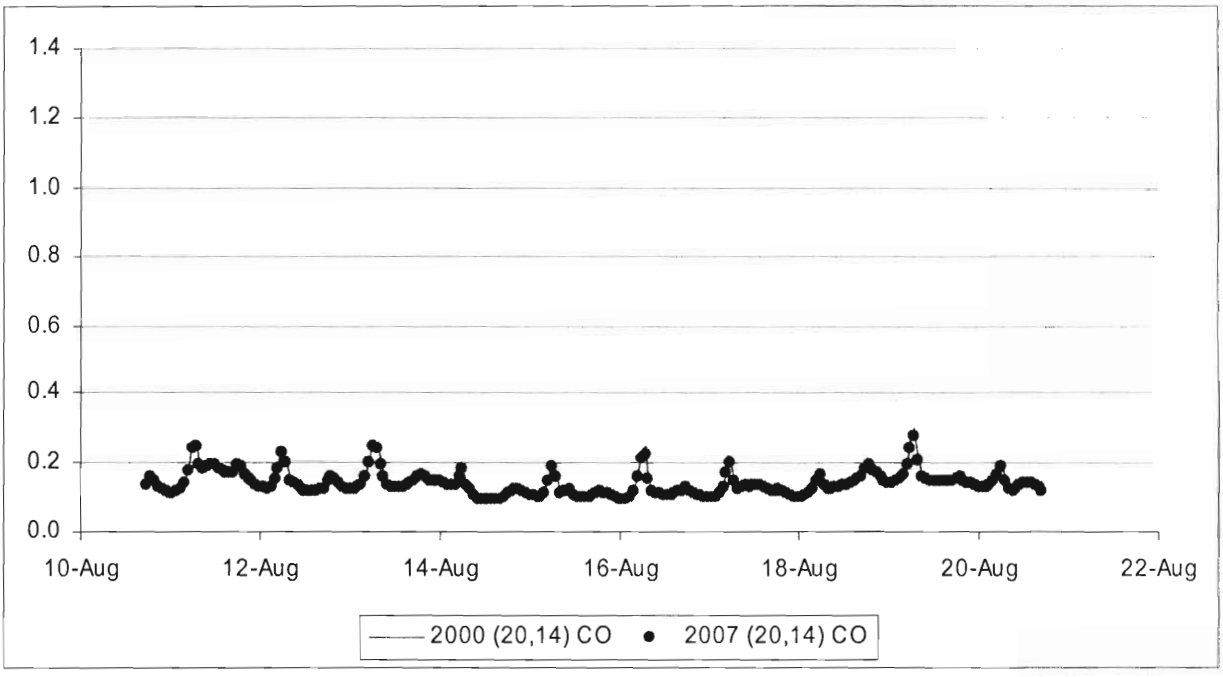

Figure 36. Continued. (c) is for the 19th column and the 14th row of grids and (d) is for the 20th column and the 14th row.

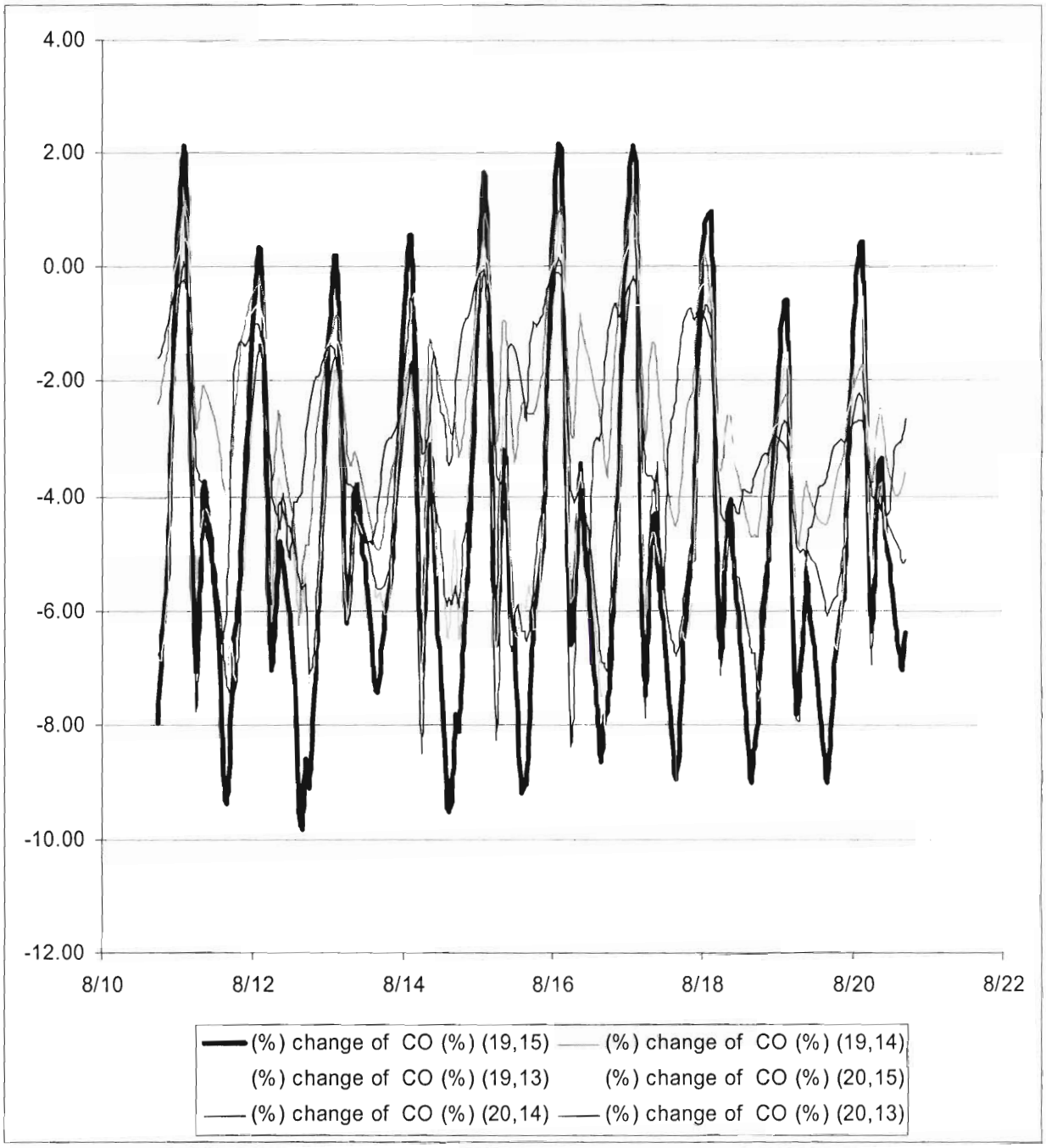

Figure 37. Changes (%) of carbon monoxide concentrations from the 2000 year to the 2007 year.

(a)

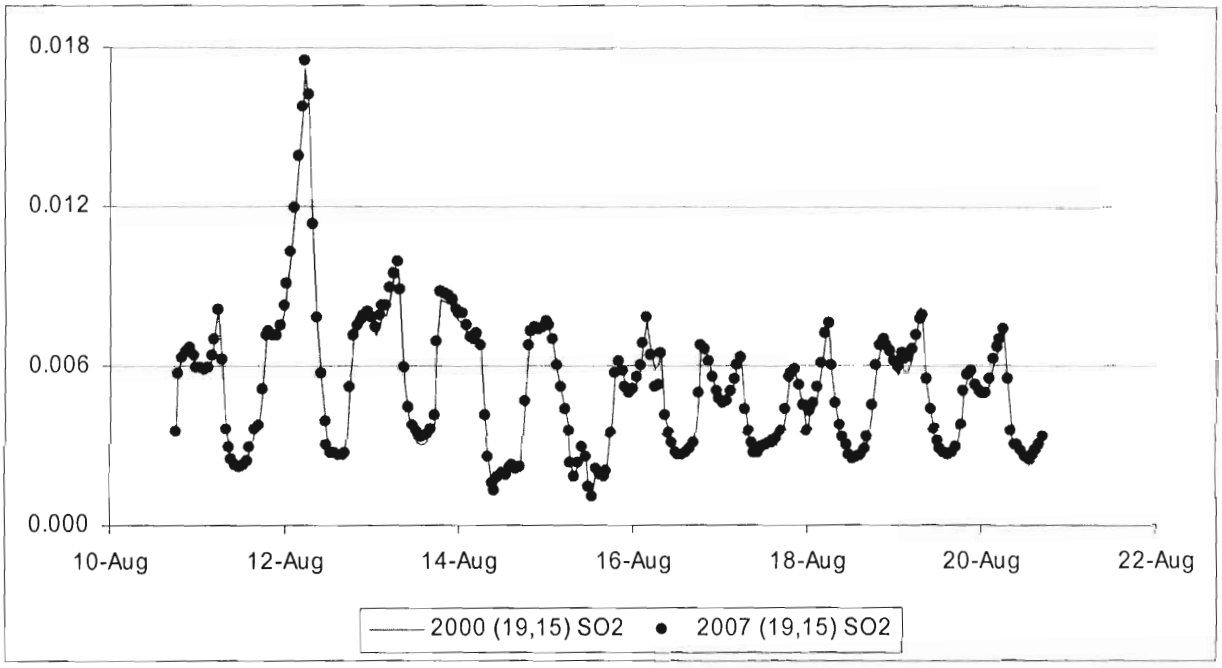

(b)

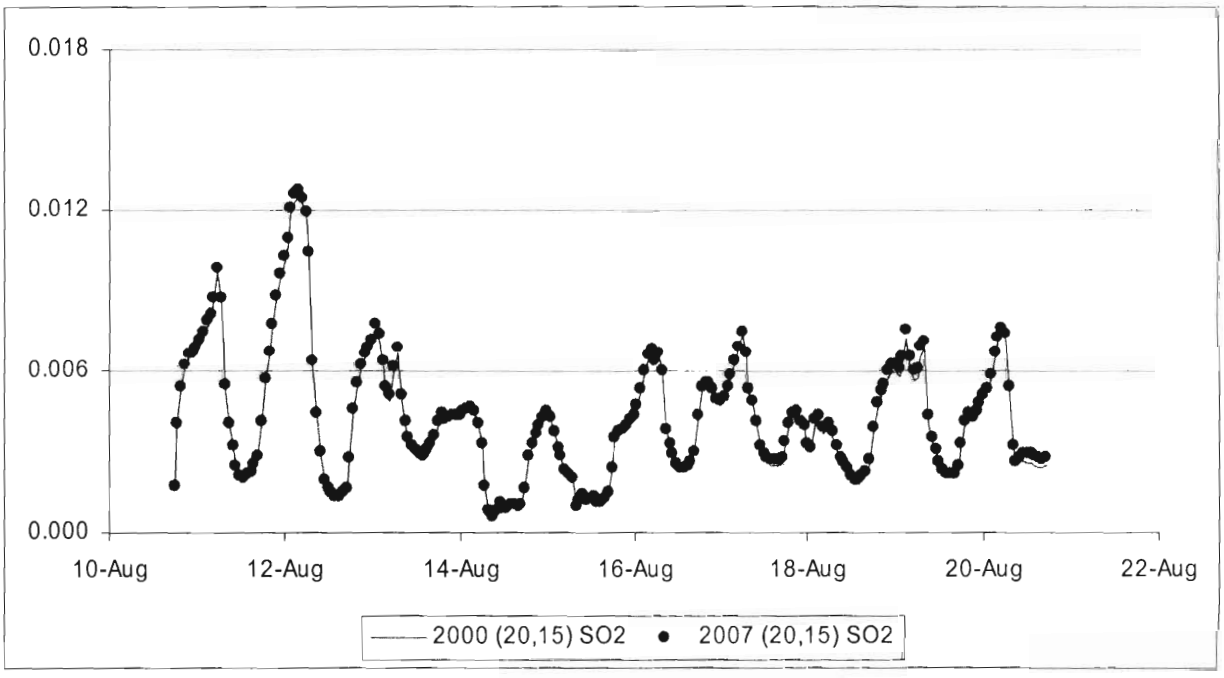

Figure 38. Comparison of the simulated hourly sulfur dioxide concentrations in 2000 and in 2007. (a) is for the 19th column and the 15th row of grids and (b) is for the 20th column and the 15th row.

(c)

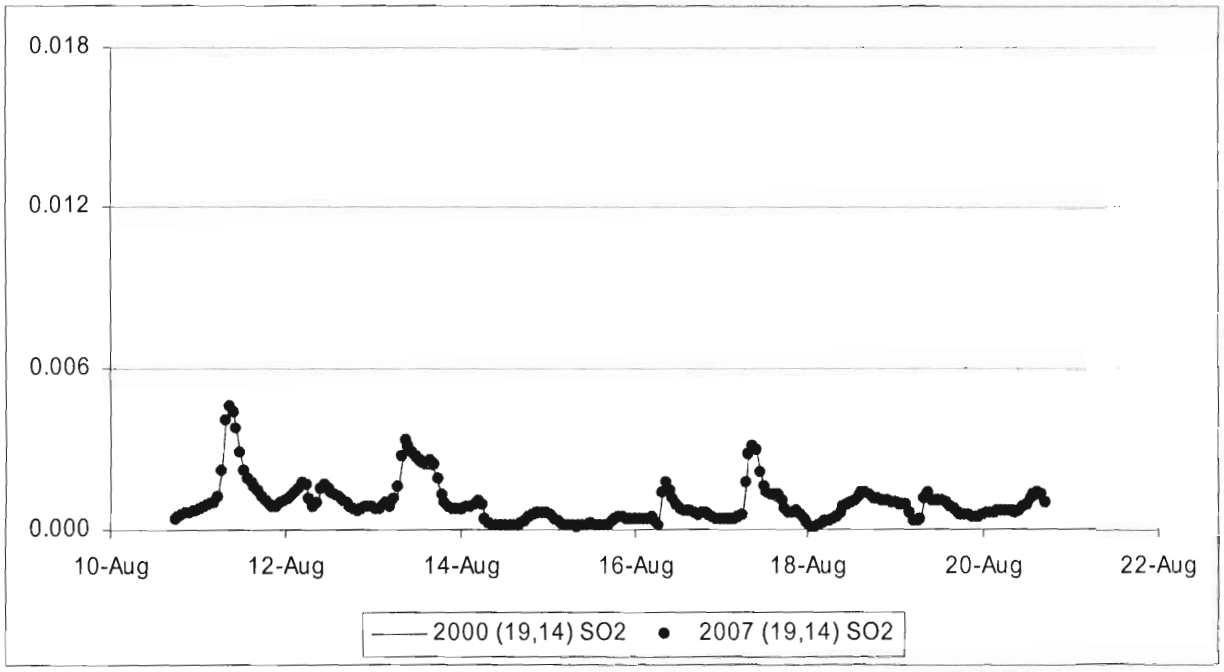

(d)

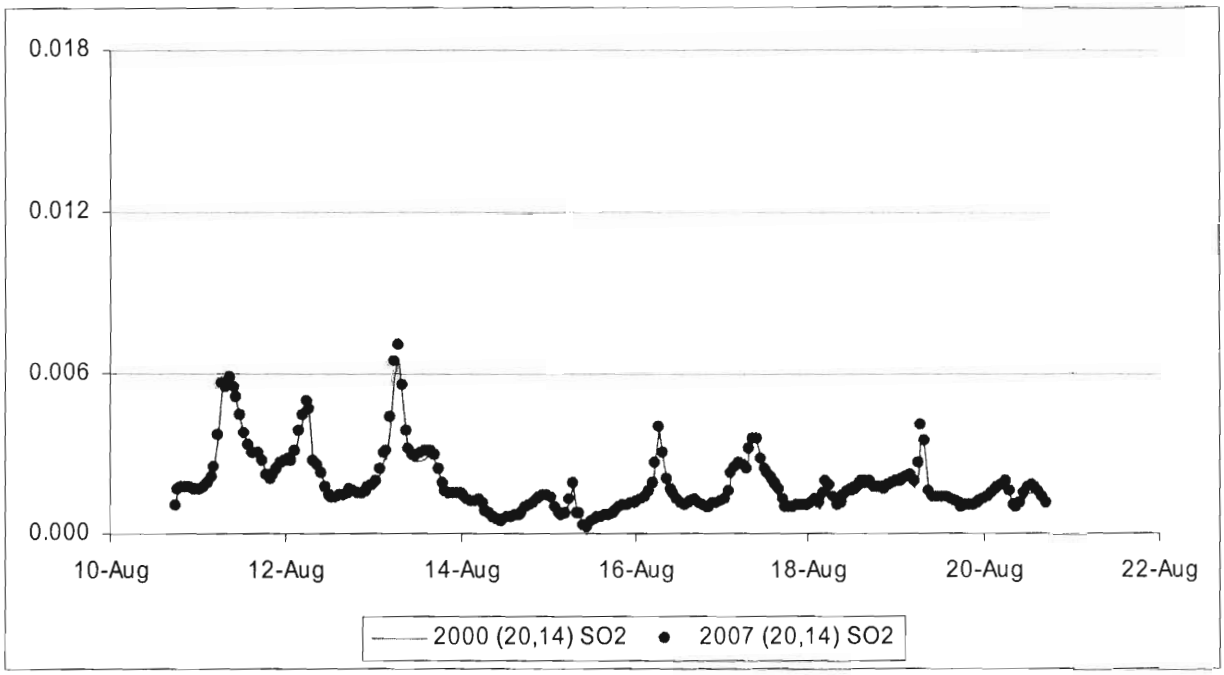

Figure 38. Continued. (c) is for the 19th column and the 14th row of grids and (d) is for the 20th column and the 14th row.

(e)

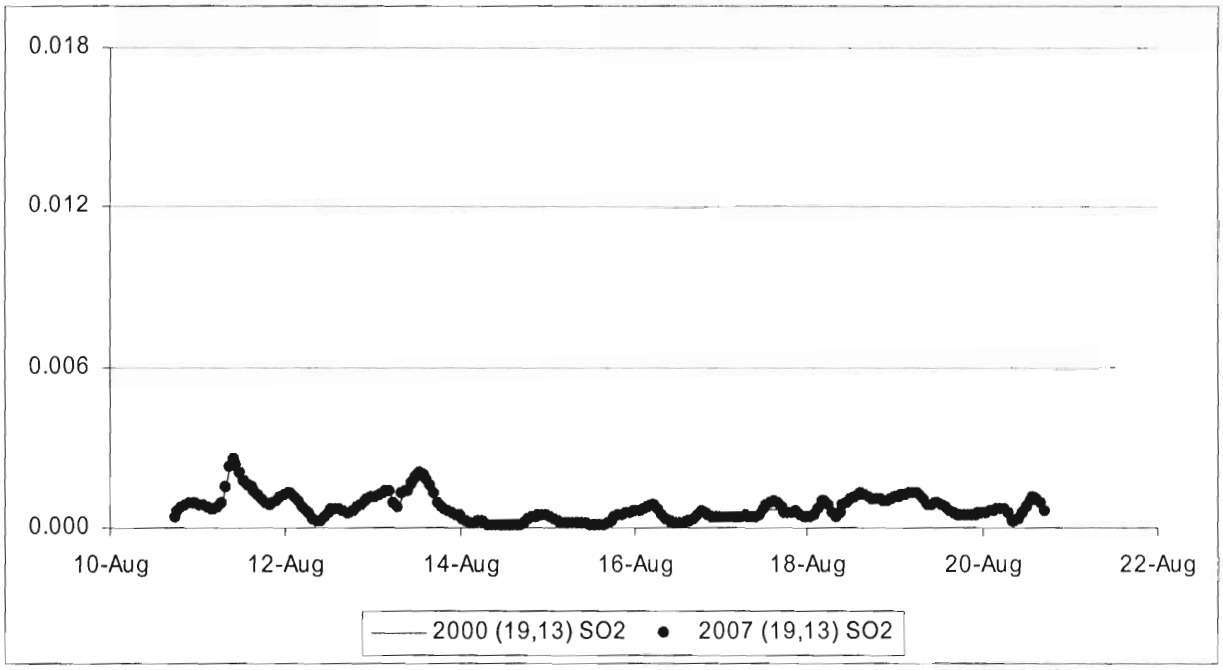

(f)

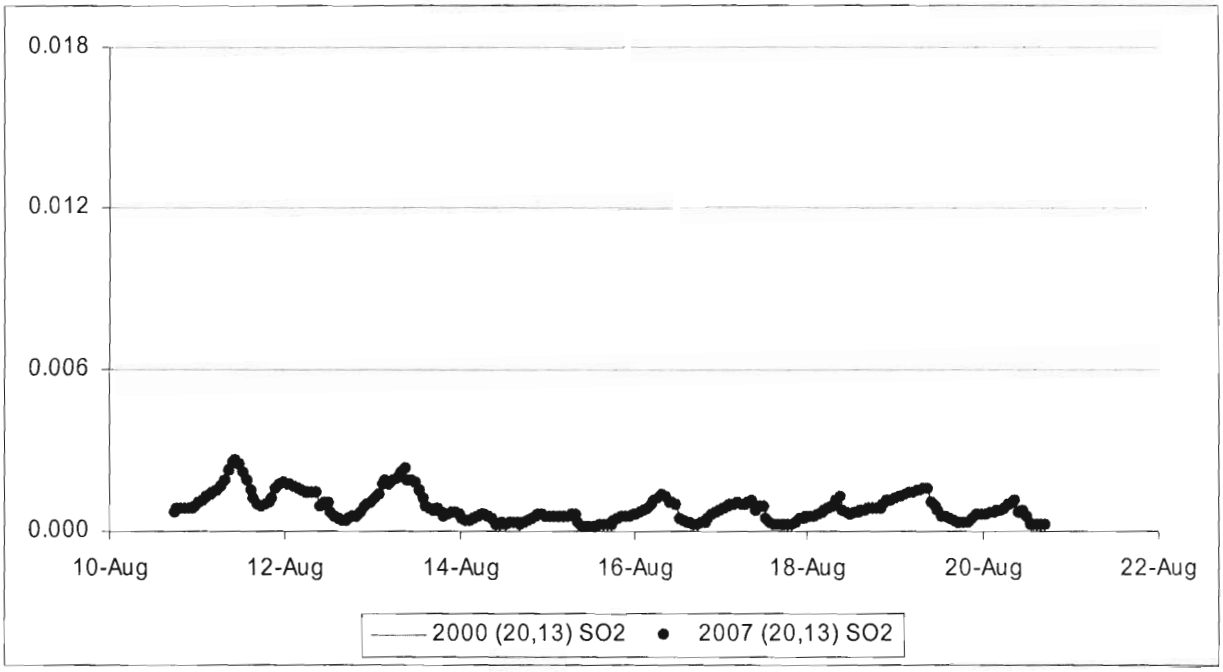

Figure 38. Continued. (e) is for the 19th column and the 13th row of grids and (f) is for the 20th column and the 13th row.

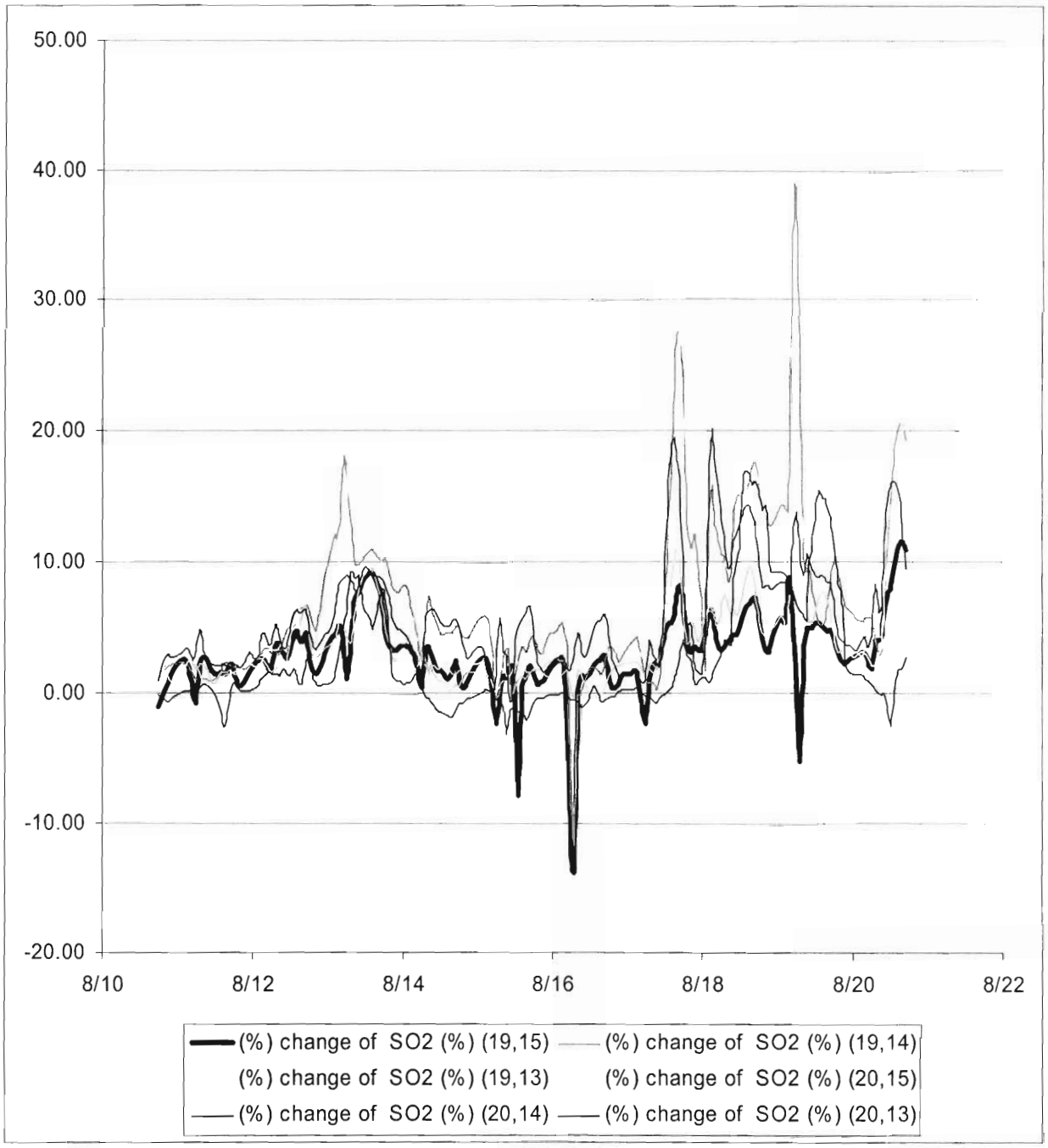

Figure 39. Changes (%) of sulfur dioxide concentrations from the 2000 year to the 2007 year.

(a)

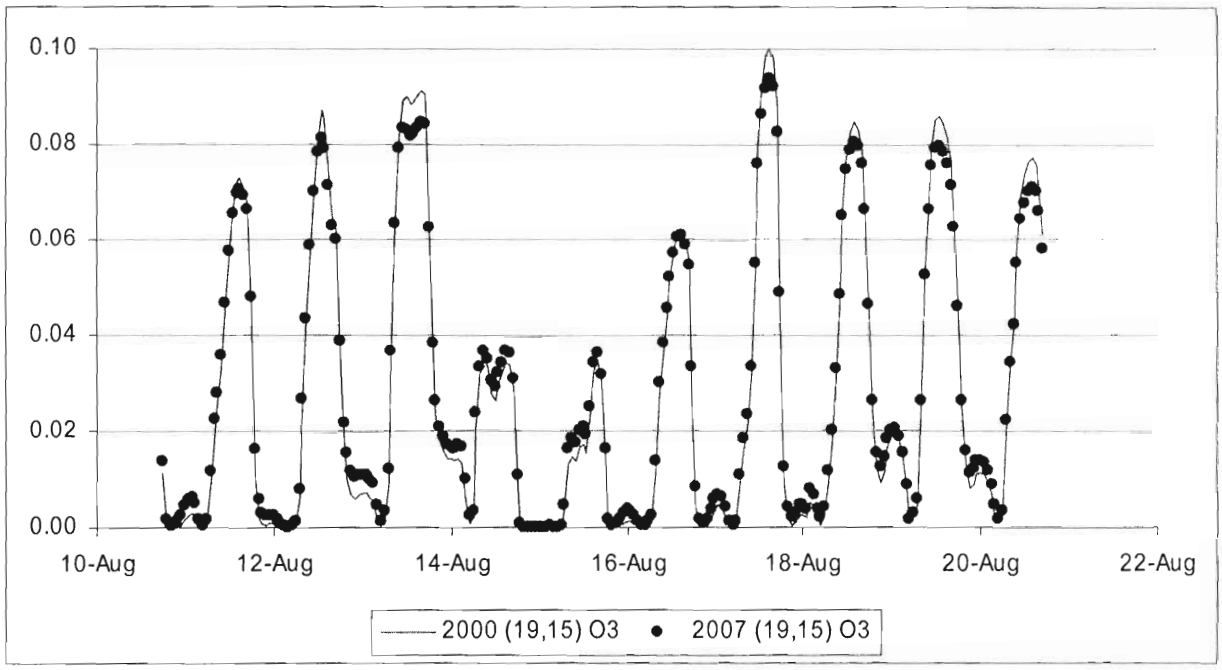

(b)

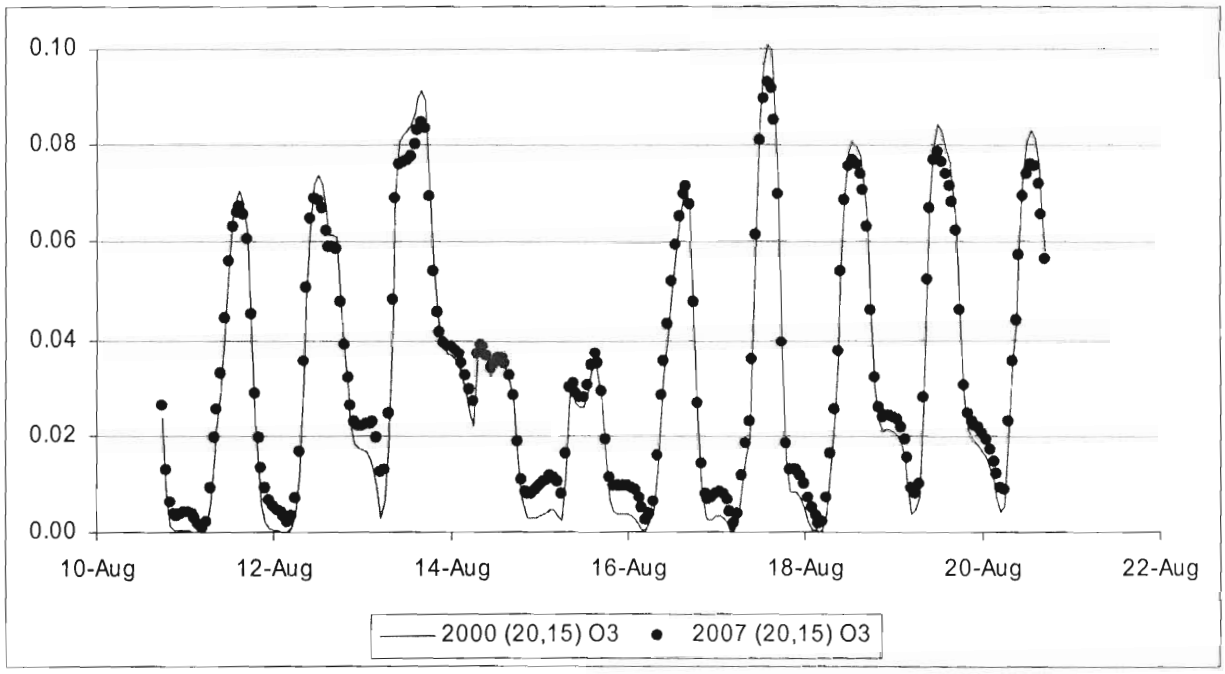

Figure 40. Comparison of the simulated hourly ozone concentrations in 2000 and in 2007. (a) is for the 19th column and the 15th row of grids and (b) is for the 20th column and the 15th row.

(c)

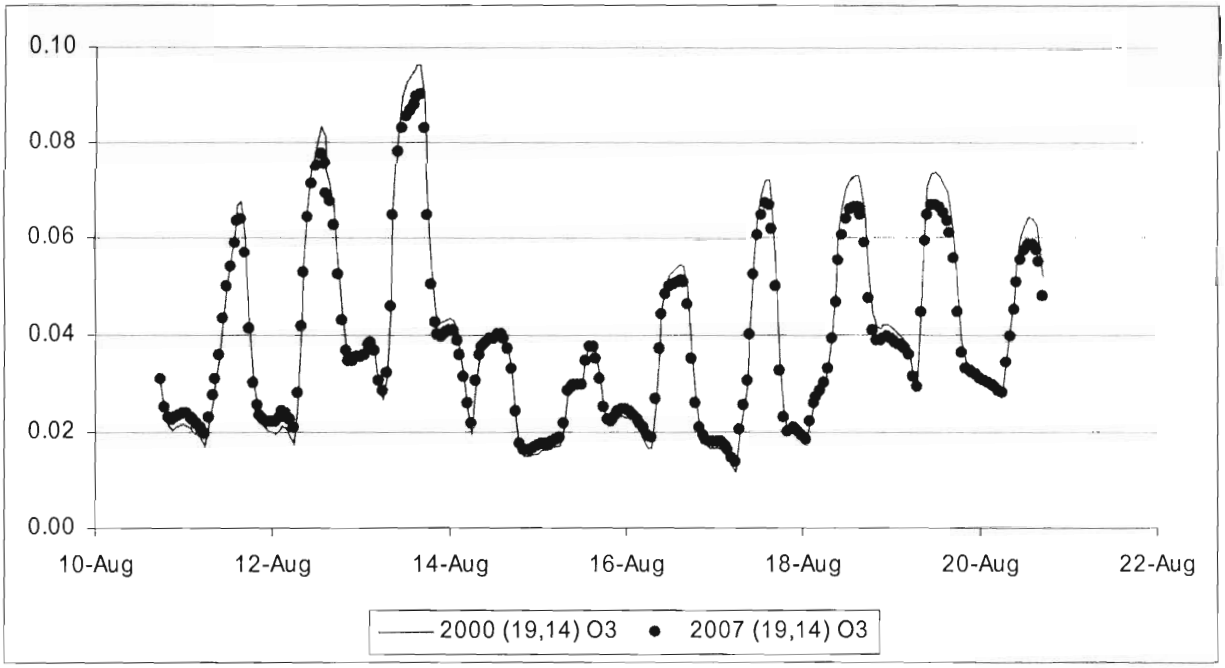

(d)

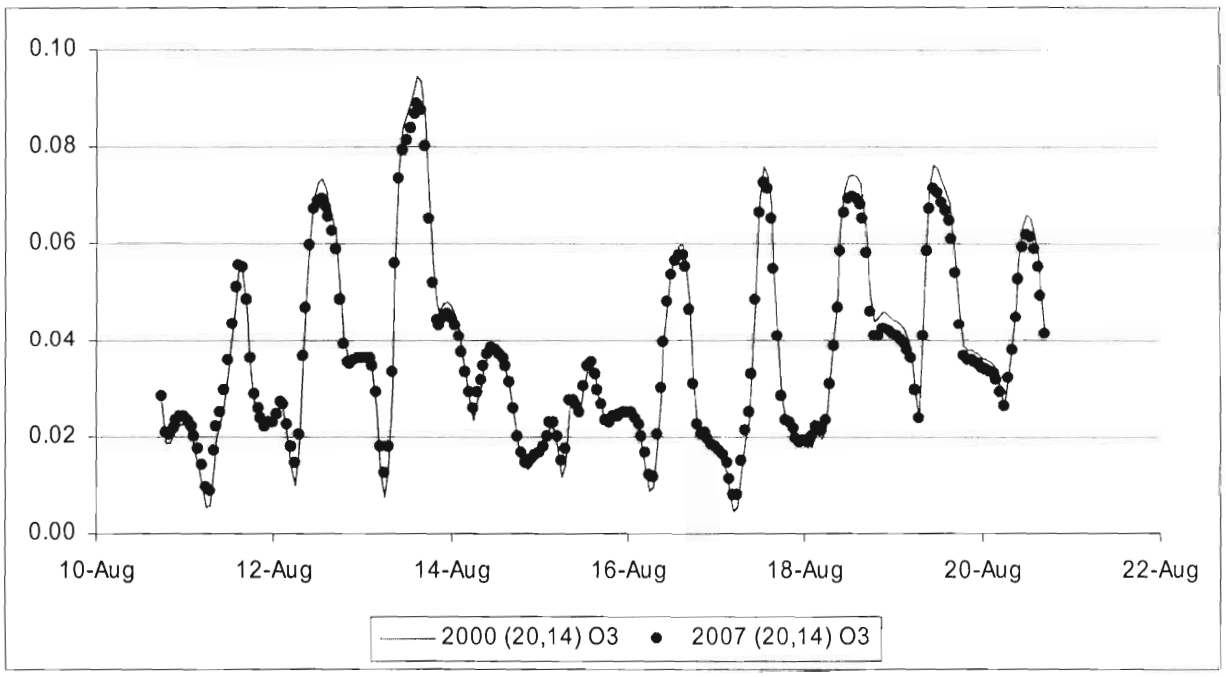

Figure 40. Continued. (c) is for the 19th column and the 14th row of grids and (d) is for the 20th column and the 14th row.

(e)

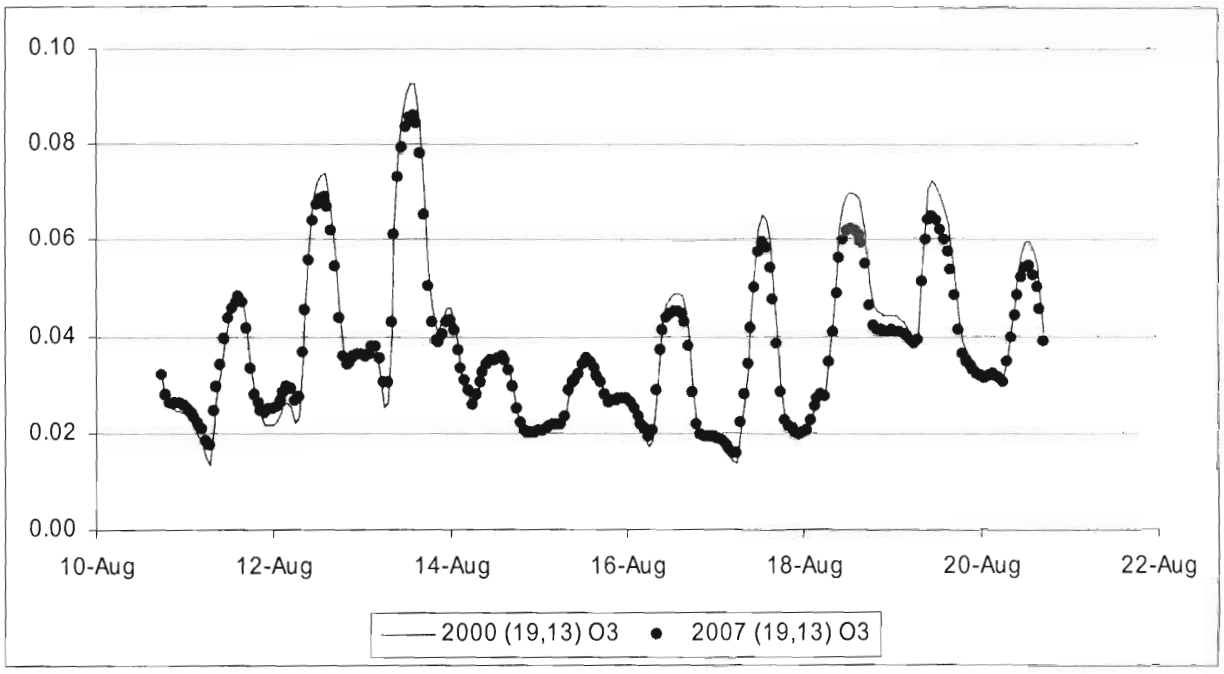

(f)

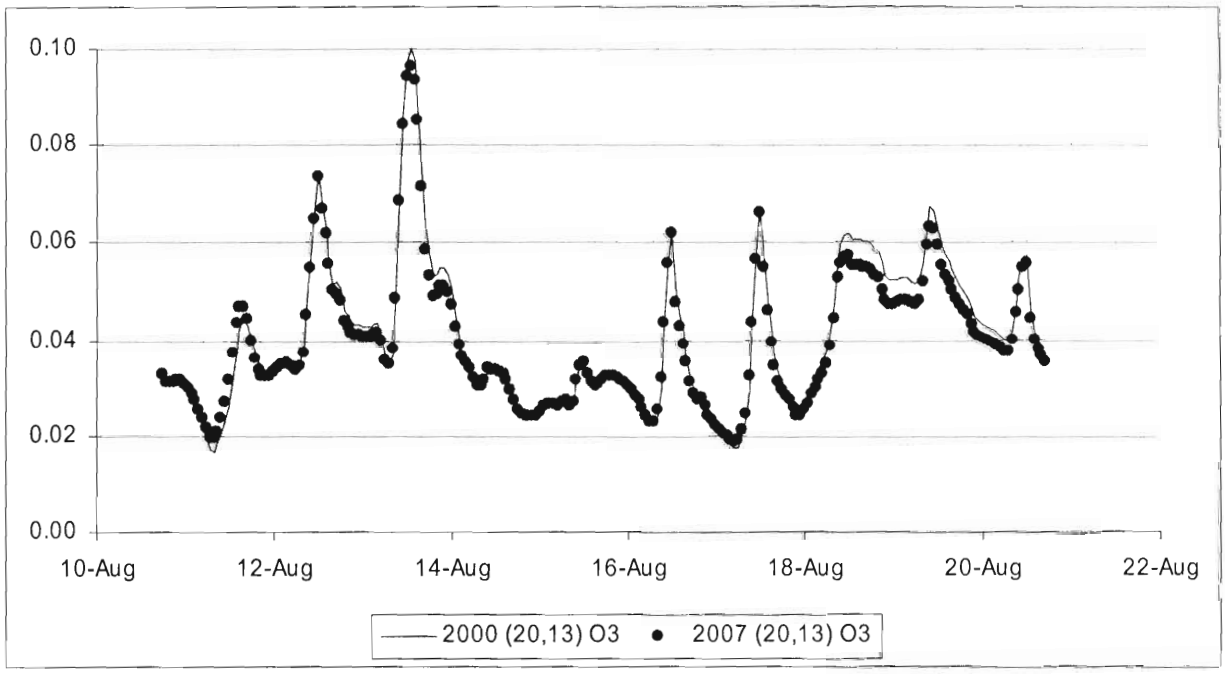

Figure 40. Continued. (e) is for the 19th column and the 13th row of grids and (f) is for the 20th column and the 13th row.

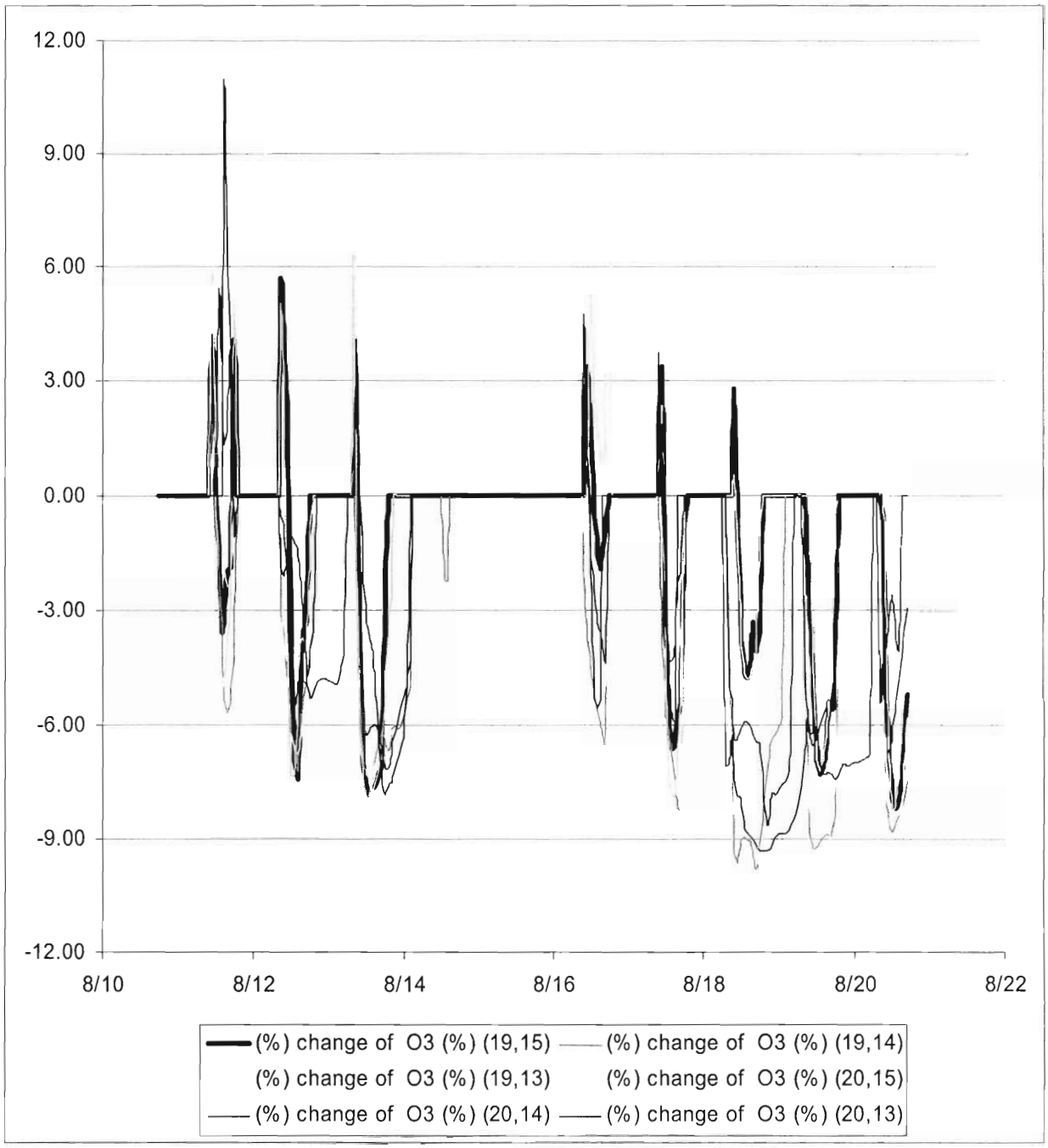

Figure 41. Changes (%) of ozone concentrations from the 2000 year to the 2007 year when ozone concentrations in 2000 were higher than 40 ppb.

(a)

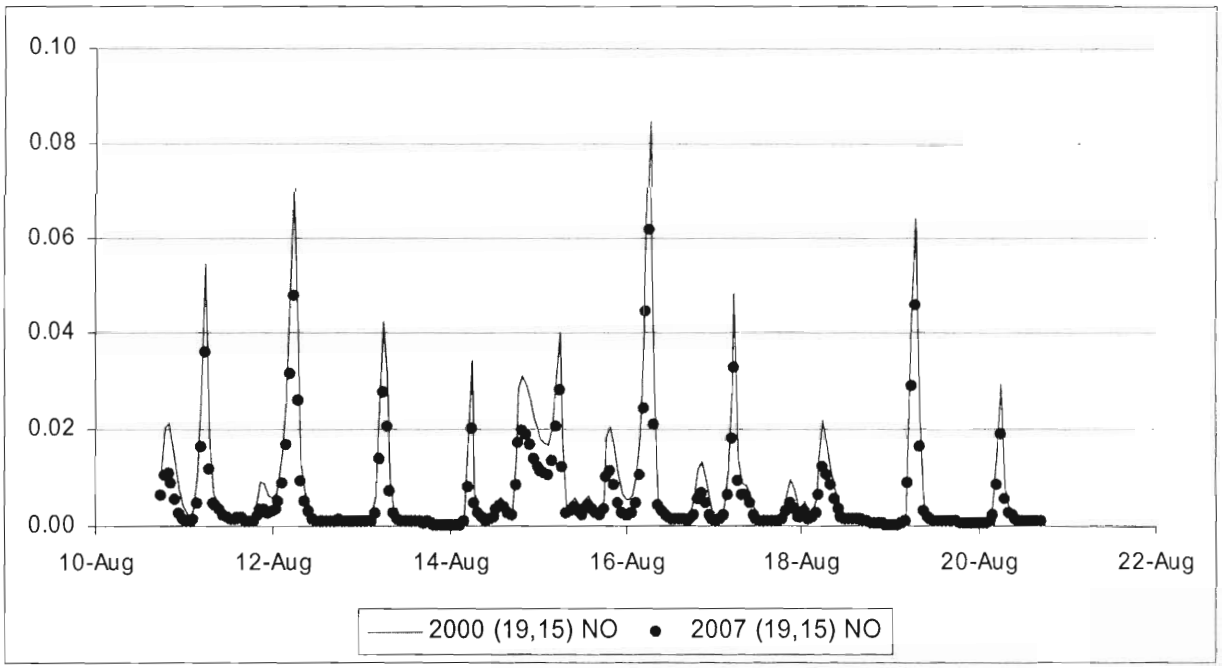

(b)

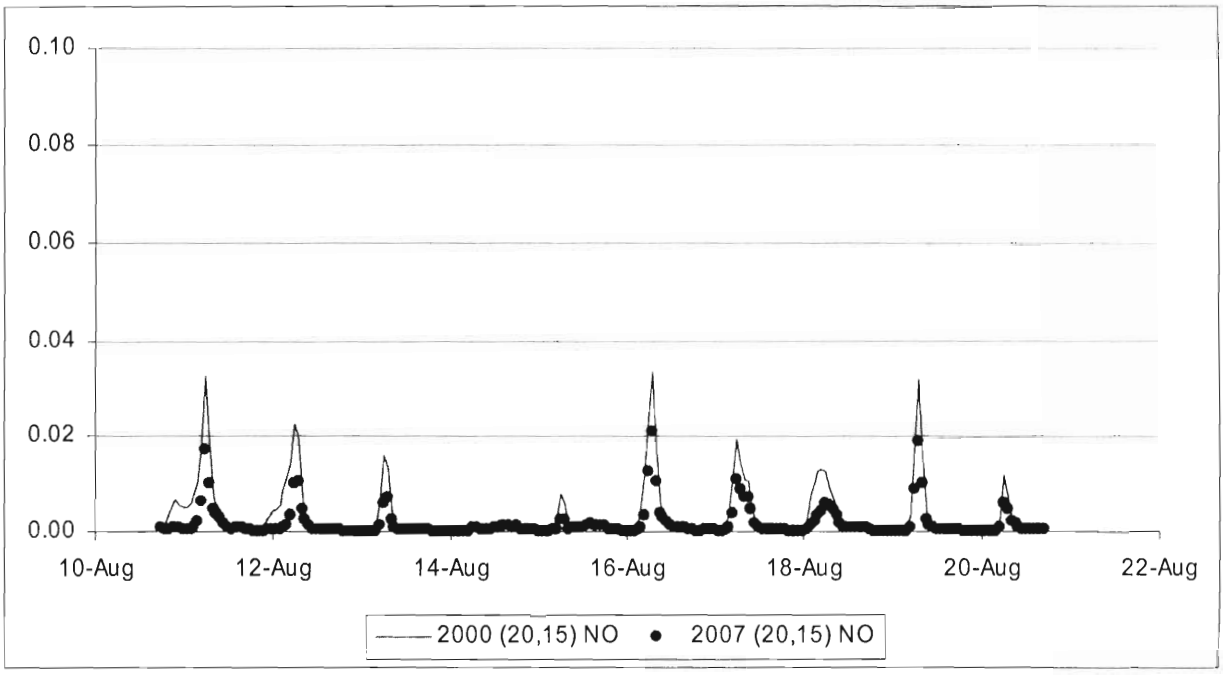

Figure 42. Comparison of the simulated hourly nitric oxide concentrations in 2000 and in 2007. (a) is for the 19th column and the 15th row of grids and (b) is for the 20th column and the 15th row.

(c)

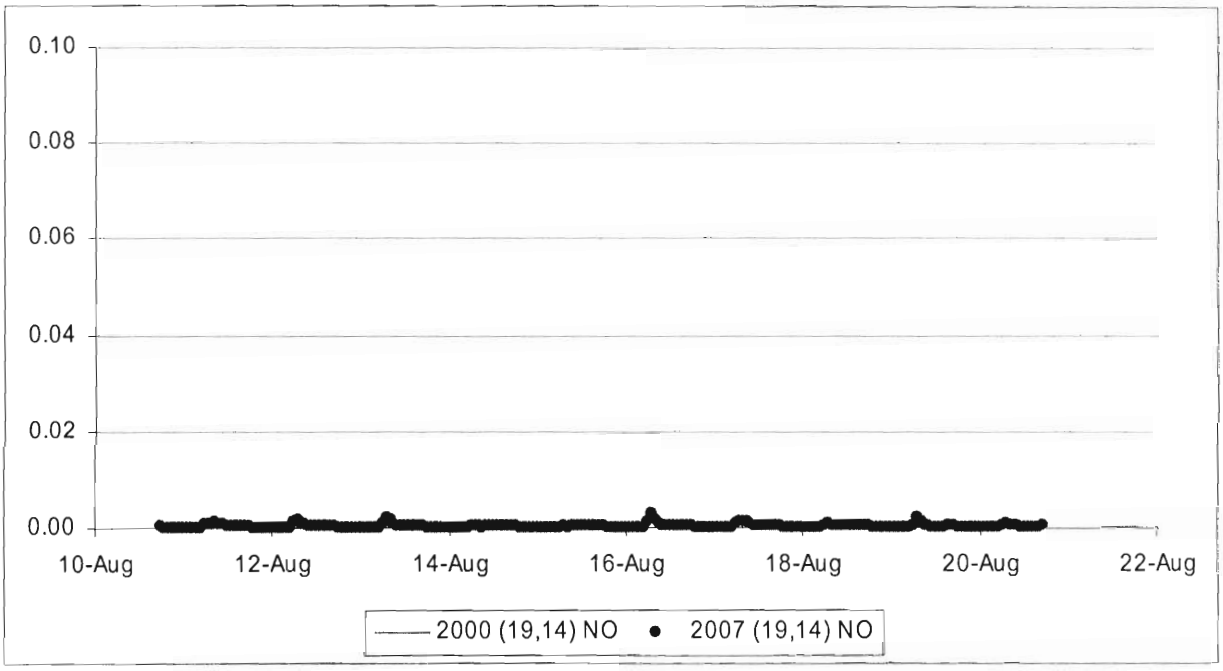

(d)

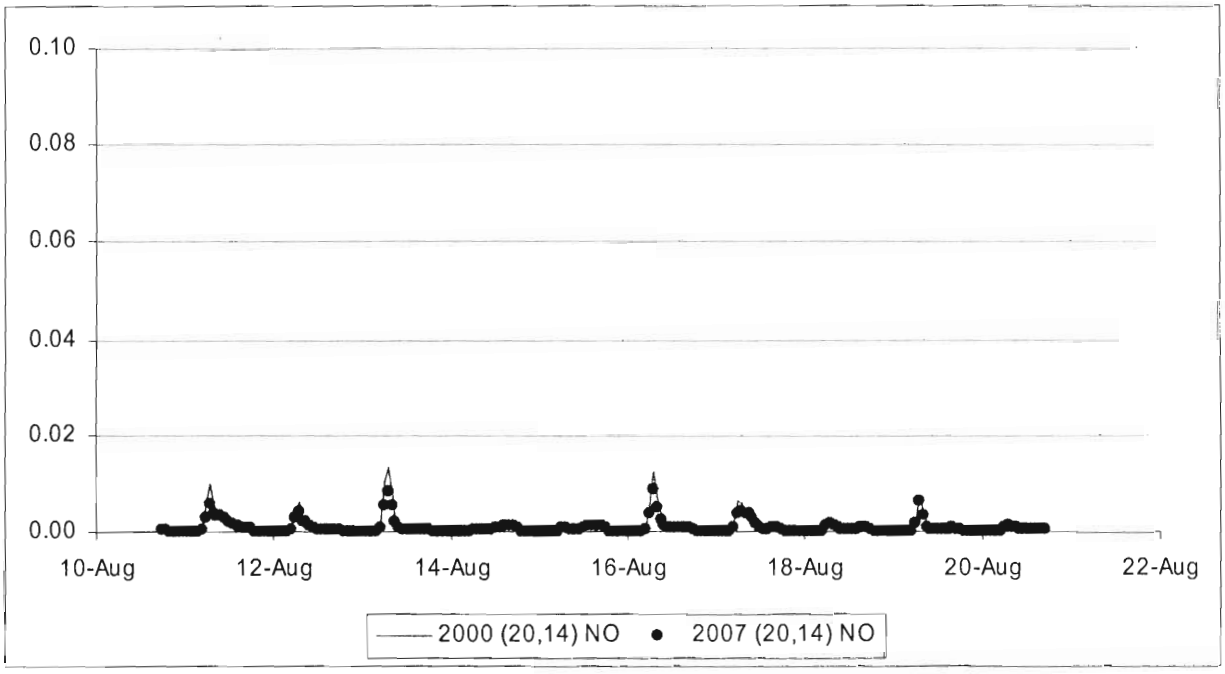

Figure 42. Continued. (c) is for the 19th column and the 14th row of grids and (d) is for the 20th column and the 14th row.

(e)

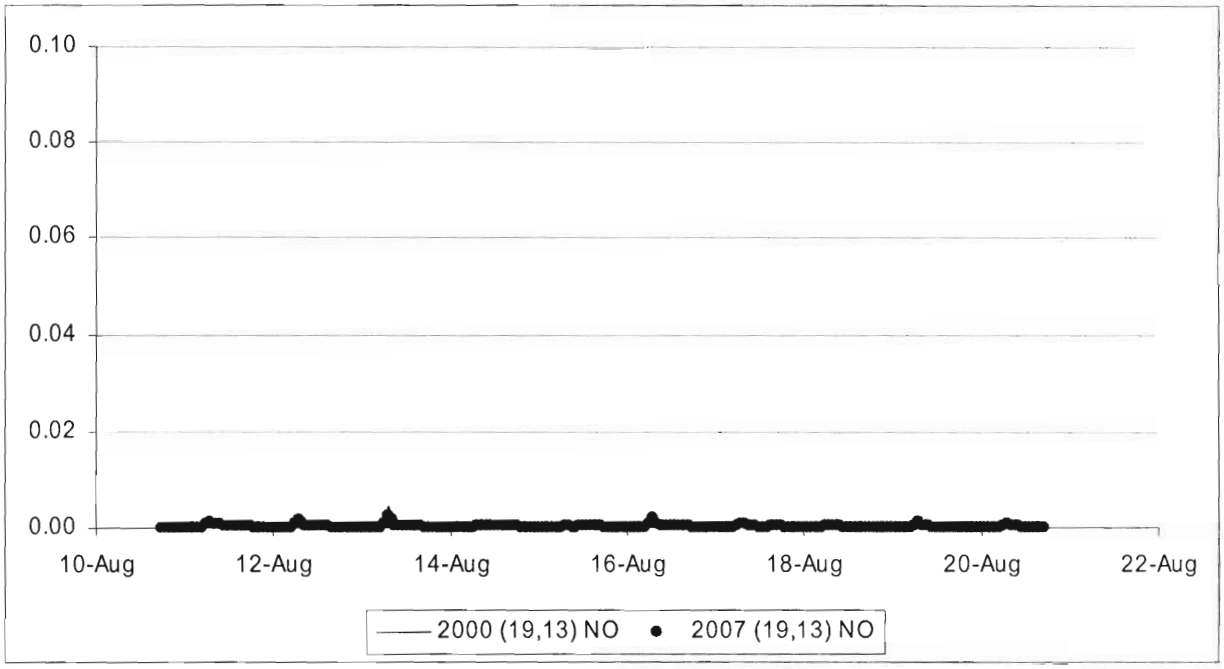

(f)

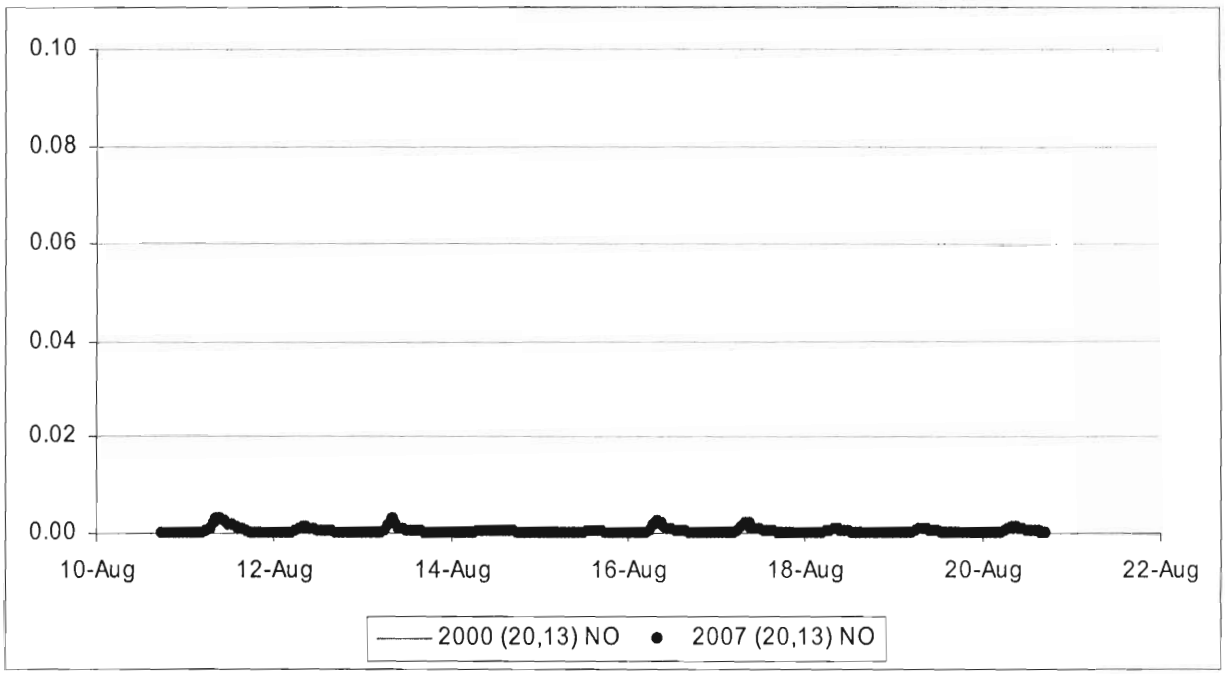

Figure 42. Continued. (e) is for the 19th column and the 13th row of grids and (f) is for the 20th column and the 13th row.

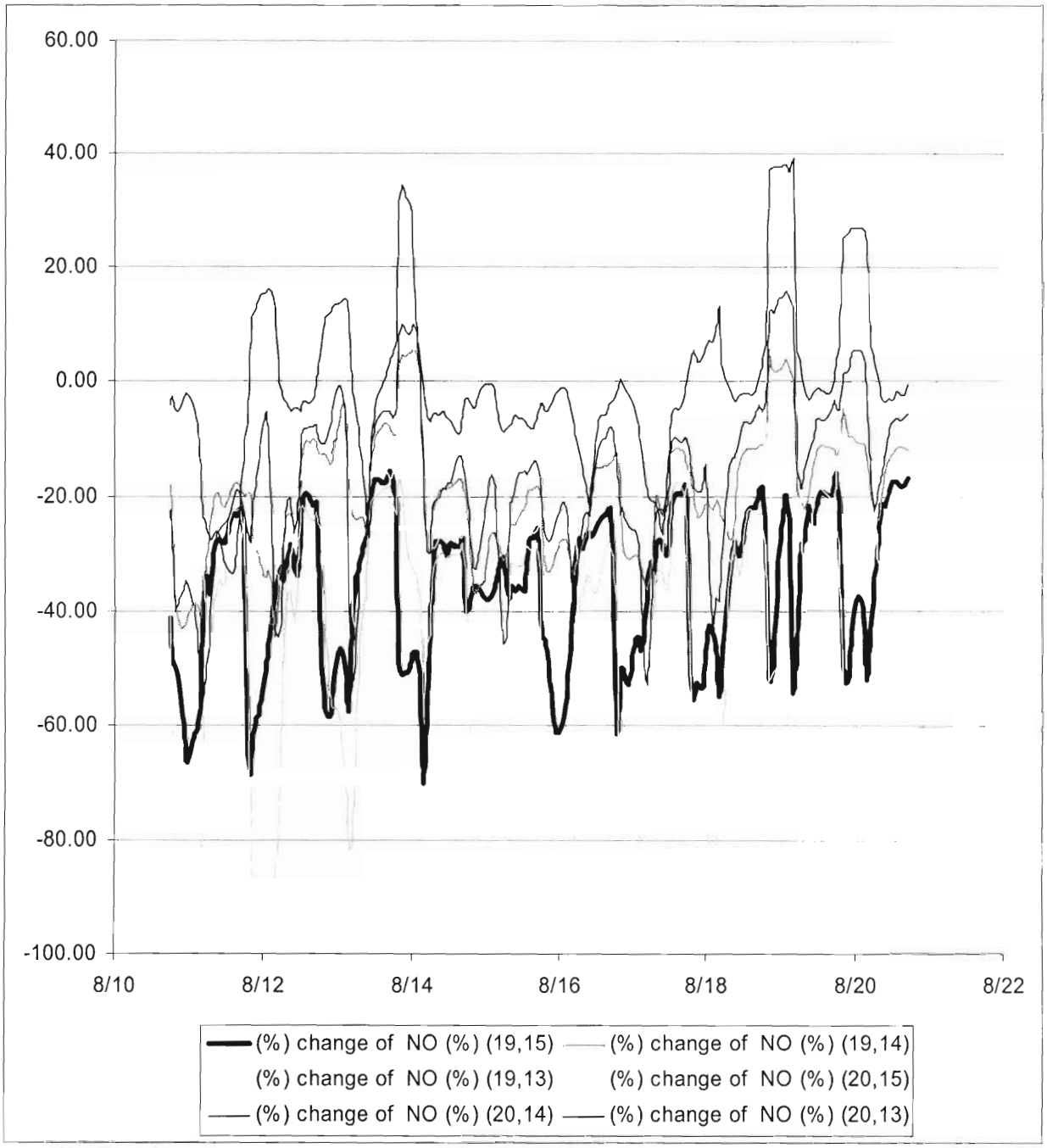

Figure 43. Changes (%) of nitric oxide concentrations from the 2000 year to the 2007 year.

(a)

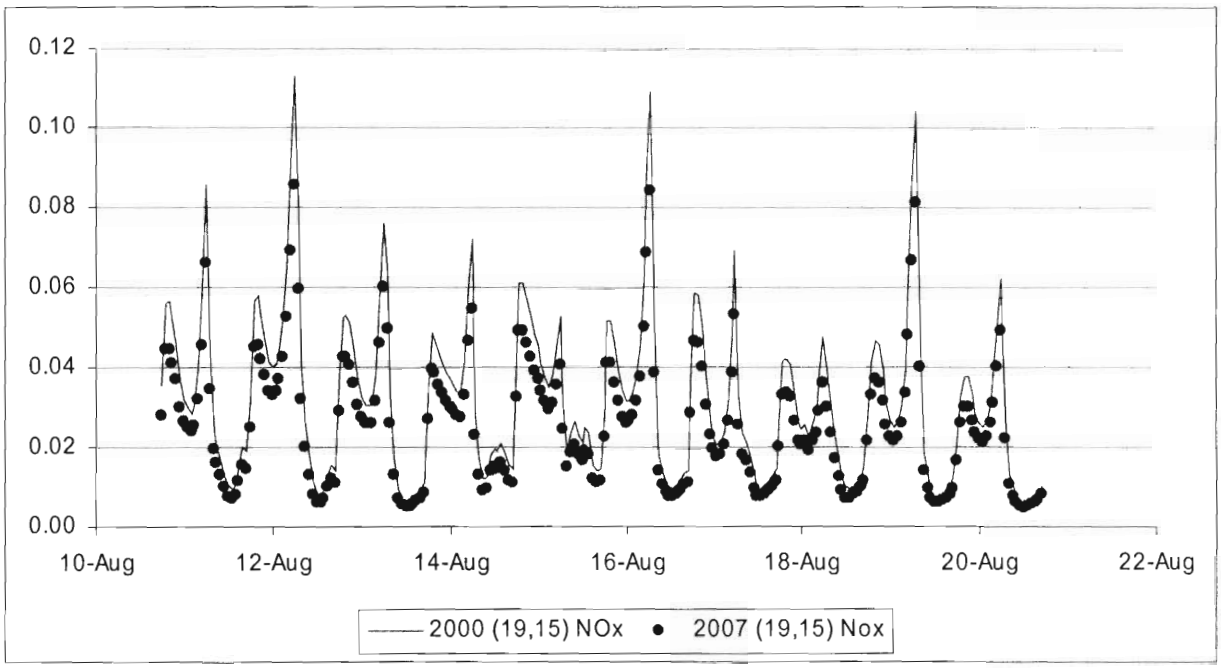

(b)

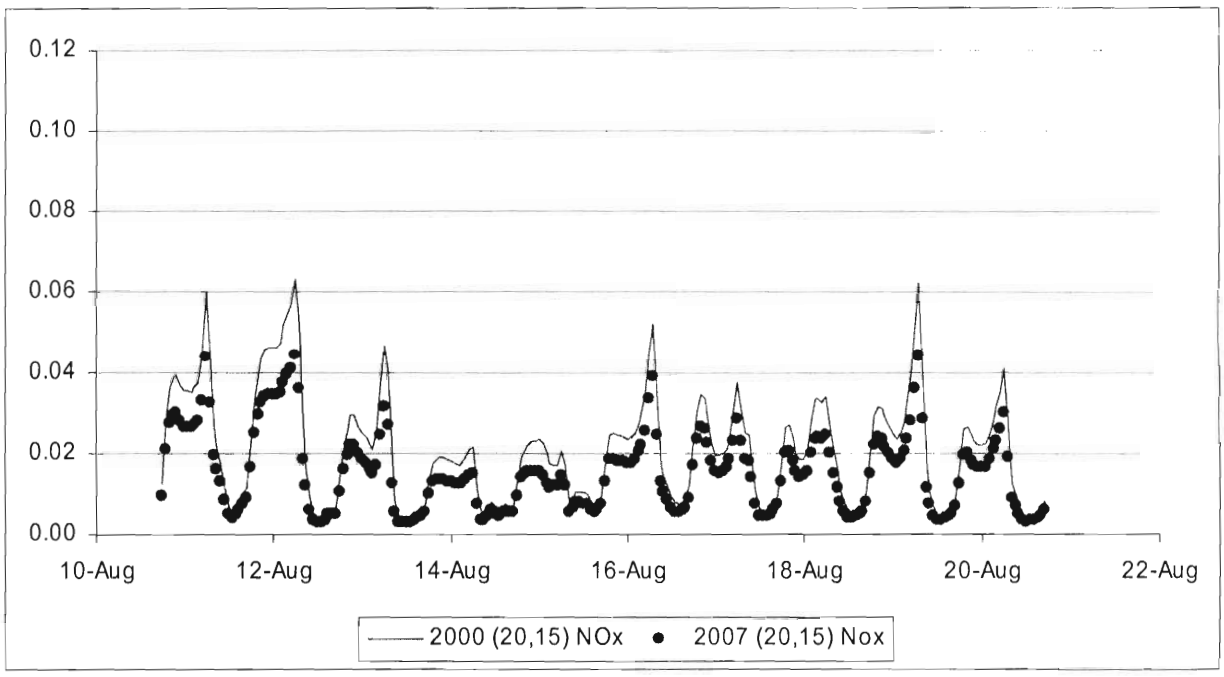

Figure 44. Comparison of the simulated hourly NOx concentrations in 2000 and in 2007. (a) is for the 19th column and the 15th row of grids and (b) is for the 20th column and the 15th row.

(c)

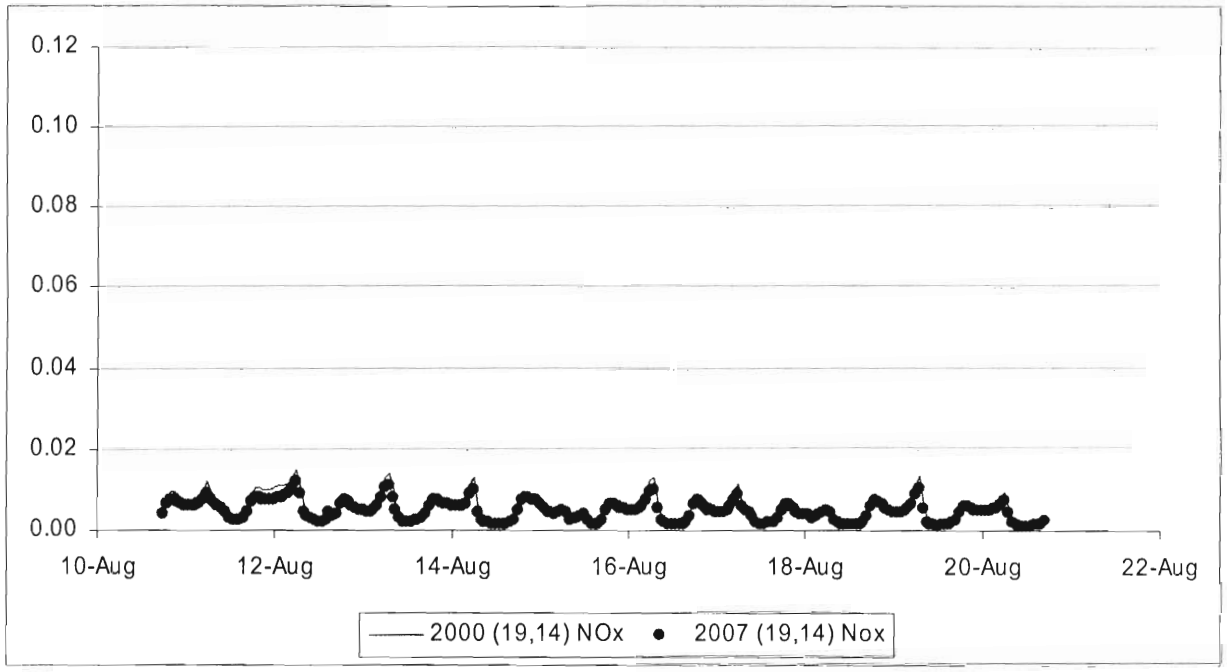

(d)

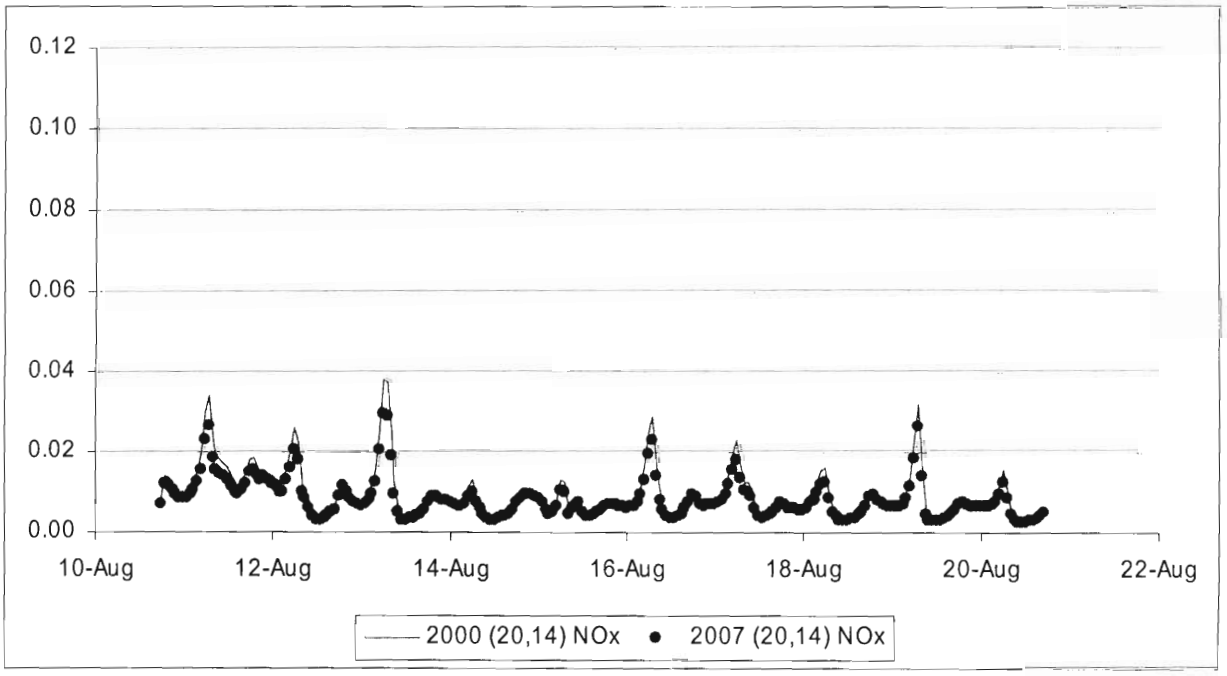

Figure 44. Continued. (c) is for the 19th column and the 14th row of grids and (d) is for the 20th column and the 14th row.

(e)

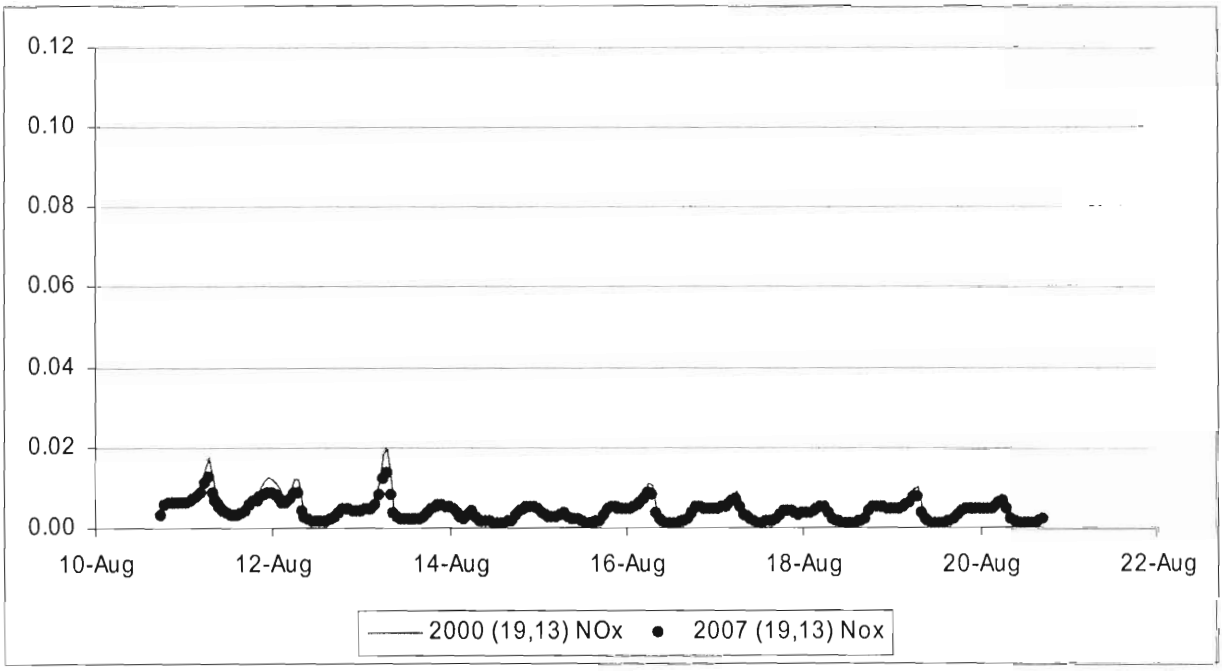

(f)

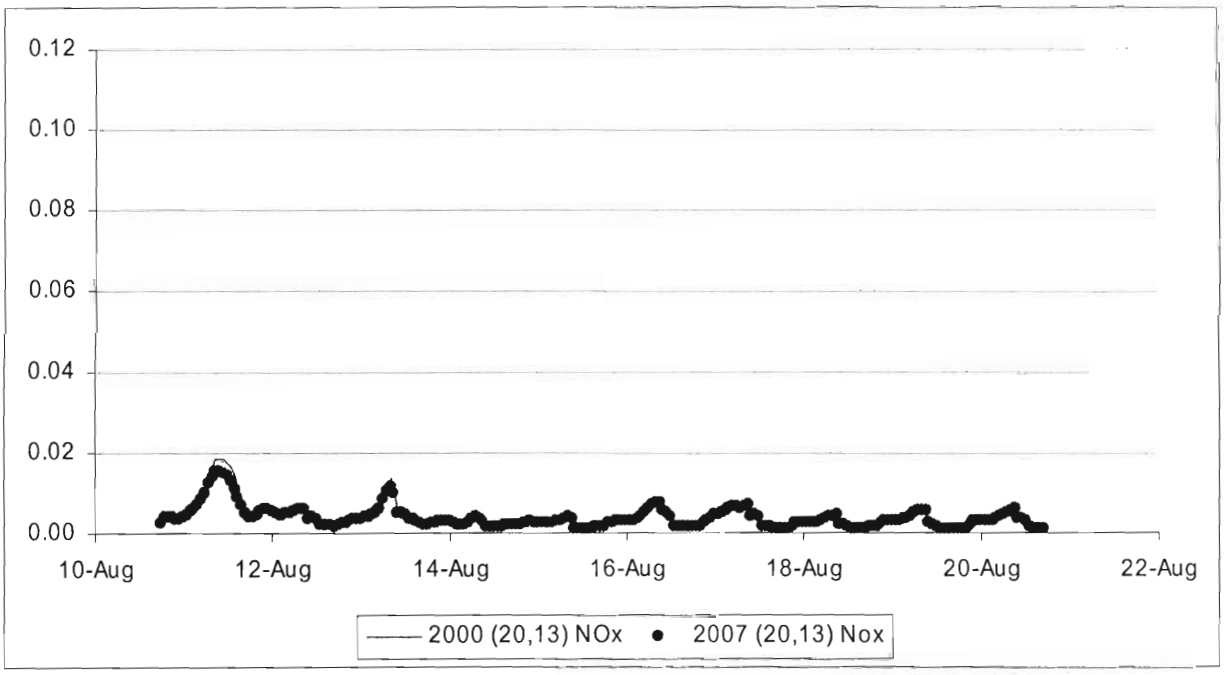

Figure 44. Continued. (e) is for the 19th column and the 13th row of grids and (f) is for the 20th column and the 13th row.

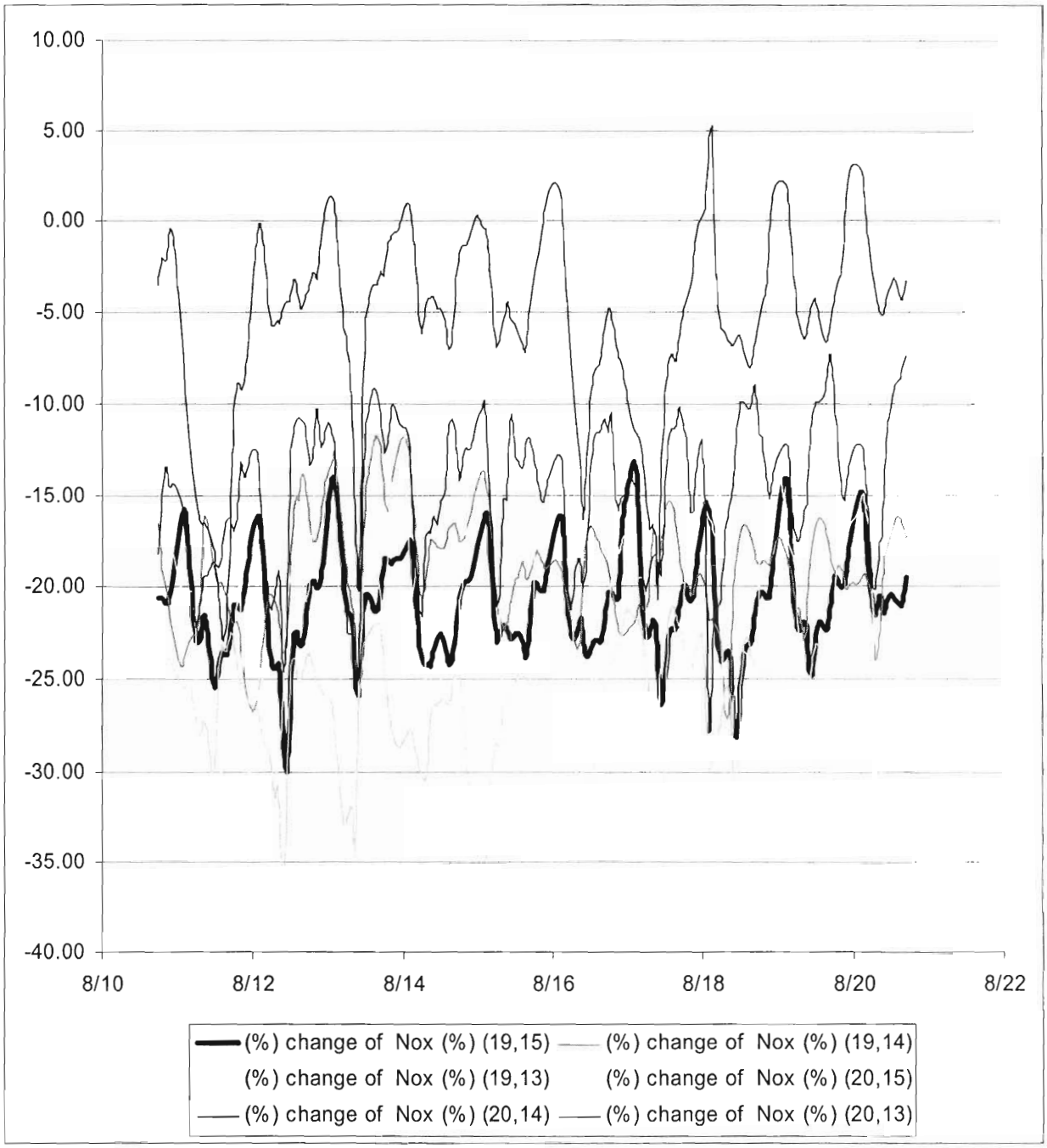

Figure 45. Changes (%) of NOx concentrations from the 2000 year to the 2007 year.

(a)

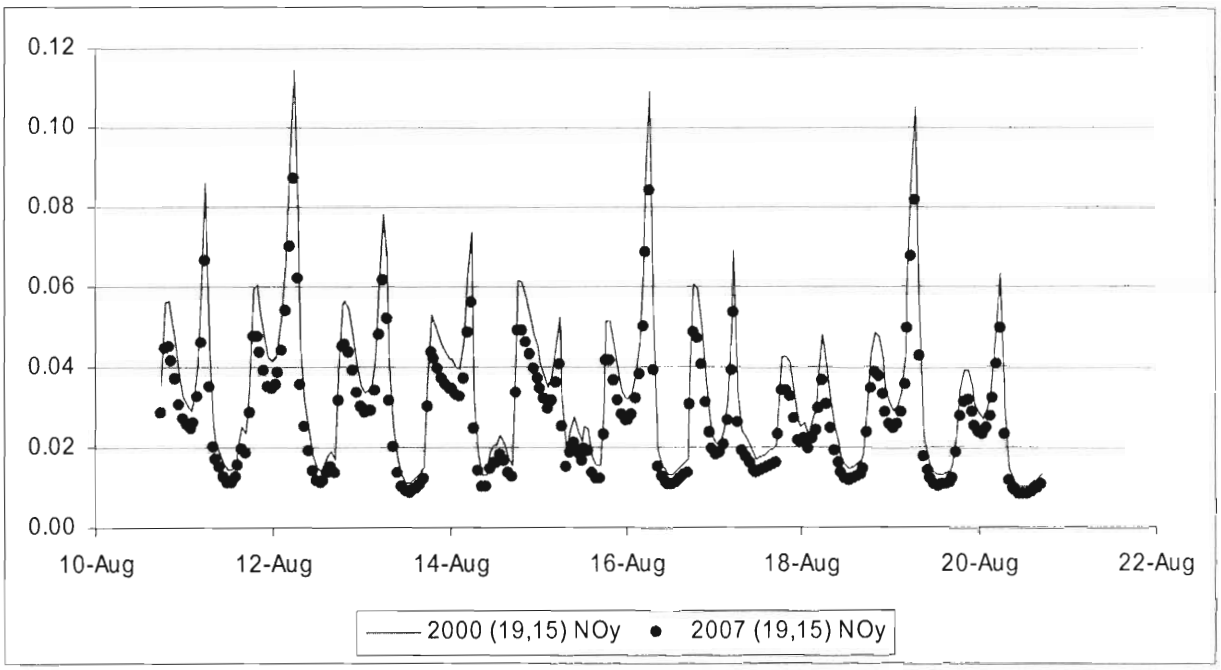

(b)

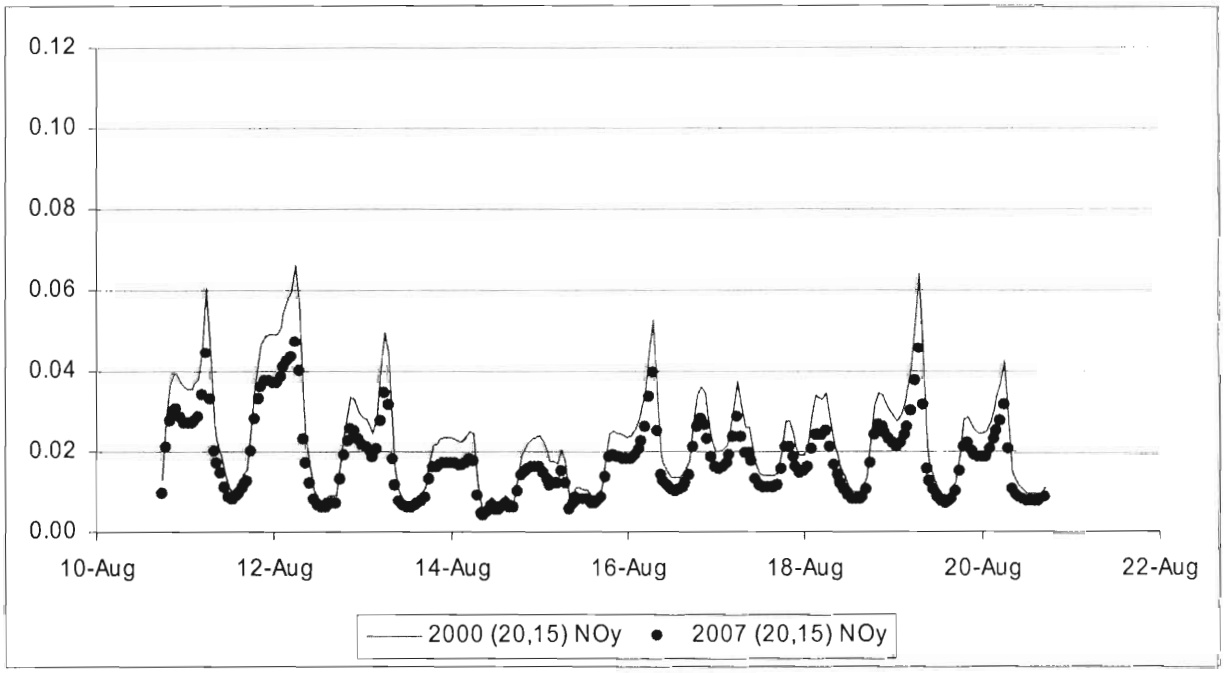

Figure 46. Comparison of the simulated hourly NOy concentrations in 2000 and in 2007. (a) is for the 19th column and the 15th row of grids and (b) is for the 20th column and the 15th row.

(c)

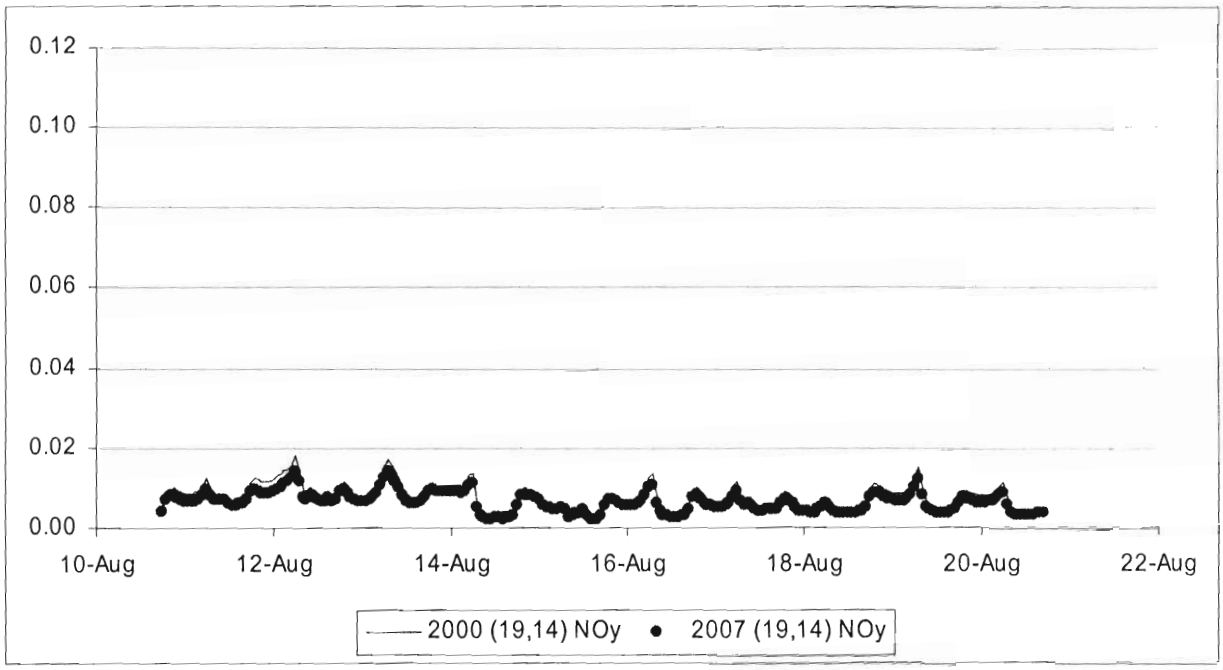

(d)

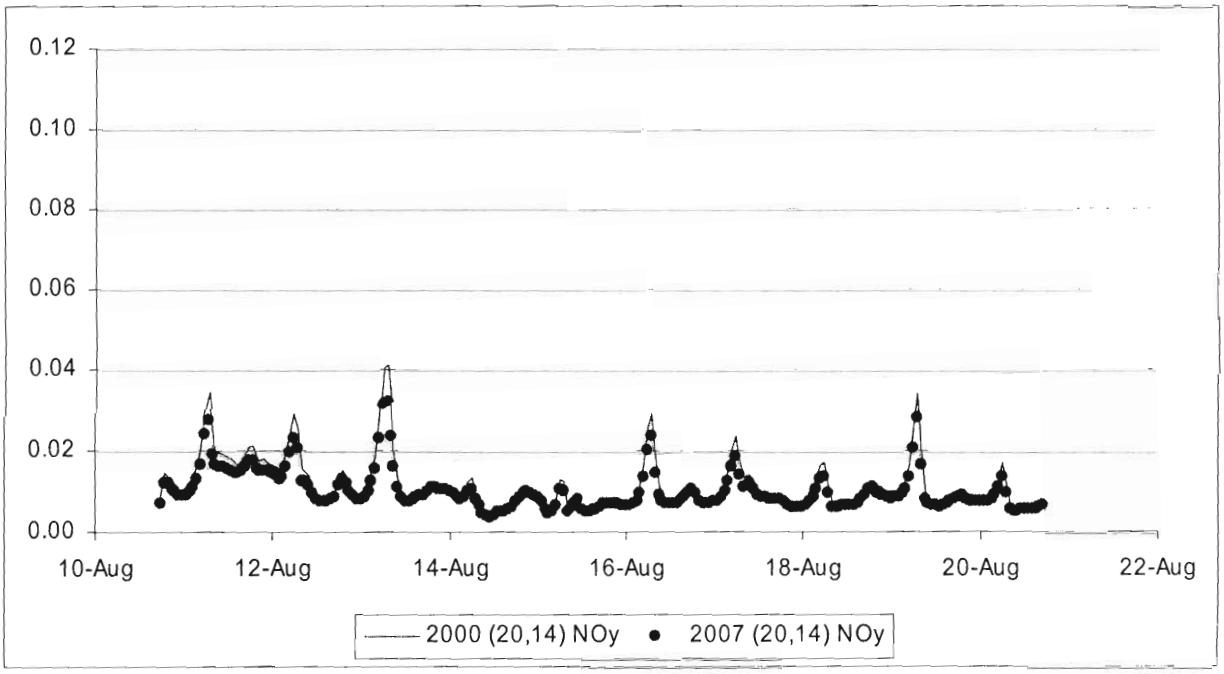

Figure 46. Continued. (c) is for the 19th column and the 14th row of grids and (d) is for the 20th column and the 14th row.

(e)

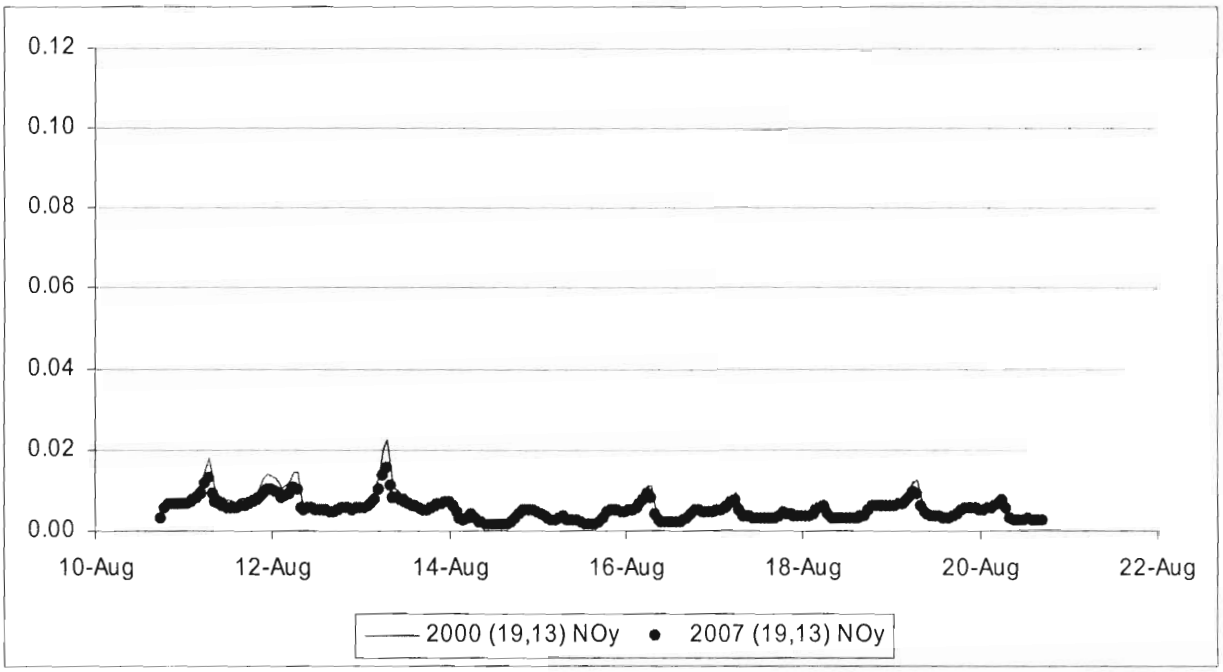

(f)

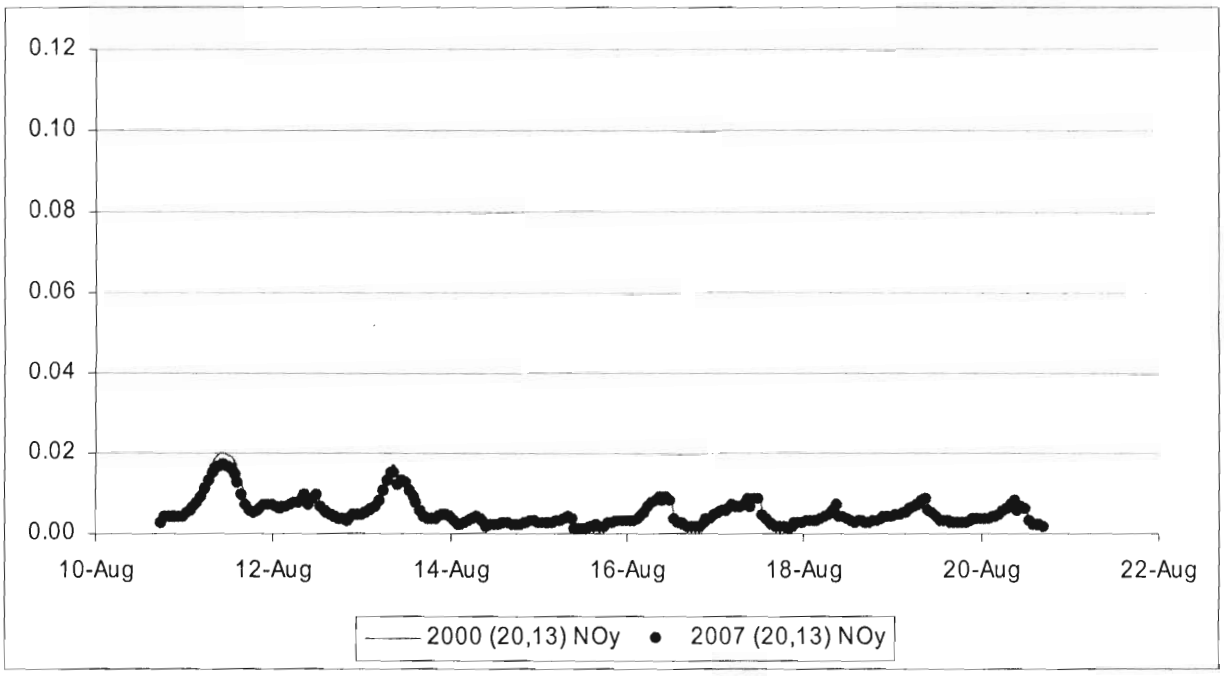

Figure 46. Continued. (e) is for the 19th column and the 13th row of grids and (f) is for the 20th column and the 13th row.

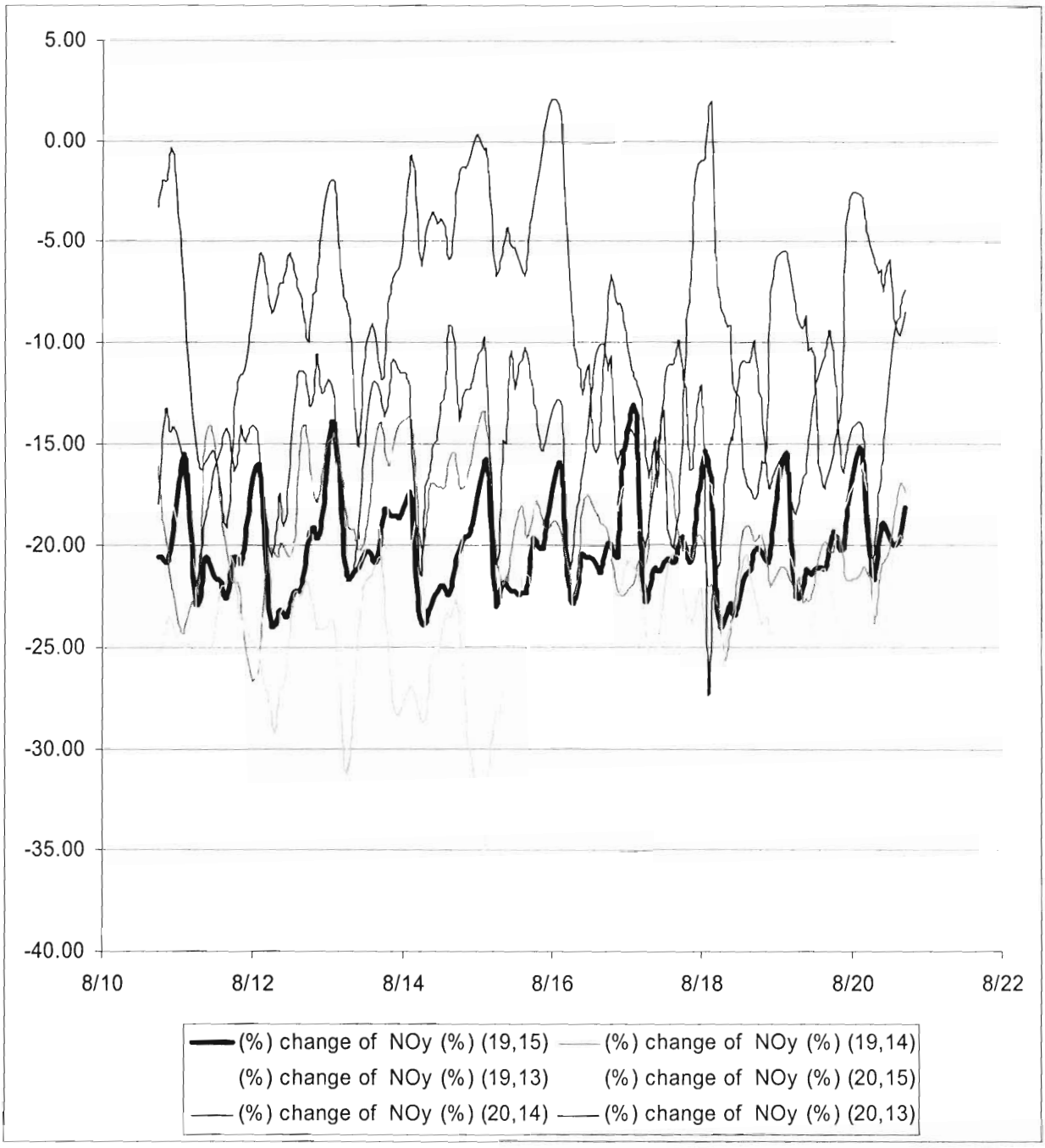

Figure 47. Changes (%) of NOy concentrations from the 2000 year to the 2007 year.

5. Conclusion

EPA provided a control strategy over the Houston area. We examined how effectively the control strategy would reduce pollutant concentrations by comparing an air quality in 2000 with that in 2007.

First, we collected an emission inventory in 2000, and modeled an air quality in the Houston area from August 11 to 20, 2000. We compared model output with measured ammonium, nitrate, sulfate, organic carbon, elemental carbon, PM 2.5 total mass, ozone, carbon monoxide, sulfur dioxide, nitric oxide and Noy concentrations. Except nitrate, which model underestimated, all modeled pollutant concentrations were very close to measured ones.

In addition, we prepared an emission inventory in 2007 based on an emission inventory in 2000. We applied EGAS (Economic Growth Analysis System) growth factors and a federal control strategy for preparing emissions in 2007. Emissions of carbon monoxide, volatile organic carbon, and NOx in 2007 were lower than those in 2000. Nevertheless, emissions of ammonia, sulfur dioxide, PM 2.5 and PM 10 in 2007 were higher than those in 2000.

Finally, we compared pollutant concentrations in 2000 and those in 2007. Amminium, sulfate, PM 2.5 and sulfur dioxide concentrations increased from 2000 to 2007. However, nitrate, organic carbon, elemental carbon, ozone, carbon monoxide, nitric oxide, NOx, and NOy concentrations decreased from 2000 to 2007